

Material characterization of an engineered spider silk protein and conception of a process for its biomimetic spinning

**Von der Fakultät für Ingenieurwissenschaften
der Universität Bayreuth
zur Erlangung der Würde eines
Doktor-Ingenieurs (Dr.-Ing.)
genehmigte Dissertation**

**von
Dipl.-Ing. David Keerl
aus
München**

Erstgutachter:	Prof. Thomas Scheibel
Zweitgutachter:	Prof. Andreas Fery
Tag der mündlichen Prüfung:	14.10.2014

Lehrstuhl für Biomaterialien
Universität Bayreuth
2014

Contents

1	Introduction	1
1.1	Biopolymers	1
1.1.1	Protein fibers	2
1.1.2	Silkworm silk	3
1.1.3	Spider silk	4
1.2	Spider silk spinning process	5
1.2.1	Spider silk protein - structure and synthesis	6
1.2.1.1	Major ampullate spidroin structure	6
1.2.1.2	Major ampullate spidroin secretion and storage	8
1.2.1.3	Biotechnological production of recombinant dragline silk proteins	9
1.2.2	Spider silk assembly process	10
1.2.2.1	The silk assembly process within a spider's spinning duct	10
1.2.2.2	Silk assembly within a technical spinning process	12
1.2.3	Fiber formation	14
1.2.3.1	Liquid-solid phase transition in the distal part of the spinning duct and fiber formation	14
1.2.3.2	Production of artificial spider silk fibers	15
1.3	Characterization of silk	18
1.3.1	Rheological characterization	18
1.3.1.1	Introduction to rheometry	18
1.3.1.2	Rheology of silk solutions	21
1.3.2	Mechanical characterization	22
1.3.2.1	Introduction to mechanical analysis	22
1.3.2.2	Mechanical analysis of silk	25
1.4	Motivation and aims of the thesis	27
2	Materials and methods	29
2.1	Materials and instruments	29
2.1.1	Chemicals	29
2.1.2	Buffers and other solutions	32

2.1.3	Consumables and tools	33
2.1.4	Instruments	34
2.1.5	Software	37
2.2	Production and purification of recombinant eADF3(AQ) ₂₄ NR3 protein	37
2.3	Protein analytical methods	37
2.3.1	SDS-PAGE	38
2.3.2	Silver staining	38
2.3.3	Immunoblotting (Western Blot)	38
2.4	Protein solution preparation methods	39
2.4.1	Preparation of a regenerated aqueous fibroin solution from <i>B. mori</i> throw- sters waste silk	39
2.4.2	Preparation of an aqueous solution from (AQ) ₂₄ NR3 protein	40
2.4.3	Preparation of (AQ) ₂₄ NR3 blends with additives	40
2.5	Preparation of artificial silk fibers from concentrated (AQ) ₂₄ NR3 solutions	42
2.5.1	Preparation of fibers using a technical pulling device	42
2.5.2	Preparation of fibers using a biomimetic spinning device	43
2.5.3	Post-treatment of artificial fibers	43
2.6	Collection of natural silk fibers	44
2.6.1	Design and construction of a laboratory housing for <i>A. diadematus</i> spiders	44
2.6.2	Catching and housing of <i>A. diadematus</i> spiders	45
2.6.3	Collecting naturally spun fibers from <i>A. diadematus</i>	45
2.6.4	Forced silking of fibers from <i>A. diadematus</i> spiders	46
2.7	Spectroscopical methods	48
2.7.1	Fluorescence spectroscopy	48
2.7.2	UV/Vis absorption spectroscopy	48
2.7.3	Fourier transform infrared spectroscopy (FT-IR)	50
2.8	Microscopical methods	52
2.8.1	Light microscopy with polarizer (PLM) or bright field modus (LMBF)	52
2.8.2	Scanning electron microscopy (SEM)	53
2.9	Material analysis methods	54
2.9.1	Rheometry	54
2.9.2	Determination of phosphate mass transfer	56
2.9.3	Determination of solvent removal using pan weighing experiments	58
2.9.4	Application of solvent removal in biomimetic spinning experiments	59
2.9.5	Mechanical characterization of natural and artificial silk fibers	60
2.9.5.1	Fiber preparation for tensile testing	60

2.9.5.2	Installation and establishment of a tensile testing setup	62
2.9.5.3	Tensile testing	63
3	Results	66
3.1	Preparation and characterization of a concentrated aqueous silk spinning dope . .	66
3.1.1	Preparation of a concentrated solution from regenerated silk fibroin	66
3.1.2	Preparation of a concentrated spinning dope from recombinant (AQ) ₂₄ NR3	67
3.1.3	Analysis of the effects of stabilizing agents on the stability of (AQ) ₂₄ NR3 solutions	70
3.1.4	Rheological characterization of flow behavior of aqueous (AQ) ₂₄ NR3 and RSF solutions	72
3.1.5	Analysis of the effects of polymeric additives on the viscosity of (AQ) ₂₄ NR3 solutions	75
3.1.6	Rheological characterization of the viscoelastic behavior of aqueous (AQ) ₂₄ NR3 and regenerated fibroin solutions	77
3.1.7	Analysis of the effects of salt on the rheological behavior of (AQ) ₂₄ NR3 and RSF solutions	79
3.1.8	Analysis of the effects of temperature on the rheological behavior of (AQ) ₂₄ NR3 and RSF solutions	80
3.1.9	Analysis of the effects of time on the rheological behavior of (AQ) ₂₄ NR3 and RSF solutions	82
3.2	Process development for biomimetic spinning	84
3.2.1	Conception and design for a biomimetic adaption of the natural spinning duct	84
3.2.2	Analysis of the effects of semipermeable membrane material, flow rate and temperature on mass transfer of phosphate ions	90
3.2.3	Characterization of solvent removal during liquid-solid transition in the spinning process	93
3.2.4	Production of artificial (AQ) ₂₄ NR3 fibers	95
3.3	Mechanical characterization of natural and artificial spider silk fibers	101
3.3.1	Establishing a fiber sample preparation procedure	103
3.3.2	Fiber diameter determination using LM or SEM	104
3.3.3	Mechanical characterization of <i>A. diadematus</i> dragline silk fibers	107
3.3.4	Influence of spinning speed on mechanical properties of <i>A. diadematus</i> dragline silk	108

3.3.5	Influence of humidity on mechanical properties of <i>A. diadematus</i> dragline silk	110
3.3.6	Mechanical characterization of (AQ) ₂₄ NR3 silk fibers	112
3.3.7	Structural characterization of biotech and natural silk fibers using FT-IR and polarized FT-IR	113
4	Discussion	116
4.1	Analysis of an aqueous (AQ) ₂₄ NR3 silk spinning dope	116
4.1.1	Influence of stabilizing agents on (AQ) ₂₄ NR3 solution stability	116
4.1.2	Rheological characterization of aqueous (AQ) ₂₄ NR3 and RSF solutions	119
4.2	Biomimetic adaptation of the natural spinning process	122
4.3	Processing of silk fibers from (AQ) ₂₄ NR3 solutions	125
4.4	Mechanical characterization of silk fibers	127
5	Summary	132
6	Zusammenfassung	135
7	Appendix	139
	Bibliography	146

List of Figures

1.1	Illustration of the natural spinning process and its implementation into a technical spinning process.	6
1.2	Illustration of shearing of a fluid	19
1.3	Illustration of typical flow curves	20
1.4	Characteristic stress-strain curves of four types of material and spider silk.	23
1.5	Comparison of engineered and true stress-strain curve for <i>A. diadematus</i> fiber.	25
2.1	Scheme for preparation of aqueous fibroin solutions from <i>B. mori</i> silk.	39
2.2	Schematic illustration of the "hand-drawing" procedure applied in this study.	42
2.3	CAD images of the original diffusion unit and spinning apparatus	43
2.4	Illustration of the post-treatment setup.	44
2.5	Spider housing	45
2.6	Scheme of silk collection from orb web	46
2.7	Forced silking - illustration of apparatus and procedure	47
2.8	Illustration of FSD FT-IR spectra of amide I band with corresponding structural assignments	51
2.9	Illustration of a typical cone-plate rotational rheometer	54
2.10	Schematic setup for ion exchange measurements	57
2.11	Illustration of pan-weighing experiment setup and solvent removal	59
2.12	Schematic overview of solvent removal procedures	60
2.13	Sample holder	61
2.14	Illustration of a tensile test procedure.	63
2.15	Exemplary error sources during tensile testing	64
3.1	Concentrating aqueous fibroin solutions	68
3.2	Concentrating aqueous (AQ) ₂₄ NR3 solutions	69
3.3	Procedure for preparation of a concentrated aqueous (AQ) ₂₄ NR3 solution.	70
3.4	Influence of stabilizing agents on the solution stability of (AQ) ₂₄ NR3	71
3.5	Rheological flow behavior of (AQ) ₂₄ NR3 and RSF solutions	72

3.6	Influence of polymeric additives on the rheological flow behavior of (AQ) ₂₄ NR3 solutions	78
3.7	Viscoelastic behavior of (AQ) ₂₄ NR3 and RSF solutions.	79
3.8	Influence of salt addition on rheological behavior of (AQ) ₂₄ NR3 solutions	80
3.9	Temperature-dependent rheological behavior of (AQ) ₂₄ NR3 and RSF solutions	81
3.10	Time-dependent rheological behavior of (AQ) ₂₄ NR3 and RSF solutions.	83
3.11	Second generation diffusion unit	84
3.12	Third generation diffusion unit	86
3.13	Membrane materials tested in this study	87
3.14	Fourth generation diffusion unit	88
3.15	Fifth generation diffusion unit	89
3.16	Diffusivity studies on different membranes applied in a technical diffusion unit	90
3.17	Water droplet formation on the surface of PES membrane	94
3.18	Mass loss over time for (AQ) ₂₄ NR3 and RSF solutions	94
3.19	Photograph of hand drawn fibers collected on the rotating mandrel	96
3.20	Time required for spinning as a function of buffer concentration	97
3.21	SEM images of natural <i>A. diadematus</i> silk and hand-drawn fibers	98
3.22	CAD Images of biomimetic spinning setups used in this study	100
3.23	Photograph of biomimetic spinning experiment including fiber formation	101
3.24	Images of the custom-made grips for tensile testing of fibers	102
3.25	New sample holder design	103
3.26	Influence of a liquid adhesive on the morphology of an (AQ) ₂₄ NR3 fiber	104
3.27	Comparison of stress-strain curves calculated based on fiber diameter determined by LMBF or by SEM	105
3.28	Comparison of fiber diameter determined by LMBF and SEM	106
3.29	Comparison of silk fibers from <i>A. diadematus</i> collected from web and by forced silking	107
3.30	Influence of reeling speed on mechanical properties of <i>A. diadematus</i> fibers	109
3.31	Influence of humidity on mechanical properties of <i>A. diadematus</i> silk fibers	111
3.32	Stress-strain curves of (AQ) ₂₄ NR3 fibers	112
3.33	FT-IR spectra of <i>A. diadematus</i> and (AQ) ₂₄ NR3 fibers	114
3.34	Polarized FT-IR spectra of spider silk fibers from (AQ) ₂₄ NR3	115
4.1	Model for stabilization of concentrated (AQ) ₂₄ NR3 solutions	118
4.2	Model for (AQ) ₂₄ NR3 assembly in solution based on rheological studies	121
4.3	Summary on evolution of diffusion unit.	123
4.4	Summary of mass transfer and solvent removal results	124

4.5	Schematic display of route to successful production of (AQ) ₂₄ NR3 fibers	127
4.6	Schematic illustration of the mechanical model proposed for native and artificial spider dragline silk	131
7.1	SEM images comparing films cast from (AQ) ₂₄ NR3 and stabilizing agent mixtures	140
7.2	Comparison of different imaging techniques for fiber diameter characterization .	141
7.3	Full list of biomimetic spinning experiments - page 1	142
7.4	Full list of biomimetic spinning experiments - page 2	143
7.5	Full list of biomimetic spinning experiments - page 3	144
7.6	Full list of hand-drawing experiments	145

List of Tables

1.1	Overview of published data for fibers produced from recombinant or regenerated silk proteins.	16
1.2	Mechanical data of spider silk fibers in comparison to other natural and synthetic fibers	26
2.5	Overview of additives to increase silk solubility used in this work.	40
2.6	Overview of polymeric additives used in this work.	41
2.7	Excitation wavelength and emission spectra.	48
2.8	Molecular extinction coefficient and molecular weight of proteins	49
3.1	Overview on concentration techniques	67
3.2	Summary of conditions tested for preparation of (AQ) ₂₄ NR3 solutions	67
3.3	Rheological fitting parameters of silk solutions	74
3.4	Overview of (AQ) ₂₄ NR3 and polymer blends.	76
3.5	Overview on calculated diffusivity factors	91
3.6	D_{ss} for (AQ) ₂₄ NR3 and RSF solutions at 45 °C and 70 °C	95
3.7	Influence of potassium phosphate (pH 8) concentration on hand drawing	96
3.8	Influence of salt on hand drawing	97
3.9	Summary of biomimetic spinning experiments from aqueous (AQ) ₂₄ NR3 solutions	99
3.10	Overview of collected data of <i>A. diadematus</i> fibers (bave) reeled at different speeds and under different environmental conditions	108
3.11	Overview of collected data for fibers made of recombinant proteins	112
3.12	Structural data obtained by FSD-analysis for natural and biomimetic fibers	113
4.1	List of cosolvents that may promote protein solubility and their mode of action	116
7.1	Tensile testing instrument evaluation	139
7.2	Overview on adhesives tested	139
7.3	Overview of data for <i>A. diadematus</i> silk, <i>B. mori</i> silk, cotton and Kevlar® fibers	141

List of Abbreviations and Symbols

<i>A. diadematus</i>	<i>Araneus diadematus</i>
<i>B. mori</i>	<i>Bombyx mori</i>
<i>E. coli</i>	<i>Escherichia coli</i>
<i>N. clavipes</i>	<i>Nephila clavipes</i>
A	alanine
ADF	<i>A. diadematus</i> fibroin
CAD	computer-aided design
CSR	controlled strain rate mode
CSS	controlled shear stress mode
Cys	cysteine
DNA	deoxyribonucleic acid
ER	escaped radial structure
ERPD	escaped radial structure with point defects
EtOH	ethanol
FS200	fibers drawn at 200 mm/s
FS60	fibers drawn at 60 mm/s
FSD	Fourier self-deconvolution
FT-IR	Fourier transform infrared spectroscopy
G	glycine
GdmHCl	guanidine hydrochloride
HFA	hexafluoroacetone hydrate
HFIP	hexafluoroisopropanol
IPA	isopropanol

List of Abbreviations and Symbols

LCST	lower critical solution temperature
LiBr	lithium bromide
LM	light microscopy
LMBF	light microscopy with bright field modus
MaSp	major ampullate spidroins
MI	minor ampullate
MWCO	molecular weight cut-off
n	number of samples
NMR	Nuclear magnetic resonance
NR	non-repetitive domain
NRC	carboxy-terminal domain
NRN	amino-terminal domain
P	proline
Phe	phenylalanine
PLM	light microscopy with polarizer
PPII	polyproline-II
Q	glutamine
rep	repetitive domain
RSF	regenerated silk fibroin
SEM	Scanning electron microscopy
TGA	Thermogravimetric analysis
Trp	tryptophan
Tyr	tyrosine
X	substitute for other amino acids such as glutamine, leucine or tyrosine
ϵ_{λ}	molecular extinction coefficient at wavelength λ [$1/Mcm$]
λ	wavelength [nm]
$A_{min,max}$	minimum or maximum absorbance []
C	mandrel circumference [mm]

c	concentration [mol/l] or [g/l]
d	layer thickness of cuvette [m]
E_λ	extinction measured at wavelength λ [$l/molcm$]
S	secondary structure content [%]
S_{mol}	molecular order parameter []
v	motor speed [mm/s] or [rpm]
α	cone angle [$^\circ$]
ΔL	change in specimen's length [m]
δt	time measured during the experiment [s]
Δy	thickness of the fluid [m]
Δl	distance or length [m]
$\dot{\gamma}$	shear rate [$1/s$]
\dot{V}	flow rate [m^3/h]
ε	tensile strain []
ε_{true}	true strain []
η	dynamic viscosity [Pas]
η_0	zero shear viscosity [Pas]
η_∞	viscosity at infinitively high shear rate [Pas]
λ	relaxation time of the viscoelastic fluid [s]
v	velocity of fluid [m/s]
ω	angular frequency [rad/s]
ρ	density [g/cm^3]
ρ_p	mass concentration of protein [g/m^3]
ρ_T	total mass density or concentration [g/m^3]
ρ_w	partial mass density of water [g/m^3]
σ	conductivity [S/cm]
σ	tensile stress [Pa]
σ_{true}	true stress [Pa]

τ	retention time of fluid in channel [s]
τ	shear stress [Pa]
A	area [m^2]
a	rate of transition between the zero shear-rate region and the power-law region []
A_0	initial cross-sectional area of the specimen [m^2]
b	fitting parameter for Power-law model []
b	membrane layer thickness [m]
D	diffusion coefficient [cm^2/s]
D_i	diffusivity []
D_{ss}	internal water diffusion coefficient [m^2/s]
E	Young's modulus (stiffness) [MPa]
F	force [N]
F_s	shearing force [N]
g	gravitational constant [$m^3/kg s^2$]
G'	elastic (storage) modulus [Pa]
G''	viscous (loss) modulus [Pa]
$h(r)$	shearing gap in dependence of r [m]
K	fitting parameter for Power-law model []
K_σ	geometrical constant for cone-plate geometry []
L	distance between two electrodes [m]
L_0	specimen's original gauge length [m]
M	torque [Nm]
m	mass after TGA measurement [g]
m_0	initial mass [g]
n	power-law exponent for Carreau-Yasuda model []
R	AC resistance [Ω]
r	radius [m]
R_m	maximum tensile strength [MPa]

rH	relative humidity [%]
T_m	critical transition temperature [$^{\circ}C$]
V	solution volume [m^3]
$V_{reactant}$	volume of reactant [m^3]
W	toughness [MJ/m^3]
x	coordinate of the diffusion direction [m]
(v/v)	volume per volume [%]
(w/v)	weight per volume [%]
Da	Dalton = kg/mol
M	Molar = Mol/l

1 Introduction

In recent years, the growing interest in the application of bio-inspired materials as higher-performing new materials or in innovative technologies [1–3] was driven by the progress of analytical and synthetic methods, enabling a more thorough understanding of molecular and structural mechanisms of biological materials [1, 4]. The application of biological principles and systems to solve technical challenges is typically referred to as biomimetics [1, 4]. In general, biomimetics is used to describe the study of formation, structure and function of biological materials and evolutionary biological processes for the purpose of mimicking products for instance by technological means [5]. Two different approaches for the study of biological concepts are usually applied: "top down" or "bottom up" [4–6]. Both approaches share 1) the elucidation of structure-function relationships by studying model systems, 2) the extraction, application and adaptation of the underlying physical and chemical design principles, and 3) the discovery of new approaches including new pathways to synthesize and manufacture new materials [5]. However, a challenge for the realization of biological principles in polymer industry is the technical and economic adaptation in large scale [6], and furthermore, the limitation of the production to the structuring of compositionally simple homopolymers and copolymers [7]. In contrast, biosynthesis controls the sequence, composition and conformation of protein fibers and produces complex multicomponent composite structures through the seamless integration of protein synthesis, mineralization and self-assembly (i.e. spontaneous organization into an ordered structure without human intervention [6]) at an unsurpassed capacity [7].

1.1 Biopolymers

In everyday's life, synthetic polymers play an important role in numerous applications, offering a large variety of material properties. In recent years, however, classical synthetic polymers were replaced in certain applications by biodegradable polymers and biopolymers, such as polysaccharides and proteins, due to the desire of having novel materials offering a combination of classical mechanical and "ecological" properties, such as biocompatibility, biofunctionality and biodegradability. Furthermore, biopolymers were also found to display optical properties like transparency, heat or electrical conductivity (e.g. DNA), and chemical properties such as resistance against cor-

rosion (e.g. cellulose) [5, 6]. Moreover, they outperform man-made counterparts although being synthesized and processed at ambient and aqueous conditions [5, 8, 9]. Amongst biopolymers, protein fibers are the most prominent representatives [7, 8, 10, 11].

1.1.1 Protein fibers

Protein fibers are essential building blocks of life, providing key functions in biological systems, such as motility, elasticity, scaffolding, stabilization and protection of cells, tissues and organisms, or forming structural materials such as hair, skin or silk [7, 10, 12, 13]. They achieve their great potential and diversity although being produced via a polymerization reaction from a comparatively small set of monomeric building blocks: 20 naturally occurring amino acids which possess various chemical properties (aliphatic, acidic, basic, polar and non-polar) [7, 8, 14]. These amino acids are linked via amide (peptide) bonds based on the protein's genetic information into a defined and unique sequence of monomers (i.e. their primary structure), yielding monodisperse linear polymers while synthetic polymers are typically heterodisperse, non-linear with a broad molecular size distribution [3, 8, 15–18]. The primary structure completely encodes the information of the protein's three-dimensional secondary structure and remarkably, only the differences in primary sequence leads to the diversity of structure, properties and biological functions [15, 19].

Polypeptide chains are able to adopt different secondary structure conformations (such as α -helix or β -sheet) and their formation and stabilization is a thermodynamically favored process driven by relatively weak non-covalent interactions (e.g. electrostatic and van-der-Waals forces, hydrophobic effects and hydrogen bonds) or covalent interactions (e.g. disulfide bridges) [8, 15, 17, 19]. The abundance of these weak interactions proved to play a vital role for production at ambient conditions [13].

Protein fibers are typically categorized based on the type of their secondary structures, such as β -turn/spiral in elastin, the α -helical motifs in keratin, the polyproline-II (PPII) triple-helix in collagens and the β -sheet fibrils in amyloid fibrils [11] or the β -sheet nanocomposites in silks [5] (and references therein). The β -sheet silk, for instance, is a remarkable proteinaceous structural material designed for mechanical function and/or extraordinary resistance to mechanical manipulation. Consequently, β -sheet structure is a very common building block for a variety of biological materials [13] making it an intriguing scaffold for advanced biomaterials [5]. Amongst the best known and investigated representatives of fibrous proteins are collagens, elastins, keratins as well as silks of silkworms and spiders.

1.1.2 Silkworm silk

Silks are fascinating and thus extensively studied protein fibers, in particular those produced from the domestic silkworm *Bombyx mori* and spiders (*Nephila clavipes*, as well as *Araneus diadematus*) for their lifelines, webs, traps, prey wrapping, or to protect their offspring [11, 20]. Silkworm silk has been commercially used as biomedical sutures for decades and in textile production for millennia (due to its superb texture and ability to bind dyes [21]) and is now rediscovered and reconsidered as a potential biomaterial in biomedical application and tissue engineering [22–24]. Although many chemically similar synthetic polymers (e.g. nylon) exist, the combination of strength and ductility [25] makes silk an ideal model for biomimetic advanced materials [5, 26]. Thus, polymer industry attempted to produce synthetic textile fibers matching silk's desirable properties, however, the poor reproducibility thereof imposes a great limit [25].

The *B. mori* raw silk fiber (bave) consists of two fibroin monofilaments (brins) enveloped in a proteinaceous sericin coat [24, 25, 27–30]. The roughly circular to elliptical brins have an average diameter of 7 μm to 16 μm [31–34], and display a core-shell type structure [24, 30, 35]. The core consists of three proteinaceous components: a heavy chain fibroin (H-chain, ca. 350 kDa), a light chain fibroin (L-chain, ca. 25 kDa) - both connected via disulfide bonds and preferentially aligned as bundles of nanofibrils along the fiber axis - and a glycoprotein (P25, ca. 30 kDa), which is non-covalently associated with both fibroins. The molar ratios of H-chain : L-chain : P25 were found to be 6:6:1 [24, 30, 35]. These fibroins, usually showing a high content of regular secondary structure characterized by alternating blocks of hydrophobic and hydrophilic domains [11, 20, 30, 36, 37], are synthesized within specialized glands, secreted into the lumen of these glands and stored prior to spinning [20, 23, 30, 36, 38, 39]. The amphiphilic character of H-chain gives rise to the formation of super-assembled transient folded structures, most likely involving micelle formation [30, 36, 37], while the repetitive hydrophobic domain accounts for the formation of anti-parallel β -sheets in the final fibers [30, 36, 37]. Generally, silk fibroin is a semi-crystalline polymer mainly consisting of two important phases: fibroin adopts a random-coil and amorphous structure (so-called silk I conformation) in solution, and an antiparallel β -sheet rich structure (silk II), formed through hydrogen bonds between adjacent peptide chains, in a fiber [28, 40, 41]. The spinning process of *B. mori* silkworm silk is similar to that of spider silk, with the fibroin undergoing a series of phase transitions: from gel to sol, from sol to liquid crystal and finally from liquid crystal to fiber. Thereby, all the individual steps are tightly controlled by environmental changes such as pH, multiple (monovalent or divalent) cations, water content (dehydration) and extensional (and shear) flow [14, 24, 27, 30, 42–45].

1.1.3 Spider silk

Spider silk produced by orb-weaving spiders reveals fascinating mechanical properties, in particular its combination of high tensile strength and elasticity, yielding an exceptional toughness (i.e. resistance to fracture) exceeding most natural or man-made fibers [46–55]. These intriguing properties have evolved over millions of years and eluded mankind even long before it longed for successful reproduction in the last decades. Cobwebs were used to staunch bleeding wounds in ancient Greece, orb webs were used for fishing in Australasia, and spider silks were later on even utilized for military purposes, e.g. for the construction of crosshairs in optical devices [53, 56]. The variety of applications is related to spider silk's properties, comprising a combination of high mechanical stability, biocompatibility, smoothness and thinness by comparison with man-made materials. In contrast to other arthropods such as silkworms, a spider is able to produce a variety of different silks with diverse properties. Female orb weaving spiders (such as the garden spider *A. diadematus*) for instance utilize five different silks during web construction, with each silk being produced in a specialized gland and its mechanical properties being tailored to fulfill a certain task [21, 46, 48, 50, 53, 57–61]. A typical orb web consists of a frame of silk which supports a wheel of silken spokes radiating from a hub; these radii in turn support the spiral thread that captures prey either by using a sticky aqueous glycoprotein coating (ecribellate spiders) or by using very fine hackled bands of silk threads combed onto the spiral thread (cribellate spider) [48, 62]. Soft spiral and tough radii work together to absorb the prey's impact and hold it aloft [21, 57], as the capture spiral absorbs high kinetic energy of prey [57] (and references therein), and the radii silk dissipates energy via viscoplastic deformation [60]. A few decades ago, the silk accounting for frame and radii of an orb web entered the focus of material sciences due to its fascinating properties [57, 58]. In addition, it is also the easiest accessible spider silk, serving as the spider's lifeline that is typically dragged behind the spider during escape and thus commonly referred to as dragline silk. This dragline silk was found to show the greatest toughness of the six silk types found in an orb web, being approximately five times higher than that of steel and three times that of man-made synthetic fibers such as Kevlar® 49 [21, 32, 49, 55, 63, 64]. The utilization as a lifeline is possible due to another remarkable property of dragline silk: it hardly twists, thus, enabling the spider to descend on it during free fall as in case of danger. This unique functional response referred to as torsional shape memory is shown by the scarce oscillation once a dragline thread is twisted and enables total (though slow) recovery of its initial form without external stimulus [49, 55, 65]. The different silk types display significant variation in their strength (from 0.02 GPa to a remarkable 1.7 GPa and extensibility (between 10 % and 500 %) [48]. Moreover, the spider's ability to tune the silk's mechanical behavior by controlling silk composition and storage conditions [61] as well as fiber extrusion conditions (by adapting the speed of silk drawing) [48, 61, 64,

66, 67] enables it to function well under a wide range of environmental conditions [20, 57, 68] and to actively respond to prey available [69] and thus nutrition [70, 71] or its own body weight [60].

Similar to silkworm silk, the exceptional properties of spider dragline silk are achieved under benign conditions, i.e. spinning at ambient temperatures and low pressures using water as solvent [32]. These properties are believed to result from its structural design, comprising β -sheet crystals that cross-link the proteins (and account for stiffness) while being embedded in a network of less organized amorphous polypeptide chains (accountable for fiber mobility) [52]. Apart from its outstanding mechanical properties, upon contact with water or a relative humidity greater than 60 %, the dragline thread starts to swell radially, leading to an increase in diameter accompanied by a shrinking in length of about 50 % [72–76]. In nature, this characteristic feature called "supercontraction" provides a helpful tool, as "worn out" silk threads within a spider's orb web can be "renewed" in the morning dew, and the web regains its initial rigidity [51, 56, 76, 77]. This feature is enabled due to the entropy-driven reorientation of silk molecules through disruption of hydrogen bonds between the spider silk proteins upon uptake of water [68, 72, 76, 78–82]. The most remarkable aspect of supercontraction is that it takes place under ambient temperatures, which is in contrast to equal processes in man-made fibers which generally require elevated temperatures or harsh solvent conditions [78]. Controlled supercontraction may also be exploited as a mechanism to tailor properties for applications [72, 82]. However, supercontraction imposes a major drawback for the creation and application of biomaterials, e.g. if one considers a bullet proof vest made from artificial spider silk worn in wet conditions [56].

The intriguing characteristics of spider dragline silk, suggested to be achieved by a optimized combination of chemistry and spinning process [9], have attracted the interest of scientists to investigate its molecular building blocks, its self-assembly properties and the fiber spinning process [53]. Thus, the technical adaptation of the natural spinning process in order to produce threads from silk proteins dissolved in aqueous solutions by mimicking the natural spinning duct using a porous or permeable compartment to implement ion exchange, acidification and water removal processes has grown greatly in interest [83–85].

1.2 Spider silk spinning process

The spinning of dragline silk is characterized by a highly concentrated liquid crystalline spinning feedstock, that undergoes an array of complex processes during the passage through the spinning duct: involving pH as well as anion induced conformational changes, shear as well as extensional

forces, and dehydration which all lead to a solid silk fiber [32, 53, 86].

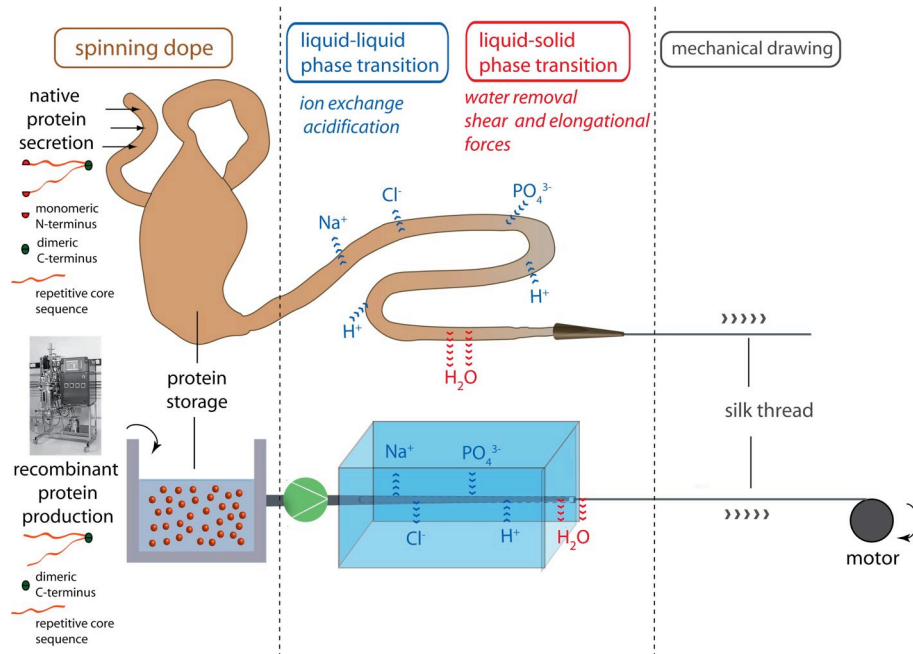


Figure 1.1 – Illustration of the natural spinning process and its implementation into a technical spinning process. The ampulla gland/sac constitutes the main storage repository and leads through a "funnel" into the tapering duct which has three loops inside a sheath and terminates in a structure known as the valve. Furthermore, the spinning dope proceeds in a narrow tubular region specialized for rapid water recovery, and the silk thread then exits at the spigot [32, 87].

1.2.1 Spider silk protein - structure and synthesis

1.2.1.1 Major ampullate spidroin structure

Dragline silk displays a core-shell type structure, with the shell consisting of a layer of minor ampullate (MI) spidroin (known as the "skin"), glycoproteins and a lipid coating [33, 35, 57, 67, 87–90]. The core mainly consists of two spidroins, secreted in the major ampullate gland, resembling in structure that of a segmented multi-block copolymer [63, 89]. The major ampullate spidroins (MaSp1 and MaSp2 (for *Nephila* species)) [91] or ADF3 and ADF4 (for *A. diadematus* fibroin) [63]) display molecular weights from 250 kDa to 350 kDa [63, 91–94]. Their primary sequence has been partly identified recently and revealed a repetitive core sequence which accounts for approximately 90 % of the amino acids of the protein [50, 95].

The repetitive sequence is composed of tandemly arrayed consensus motifs: large hydrophobic alanine-rich stretches (A_n or $(GA)_n$, with A for alanine and G for glycine), and more hydrophilic glycine-rich stretches, (GPGXX or GGX, with P for proline and X often representing glutamine, alanine, leucine, or tyrosine) [53, 63, 95]. The composition and repetitiveness of the core sequence of MA spidroins distinguishes the amino acid composition (unusually high content of G, X, A and P in addition with an extremely low content of charged amino acids) from that of other structural proteins [53, 73, 96]. Moreover, the repetitive core region largely determines the macroscopic properties of the fiber and in particular its mechanical behavior [97, 98]. On the one hand, the alanine-rich motifs have been found to form either the highly oriented crystalline β -sheet stacks (A_n) or the non-oriented linker between the crystalline region and the amorphous matrix ($(GA)_n$), both accounting for the extraordinary tensile strength of the fiber [63, 79, 99–105]. The glycine-rich motifs, on the other hand, have been discovered to be involved in providing the fiber's elasticity, e.g. by forming the amorphous matrix (3_1 -helix) connecting crystalline regions (GGX motif) [63, 100, 103–105] or by forming elastic β -turn spirals (GPGXX motif) [63, 105, 106].

The core sequence is flanked by highly conserved non-repetitive (NR) regions (90 to 140 amino acids) at the carboxy-terminal (NRC-domain) [93–95, 107, 108] and amino-terminal (NRN-domain) ends [95, 109–113]. Unlike the core domain, both terminal domains are mainly composed of five α -helical bundles, although with different folds and neither one having structural homologues so far. The NRN-domain displays a higher homology and thus a more conserved function [107, 112, 114], while the NRC-domain displays the proteins' most hydrophobic part [94, 107] and a high content in charged amino acids [94, 95, 107]. Furthermore, the NRC-domain typically exists as a parallel dimer assisted by the permanent linking of α -helices via disulfide bonds [98]. Recent studies have revealed that both terminal domains act as environmentally triggered structural switches, significantly influencing the solubility as well as the initiation of fiber assembly [98, 107, 112, 114, 115]. The NRC-domain was found to be essential for the controlled switching between storage and assembly forms of silk proteins as a function of environmental conditions [94, 98, 107, 114, 116, 117] and to play a role in the alignment of spidroins which accounts for higher molecular weight and improved mechanical properties [93–95]. The NRN-domain was observed to be responsible for the regulation of spidroin assembly by inhibiting precocious aggregation during storage as well as accelerating and directing self-assembly as the pH is lowered along the spider's extrusion duct [98, 111, 112, 114, 115, 118]. However, the mechanisms involved, in particular regarding the NRN-domain, are still up for discussion. It was shown, that at pH above 7 the NRN-domain is monomeric due to the destabilization of the dimers by a trap-and-trigger mechanism. While upon acidification, the same mechanism acts as a stabilizing trap, locking the monomers into antiparallel dimers via electrostatic interactions between the protonated acidic residues at the hydrophobic interface [98, 107, 114, 115, 118].

These features led to the conclusion that silk's primary structure is extremely important for fiber formation and the characteristic features of the solid silk fiber [40, 53, 94].

1.2.1.2 Major ampullate spidroin secretion and storage

The major ampullate gland, where the MaSp proteins are secreted and stored, consists of two distinct transverse zones: the A-zone, occupying the long tail and the B-zone, comprising the wider part of the sac to the funnel [32, 86, 87, 92, 119]. The epithelium of the A-zone is composed of tall columnar cells [120] which secrete a metastable aqueous and highly viscous solution of 20 % to 30 % (w/v) [40, 63, 102, 121], the so-called "spinning dope" [32, 62, 63, 87, 92, 102, 119, 122–125]. The freshly synthesized, rod-shaped spider silk proteins were found to adopt a cholesteric liquid crystalline phase [38], in which neighboring molecules spontaneously orient their long axis in parallel to each other and perpendicular to the secreting epithelium in a so-called escape texture [32, 126, 127]. However, other studies observed the tightly hexacolumnar-packed molecules to form many small spherical droplets yielding a gel-like spinning dope which flows from A-zone to B-zone [86, 87, 128]. These droplets grow by coalescence under the influence of hydrophobic interactions [129] before being drawn out into long thin structures [86, 87]. The latter observation can be related to the amphiphilic character of the silk protein, which promotes appropriate solubility and the formation of mesogenic liquid crystals for controllable assembly [40, 94, 107, 130].

Alike the *B. mori* fibroin, the spider spidroin's structural conformation in the spinning dope within the A-zone differs significantly from that in the final dragline silk fiber, displaying predominantly characteristics of an unfolded protein (mainly random-coil and PPII helix-like structures) [102, 119, 122, 131]. In particular the PPII helix-like regions (adopted by glycine residues) [14, 132], but also the environment in the glands [133], play a key role in achieving the two opposite constraints of maintaining stability as well as avoiding premature self-aggregation during storage and initiating the phase transition from gel to solid during the spinning process [37, 94, 95, 122]. The stability of MaSp in the spinning dope is achieved by the PPII helix-like regions through preferential formation of intermolecular hydrogen bonds between side chains and solvent, thus, preventing the formation of intramolecular hydrogen bonds [102, 122]. Upon induction of shear and elongational forces, these PPII helix-like regions can be readily transformed into a β -sheet structure [122].

In the B-zone, where the structure shifted towards predominantly β -sheets [129, 132], the orb-web spiders also secrete coat protein(s), for instance the glycoproteins that help to plasticize the thread by maintaining a high water content, and thus influence the mechanical properties [32, 62, 87, 89,

119]. Chemical analysis revealed that the skin showed increased resistance to chaotropic agents and acids compared to the core, acting as a supplementary protection for the silk fiber [89].

1.2.1.3 Biotechnological production of recombinant dragline silk proteins

The ability to produce spider silk proteins in sufficient amounts and in a cost-effective way is essential for the application of spider silk in high-performance materials. Since the farming of spiders is hampered by their territorial and cannibalistic behavior [134, 135], the biotechnological production of spider silk proteins represents a promising alternative owing to its potential for large-scale production of proteins with precisely designed primary sequences [9, 63, 136–140]. Thereby, the genetic information of the desired protein has to be transferred to an expression host, such as bacteria, which is cultured in a fermentation process until offering optimum conditions for protein production. Then, protein synthesis is induced, and the desired protein is isolated from the expression host at the end of the process.

Long spider silk gene sequences have been analyzed [137], but their successful biotechnological production in expression hosts has been hampered in particular due to the highly repetitive nature of the underlying genes, as well as the high gc-content, the length of the constructs and the specific codon usage of spiders [63, 138, 141–144]. Approaches to produce recombinant spider silk proteins have included genetically modified bacteria (e.g. *Escherichia coli*) [106, 141, 142, 145–147], yeasts [148, 149], plants [150, 151], insect [152, 153] and mammalian cells [154] as well as transgenic animals [155, 156]. Despite the use of different host systems, the expressed spider silk proteins displayed much lower molecular weights than their native counterparts [143]. Although one group produced a native-sized protein in a metabolically engineered *E. coli* [157], as of today, no successful expression of full length spider silk clones has been achieved. However, the size of the recombinant proteins and the distribution of modular repeat units play an important role in silk protein assembly and material functions, as more repeating units allow an increased number of inter-chain and intra-chain interactions [9, 157]. Furthermore, the absence of some protein domains is assumed to severely affect the quality of the resulting silk, either because of improper assembly or loss of material properties [143].

To overcome the mentioned hurdles, scientists have put remarkable efforts into developing various cloning and production strategies using recombinant DNA technology to design specific spider silk-like genes with precisely specified amino acid sequences mimicking those of natural silk fragments [138, 141, 143, 154]. Furthermore, the production of a new generation of silk-like proteins by extending these genetic design concepts to a broader range of chemistries, such as other types of protein block copolymers and fusion or chimeric proteins is enabled [9, 138, 143,

158, 159]. Moreover, this technique offers the advantage of precisely controlling both molecular mass and amino acid monomer sequence, enabling a level of control over physical properties and functionality not achievable with standard chemical polymerization technologies [141]. In terms of gene design several approaches have been employed [63, 142, 151, 153–155]. Among others, a cloning system enabling the creation of artificial spider silk genes by seamlessly joining solid-phase synthesized oligonucleotides was developed [63, 160]. This method provides the opportunity to mimic the modular arrangement of spider silk consensus motifs and to adjust the codon usage according to the needs of the designated expression host. Thereby, a variety of spider dragline silk-like proteins were produced in *E. coli* based on sequences from *A. diadematus* dragline silk proteins [152, 160]. The repetitive sequence of ADF3 was mimicked by the design of two modules, with one (termed A) being derived from the poly-alanine containing consensus sequence, while the other module (termed Q) comprises four repeats of the GPGQQ motif [63, 160]. In contrast, the repetitive part of ADF4, which is generally composed of a single conserved repeat unit displaying only slight variations, was mimicked by design of one consensus module (termed C) [63, 160]. All of the synthetic genes could be combined with a NRC-region mimicking the carboxy-terminal domain and containing the only cysteine residue enabling the formation of an intermolecular disulfide bridge [63, 160, 161]. Based on its amino acid sequence, the recombinant (AQ)₂₄NR3 used in this work, is an amphiphilic protein with a monomeric molecular weight of 106 kDa [160, 161].

1.2.2 Spider silk assembly process

1.2.2.1 The silk assembly process within a spider's spinning duct

The assembly pathways of natural spider silk proteins upon processing through the spinning duct have been explained in detail in literature, revealing that besides dope composition and spinning speed, changes in the environmental conditions such pH value and presence of ions are of paramount importance [9, 32, 43, 53, 86, 121, 125, 127, 137]. Upon transfer through the spinning duct, a transition from mainly random coil and α -helical (more likely 3_1 -helical) conformation in the native dope to the β -sheet conformation of the fiber was observed, although some native structural elements were still retained in the amorphous phase of the final fiber [119, 123, 124, 131]. Similar observations have been made for the spinning process in *B. mori* silkworms.

As mentioned, the highly concentrated aqueous spinning dope displays liquid crystalline properties [63, 123–125], combining the properties of a liquid (e.g. anisotropic viscous behavior of sufficiently concentrated solutions) and of a crystalline solid (e.g. anisotropic elastic behavior)

[162], and is further responsive to temperature as well as pH changes [127]. Spinning from a liquid crystalline material has revealed several advantages, being virtually free of the uncontrolled reorientation of molecules after emergence from the die and reducing the force required to spin a thread [32]. Molecules that form liquid crystalline structures are usually long and straight with a tendency to line up against each other or any adjacent surface. Thereby, nematic crystals are ordered in parallel, smectic crystals in parallel as well as in layers, and cholesteric crystals are ordered in a pseudo-helical or screw-carpet fashion [6, 162, 163]. This feature observed in fibrous biopolymers [6] helps the spider to control the folding and crystallization of its silk proteins at benign conditions [32, 86]. Depending on the class of liquid crystal and the amount of material that is orientated in any particular direction, mechanical properties and the direction of those properties in the resulting material can be very closely controlled [6]. The orientational order of the liquid crystalline dope is known to significantly change along the silk spinning pathway and particularly in the tubular extrusion duct just before the draw down of the fiber. This evolution of orientational order is extremely important, because it determines the processability of the material (by affecting its viscosity) [30, 32, 55, 86, 90, 126, 164], the microstructural details and thus the mechanical properties of the solidified silk fiber [32, 86, 126, 164].

The spinning dope within the ampulla revealed characteristics of an unfolded protein present in a cholesteric liquid crystalline phase. The relatively low elongational flow rates within the ampulla and the early part of the spinning duct are assumed to prevent premature crystallization of the feedstock before high shear rates are applied [32, 38, 86, 119]. Upon flow from ampulla to the first limb of the spinning duct, a natural analogous to the die used in artificial spinning [32], the viscous silk protein solution turns and untwists into a lyotropic nematic liquid crystalline mesophase (i.e. an intermediate phase) [32, 37, 38, 86, 90, 102, 126]. The spider silk proteins retain this so-called escaped nematic orientation until they enter the second limb of the spinning duct. Furthermore, the moderate extensional flow appears to be the driving force for onset of the conformational transition from random coil and PPII helix-like to mainly β -sheet [32], and thus the orientational ordering of the silk proteins [119].

In the second limb of the duct, the spidroins are further re-organized into disk-shaped bilaminar micelles with their long-axes perpendicularly arranged to the disk's plane [32, 42, 86, 127]. This improved orientation and molecular alignment within the dope, commonly known as cellular optical texture [42], is achieved under relatively low stress forces, and is likely driven by the slow increase in elongational flow rate due to the hyperbolic geometry (i.e. slow reduction in diameter) of the duct, a slight acidification of the spinning dope by addition of hydrogen ions [40, 43, 44, 57, 86, 87, 116, 125, 132], and a change in element composition (increase of metallic ion potassium and decrease of sodium) [121, 125, 165].

Finally, in the third limb, epithelial cells with apical microvilli resorb water, a process additionally facilitated by the thin cuticle lining (a hollow fibre dialysis membrane analogue) which is thought to enable rapid removal of water and change in ionic composition [32, 116, 166]. Assuming a rapid convective removal of water, a numerical model proposed that the process is solely governed by the rate-limiting internal diffusion, which will result in increased fiber plasticity, since intra- and intermolecular hydrogen bonds have a longer time to re-orient [167, 168]. The combination of increase in viscosity (due to water extraction) and wall shear forces (due to exponential increase in linear velocity caused by the convergent geometry) is thought to pull out the cellular texture by pre-orientating the molecules uniaxially in the distal part of the third limb [86], initiating the development of early β -sheet structures [40, 90, 119, 169]. This pre-orientation is suggested to reduce the viscous drag of the feedstock and, thus, the energy required to produce an axial alignment of the molecules [127]. At the tubular extrusion duct of a spider, the silk dope contains a metastable escaped radial structure with point defects (ERPD) [32, 86, 126, 127, 164]. ERPD is regularly observed when nematic liquid crystals are confined in cylindrical tubes with lateral surfaces enforcing strong radial anchoring, i.e. the molecules are forced to orient radially at the surface [126]. Upon approaching the very end of the third ductal limb, accelerating elongational flow and shear forces lead to an elongation and alignment of the disk-like structures [87], initiating phase separation [169] and formation of most of β -sheets [119]. Thereby, the ERPD structure evolves into a defect-free predominantly axial escaped radial (ER) β -sheet rich structure [86, 126], which is retained in the solidified fiber [86, 126].

1.2.2.2 Silk assembly within a technical spinning process

Today, mainly two different approaches for investigating silk assembly *in vitro* have been employed [170]: 1) using reconstituted/regenerated silk dopes produced by dissolving native silk fibers in harsh solvents (e.g. lithium bromide (LiBr) or hexafluoroisopropanol (HFIP)) [171–178] or 2) using recombinant silk proteins dissolved in aqueous solutions (native-like conditions). Using regenerated *B. mori* fibroin solutions, the Kaplan group tried to clarify the process of silk self-assembly during natural spinning [37]. Remarkably, in contrast to the liquid crystalline theory for native silk dope, they observed the formation of micelles in water, which at higher concentration coagulate into globules that are elongated upon transfer through the spinning duct into fibrillar structures and finally into a fiber [37]. This observation was related to the amphiphilic liquid crystalline character of fibroins. Lyotropic liquid crystals (i.e. liquid crystals that are able to undergo phase transitions dependent on the concentration of its basic compound) with amphiphilic character display a concentration-dependent self-assembly behavior in solution: at low concentration they spontaneously assemble into micelles, while at higher concentrations they are ordered into

hexagonal columns [162, 174].

Although *in vitro* as well as *in vivo* studies highlighted the same aspects of silk protein pre-orientation, several important effects influencing secondary, tertiary and quaternary structures of the proteins have not been considered. Similar to native spidroins, recombinant spidroins in solution have been reported to fold into hairpin structures essential for the formation of antiparallel β -sheet structures in mature fiber [179]. This process is mainly driven by the Alanine-rich segments that are predicted to form helical structures in solution and are believed to constitute the β -sheets in the fiber [101, 179]. Glycine-rich segments however, generally lack a charged residue, and short segments likely form β -turns, while long segments likely form random coil or helical structures [179]. Studies using recombinant spidroins revealed that the minimal requirements for prominent fiber formation are four poly-AG-rich co-repeats and a NRC-domain [179].

Upon passage through the spinning duct, the proteins encounter remarkable changes in their solvent environment, leading to salting-out effects accompanied by structure formation. The role of processing, in combination with the primary structure, plays a critical role in silk material properties [9]. Similar to conditions found *in vivo*, *in vitro* processing and assembly of silk proteins was also influenced by ionic environment, pH and physical stress [87, 158, 180, 181]. In general, the stability of proteins in an aqueous solution is affected by its surrounding ions: according to studies by Hofmeister in the early 20th century, chaotropic ("salting-in") ions stabilize soluble proteins, while kosmotropic ("salting-out") ions promote structure formation and protein aggregation [182–184]. Salting-in salts such as sodium chloride, as found in the spider's storage dope, inhibit aggregation and assembly of the silk proteins and even prevent liquid-liquid phase separation. Moreover, as soon as sodium chloride is exchanged against "salting-out" ions, structure formation starts [161]. The "salting-out" effect depends not only on the employed ions but also on the sequence of the repetitive core and the flanking NR domains which amplify the response of the repetitive (rep) domain to factors promoting "salting-out" [160, 185]. Studies on the effects of acidification revealed that at pH 7.2, at which silk proteins are stored in the lumen of the spinning gland, the presence of above-mentioned salts did not affect the silk protein, whereas at pH 6, where the fiber assembles, a more pronounced effect was observed [32]. This pH drop correlated well with rheological findings on shear sensitivity that was found to be weak at pH 6.8 and strong at pH 6.3 [121]. Acidification of silk proteins results in neutralization of typically negatively charged glutamate residues, thereby promoting hydrophobic interactions. As a consequence, the spinning dope undergoes gelation, resulting in an increased viscosity which in combination with rapid extensional flow supports fiber formation [32, 40, 44, 86, 125, 181]. At a pH above 8.5, phase separation of (AQ)₂₄NR3 was inhibited due to deprotonation of tyrosine residues, as the resulting anionic tyrosylates increased the hydrophilicity of the protein and thus reduced inter-chain

hydrophobic interactions [161].

In order to analyze more closely the influence of environmental conditions and kinetics during silk assembly a microfluidic device was employed. Therein, the ion concentrations and pH value could be precisely controlled and simultaneously physical stress could be applied upon channel design [180]. It was detected that silk fibers formed only after addition of phosphate in combination with elongational flow. The latter one alone did not affect the structural state of the employed silk proteins, whereas salting-out in the absence of elongational flow only led to the formation of spherical aggregates [180]. It could be shown that fibers resulted from pre-formed spherical aggregates that were forced into contact by the elongational flow in the microfluidic channel [180]. The resulting fibers were highly flexible, showing structurally highly-ordered patches (mainly β -sheet rich) along the thread. The surface of the fibers obtained grainy structures, leading to the assumption that the resulting fibers are still not mature and in fact likely represented an early or intermediate stage of fiber formation [180]. Thus, the precise control of the ionic environment within the spider's spinning duct proves to be crucial for formation of a tough insoluble thread and for devising mimetic processes to spin silk proteins industrially [83–85, 180].

1.2.3 Fiber formation

1.2.3.1 Liquid-solid phase transition in the distal part of the spinning duct and fiber formation

The final step of the spinning process is the transition from a high density liquid into a solid phase starting in the distal part of the duct [32, 86, 116, 169]. The hyperbolic geometries of natural spinnerets ensure a gradual and linear increase in the shear rate through the duct [26]. The resulting rapid flow is suggested to force the dope molecules to align in order to promote thorough hydrogen bonding accompanied by water expulsion [133, 169]. As a consequence, a strain-induced liquid-solid phase transition is initiated, in which concentrated spinning dopes separate into a solid protein-rich phase (the thread) surrounded by an aqueous protein-poor phase [32, 86, 168, 169], which is contrary to previous postulations that solidification occurs solely upon contact with air [32, 38, 87, 186, 187].

The accompanied thinning/drying process of the viscoelastic fluid filament (often referred to as "necking") is driven by capillary pressure as well as internal diffusion of water, and is resisted by the viscoelastic stress in the elongating filament as described by the time-evolutionary necking model [188, 189]. In this model, the necking rate is modulated by accessory evaporation of solvent from the thread, since the evaporation rate increases with time, due to the increasing surface area-

to-volume ratio. Furthermore loss of water leads to an increase in fluid viscosity and an additional slow-down in the necking rate [189]. The resistance of a fluid filament to further stretching is characterized by its extensional viscosity properties, which increase a hundred fold during capillary thinning. At large strains, the filament undergoes strain-hardening, which inhibits capillary break up and finally stabilizes the filament. The combined action of molecular elongation and solvent evaporation ultimately yields a solid, uniform fiber with constant diameter [188].

The semi-solid intermediate/premature fiber is then moved through the final part of the duct by a pumping mechanism, involving the cooperative work of two muscles, and exits through a spigot (often referred to as a valve) [32, 87, 116]. Shortly before the fiber exits the spider's abdomen, the lips of the spigot, fitting tightly around the emerging silk fiber, remove most of the remaining residual water and molecules are locked into their final orientation [32, 169, 187]. The fiber formation is completed after exiting the spigot, caused by the combination of drawing and loss of water due to evaporation in air. Factors influencing the evaporation process include the fiber radius, time of exposure to air, atmospheric humidity as well as temperature, and the speed of air flow [190]. However, solvent evaporation is not essential for fiber formation, as some natural silks were successfully spun in aqueous environments [32, 38, 87, 186]. The tapered nature of the duct allows the point of drawdown to move along the duct in dependence of the rate of spinning, resulting in thread diameters adjusted to the speed of spinning [32, 191]. Silks further tend to display a moderate, positive Poisson ratio, with a linear relationship between diameter and extension, resulting in improved mechanical properties of the fiber [190]. Similar to *B. mori*, the freshly drawn dragline silk fiber is a two filament bave. In most cases, it is fixed to a substrate (using a silk from the spider's piriform gland) immediately after drawing before further drawing by moving or descending using the spider's body weight and/or force of gravity is exerted. Alternatively, dragline silks are drawn out by a spider with its hind legs [32, 37, 58, 63, 192, 193].

1.2.3.2 Production of artificial spider silk fibers

Although several studies investigated artificial spinning of spider silk, silk fibers so far displayed inferior mechanical properties compared to natural silks. This can be related e.g. to the lower molecular weight compared to natural silk molecules [157], as molecular weight was found to affect the molecular orientation within polymers, with lower weight resulting in less orientation [194].

It should be noted that the natural spinning process is a rapid and concerted combination of extrusion and drawing (= pultrusion), distinguishing it from any known method of producing synthetic polymer fibers, where physical transformation, spinning and drawing are sequential [32, 87, 90,

Table 1.1 – Overview of published data for fibers produced from recombinant or regenerated silk proteins.

sample	solvent (fiber production / post-treatment)	molecular weight [kDa]	elongation to break [%]	tensile strength [MPa]	toughness [MJ m ⁻³]	diameter [μm]
avg. (AQ) ₂₄ NR3	aqueous buffer	106.3	10.8 ± 3.1	64.6 ± 26.0	3.0 ± 0.2	11.7 ± 4.2
best (AQ) ₂₄ NR3	aqueous buffer	106.3	32.3	143.4	24.6	10
avg. (AQ) ₂₄ NR3	aqueous buffer / ethanol vapor	106.3	7.4	72.1	2.3	11.7 ± 4.2
post-treated						
best (AQ) ₂₄ NR3	aqueous buffer / ethanol vapor	106.3	29.9	152.3	23.6	10
post-treated						
96mer [157]	HFIP	284.9	15 ± 5	508 ± 108	n.a.	n.a.
32mer [157]	HFIP	100.7	< 4	< 200	n.a.	n.a.
(MaSp1) ₂₄ - as-spun [195]	HFIP	70	3.1 ± 1.8	35.7 ± 8.4	0.9 ± 0.6	40.9 ± 4.0
(MaSp1) ₂₄ - post-treated [195]	HFIP / post-stretched in 75 % IPA	70	22.8 ± 19.1	132.5 ± 49.2	23.7 ± 18.5	17.4 ± 5.0
Y1S820-P hand-drawn [196]	HFIP	58	46.9 ± 23.0	22.9 ± 15.8	5.6 ± 5.1	22.9 ± 10.1
Y1S820-P post-treated [196]	HFIP (post-stretched in 90 % IPA, then in water)	58	29.6 ± 20.5	96.2 ± 28.8	22.6 ± 15.7	14 ± 8.7
2Ex12 - as-spun [197]	HFIP	71	3.6 ± 2.6	49.5 ± 7.8	n.a.	74.1 ± 33.9
RSF-6x [178]	LiBr (post-stretched in hot ammonium sulphate)	n.a.	27.7 ± 4.2	450 ± 20	100.6 ± 18.1	10.8 ± 2.4
capillary dry-spun RSF [45]	LiBr (post-treated in ethanol)	n.a.	16	298 ± 61	n.a.	15 ± 2
RSF - hand-drawn [198]	aqueous buffer	n.a.	18.5 ± 8.5	125 ± 15	n.a.	9

116, 154, 199]. Furthermore, the consideration of the internal water removal process, spin dope fluid behavior, and environmental influences imposed additional challenges to the technical mimicking of the natural spinning process [32, 53, 87, 90, 116, 154, 199]. Production of artificial spider silk fibers can be obtained by two different approaches: 1) spinning from regenerated silk dopes and 2) spinning from solutions of recombinant silk proteins. Most of the previously applied techniques to produce fibers have focused on the application of established technical spinning procedures such as solvent extrusion, wet-spinning through a coagulation bath, electrospinning or microfluidic approaches [17, 53, 63, 139, 154, 157, 195, 200–208].

The use of a highly concentrated silk solution as a prerequisite for successful technical spinning of silk fibers [178], in line with the supposition that spidroin length correlates with strength of fibers, has resulted in frequent use of denaturing agents and organic solvents due to the limited yield and solubility of regenerated and recombinant silk proteins in aqueous solutions [138, 147, 154, 161, 204, 209]. Regenerated silk solutions were usually prepared by dissolving a large amount of natural silk fibers in strong chaotropic agents, such as highly concentrated LiBr solutions, HFIP, hexafluoroacetone hydrate (HFA) or formic acid amongst others [17, 200, 210, 211]. However, the number of studies on spider silk is limited since most studies were performed using silk from *B. mori* silkworms due to higher availability and easier accessibility [45, 79, 178, 210, 212, 213]. Only few studies have been conducted using regenerated spider dragline silk solutions prepared in HFIP [206, 207] or 8M guanidine hydrochloride (GdmHCl) solution [198].

Considerable progress has been made in the past concerning wet-spinning of recombinant proteins dissolved in organic solvents [195–197, 205, 214, 215]: e.g. a high-molecular weight silk analogue (289.4 kDa) displayed a tensile strength of up to 500 MPa and elongation to break of 10 % to 20 % [157]. Applying a novel post-stretching procedure using an aqueous isopropanol (IPA) bath (75 % (v/v) IPA and 25 % (v/v) water), yielded fibers with a maximum tensile strength of 233.5 MPa and elongation to break of 31.3 % [195]. A major drawback of organic solvents is that they severely degrade the silk proteins, that they can not be fully removed from the artificial fiber [206], and that they are too expensive or toxic for use in industrial processes. Recently, some research groups have successfully produced fibers from recombinant silk proteins dissolved in aqueous solutions by hand-drawing [161, 198, 215]. Although it was observed that pulled fibers were typically superior than as-spun fibers due to improved molecular organization [195, 211, 215], the mimicry of the natural (aqueous) spinning process is far from being accomplished since the mechanical properties of pulled fibers were still inferior than those of natural silk. By successfully applying a double post-spin procedure in which as-spun fibers were post-stretched in 90 % (v/v) IPA and 10 % (v/v) water and shortly incubated in water, the mechanical properties could be improved to a tensile strength of up to 125 MPa, elongation to break up to 50 %, with fibers thinner than 23 μ m [196].

These results indicated that post-spin drawing improved mechanical properties of silk fibers, due to improved molecular alignment, increased β -sheet content and reduced amount of defects in the fiber [154, 178, 195, 196, 207, 213, 216, 217]. Apparently, this effect was enhanced in the presence of coagulation baths, containing solvents known to induce protein conformation to β -sheet rich structures through strong preferential interaction with spidroin, thereby destabilizing non-local hydrophobic interactions and enhancing polar interactions (hydrogen bonds) [129, 218]. Water-stretched fibers were shown to display significant tensile strength increases due to increased β -sheet fractions in the fiber, although the content is not as high as that observed in native spider silks [104, 195, 219–221]. Fibers post-stretched in organic coagulation baths, in contrast, often displayed inferior appearance (brittle) and properties, caused by the rapid conformation transition from random coil to β -sheet structure, and the isotropic formation of crystallites without proper orientation [178, 195, 213, 217, 222, 223]. The rate at which conformation transition occurs is crucial to the behavior of the silk during drawing and consequently its mechanical properties. At slow rates, fibers displayed irregular cross-sections or were not formed at all, while at fast rates, the resulting fibers were brittle [178]. Therefore, a carefully composed hot ammonium sulphate coagulation bath was used for wet-spinning and post-spin drawing of fibers, allowing the protein chains sufficient freedom of movement to permit further alignment during extrusion and post-drawing [178]. Another group established a wet-spinning procedure using the osmotic stress of silk solution to precisely control composition and corresponding crystalline structure of regenerated silk fibroin (RSF) before spinning [208].

1.3 Characterization of silk

1.3.1 Rheological characterization

1.3.1.1 Introduction to rheometry

Rheometry, often referred to as rheology, is the experimental characterization of a material's rheological behavior. It provides information about the flow and deformation behavior of liquids or soft solids, such as gels due to the application of force [224]. Rheometry furthermore comprises the theoretical aspects of elasticity, plasticity and fluid dynamics (non-Newtonian fluids) of these materials and deals with their basic properties such as viscosity, elasticity and plasticity. Rheological tests are also conducted to provide information on the degree of intermolecular associations present in the solution [133, 211, 225].

Figure 1.2 illustrates the shearing of a fluid between two boundary plates. Upon application of

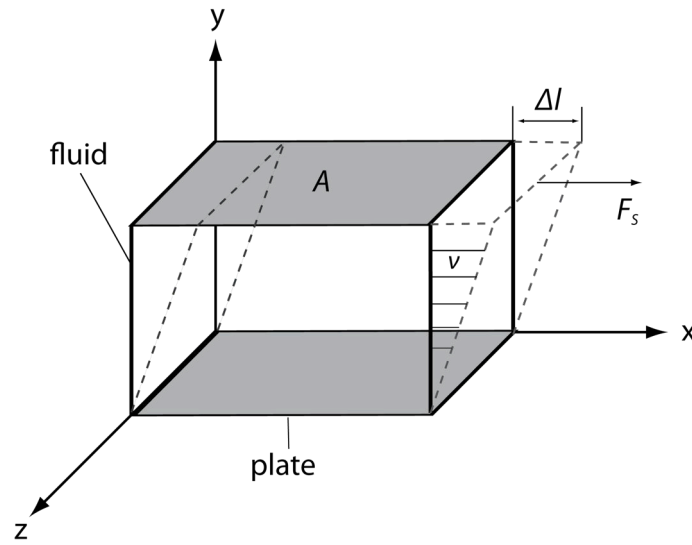


Figure 1.2 – Illustration of shearing of a fluid: F_s = shearing force, A = area of boundary plate, Δl = distance along which fluid is sheared and v = velocity of fluid.

a shearing force F_s , the upper plate starts to move in the direction indicated by the arrow. As a consequence, the fluid between both plates starts to move until the force is removed. As the lower plate does not move, and assuming no slip between liquid and plate, a velocity gradient is formed in the fluid with increasing velocity from the lower to the upper plate.

This behavior is described by

$$\dot{\gamma} = \frac{\Delta v}{\Delta y} \quad (1.1)$$

with $\dot{\gamma}$ being the shear rate [1/s], v being the velocity of the fluid [m/s] and Δy being the thickness of the fluid [m].

Shear stress τ [Pa] is defined as the shearing force F_s [N] divided by the area A [m²] over which it is applied, according to

$$\tau = \frac{F_s}{A} \quad (1.2)$$

Rheological behavior is often described by a constitutive equation ("rheological equation of state"), which relates the tensorial state of stress in a complex fluid to the entire deformation history imposed on it. This constitutive equation may be constructed empirically or derived from

molecular-based kinetic theories [226]. The most simple form of rheological behavior typically used to describe Newtonian liquids is given by

$$\eta = \frac{\tau}{\dot{\gamma}} \quad (1.3)$$

in which shear rate $\dot{\gamma}$ and shear stress τ are associated via a dynamic viscosity η [Pas]. This relationship is equivalent to Hooke's law for solids, and thus is limited to linear stress-strain relationships. However, the typical flow behavior (relationship between shear stress (or viscosity, respectively)) of materials is more complex as shown in the following flow curve diagram (see Figure 1.3).

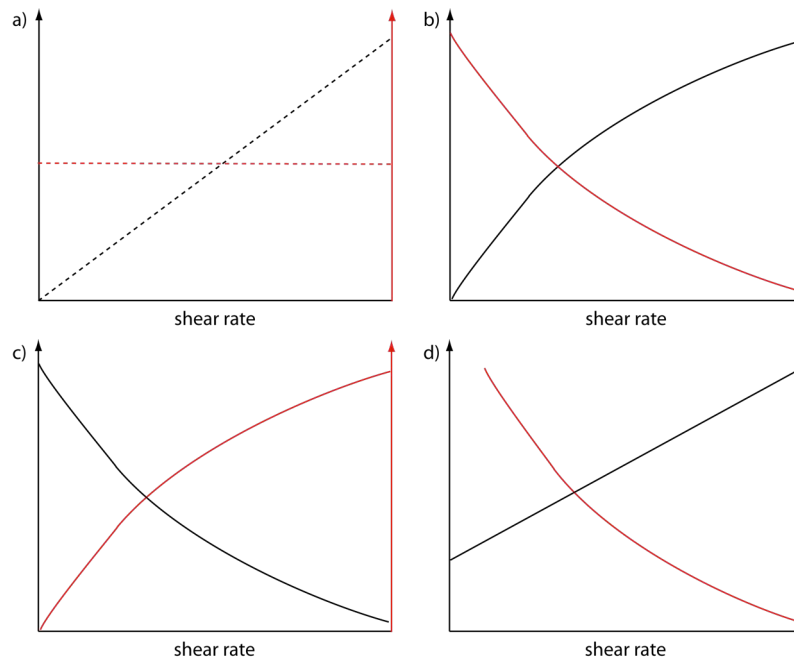


Figure 1.3 – Illustration of typical flow curves: a) Newtonian fluid, b) shear thinning fluid, c) shear thickening fluid and d) Bingham plastic (red: viscosity; black: shear stress).

Figure 1.3 shows the four most common types of materials as characterized by their flow behavior. A Newtonian fluid is characterized by a linear shear stress and shear rate relationship (Figure 1.3a). This is equivalent to a constant viscosity over the entire shear rate regime, indicating that the viscosity of the fluid is independent of shear rate and time at constant temperatures. If the relationship between an imposed shear rate and the resulting shear stress is nonlinear the fluid is called "non-Newtonian". Non-Newtonian fluids display different behaviors: 1) "shear thinning" fluids display a decrease of viscosity with increasing shear rate (Figure 1.3b), 2) dilatant materials

display a "shear thickening" behavior, indicated by increasing viscosity with increasing shear rate (Figure 1.3c) and 3) Bingham plastics behave like solids at low shear rates until a certain yield stress is surpassed and viscosity starts to decrease, i.e. the material begins to flow (Figure 1.3d). These three types of materials have one thing in common: they are time-independent. However, time-dependent flow behavior can also be observed in materials and can be distinguished into two different behaviors. Thixotropic behavior characterizes a time-dependent shear thinning at constant shear rate, i.e. at the beginning the material is highly viscous, but with proceeding time, the shear stress starts to act on the material's structure and the material begins to flow. Typically, thixotropic materials recover their original state after a period of relaxation. In contrast, rheopectic materials show time-dependent shear thickening at constant shear rate. Moreover, rheopectic materials do not immediately recover their original state upon removal of shear load.

1.3.1.2 Rheology of silk solutions

Rheological studies allowed the elucidation of mechanistic details of the dope and the process of moving a semi-solid spinning dope through a convergent die-like spigot providing additional key insights into fiber properties [44, 121, 133, 170, 188, 211, 214]. Moreover, rheology proved to be a useful tool to evaluate the spinnability of regenerated or recombinant solutions in particular with regard to the sample concentration, as higher concentrations yielded a higher viscosity (and better "spinnability") and ultimately fibers with higher strength [26, 211, 214].

As mentioned before, silk is a liquid crystalline solution which typically displays the rheological flow behavior of a non-Newtonian fluid. Furthermore, the stress forces along and across the flow lines of the non-Newtonian solutions were observed to be highly dependent on the concentration of the solution. This feature offers several advantages, in particular reducing the metabolic costs of silk production and the energy required to produce very fine fibers from narrow spinning ducts [32]. It was estimated from rheological studies that the force required to move the silk dope through the spigot is 500 times lower than if silk were a viscous Newtonian fluid [44, 121]. However, studies on rheological flow curves of native silk dopes have identified a different and more complex behavior, showing that in the limit of low shear rates the relationship between stress and shear rate is reduced to a simple linear one, corresponding to a simple Newtonian fluid [44, 133, 188, 211, 227]. The resulting steady shear viscosity approaches a constant value defined as the zero-shear rate viscosity. Upon a critical shear rate, the Newtonian behavior switches to a non-Newtonian behavior, indicated by shear thinning in the high shear rate regime [44, 133, 188, 211, 227]. The critical shear rate for onset of shear thinning can be related to the longest relaxation time of the solution, i.e. the time to resolve the entanglements between chains. The slope of the shear

rate response in the shear thinning regime was found to be strongly influenced by intermolecular interactions between chains or chain and solvent [44]. These findings correlated well with observations that silk in the lumen becomes increasingly birefringent and ordered upon passage through the duct due to the mechanical and frictional forces. The position of onset of marked birefringence was observed to vary with spinning conditions but correlated well with the point in the secretory pathway at which the fibroin solution reached a calculated critical shear rate required for conversion into a β -sheet rich-state [24]. Upon passage through the spinning duct, silk is also exposed to elongational forces, and extensional rheometry revealed an increasing resistance of silk to stretching with time and strain imposed, which is not contradictory to the shear thinning behavior, and leads to a viscoelastic fluid filament [188, 228, 229].

Other rheological studies have investigated the role of pH and salt (potassium, sodium and calcium) on native silk solutions, showing that altering the pH of native dopes reversibly changed the behavior from liquid-like to solid-like [30, 44]. It was assumed that a reduction in pH offsets the balance of repulsive and attractive forces responsible for the maintenance of the liquid crystalline state and allows the hydrophobic blocks to approach one another to produce hydrophobic interactions which stabilize the gel [44]. Rheological characterization of the spinning dope was also used to elucidate the effects of spinning temperature on the mechanical properties of silk fibers [191]. The effects can be related to a transformation of the dope from opaque to white solid above 55 °C, attributed to a transition from random-coil to β -sheet [133]. Holland and collaborators have measured the rheological properties of natural and reconstituted silk solutions over a wide range of concentrations and made the remarkable observation that the viscosity of natural silk solutions is about 5 orders of magnitude greater than that of reconstituted silk [133, 211].

1.3.2 Mechanical characterization

1.3.2.1 Introduction to mechanical analysis

The selection of a material for a specific application is based on the mechanical loading forces it is exposed to during usage, as materials display diverse mechanical properties and respond differently to external loads. Materials are typically characterized by shearing, bending or tensile testing in which they are exposed to load applications corresponding to those expected in their destined technical application. Fibers or fibrous materials for instance are characterized by tensile testing, a quasi-static destructive technique often conducted according to standardized procedures (e.g. ASTM D3379-75 (Standard Test Method for Tensile Strength and Young's Modulus for High-Modulus Single-Filament Materials) or EN-ISO 527-1 (for polymers)). Thereby, in order

to determine the material's response under uniaxial loading, a specimen of defined dimensions is exposed to a tensile load (by application of a force) which ultimately results in the specimen's deformation until failure.

Both deformation (= displacement) and load can then be used to calculate stress σ [Pa] and strain ε (assuming a constant cross-sectional area during the testing procedure), to compare a material's mechanical properties using the following relationships

$$\sigma = \frac{F}{A_0} \quad (1.4)$$

and

$$\varepsilon = \frac{L - L_0}{L_0} \cdot 100\% = \frac{\Delta L}{L_0} \cdot 100\% \quad (1.5)$$

with F being the force applied [N], A_0 the initial cross-sectional area of the specimen [m²], L_0 being the specimen's gauge length [m] and ΔL being the change in specimen's length [m].

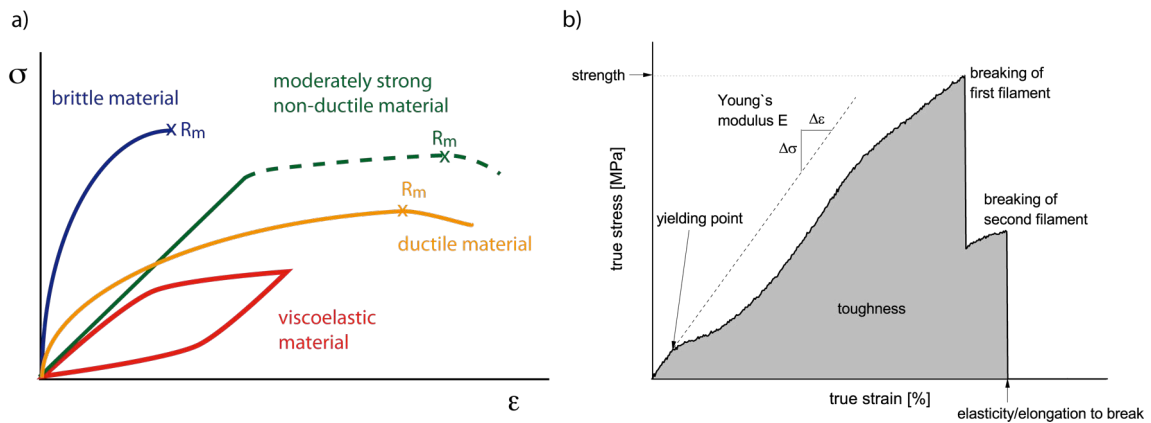


Figure 1.4 – Characteristic stress-strain curves of a) four different classes of materials (R_m = maximum tensile strength [MPa]) and b) exemplary of a spider silk fiber.

Stress and strain are typically plotted as a stress-strain curve characteristic for each material (see Figure 1.4a) which can be used to determine typical material properties. In general, each material displays an elastic behavior at low load forces, characterized by a linear stress-strain relationship to the yield point, in which all deformation is recoverable and the material will return to its initial shape when the load is removed. The tensile strength measures the force required to pull a material to the point where it breaks, i.e. the maximum amount of tensile stress that it can be subjected to before failure. Above the yielding point, the material displays irreversible deformation which is

characteristic for the type of material: brittle materials immediately break once the yield point is passed, moderately strong non-ductile materials show a plastic deformation in form of strain hardening, i.e. the material shows a non-linear increase in stress with increasing strain up to ultimate strength. Ductile materials display a plastic deformation, so-called creeping, while viscoelastic materials are characterized by elastic and viscous behavior as indicated by the hysteresis. Therefore, the yielding point displays the transition from elastic to plastic deformation (i.e. irreversible deformation).

The slope of the stress-strain curve in the elastic regime (see Figure 1.4b) can be used to calculate the Young's modulus E [MPa], i.e. the stiffness of the material, using Hooke's law:

$$E = \frac{\Delta\sigma}{\Delta\epsilon} \quad (1.6)$$

It should be noted that the aforementioned standardized procedures were conducted by using ideal testing conditions and standardized samples, both not feasible in case of biological materials. Young's modulus, for instance, is determined according to EN-ISO 527-1 by calculating the slope of the stress-strain curve between 0.05 % and 0.25 %.

The area below the stress-strain curve is the toughness W [MJm^{-3}], a measure for the energy required to cause material failure and can be calculated using

$$W = \int_{\epsilon_{\min}}^{\epsilon_{\max}} \sigma \cdot d\epsilon \quad (1.7)$$

Silks, like many polymers, display a so-called necking phenomenon, that means the cross-sectional area of a specimen decreases substantially due to plastic flow [191, 230]. This leads to a reversal of the engineering stress-strain curve where decreasing stress correlates to increasing strain because engineering stress and strain are calculated assuming initial cross-sectional area. This can be corrected by applying true stress and true strain calculated according to Equation 1.8 and Equation 1.9 [231], assuming a constant fiber volume [69, 191, 232, 233].

$$\sigma_{\text{true}} = \frac{F}{A} = \frac{F \cdot L}{A_0 \cdot L_0} \quad (1.8)$$

where F is the force applied to the specimen [N], A is the estimated cross-sectional area of specimen calculated from initial cross-sectional area A_0 [m^2], L is the instantaneous length of the fiber [m] at each extension value and L_0 is the original gauge length of the fiber [m] [232].

Alternatively, fiber diameters were measured prior to or after tensile testing, and the determined values were applied in true stress calculations (Equation 1.8) [69, 191, 232, 233].

$$\epsilon_{\text{true}} = \ln \frac{L}{L_0} \quad (1.9)$$

where L is the instantaneous length of the fiber at each extension value and L_0 is the original gauge length of the fiber [232]. A comparison of true and engineered stress and strain values is shown in Figure 1.5.

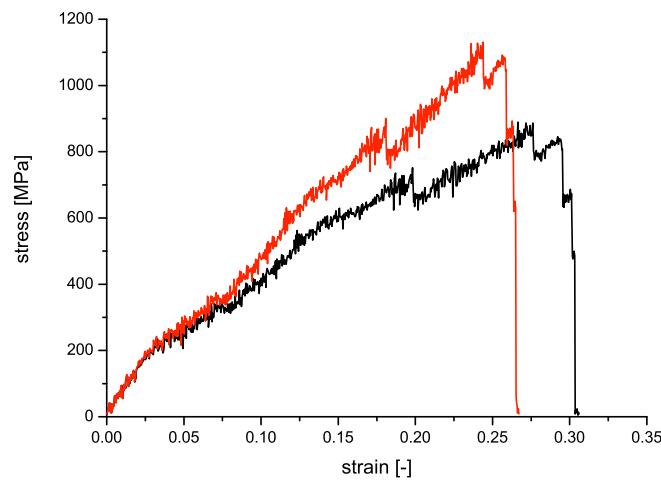


Figure 1.5 – Comparison of engineered (black) and true (red) stress-strain curve for *A. diadematus* fiber.

1.3.2.2 Mechanical analysis of silk

Silk fibers are very thin with diameters usually in the order of a few micrometers limiting their potential for mechanical characterization to tensile testing techniques [55]. The thinness results in irreversible deformation of silk fibers albeit their tremendous strength at very small load forces (in the mN range). In order to generate meaningful mechanical data, the tensile testing system applied must thus provide high accuracy in this regime which is achieved by using high precision load cells and displacement transducers. In general, two approaches for tensile testing of thin micro fibers were established in the past. The first approach uses custom-built tensile testing systems equipped with commercial high-precision load cells and displacement transducers [74, 191, 234].

1.3 Characterization of silk

The other approach uses commercial tensile testing systems (e.g Instron) with precision load cells with less than 2.5 N [25, 33, 67, 235–237], systems with high-precision load cells (less than 1 N (Nano Bionix system, MTS Systems Corp., Oak Ridge, USA) [232, 238–241] or commercial linear extensometers [80, 242].

Table 1.2 – Mechanical data of spider silk fibers in comparison to other natural and synthetic fibers (unless otherwise noted, data is obtained from [52]).

sample	tensile strength [MPa]	elongation to break [%]	toughness [MJ m ⁻³]
spiders			
<i>A. diadematus</i> MA silk [230, 239]	1150 ± 140	35 ± 7	141 ± 77
<i>A. diadematus</i> capture spiral [230]	1338 ± 80	476 ± 16	163
<i>Araneus sericatus</i> MA silk [48]	1100	27	160
<i>Argiope trifasciata</i> [67]	600 ± 50	30 ± 2	90 ± 10
<i>A. trifasciata</i> [239]	1200 ± 3	23 ± 0.6	116 ± 4
<i>N. clavipes</i> [239]	1000 ± 4	20 ± 1.1	111 ± 6
<i>N. edulis</i> [32]	1150 ± 200	39 ± 8	165 ± 30
<i>Lactrodectus hesperus</i> [239]	1000 ± 5	45 ± 3.4	181 ± 11
<i>Caerostris darwini</i> [243]	1850 ± 340	33 ± 8	270 ± 69
other natural fibers			
<i>B. mori</i> [67]	650 ± 40	12 ± 1	50 ± 10
flax fiber [244]	1339 ± 486	3 ± 0.8	n.a.
tendon collagen	150	12	7.5
wool, 100 % rH	200	50	60
synthetic fibers			
elastin	2	150	2
synthetic rubber	50	850	100
Nylon	950	18	80
Kevlar® 49	3600	2.7	50
carbon fiber	4000	1.3	25
high-tensile steel	1500	0.8	6

Table 1.2 provides an overview over selected mechanical data of spider silk fibers in comparison with typical natural and synthetic fibers. The qualitative patterns of silk’s tensile behaviors followed the same trend for all species, however details varied across species. The strength of silk fibers was found to be in the regime of steel and flax fiber and only two to three times lower than that of the strongest synthetic materials. Furthermore, silk offered higher extensibility (nearly 10 times) compared to those materials, yielding a toughness higher than that of steel and Kevlar® 49. These intriguing mechanical properties of silk are a result of its desired functionality. MA silk fibers in an orb-web typically experience loads at right angles to their long axis, which imposes an interesting constraint on their properties: a balance between strength and elasticity (loaded normal to long axis) is required to allow for absorption of high kinetic energies upon prey impact [21, 48, 52].

Since silk is a viscoelastic material, its mechanical properties vary strongly with the silk drawing speed, indicating a strong linear relationship. This corresponds to strong effects on protein folding and molecular interactions, with higher draw rates (i.e. increased shear forces and forces of elongational flow) reducing the time required for protein alignment [48, 52, 169, 191]. Three common drawing effects have been observed for spider silk: 1) during the rapid vertical descent method the exertion of friction forces up to more than twice the spider's body weight was observed resulting in strong fibers [193]; while 2) during free fall, silk was spun at low forces of approximately 10 % of spider's body weight without applying any additional frictional force and yielded moderately strong fibers [192, 193]; and 3) during undisturbed climbing fibers were spun which represent the lowest limit in stress-strain curves [72, 193]. Besides the active controls employed by a spider, silk fiber properties represent conditions of spinning dope material and processing (e.g. environmental influences such as diet, temperature and humidity as well as body weight) which must be complementary to each other [20, 21, 58, 70, 96, 169, 187, 191, 211, 234, 245]. The spider's active tensile control during silk drawing allows the production of a tailored material ideally suited for either an inhabited environment or immediate needs, and consequently leads to the broad range and variability of mechanical properties of dragline fibers [246]. However, it should be pointed out that the marked variability of their mechanical properties is a major drawback concerning the mechanical characterization [64, 67, 234, 246]. Silk fibers exposed to high humidity apparently showed a rubber-like behavior in the stress-strain curve [68, 77, 80, 186, 242, 247–249]. Moreover, spider silk MAS fibers showed an unique feature in aqueous environment: supercontraction [66], indicated by extreme shrinkage of the fiber (more than 50 % of its initial length) and significant changes of the mechanical properties turning the material rubber-like [40, 51, 52].

1.4 Motivation and aims of the thesis

The intriguing mechanical properties of silk fibers have made them a very popular high-performance material with enormous potential in biomedical applications, e.g. wound dressing, sutures and tissue engineering [7, 9, 23, 57, 250–252], technical applications such as in filter, membrane or paper fabrication [7, 9, 57], in textiles or other structural fabrics [57] or in special applications such as ropes or fishing nets [56] or as optical materials [253, 254]. However, the limited accessibility of spider silk thus far have resulted in the commercial silk industry being almost entirely based on the application of *B. mori* silk [22]. Yet the natural fibers also have shortcomings regarding long-term durability of mechanical performance [255], which can only be addressed by chemical modification of the natural silk fibers or by spinning new fibers from

regenerated or recombinant silk proteins [35] (and references therein).

Although recent progress has been made in the processing of recombinant silk proteins into various morphologies for technical application [256], such as films [257, 258] encapsulated beads [259], hydrogels [260], or even electrically conductive and photoluminescent silk fibers [261], the pinnacle of silk research, the production of native-like silk fibers from recombinant or regenerated silk proteins, has not been reached. In particular the application of standard spinning technologies, such as wet-spinning, for regenerated or recombinant silk solutions has failed so far. The aim and the focus of this work thus laid on the conception and application of the first technical and biomimetic adaptation of the natural spinning process. Therefore, rheological studies of a recombinant silk spinning dope were carried out to elucidate the solution's "spinnability" and to compare the behavior of a recombinant silk solution with that of a native spinning dope. Furthermore, the processes accounting for the phase transitions within the natural spinning duct, such as the change in ionic composition and water removal, were investigated *in vitro* to shed more light on the prerequisites for successful fiber formation.

Additionally, a comprehensive set of mechanical data for *A. diadematus* dragline silk collected at different spinning conditions (using forced silking) and tested at different relative humidities was obtained. The data will provide more information on the mechanical and structural properties of dragline silk.

2 Materials and methods

2.1 Materials and instruments

2.1.1 Chemicals

chemical	company
1,1,1,3,3,3-Hexafluoro-2-propanol (HFIP)	Alfa Aesar, Karlsruhe, Germany
2-Mercaptoethanol	Carl Roth GmbH + Co. KG, Karlsruhe, Germany
2-Amino-2-hydroxymethyl-1,3-propanediol (Tris)	Carl Roth GmbH + Co. KG, Karlsruhe, Germany
3-morpholinopropane-1-sulfonic acid (MOPS)	Carl Roth GmbH + Co. KG, Karlsruhe, Germany
acetic acid, 100% p.a.	Carl Roth GmbH + Co. KG, Karlsruhe, Germany
acrylamide (Rotiphorese® Gel 40, 37.5:1)	Carl Roth GmbH + Co. KG, Karlsruhe, Germany
alginate sodium salt, for biochemistry	Sigma Aldrich Chemie GmbH, Steinheim, Germany
ammonium hydrogen carbonate ((NH ₄)HCO ₃)	Carl Roth GmbH + Co. KG, Karlsruhe, Germany
ammonium persulfate (APS), p.a.	Carl Roth GmbH + Co. KG, Karlsruhe, Germany
ammonium sulfate ((NH ₄) ₂ SO ₄)	Carl Roth GmbH + Co. KG, Karlsruhe, Germany
bromophenol blue sodium salt	Merck KGaA, Darmstadt, Germany
calcium chloride dihydrate (CaCl ₂ · 2H ₂ O)	Carl Roth GmbH + Co. KG, Karlsruhe, Germany
chitosan	provided by Dr. Humenik, University of Bayreuth (UBT), Germany
cholic acid sodium salt	Carl Roth GmbH + Co. KG, Karlsruhe, Germany
cotton flake	Wollknoll GmbH, Oberrot- Neuhausen, Germany
D-sorbitol	Carl Roth GmbH + Co. KG, Karlsruhe, Germany

diammonium hydrogen phosphate ($(\text{NH}_4)_2\text{HPO}_4$)	Carl Roth GmbH + Co. KG, Karlsruhe, Germany
dipotassium hydrogen phosphate (K_2HPO_4)	Carl Roth GmbH + Co. KG, Karlsruhe, Germany
ethanol, 100% p.a.	Carl Roth GmbH + Co. KG, Karlsruhe, Germany
ethylenediaminetetraacetic acid (EDTA)	Carl Roth GmbH + Co. KG, Karlsruhe, Germany
fat-free powdered milk, blotting grade	Carl Roth GmbH + Co. KG, Karlsruhe, Germany
formaldehyde, 37% p.a.	Carl Roth GmbH + Co. KG, Karlsruhe, Germany
glycerol (Rotipuran [®]), p.a.	Carl Roth GmbH + Co. KG, Karlsruhe, Germany
glycine, p.a.	Carl Roth GmbH + Co. KG, Karlsruhe, Germany
guanidinium thiocyanate (GdmSCN)	Carl Roth GmbH + Co. KG, Karlsruhe, Germany
hydrochloric acid (HCl), 37%	Sigma Aldrich Chemie GmbH, Steinheim, Germany
isopropanol, 100% p.a.	Carl Roth GmbH + Co. KG, Karlsruhe, Germany
Kevlar [®] fiber (aramidrovig 805tex)	R&G GmbH, Waldenbuch, Germany
L-arginine	Carl Roth GmbH + Co. KG, Karlsruhe, Germany
L-glutamic acid	Carl Roth GmbH + Co. KG, Karlsruhe, Germany
Lumi-Light ^{Plus}	Roche Diagnostics GmbH, Mannheim, Germany
methanol, 100% p.a.	Carl Roth GmbH + Co. KG, Karlsruhe, Germany
N-2-hydroxyethylpiperazine-N'-2-ethane- sulfonic acid (HEPES)	Carl Roth GmbH + Co. KG, Karlsruhe, Germany
N,N-dimethylmethanamine oxide (TMAO)	Alfa Aesar, Karlsruhe, Germany
N,N,N',N'-tetramethylethylenediamine (TEMED)	Carl Roth GmbH + Co. KG, Karlsruhe, Germany
ortho phosphoric acid (H_3PO_4), 85%	Carl Roth GmbH + Co. KG, Karlsruhe, Germany
polyacrylamide (PAA), 10 kDa	Sigma Aldrich Chemie GmbH, Steinheim, Germany
polyacrylamide (PAA), 5 MDa	Sigma Aldrich Chemie GmbH, Steinheim, Germany
polyacrylonitrile (PAN)	Sigma Aldrich Chemie GmbH, Steinheim, Germany

polyacetylene (PAC)	Sigma Aldrich Chemie GmbH, Steinheim, Germany
polyethylene glycol (PEG), 4 kDa	Carl Roth GmbH + Co. KG, Karlsruhe, Germany
polyethylene glycol (PEG), 20 kDa	Carl Roth GmbH + Co. KG, Karlsruhe, Germany
polyethylene glycol (PEG), 35 kDa	Carl Roth GmbH + Co. KG, Karlsruhe, Germany
polyethylene glycol (PEG), 100 kDa	Sigma Aldrich Chemie GmbH, Steinheim, Germany
polyethylene glycol (PEG), 600 kDa	Sigma Aldrich Chemie GmbH, Steinheim, Germany
poly(lactic-co-glycolic acid) (PLGA)	Sigma Aldrich Chemie GmbH, Steinheim, Germany
polyvinyl alcohol (PVA, Mowiol [®] 4-88)	Carl Roth GmbH + Co. KG, Karlsruhe, Germany
potassium dihydrogen phosphate (KH ₂ PO ₄)	Carl Roth GmbH + Co. KG, Karlsruhe, Germany
potassium sulfate (K ₂ SO ₄)	Carl Roth GmbH + Co. KG, Karlsruhe, Germany
Precision Plus Protein [™] Standard Dual Color	Bio-Rad Laboratories GmbH, Muenchen, Germany
silicone oil M5, M200, M1000	provided by Appl. Mechanics & Fluid Dynamics, UBT, Germany
silver nitrate (AgNO ₃)	Carl Roth GmbH + Co. KG, Karlsruhe, Germany
sodium acetate	Carl Roth GmbH + Co. KG, Karlsruhe, Germany
sodium carbonate (Na ₂ CO ₃)	Carl Roth GmbH + Co. KG, Karlsruhe, Germany
sodium carboxymethyl cellulose (viscose)	Sigma Aldrich Chemie GmbH, Steinheim, Germany
sodium chloride (NaCl)	Carl Roth GmbH + Co. KG, Karlsruhe, Germany
sodium dodecyl sulfate (SDS), pellets	Carl Roth GmbH + Co. KG, Karlsruhe, Germany
sodium hydrogen carbonate (NaHCO ₃)	Carl Roth GmbH + Co. KG, Karlsruhe, Germany
sodium dihydrogen phosphate (NaH ₂ PO ₄)	Carl Roth GmbH + Co. KG, Karlsruhe, Germany
sodium hydroxide (NaOH)	Carl Roth GmbH + Co. KG, Karlsruhe, Germany
sodium thiosulfate pentahydrate (Na ₂ S ₂ O ₃ · 5H ₂ O)	Carl Roth GmbH + Co. KG, Karlsruhe, Germany

Spectra/Gel [®] absorbent	Carl Roth GmbH + Co. KG, Karlsruhe, Germany
T7-tag [®] Antibody HRP conjugate	Merck KGaA, Darmstadt, Germany
throwsters waste silk <i>B. mori</i>	Wollknoll GmbH, Oberrot- Neuhausen, Germany
Tween [®] 20, molecular biology grade	Carl Roth GmbH + Co. KG, Karlsruhe, Germany
urea	Carl Roth GmbH + Co. KG, Karlsruhe, Germany

All other non-listed chemicals used in this work were either purchased from Sigma Aldrich Chemie GmbH (Steinheim, Germany) or Carl Roth GmbH (Karlsruhe, Germany).

2.1.2 Buffers and other solutions

solution	composition
Tris/HCl stock solution	1 M Tris, add HCl to desired pH
dialysis buffer A	10 mM Tris/HCl pH 8
dialysis buffer B	10 mM Tris/HCl pH 8 and 100 mM NaCl
dialysis buffer C	10 mM Tris/HCl pH 8, 100 mM NaCl and 4.3 g/L cholic acid sodium salt
potassium phosphate buffer ($K_xH_{3-x}PO_4$) pH 6	87.7% (v/v) KH_2PO_4 + 12.3% (v/v) K_2HPO_4
$K_xH_{3-x}PO_4$ buffer pH 7	39% (v/v) KH_2PO_4 + 61% (v/v) K_2HPO_4
$K_xH_{3-x}PO_4$ buffer pH 8	5.3% (v/v) KH_2PO_4 + 94.7% (v/v) K_2HPO_4
$CaCl_2$ -EtOH- H_2O	$CaCl_2 \cdot 2H_2O$, ethanol + H_2O (mole ratio 1:2:6)
10x SDS-PAGE buffer	0.25 M Tris/HCl, 1% (w/v) SDS + 1.92 M glycine, set to pH 8.4 - 8.9
4x Laemmli buffer	250 mM Tris/HCl (pH 6.8), 8% (w/v) SDS, 40% (v/v) glycerol, 0.04% (w/v) bromophenol blue + 20% (v/v) 2-Mercaptoethanol
10% SDS separating gel	375 mM Tris/HCl (pH 8.8), 10% (v/v) Rotiphorese [®] Gel 40 + 0.1% (w/v) SDS
10% SDS stacking gel	125 mM Tris/HCl (pH 6.8), 4.5% (v/v) Rotiphorese [®] , 0.06% (w/v) SDS and a small amount of bromophenol blue
Fix 1 solution	30% (v/v) ethanol + 10% (v/v) acetic acid
Fix 2 solution	0.4 M sodium acetate, 0.5% (v/v) acetic acid + 30% (v/v) ethanol set to pH 6; add 1 g/L $Na_2S_2O_3$ shortly before use

2.1 Materials and instruments

silver staining solution	6.5 mM AgNO ₃ and 25 µl 37% formaldehyde in 100 ml MilliQ-water
developer solution	1.25 g Na ₂ CO ₃ and 20 µl 37% formaldehyde in 50 ml MilliQ-water
stop solution	50 mM EDTA (pH 7.5)
Western Blot transfer buffer	48 mM Tris/HCl, 39 mM glycine, 1.3 mM SDS and 20% (v/v) methanol
10x phosphate buffered saline (PBS) solution (pH 7.4)	40 mM Tris/HCl, 160 mM Na ₂ HPO ₄ x 2 H ₂ O and 1.15 M NaCl

All solutions were prepared using "ultrapure" water obtained from Milli-Q systems (Millipore Corporation, Billerica, MA, USA). Potassium phosphate buffers were prepared according to a pH table for phosphate buffers (www.roche-applied-science.com/labfaqs). Final pH values of all buffers were verified using a pH meter.

2.1.3 Consumables and tools

consumable or tool	company
all-purpose glue	UHU GmbH & Co. KG, Germany
adhesive tape: tesa [®] double-sided	TESA SE, Hamburg, Germany
canuli: Sterican [®] (diverse sizes)	B. Braun AG, Melsungen, Germany
Contacta Professional (modeling glue)	REVELL GmbH & Co. KG, Germany
cuvettes: Quarz Suprasil [®] (QS 105.200)	Hellma GmbH & Co. KG, Muehlheim, Germany
dialysis membranes: Spectra Por [®] (various MWCO)	Spectrum Laboratories Inc., Rancho Dominguez, CA, USA
filter: poly ether sulfone (PES)	EMD Millipore Corp., Billerica, MA, USA
membrane discs (0.45 µm)	
fine tweezers and fine scissors	C. Roth GmbH + Co. KG, Karlsruhe, Germany
membrane: cellulose Thomapor [®] Biospectra (ID: 0.2 mm, MWCO 13 kDa)	Reichelt Chemietechnik GmbH, Heidelberg, Germany
membrane: ceramic (ID: 0.8 mm, MWCO 10 kDa)	KERAFOL GmbH, Eschenbach, Germany
membrane: PES (ID: 0.8 mm, MWCO 10 kDa)	Microdyn Nadir GmbH, Wuppertal, Germany
micro tubes: 1.5 & 2 ml	Sarstedt AG, Nuembrecht, Germany
nail polish: Maybelline Jade Express Finish	L' Oreal GmbH, Germany
petri dishes (92 x 16mm)	Sarstedt AG, Nuembrecht, Germany
petri dishes (35 x 10mm)	Sarstedt AG, Nuembrecht, Germany

2.1 Materials and instruments

pipette tips (diverse types and sizes)	Sarstedt AG, Nuembrecht, Germany
polyester filter, non-woven	Sandler AG, Schwarzenbach, Germany
reagent and centrifugal tubes: 15 & 50 ml	Sarstedt AG, Nuembrecht, Germany
Roti [®] -PVDF membrane	C. Roth GmbH + Co. KG, Karlsruhe, Germany
SEM specimen stubs	Agar Scientific Ltd., Essex, UK
SEM adhesive carbon discs	Agar Scientific Ltd., Essex, UK
SEM Thermanox [®] plastic cover slips	Nalge Nunc Int., Rochester, NY, USA
serological pipettes: 10 & 25 ml	Sarstedt AG, Nuembrecht, Germany
sterile syringe filter: PES, 0.22 µm	Sarstedt AG, Nuembrecht, Germany
sterile syringe filter: PES, 0.45 µm	Sarstedt AG, Nuembrecht, Germany
syringe: Injekt-F 1ml	B. Braun AG, Melsungen, Germany
syringe: Omnifix [®] (2 - 20 ml)	B. Braun AG, Melsungen, Germany
Vivaspin [®] 20 (MWCO 10 kDa)	Sartorius AG, Goettingen, Germany
Vivacell 250 (MWCO 10 kDa)	Sartorius AG, Goettingen, Germany
Whatman [®] filterpaper (0.34 mm)	C. Roth GmbH + Co. KG, Karlsruhe, Germany

2.1.4 Instruments

instrument	model	company
anti-vibration system	Halcyonics Micro 60	Accurion GmbH, Goettingen, Germany
balances	Discovery (fine balance)	OHAUS Europe GmbH, Naenikon, Switzerland
	Acculab ALC-3100.2	Sartorius AG, Goettingen, Germany
centrifuges	Heraeus [™] Fresco [™] 17	Thermo Scientific, Waltham, MA, USA
	Heraeus [™] Pico [™] 17	
	Heraeus [™] MULTIFUGE [™] 1 S-R	
	Sorvall [™] RC 6 plus	
conductivity meter	Qcond 2200	Merck Eurolab, Darmstadt, Germany
	FG3 - FiveGo [™] Kit	Mettler Toledo GmbH, Giessen, Germany
freeze dryer	Alpha 1-2 LDplus	M. Christ GmbH, Osterode am Harz, Germany
heat block	VWR Digital Heat Block	VWR International GmbH, Darmstadt, Germany
heater & stirrer	IKA [®] RCT Basic	IKA [®] -Werke GmbH & Co KG, Staufen, Germany

2.1 Materials and instruments

high pressure homogenizer	Niro Soavi Panda 2k	GEA Niro Soavi, Luebeck, Germany
humidity control	microcontroller 5100 humidifier 5462 dehumidifier (dry gas) 5465	Electro-Tech Systems Inc., Glenside, PA, USA
microscope, stereo	Zeiss 475002	Carl Zeiss AG, Oberkochen, Germany
microscope, light	Leica DMI3000B objective: 40x	Leica Mikrosystem Vertrieb GmbH, Wetzlar, Germany
microscope, scanning electron (SEM)	1540EsB Cross Beam (Metals and Alloys, UBT) Zeiss 1530 FESEM (Macromolecular Chemistry I (MC I), UBT) Quanta 200 (Friedrich-Baur-Institute of Biomaterials, Bayreuth)	Carl Zeiss GmbH, Jena, Germany
moisture analyzer	Sartorius MA150	FEI Europe, Eindhoven, The Netherlands Sartorius AG, Goettingen, Germany
pH meter	Lab 860	Schott AG, Mainz, Germany
pipettes	Eppendorff Research	Eppendorf AG, Hamburg, Germany
pipetting robot	Gilson GX-271 Liquid Handler power supply: Power 508 pump: Gilson 402 (100 μ l and 10 ml syringe) Racks: 29LE (micro tubes), 22 (reagent tubes)	Gilson, Inc., Middleton, WI, USA
pump	syringe: Harvard 33 micro annular gear: mzs-2905 micro annular gear: mzs-4605	Harvard Apparatus, MA, USA HNP Mikrosysteme GmbH, Parchem, Germany
rheometer	Physica MCR-500 (Appl. Mechanics & Fluid Dynamics) cone-plate 50 mm, 1° AR-G2 cone-plate 40 mm, 0.5° cone-plate 20 mm, 0.5°	Anton Paar Germany GmbH, Ostfildern, Germany
rotating mandrel (custom built)	rotating step motor: QMOT motor QSH5718 gear belt: LEZ 1 Silicon 2870, shore hardness 70 (Shore-A)	TA Instruments, Eschborn, Germany Trinamic Motion Control GmbH, Hamburg, Germany isel Germany AG, Eichenzell, Germany supplied by Uni Bayreuth

2.1 Materials and instruments

rotator, shaker	Rotamax 120	Heidolph Instruments GmbH & Co KG, Germany
	Intelli-Mixer RM-2S	Elmi Ltd, Riga, Latvia
Sodium dodecyl sulfate	SDS apparatus: Mighty Small II	Hoefer Inc., MA, USA
polyacrylamide gel	SE250 (10 x 8 cm)	
electrophoresis (SDS-PAGE)	power supply: BluePower™ 500 Plus	Serva Electrophoresis GmbH, Heidelberg, Germany
spectrophotometer, UV/Vis absorption	Varian Cary® 100	Agilent Technologies GmbH & Co.KG, Germany
	Genesys 10™	Thermo Scientific, MA, USA
	NanoDrop™ ND-1000	PEQLAB Biotechnologie GmbH, Erlangen, Germany
spectrophotometer, fluorescence	FluoroMax® 3	HORIBA Jobin Yvon Ltd., Stanmore Middlesex, UK
spectrometer, FTIR	Tensor 27 IR-Spectrometer detector: MCT measurement units: MIRacle germanium-ATR-crystal microscope: Hyperion™ 1000 objectives: ATR 20x, 15x IR filter: IR-polarizer A675P1	Bruker Optics GmbH, Ettlingen, Germany
sputter coater	Cressington 208HR (MC I, UBT)	Cressington Scientific Instruments Ltd., Watford, England, UK
sputter thickness controller	Cressington 208HR mtm20 (MC I, UBT)	
tensile testing	BOSE Electroforce® 3220 load cells: 0.5N and 2.5 N saline bath incl. control unit	BOSE Electroforce® Inc., Eden Prairie, MN, USA
thermomixer	Thermomixer compact/ comfort	Eppendorf AG, Hamburg, Germany
ultracentrifuge	Optima™ MAX-XP (rotor: TLA-55)	Beckmann Coulter Inc., CA, USA
vortex	VV3	VWR International GmbH, Darmstadt, Germany
Western Blot	blotting apparatus: Fastblot B43 detection: Ultima Pro	Biometra GmbH, Goettingen, Germany Hoefer Inc, MA, USA

2.2 Production and purification of recombinant eADF3(AQ)₂₄NR3 protein

2.1.5 Software

software	company
Adobe® Acrobat® 8.0 Professional	Adobe Systems, San Jose, CA, USA
Adobe® Illustrator CS3 (Win/Mac)	Adobe Systems, San Jose, CA, USA
Adobe® Photoshop CS3 (Win/Mac)	Adobe Systems, San Jose, CA, USA
BibDesk 1.6.3	http://bibdesk.sourceforge.net/
CorelDRAW® X4	Corel Corporation, Ottawa, Canada
ExPASy - SIB Bioinformatics Resource Portal	http://expasy.org/
ImageJ 1.42q (win/Mac)	National Institute of Health, USA
Mac OS X 10.9.5	Apple Inc., Cupertino, CA, USA
MacTex 2012-2014	http://tug.org/mactex/
Microsoft® Windows XP, Vista and 7	Microsoft Corp., Redmond, WA, USA
Microsoft® Office 2007	Microsoft Corp., Redmond, WA, USA
Opus 5.0	Bruker Optics Corp., MA, USA
OriginPro 8.1G	OriginLab Corp., MA, USA
ProEngineer Wildfire 5.0	PTC, Needham, MA, USA
TA Rheology Advantage™ AR 5.7	TA Instruments Ltd, DE, USA
WinTest® 4.1	BOSE, Eden Prairie, MN, USA

2.2 Production and purification of recombinant eADF3(AQ)₂₄NR3 protein

The recombinant spider silk protein (AQ)₂₄NR3 used in this work was kindly provided by Andreas Schmidt and Johannes Diehl. The purification of (AQ)₂₄NR3 was based on the established protocol by Huemmerich [160], which was further modified and optimized in the course of this work by Andreas Schmidt and Johannes Diehl. Briefly, *E. coli* cells were disrupted using a high pressure homogenizer and cell debris was removed by centrifugation. The protein was then purified using heat treatment (at ~65 °C), NH₄SO₄ precipitation and dialysis against a NH₄HCO₃ buffer. Finally, the purified (AQ)₂₄NR3 protein was freeze dried and stored at –20 °C until use.

2.3 Protein analytical methods

The identity and purity of (AQ)₂₄NR3 protein batches was assessed using standard protein analytical methods.

2.3.1 SDS-PAGE

SDS-PAGE is a technique widely used to separate proteins based on their electrophoretic mobility (i.e. based upon the protein's molecular size and charge). The running behavior of the protein depends on the protein's size and shape and can be controlled by the concentration of the applied polyacrylamide gels. Furthermore, the unspecific binding of SDS to the protein masks the protein's charge and results in a denatured protein (i.e. the protein's appearance is more linearized). Consequently, separation is only affected by the molecular size while other factors such as charge or tertiary conformation can be neglected.

SDS-PAGE gels were prepared according to the standard lab procedure of the chair. Briefly, the separating and stacking gels were cast successively into the gel caster and then transferred to the SDS apparatus filled with 1 x SDS-PAGE buffer. Meanwhile, samples for SDS-PAGE were prepared by mixing (AQ)₂₄NR3 (diluted to a concentration in the $\mu\text{g}/\mu\text{l}$ range) with 1x Laemmli buffer and heating for 5 min at 95 °C. Electrophoretic runs were performed at a constant amperage of 30 mA per gel for ~50 min. For molecular weight estimation, a reference marker was added.

2.3.2 Silver staining

In order to visualize proteins after SDS-PAGE separation, a silver staining procedure (detection limit ~0.01 μg) was conducted as follows. The SDS-PAGE gel was incubated in Fix 1 solution for 10 min and afterwards in Fix 2 solution for 30 min. The gel was then washed and rehydrated with Milli-Q water (four times for a few minutes) before the silver staining solution was added for 30 min to 45 min, in a box covered with aluminum foil to avoid exposure to light. In the next step, the gel was treated with developer solution until the desired intensity of staining was achieved. The reaction of silver nitrate to elementary silver was stopped through addition of EDTA stopping solution. The gel was then rinsed with Milli-Q water, imaged and dried in a gel dry solution for storage.

2.3.3 Immunoblotting (Western Blot)

In order to identify specific proteins, the Western Blot, a widely accepted immunologic detection technique, was used. In a first step, the proteins that were separated by SDS-PAGE were transferred onto a PVDF membrane using a western blotting apparatus. Before blotting, the Roti-PVDF membrane was activated in methanol for 20 s to 30 s and then rehydrated by rinsing with Milli-Q

water. Then, the membrane as well as 8 layers of Whatman[®] paper were incubated in the western blot transfer buffer for five minutes. Finally, the gel and the Roti-PVDF membrane (on top of the gel) were stacked between the Whatman[®] paper layers and protein transfer was generated by applying a constant amperage of 0.8 mA per cm² gel for 70 min.

To prevent unspecific antibody binding, the membranes were blocked by incubation in a 5 % non-fat dry milk - 1x PBS solution for at least 15 min. After removal of the non-bonded blocking reagent by rinsing repeatedly with 1x PBS solution, the membrane was placed into a dilute solution (1:5000) of antibody for 30 min to 45 min at room temperature. Following extensive washing in a 1x PBS solution, the bound antibody was detected by a chemiluminescent detection procedure using Lumi-Light^{Plus}.

2.4 Protein solution preparation methods

2.4.1 Preparation of a regenerated aqueous fibroin solution from *B. mori* throwsters waste silk

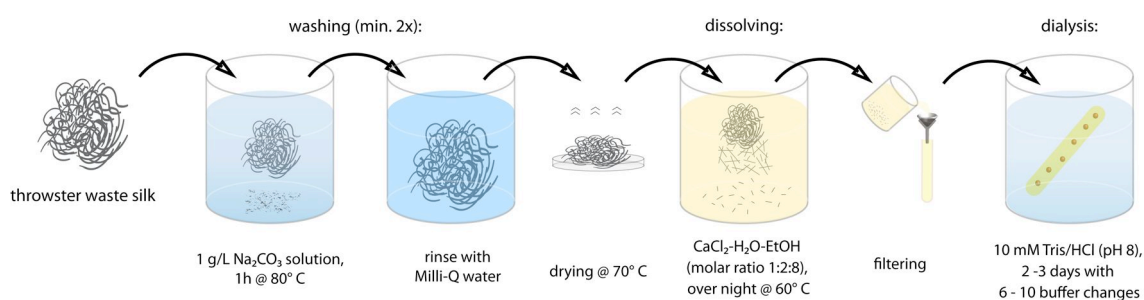


Figure 2.1 – Scheme for preparation of aqueous fibroin solutions from *B. mori* throwsters waste silk.

A procedure described previously [262–264] using CaCl₂–EtOH–H₂O as dissolving agent, was adopted and established for the preparation of aqueous fibroin solutions (see Figure 2.1).

The *B. mori* throwsters waste silk purchased from Wollknoll GmbH was washed for one hour in 0.1 % (w/v) sodium carbonate at 80 °C and then carefully rinsed with Milli-Q water in order to remove sericin debris and other impurities. Degumming and rinsing were repeated at least once before the silk was dried in an oven at ~70 °C for a few hours. After drying, the silk was dissolved over night in the CaCl₂–EtOH–H₂O solution at 60 °C under continuous stirring. The solution was filtered in order to remove impurities and insoluble fragments using a non-woven polyester filter. To remove the strong dissolving agent, the fibroin solution was dialyzed against an aqueous buffer using dialysis membranes with a MWCO of 6 kDa to 8 kDa. Dialysis was conducted against

an aqueous 10 mM Tris/HCl (pH 8) buffer for 3 to 4 days at 4 °C (with minimum 50 fold volume excess of buffer). The buffer was changed 6 to 10 times during dialysis in order to achieve a minimum dilution of a billion fold. The fibroin solution was then stored at 4 °C until use. For measurements, e.g. rheology, the density of the RSF was assumed as $\rho = 1.36 \text{ g cm}^{-3}$ according to earlier studies [227].

2.4.2 Preparation of an aqueous solution from (AQ)₂₄NR3 protein

Similar to fibroin, purified recombinant (AQ)₂₄NR3 had to be dissolved in strong denaturants such as 6 M GdmSCN or 8 M urea. The dissolved (AQ)₂₄NR3 was then transferred to the desired buffer solution A, B or C (see Section 2.1.2) by dialysis. Dialysis was performed with a minimum 100 fold excess in volume for 2 to 3 days at 4 °C and yielded solutions up to ~5 % (w/v). Concentrated solutions of (AQ)₂₄NR3 with concentrations between 6 % to 25 % (w/v) were prepared by centrifuging the as-dialyzed aqueous (AQ)₂₄NR3 solution in Vivaspin® 20 ultrafiltration tubes at 4000 x g and 12 °C to 17 °C. The concentrated (AQ)₂₄NR3 spinning dope solutions could then be stored for 14 days at 4 °C until use.

2.4.3 Preparation of (AQ)₂₄NR3 blends with additives

Table 2.5 – Overview of additives to increase silk solubility used in this work.

additive stock solution	c _{additive} used [M]
4 M sorbitol	0.5
	1.0
	1.5
8 M urea	0.2
	0.4
	1.0
0.25 M L-arginine (Arg) & 0.25 M L-glutamic acid (Glu)	0.05
	0.1
1 M PEG (4 kDa)	0.005
	0.02
	0.04
5 M TMAO	0.2
	0.5
	1.0
TMAO & urea (1:2 molar ratio)	0.2/0.4

The as-dialyzed (AQ)₂₄NR3 stock solution (in dialysis buffer B to avoid potential stabilizing effects related to sodium cholate) was prepared as a ~2 % (w/v) solution, while additive stock solu-

tions were prepared by dissolving the desired amount of additive in Milli-Q water (see Table 2.5). Different mixtures of both stock solutions were prepared using a pipetting robot to yield final additive concentrations according to Table 2.5 and a final (AQ)₂₄NR3 concentration of ca. 1.2 % (w/v). The solutions were carefully, but thoroughly mixed using the pipetting robot and the blend solutions were stored at room temperature for 14 days. Throughout this period, the stability of the solutions was monitored by determination of (AQ)₂₄NR3 concentration in the soluble supernatant after 1, 4, 7 and 14 days using UV/Vis spectroscopy [265]. Scanning electron microscopy (SEM) was used to qualitatively monitor aggregates formed during this process with regard to size and morphology.

Table 2.6 – Overview of polymeric additives used in this work.

polymer	molecular weight [kDa]	polymer [% (v/v)]	(AQ) ₂₄ NR3 [% (v/v)]
25 % (w/v) PEG	35	20	80
		50	50
		80	20
2.5 % (w/v) PEG	600	20	80
		50	50
		80	20
100 % (w/v) glycerol	92.1	20	80
		50	50
		80	20
50 % (w/v) PAA	10	20	80
		50	50
		80	20
2.5 % (w/v) PAA	5000	20	80
		50	50
		80	20
15 % (w/v) PVA	31	20	80
		50	50
		80	20
2 % (w/v) alginate	0.176	20	80
		50	50
		80	20

Polymeric additive stock solutions were prepared by dissolving the desired amount of polymer in Milli-Q water (see Table 2.6). The as-dialyzed (AQ)₂₄NR3 stock solution (in dialysis buffer C as stabilizing effects related to sodium cholate were desired in this study) was set to a concentration of ~3 % (w/v). The different aqueous (AQ)₂₄NR3 and polymer blend solutions were prepared using the pipetting robot according to Table 2.6 and thoroughly mixed over night at 130 rpm.

2.5 Preparation of artificial silk fibers from concentrated (AQ)₂₄NR3 solutions

2.5.1 Preparation of fibers using a technical pulling device

Fibers were produced by mixing equal volumes of an 11 % to 20 % (w/v) (AQ)₂₄NR3 solution and solutions of either 1 M potassium phosphate (pH 8), 1 M diammonium hydrogen phosphate (pH 7.9), 1 M ammonium sulfate (pH 5) or 1 M sodium dihydrogen phosphate (pH 4). Immediately after mixing, the appearance of viscous gel-like aggregates was observed. These aggregates could easily be separated from the solution and following a short period of drying be drawn into fibers using fine tweezers. These fibers were immediately transferred to a rotating mandrel (see Figure 2.2) and collected at a reeling speed of 2 mm s⁻¹. After fiber formation, fibers were left on the mandrel over night (at typical laboratory conditions in the range of 20 °C to 30 °C and 35 % to 45 % relative humidity) before being prepared for tensile testing.

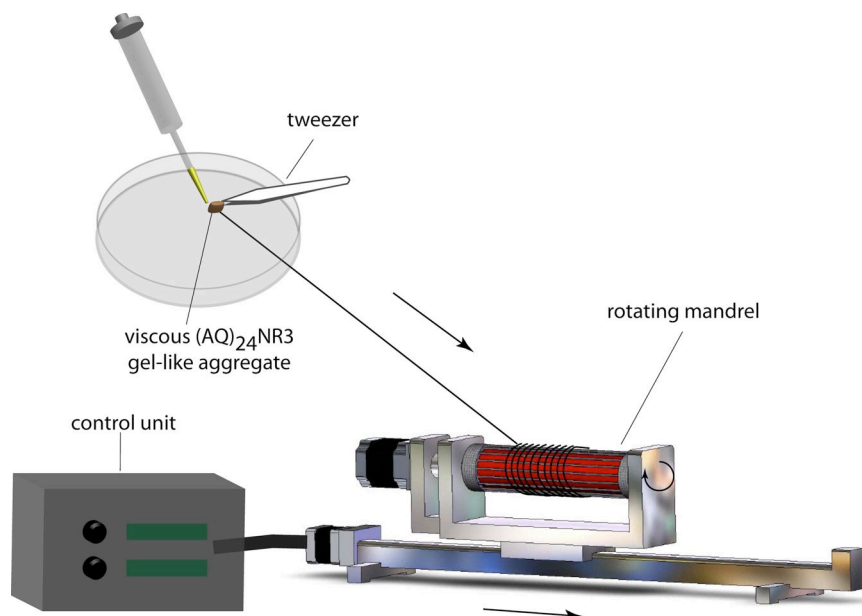


Figure 2.2 – Schematic illustration of the procedure applied in this study to produce "hand-drawn" fibers from a viscous drop of (AQ)₂₄NR3 solution.

2.5.2 Preparation of fibers using a biomimetic spinning device

Based upon a granted patent for the production of threads from silk proteins [83], a device for biomimetic spinning had been designed and constructed by Daniel Huemmerich (see Figure 2.3). The main components of this initial setup included a custom-built syringe pump (for processing of the protein solution) and a small diffusion unit constructed from a 2 or 5 ml syringe. This syringe was filled with a mixture containing 40 % (v/v) acrylamide and 0.5 M potassium phosphate buffer (pH 8). A fine needle (diameter of ~ 0.7 mm) was placed inside the syringe in order to create the flow channel, while the mixture of acrylamide and phosphate polymerized upon addition of APS (10 % (w/v)) and TEMED (0.1 % (v/v)). After polymerization, the needle was removed and imperviousness of the flow channel was tested with water. Initial spinning tests were performed with this setup.

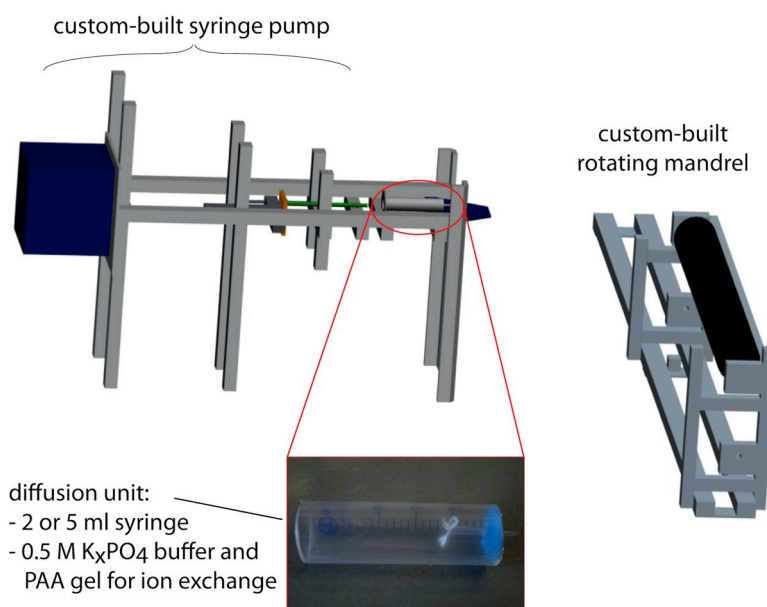


Figure 2.3 – CAD images of the original diffusion unit and spinning apparatus for biomimetic spinning developed by Dr. Huemmerich.

2.5.3 Post-treatment of artificial fibers

Fibers produced from (AQ)₂₄NR3 or RSF were post-treated using a steam annealing procedure, as shown in Figure 2.4. In this procedure, fibers were collected from the rotating mandrel and transferred to a small piece of fly-screen fixed to a metal ring holder. The holder was placed inside a glass beaker that was filled either with water or ethanol (the solution surface was kept well below

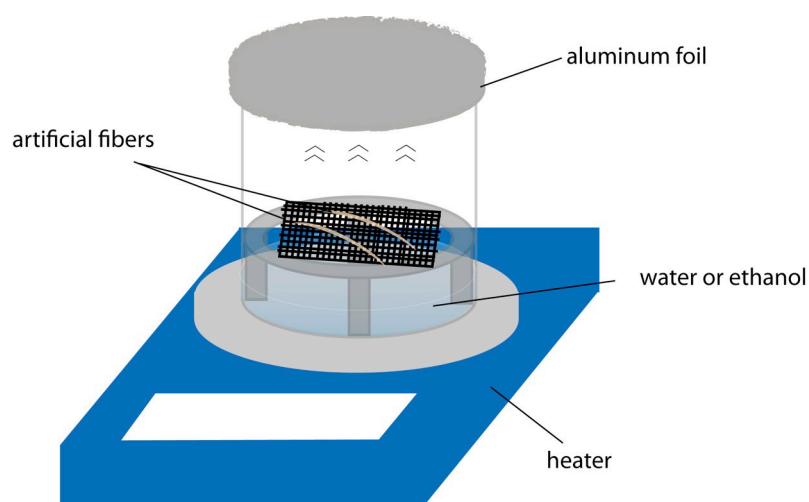


Figure 2.4 – Illustration of the post-treatment setup applied in this study.

the fly-screen). For steam annealing, the beaker was covered with aluminum foil and then placed on top of a heater and temperatures were set to 90 °C for water or 40 °C for ethanol in order to control evaporation over night.

2.6 Collection of natural silk fibers

2.6.1 Design and construction of a laboratory housing for *A. diadematus* spiders

In order to have a high number of fiber samples readily available for material analysis, a method for housing *A. diadematus* spiders in a laboratory environment was established, in which they were allowed to build orb-webs. Based upon *A. diadematus* webs being in the range of 20 cm to 50 cm the housing was designed respectively [135]. Construction of the spider house has been described in literature [135, 234, 266]: based thereon, four wood ledges (with a length of 30 cm and a width of 5 cm) were fixed together to form a rectangular frame. Inside the frames a black rubber tape was applied, assisting the spider with walking and easing web attachment. Each of the four frames was additionally equipped with a handle on top to ease pulling the frame out of the rack. Three of those frames were stacked in a rack, separated by 2 mm thin transparent plexiglass shields (see Figure 2.5), while the fourth frame was used as a substitute for web collection. Separation of individual frames and spiders, respectively is essential due to their cannibalistic behavior [135]. The plexiglass shields had a smooth surface to prevent web attachment. The transparency of these shields allowed better observation of the spiders and guaranteed a normal day and night cycle, an important factor for a regular web building routine [135]. Based on this initial setup, several other

individual frames with varying dimensions for other spider species (e.g. *Nephila edulis*) were later constructed at the chair using Macrolon®.



Figure 2.5 – Spider housing used in this study; left: CAD-design and right: photograph of actual housing.

2.6.2 Catching and housing of *A. diadematus* spiders

The aforementioned cannibalistic behavior of *A. diadematus* spiders allowed the housing of at most three spiders at the same time in one rack. Female sub-adult *A. diadematus* spiders (which are supposed to thrive better in laboratory conditions [135]) were collected in the Bayreuth area and housed in the aforementioned frames (see Section 2.6.1). Spiders were fed regularly with various sorts of flies or fly larvae and supplied with tap water [135, 191, 234]. They finally reached a body weight of ca. 200 mg to 250 mg at the time of silking. Housing conditions were in accordance with typical laboratory conditions in the range of 20 °C to 30 °C and 35 % to 45 % relative humidity. This method enabled the housing of spiders in the laboratory for more than 6 months, including occasional cocoon building.

2.6.3 Collecting naturally spun fibers from *A. diadematus*

Collection of naturally spun silk (see Figure 2.6), i.e. silk spun during orb web building, was based on a method described in literature [230]. First, the spider was separated from its web and transferred to a separate frame. Next, two cardboard templates that mimic the design of an orb web were attached to the web from both sides, using the web's initial stickiness and double-sided adhesive tape. In the final step, the web was cut from the frame using scissors or blades and individual fibers could be collected carefully and mounted onto the sample holders using fine

tweezers. Unlike other methods in which the silk was cut from the web with a hot soldering iron [241] or a hot wire [230], in this work scissors and blades were used for simplicity and to avoid potential fiber degradation due to heat. All naturally spun silk fiber samples were collected during a period of 6 weeks from clean and undamaged webs built by adult female spiders with a body weight of ca. 200 mg to 250 mg.

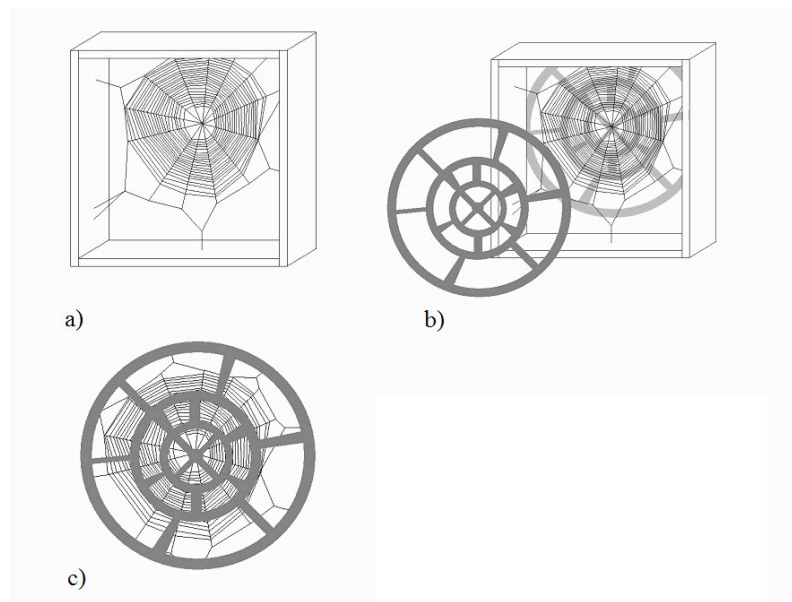


Figure 2.6 – Scheme of silk collection from orb web: a) isolated web; b) placing web between two cardboard templates using adhesive tapes and c) collected web.

2.6.4 Forced silking of fibers from *A. diadematus* spiders

Forced silking is a method originally established to reel spider silk with low variance of silk properties [66, 192, 193, 267, 268]. For this purpose, a forced silking setup based on the original setup proposed by Work and Emerson [267] later used in several other studies [90, 234, 268] was built (see Figure 2.7a)).

The main component of this setup is a rotating take-up mandrel controlled by a QMOT motor QSH5718. This two phase hybrid step motor is optimized for micro stepping and enables precise control at low rotational speeds. The mandrel itself is covered with a silicon coating easing the pick-up of fibers from the mandrel. On both ends of the mandrel, one side of a hook-and-loop tape was fixed. Furthermore, a collar (see Figure 2.7a)) consisting of 17 stainless steel rods (2.5 mm diameter) sewn in parallel onto the counter-side of the hook-and-loop tapes was built. The two rods that are opposed to each other when the collar is closed around the mandrel are covered

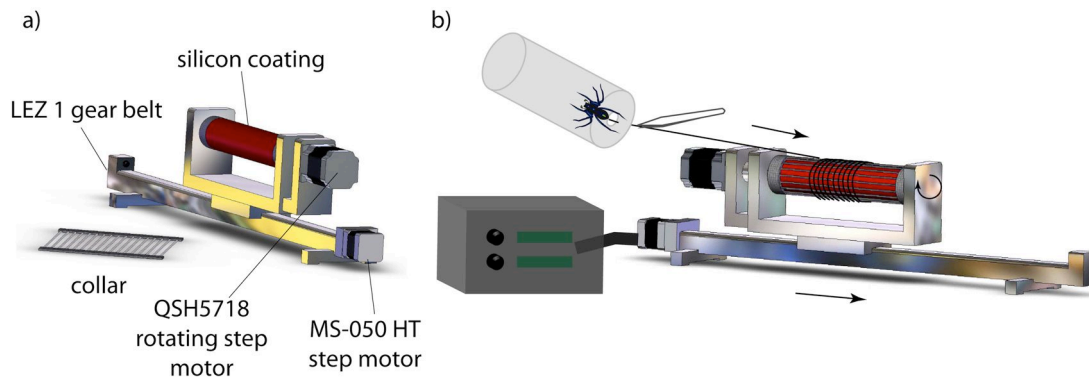


Figure 2.7 – a) Scheme of forced silking apparatus. b) Illustration of forced silking procedure.

with a small strip of double-sided adhesive tape before silking was started. The initial continuous fiber could thus be divided into samples of a length equal to the mandrel circumference by simply cutting between both adhesive tapes. The collar offers the advantage of significantly simplifying fiber pick-up for sample preparation. The mandrel and its motor were built on a sledge that can be moved axially using a commercially available gear belt LEZ 1. The gear belt is controlled by a second independent step motor MS-050 HT, working very precisely in the range of 0.1 mm s^{-1} to 250 mm s^{-1} . It is noteworthy, that due to the motor setup, the rotating speed was controlled via *rpm* instead of mm s^{-1} . Therefore, the desired reeling speed had to be converted into *rpm*. One turn by the mandrel could thereby be set equal to the mandrel circumference of 20 cm, since the effects due to the axial movement were negligible ($<1\%$) even at maximum axial and rotational speeds. The motor speed was thus calculated according to the following relationship:

$$v_{[\text{rpm}]} = \frac{v_{[\text{mm/s}]} \cdot 60_{[\text{s/min}]}}{C_{[\text{mm}]}} \quad (2.1)$$

with C being the mandrel circumference [mm].

The reeling speeds of 200 mm s^{-1} and 60 mm s^{-1} corresponded to 60 and 18 rpm, respectively. The whole setup enables reeling of silk fibers at a defined rate and with defined distances between them, easing the collection of individual fibers for material analysis.

For the forced silking procedure, spiders were collected from their housing using a 50 mL reagent tube. The reagent tube could further be used to loosely immobilize the spider without using anesthetics, which were found to significantly affect mechanical properties of silk [269]. For this purpose, a hole, small enough to avoid the spider's escape, was punched into the bottom of the reagent tube. Using fine tweezers, the dragline silk could be pulled from the spider's spigot

through this hole and transferred carefully to the collar where it was fixed onto the double-sided adhesive tape. Immediately after fixation, the motors were started and the silk was reeled at the desired speeds.

2.7 Spectroscopical methods

2.7.1 Fluorescence spectroscopy

Fluorescence spectroscopy is an electromagnetic spectroscopical technique which analyzes a sample's fluorescence emission. Fluorescence emission is observed when electrons of a sample return from an excited state (due to irradiation at a certain wavelength) to their ground state, thereby emitting radiation of a different wavelength. For proteins, the fluorescence originates from phenylalanine (Phe), tyrosine (Tyr) and tryptophan (Trp) residues, with contributions of Trp residues usually dominating [11].

In this work, the fluorescence of Trp and Tyr residues was used to estimate the purity of recombinant (AQ)₂₄NR3, since (AQ)₂₄NR3 lacks the fluorescence dominating Trp residues. Thus, emission spectra for Tyr and Trp were recorded by measuring the intensity of fluorescent light emitted by (AQ)₂₄NR3 samples when excited at a defined wavelength (see Table 2.7). The spectra obtained were then overlaid to evaluate if Trp spectra affected the Tyr spectra, which is indicative for the existence of other proteins in the sample.

Table 2.7 – Excitation wavelength and emission spectra.

amino acid	excitation wavelength	emission spectrum
Tyr	275 nm	290 - 400 nm
Trp	295 nm	310 - 400 nm

2.7.2 UV/Vis absorption spectroscopy

UV/Vis absorption spectroscopy, a routine technique for quantitative determination of proteins, was used to determine the concentration of proteins in solution as well as the stability of (AQ)₂₄NR3 in the presence of solubility additives. Molecules exposed to light with an energy that matches a possible electronic transition within the molecule, absorb light while the electron is promoted to a higher energy level. The UV/Vis spectrometer records the wavelength at which absorption occurs and the quantum of absorption at each wavelength. The resulting spectrum is typically presented as a graph of absorbance (A) versus wavelength. In the case of proteins,

the excitation results in characteristic spectra with absorption maxima in the near-UV range (<240 nm) and at wavelengths between 260 nm and 280 nm. The near-UV range is related to the peptide backbone and thus is not useful for concentration or protein stability determination. In contrast, the pronounced absorption between 260 nm and 280 nm is related to a valence electron transfer of aromatic amino acids, in particular Trp and Tyr, and to a lesser extent of Phe and cystine (Cys) [270, 271]. Based on a method by Gill and Hippel [272] the wavelength-dependent extinction coefficient of recombinant spider silk proteins can be determined from the primary structure of a protein and is calculated according to

$$\epsilon_{\lambda, \text{protein}} = \epsilon_{\lambda, \text{Trp}} \cdot n_{\text{Trp}} + \epsilon_{\lambda, \text{Tyr}} \cdot n_{\text{Tyr}} + \epsilon_{\lambda, \text{Cys}} \cdot n_{\text{Cys}} \quad (2.2)$$

using the software Protparam (see Table 2.8).

Table 2.8 – Molecular extinction coefficient and molecular weight of proteins used in this study calculated using Protparam.

protein	molar extinction coefficient @ 280 nm [M ⁻¹ cm ⁻¹]	molecular weight [kgmol ⁻¹]
(AQ) ₂₄ NR3	75990	106.3
eADF3(AQ24)	71520	94.5
eADF4(C16NR4)	49170	56.4
eADF4(C16)	47680	47.7
eADF4(C32NR4)	96850	104.1
eADF4(C32)	95360	93.8
fibroin heavy chain (hc)	473480	391.6
fibroin light chain (lc)	27515	27.7
fibroin P25	31900	25.2
fibroin avg (hc:lc:P25 = 6:6:1)	233682	195.5

The calculated molecular extinction coefficients can be used to determine the protein concentration based on the relation between concentration, extinction coefficient and measured extinction described by the Beer - Lambert law:

$$E_{\lambda} = \epsilon_{\lambda} \cdot c \cdot d \quad (2.3)$$

with E_{λ} : extinction measured at wavelength λ [l/molcm], ϵ_{λ} : molecular extinction coefficient at wavelength λ [M⁻¹cm⁻¹], c : protein concentration [mol/l] and d : layer thickness of cuvette [m].

For the determination of protein concentrations, UV spectra were recorded between 230 nm and 340 nm using a Thermo Scientific Genesys 10 Photometer for dilute solutions or a NanoDropTM ND-1000 for concentrated solutions. The protein solutions were diluted before measurements to obtain a maximum absorption below the instruments' limits at 280 nm. All measurements were performed three times for each sample. Usually, centrifugation was avoided due to the shear sensitivity of (AQ)₂₄NR3 solutions [117]. Only if absolutely necessary (e.g. high turbidity of solution), samples were carefully centrifuged before measurement.

2.7.3 Fourier transform infrared spectroscopy (FT-IR)

In infrared spectroscopy, electromagnetic radiation in the mid-infrared range (at wavelengths between 50 μm and 2.5 μm which corresponds to wavenumbers of 200 cm^{-1} to 4000 cm^{-1}) is passed through a sample and some part of the radiation is absorbed by the sample while the rest of it is transmitted. The absorption of infrared radiation induces specific vibrational transitions between atomic bonds, affecting the dipole moment of a molecule resulting in an unique infrared spectrum. Therefore infrared spectroscopy can be used to qualitatively analyze a material. In FT-IR spectroscopy, an optical device called Michelson interferometer is employed to create an interferogram based on absorption and transmission of IR radiation. The interferogram is then used to calculate a spectrum using Fourier transformation. In the case of proteins, FT-IR spectroscopy can be used to gain insight into their secondary structure. Moreover, the assignment of individual amino acid residues to distinct conformations is partially possible [273]. The majority of a protein's infrared spectrum is related to independent vibration modes of the peptide backbone and bonds, which display nine characteristic bands: amide A and B as well as amide I-VII [274, 275]. Amide I and II bands are typically used to determine the secondary structure of proteins as the characteristic vibrations for different secondary structures elements typically appear in the regime of these bands. The amide I band (at 1600 cm^{-1} to 1700 cm^{-1}) for instance is mainly associated with stretching vibrations (70 % to 85 %) caused by the peptide carbonyl C=O group and is directly related to backbone conformation. The amide II band (at 1500 cm^{-1} to 1580 cm^{-1}) in contrast, represents N-H bending vibrations (40 % to 60 %) as well as C-N stretching vibrations (to 18 % to 40 %) and is sensitive to conformational changes. The other amide bands result from complex coordinate displacements or out-of-plane motions. The most efficient technique to study fiber microstructure by infrared spectroscopy is the application of attenuated total reflectance (ATR) using e.g. a germanium crystal. The crystal allows circumventing the limitation of conventional ATR accessories that required several filaments to obtain spectra with a sufficiently high signal-to-noise ratio [276].

In this work, FT-IR spectra of fibers were recorded using the Bruker Hyperion 1000 FT-IR microscope with an ATR objective. For each measurement in ATR mode, 125 scans were conducted with a resolution of 4 cm^{-1} in a range of 5000 cm^{-1} to 800 cm^{-1} and cumulated to yield the final spectrum. The spectra were obtained with atmospheric compensation and corrected using a background spectrum and baseline correction using the Opus 5.0 software.

Secondary structure was determined by Fourier self-deconvolution (FSD) of the infrared spectra covering the amide I region (1720 cm^{-1} to 1590 cm^{-1}) using Opus 5.0 software and Origin 8.1G, according to a procedure described by Hu and coworkers [173]. The amide I band was subjected to a baseline correction and smoothing procedure prior to the automatic FSD using the following parameters: Lorentzian fit with noise reduction set to 0.3 and bandwidth set between 23 and 27. These settings enhance the interferogram at higher mirror deflections which results in improved resolution of the spectrum and sharper bands. The resulting new spectrum was again baseline corrected in the region 1705 cm^{-1} to 1590 cm^{-1} and peak fitting performed using Gauss-oscillation (Levenberg - Marquardt fit) with positions as described by Hu and coworkers [173]. At minimum three FSD runs were performed to obtain the mean average. The assignments were made according to Figure 2.8 [173, 258].

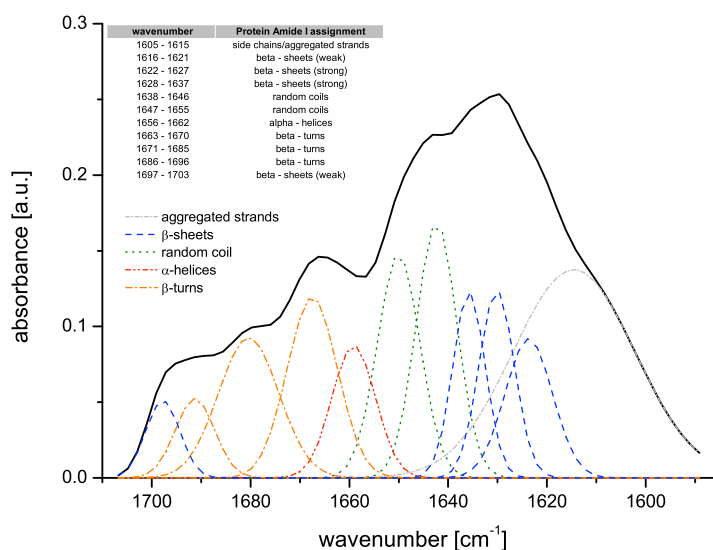


Figure 2.8 – Illustration of FSD FT-IR spectra of amide I band and corresponding structural assignments according to [173].

The percentage of the different secondary structure elements could be calculated using the normalized integrals of each curve according to the following relationship:

$$\begin{aligned} \text{secondary structure (S) content [\%]} &= \\ &= \frac{\sum \text{integrals assigned to S}}{\sum \text{of all integrals}} \cdot 100\% \end{aligned} \quad (2.4)$$

Polarized FT-IR spectroscopy enables the investigation of the orientation of distinct bonds or transition moments in the analyte. Polarized FT-IR measurements of fibers were conducted using the 15x Objective of a Bruker Hyperion 1000 FT-IR spectrometer with polarizing filters at 0 and 90 degrees. In case of perfectly aligned fibers all transition moments are parallel, resulting in a near-zero maximum absorbance when the beam is polarized perpendicular to the fiber's orientation axis [273]. The analysis is focused in the spectral region between 1100 cm^{-1} and 900 cm^{-1} because this region contains amino acid-specific bands. The molecular order parameter S^{mol} can be calculated by the following equation

$$S^{\text{mol}} = \frac{A_{\text{max}} - A_{\text{min}}}{A_{\text{max}} + 2A_{\text{min}}} \quad (2.5)$$

with A_{max} and A_{min} being the maximum and minimum absorbance [273].

2.8 Microscopical methods

2.8.1 Light microscopy with polarizer (PLM) or bright field modus (LMBF)

The determination of fiber diameter is essential to correctly assess the fiber's mechanical properties, since even small deviations in fiber diameter due to measurement inaccuracies or false assumptions have a significant effect on tensile strength. Due to the thinness of the silk fibers, only LM and SEM techniques appeared to be suitable according to earlier studies [60, 70, 191, 277].

Successfully tensile tested fibers were collected and micrograph images were obtained using a Leica DMI3000B Inverted Microscope with a 40x objective for bright field mode and additional polarizing filters for polarized mode. Fiber diameters were measured at 3 to 5 different spots along a $\sim 2\text{ mm}$ long fiber using the imaging software ImageJ 1.42q. The mean diameter of a fiber required for the calculation of stress values of individual fibers [195] was calculated from these values using Origin 8.1G.

2.8.2 Scanning electron microscopy (SEM)

Scanning electron microscopy (SEM) is an electron microscopy technique in which a sample is scanned with a beam of electrons in a raster scan pattern, yielding images with high resolution and large depth of field. In particular the large depth of field results in characteristic three-dimensional appearance of SEM images which make this technique useful for analysis of structure and morphology of samples. The technique involves a thin, focused electron beam (diameter ~ 5 nm) with an energy typically in the range between 0.2 and 40 keV. This fine electron beam scans the surface of a sample usually in a high vacuum in order to avoid interactions between the electron beam and air. Consequently, the electron beam only interacts with the sample resulting in emission of secondary electrons due to inelastic scattering out of the sample surface. The resulting scattering signal can be detected and provides the information about sample morphology [11].

Prior to imaging in the microscope, specimens must be electrically conductive, at least at the surface, and moreover electrically grounded in order to prevent the accumulation of electrostatic charge at the surface. Before imaging, all samples were sputtered with a 2 nm thick platinum coating, using a Cressington 208HR high resolution sputter coater combined with a mtm 20 thickness controller.

To analyze size and morphology of aggregates obtained from (AQ)₂₄NR3 and solubility additive mixtures, samples were prepared by casting 5 μ l of the mixtures immediately and 14 days after mixing onto ThermanoxTM plastic cover slips. Samples were washed three times with Milli-Q water to remove salt or other water-soluble particles and air-dried. Larger, visible aggregates that formed after 14 days were obtained by centrifugation at 17000 x g for 10 min. After washing twice with Milli-Q water these aggregates were placed onto the ThermanoxTM plastic cover slips and air-dried.

Natural and artificial fibers were prepared directly on SEM adhesive carbon discs. SEM images were recorded with an incident electron beam of 3 kV to 5 kV at a working distance of 4 mm to 5 mm using a Zeiss 1540EsB Cross Beam by Claudia Bluem and Dr. Hendrik Bargel, a Zeiss 1530 FESEM by Johannes Diehl or a Quanta 200 by Andreas Schmidt.

2.9 Material analysis methods

2.9.1 Rheometry

Depending on the application and viscosity regime of the material investigated, different types of rheometer are typically applied. To investigate the viscoelastic behavior of polymeric solutions, a rotational rheometer is commonly applied in combination with a plate-plate or cone-plate geometry. The latter geometry was used throughout this work and thus is presented in more detail in the following (see Figure 2.9). Earlier studies on native silk dope showed that the cone-plate geometry allowed to study small and highly concentrated samples with minimal shear history caused by the loading [133, 214].

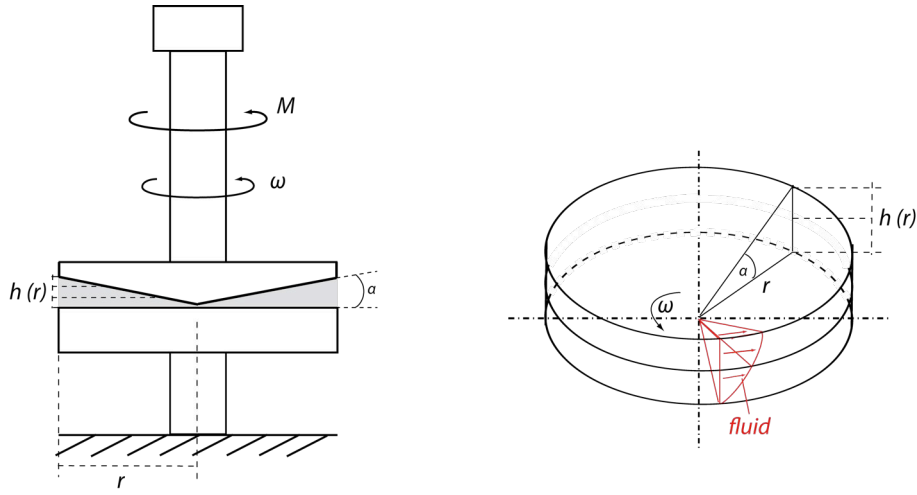


Figure 2.9 – Illustration of typical rotational rheometers for shear rheometry using cone-plate geometry; r = radius of cone [m]; $h(r)$ = shearing gap in dependence of r [m]; α = cone angle [$^\circ$]; M = torque [Nm] and ω = angular frequency [rad/s].

In a rotational rheometer with cone-plate geometry, the sample is typically placed between a stationary plate (bottom) and a movable cone, which are orientated coaxially to each other. The cone is characterized by its dulled geometry as indicated by the very small cone angle $\alpha = 0.5^\circ$, and its peak is in the center of the stationary plate. The selection of very small cone angles enables to set the shearing gap $h(r)$ equal to the arc length at distance r

$$h(r) = r \cdot \tan(\alpha) \cong r \cdot \alpha \quad (2.6)$$

Moreover, it enables the assumption that the circumferential velocity is proportional to the ra-

dius, which excludes the influence of radius on shear rate. In combination with a homogeneous distribution of shear velocity within the shearing gap provided by cone-plate geometry, complex mathematical corrections become obsolete. Due to Newton's third axiom "*actio est reactio*", the torque (which is measured by the rheometer) acting on plate and cone are equivalent, thus only the fluid transfers the torque within the shearing gap. Applying the geometrical constant for cone-plate geometry

$$K_{\sigma} = \frac{3}{2 \cdot \pi \cdot r^3} \quad (2.7)$$

allows the calculation of shear stress τ using the constitutive equation

$$\tau = K_{\sigma} \cdot M = \frac{3 \cdot M}{2 \cdot \pi \cdot r^3}. \quad (2.8)$$

Consequently, based on known instrument dimensions, defined shear rate and measured torque data, the viscosity can now be obtained by

$$\eta = \frac{\tau}{\dot{\gamma}} = \frac{3 \cdot M}{2 \cdot \pi \cdot r^3} \cdot \frac{\tan(\alpha)}{\omega} \quad (2.9)$$

Rotational rheometer are typically run in two different ways: controlled shear stress (CSS) or controlled strain rate (CSR). In CSS mode, the sample is loaded with a defined torque, and the resulting strain or strain rate is measured. In CSR mode, a defined shear rate is applied and the resulting torque (stress) is determined. The latter mode is a common technique to determine a material's viscosity.

In this work, rheological measurements were performed using a TA Instruments AR-G2 stress-controlled rotational rheometer with a Peltier temperature regulator unit and a solvent trap to avoid sample dehydration. In order to verify the accuracy of the rheometer, testing was performed on benchmark Newtonian fluids (silicon oils M200, M500 and M1000). All measurements were performed at 25 °C, ensuring solution state conditions [227], using a cone-plate geometry with 40 mm diameter and 0.5° angle. Flow curve diagrams of viscosity η as a function of shear rate $\dot{\gamma}$ were determined by increasing the shear rate logarithmically from 0.01 s⁻¹ to 300 s⁻¹, which is well within the range of shear rates calculated based on silk gland geometry and observed spinning rates during fibroin passage through the anterior region of the gland [30]. The storage and loss moduli, G' and G'' , were measured as a function of angular frequency ω in the range

of 188.5 rad s^{-1} to 1.88 rad s^{-1} . Thixotropy measurements were performed in CSR mode. The measurement itself was conducted as a loop test in form of a CSR ramp test: 1) shear rate was increased from 0 s^{-1} to 300 s^{-1} (so-called up curve), then 2) shear rate was kept constant at 300 s^{-1} (so-called hold peak with odd numbers), then 3) shear rate was decreased from 300 s^{-1} to 0 s^{-1} (so-called down curve) and 4) finally shear rate was kept constant at 0 s^{-1} (so-called hold peak with even numbers).

Temperature sweeps measurements were conducted at the Chair of Applied Mechanics and Fluid Dynamics, assisted by Markus Horn, using a Physica MCR 500. Samples were exposed to a constant shear rate $\dot{\gamma}$ of 1 s^{-1} and temperature was increased by 5°C every five minutes from 5°C to 45°C . After resting at 45°C for 10 min, temperature was decreased by 5°C every five minutes from 45°C to 5°C . Investigations of temperature dependence of rheological behavior were conducted using a TA Instruments AR-G2 rheometer, with a constant shear stress of 2.5 GPa applied while the temperature was increased by 1°C per minute.

2.9.2 Determination of phosphate mass transfer

Mass transfer usually describes the net transfer of mass from one location to another, e.g. as found in a diffusive process through a semipermeable membrane. The driving force for a diffusive mass transfer process through a semipermeable membrane is the osmotic pressure caused by a concentration gradient of a solute between one side of the membrane and the other. Studies on the silk spinning process have revealed that an increase in potassium phosphate concentration in the spinning dope during spinning triggers fiber formation [121, 125, 165]. Moreover, it was observed that the addition of phosphate to the engineered silk solutions is essential for successful spinning of artificial silk fibers [180]. A potential technique for controlled addition of phosphate to the spinning dope is the use of osmotic driven mass transfer through a semipermeable membrane.

Phosphate concentrations were determined by conductivity measurements, a routine technique to measure the ionic content of solutions in industrial applications. Conductivity σ [S/cm] is typically determined by measuring the AC resistance R [Ω] of the solution between two electrodes (of area A) separated by a fixed distance L according to the following relation

$$R = \frac{L}{\sigma \cdot A} \quad (2.10)$$

The conductivity data enables the determination of the concentration of electrolytes knowing the ionic composition and reference values obtained from a standard plot. First, a standard plot of

conductivity over concentration for aqueous phosphate solutions with concentrations between 0 M and 1 M (in steps of 25 mM between 0 M and 0.3 M and steps of 50 mM between 0.3 M and 1 M) was determined. The resulting data points could be best described by a linear fit following the relation

$$\sigma = a + b \cdot c \quad (2.11)$$

with c being the phosphate concentration [mol/l].

Due to conductivity measurement limitations in the presence of a highly concentrated protein solution (high viscosity), the mass transfer was simulated using only aqueous Tris/HCl pH 8 buffer solution in which the protein would later be dissolved. The experimental setup designed for mass transfer determination by conductivity measurements is displayed in Figure 2.10.

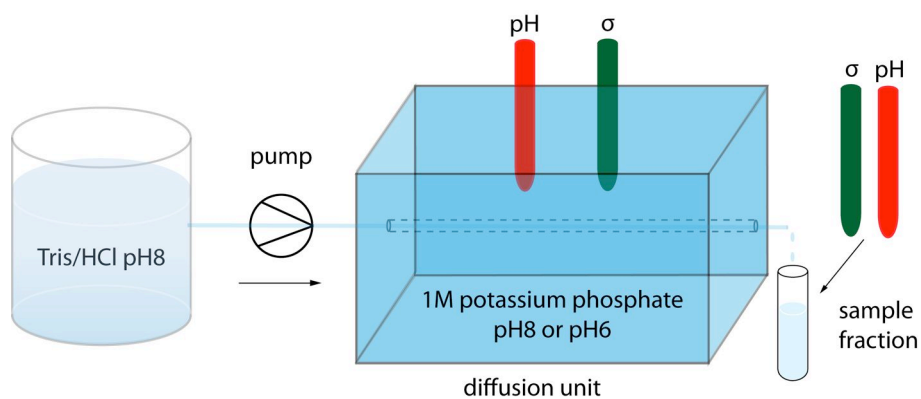


Figure 2.10 – Schematic setup for ion exchange measurements
(σ = conductivity; dotted lines symbolize the semipermeable membrane).

Tris/HCl pH8 buffer was pumped through the membranes at flow rates calculated to either match the retention time or diffusivity. Retention time, i.e. the residence time of a particle in a channel, could be determined according to the following relationship:

$$\tau = \frac{V_{\text{reactant}}}{\dot{V}} = \frac{r^2 \cdot \pi \cdot l}{\dot{V}} \quad (2.12)$$

with r being the radius of the cylindrical channel, l being the channel length and \dot{V} being the flow rate [m³/h].

During the experiment, pH and conductivity were monitored in the diffusion unit and determined to be constant throughout the experiment. Samples were collected at the exit of the diffusion unit

in ~ 1.5 ml to 2 ml fractions and were allowed to equilibrate for 30 min before pH and conductivity were determined. The conductivity of Tris/HCl pH 8 buffer (usually between $670 \mu\text{S cm}^{-1}$ and $750 \mu\text{S cm}^{-1}$) was subtracted from the measured conductivity and the corrected value was recalculated into phosphate concentration using standard interpolation formula according to

$$c = c_0 + \frac{(c_1 - c_0) \cdot (\sigma - \sigma_0)}{\sigma_1 - \sigma_0} \quad (2.13)$$

with σ being the conductivity measured, c_0 being the next lower limit of phosphate concentration and σ_0 its corresponding conductivity, c_1 being the next upper limit of phosphate concentration and σ_1 its corresponding conductivity as determined by standard curves. The results were confirmed by calculation using the data obtained from linear regression fits (based on Equation 2.11).

Temperature dependency of mass transfer was measured by placing the diffusion unit into a temperature controlled water bath and monitoring the temperature inside the diffusion unit.

2.9.3 Determination of solvent removal using pan weighing experiments

Thermogravimetric analysis (TGA) is a method to remove solvent from a sample via application of heat. The resulting loss of mass is typically recorded by a balance.

$$\text{moisture [\%]} = \frac{m_0 - m}{m_0} \cdot 100\% \quad (2.14)$$

with m_0 being the initial mass [g] and m being the mass after measurement [g].

Kojic and coworkers established a pan-weighing setup to observe the mass loss over time for a small amount of native silk dope extracted from major ampullate gland of a female *N. clavipes* spider [168]. The results were used to establish a numerical model to obtain the diffusion coefficient of water, the parameter describing the internal diffusion of water through the dope, assumed to govern solvent removal within the spinning process, while the accompanying convective resistance to evaporation of solvent from the fiber surface is almost negligible [167, 168].

In order to gain insight into heat-induced solvent removal from $(\text{AQ})_{24}\text{NR3}$ and RSF solutions, pan-weighing experiments in this work were performed using a Sartorius MA150 moisture analyzer. For these experiments, 1 ml of each sample was cast into a $35 \text{ mm} \times 10 \text{ mm}$ petri dish.

Then, the sample was heated within seconds to either 45 °C or 70 °C and loss of mass over time was recorded and plotted in a diagram using Origin 8.1G.

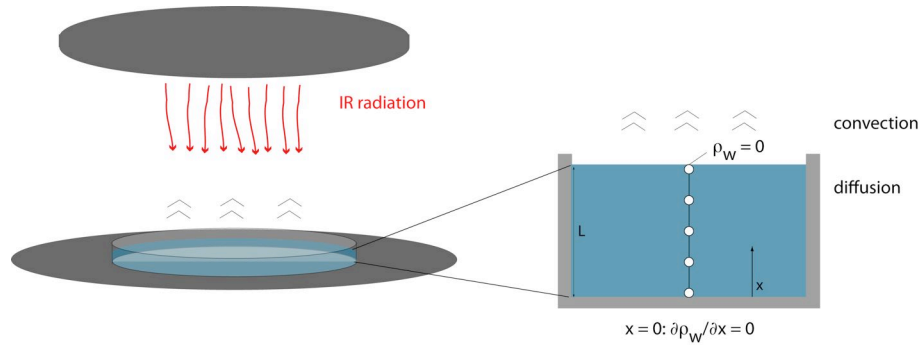


Figure 2.11 – Illustration of pan-weighing experiment setup and finite-element model of solvent removal [167].

The diffusion of water in the pan-weighing experiment can be considered as a one-dimensional process (see Figure 2.11) [167] best described by

$$\frac{\delta \rho_w}{\delta t} - \frac{\delta}{\delta x} \cdot [\rho_T \cdot D_{ss} \cdot \frac{\delta}{\delta x} \cdot \frac{\rho_w}{\rho_T}] = 0 \quad (2.15)$$

where ρ_w is the water partial mass density (concentration) [g/m³], x is the coordinate of the diffusion direction [m], ρ_T is the total mass concentration (total mass per unit volume of solution) [g/m³],

$$\rho_T = \rho_w + \rho_p \quad (2.16)$$

where ρ_p is the concentration of protein.

With mass concentrations ρ_i and time t [s] being measured during the experiment and x known from the petri dish dimensions, the internal water diffusion coefficient D_{ss} [m²/s] could be calculated for different concentrations of fibroin and (AQ)₂₄NR3 and temperatures in this work.

2.9.4 Application of solvent removal in biomimetic spinning experiments

Figure 2.12 illustrates both technical approaches for solvent removal tested in this study. A promising approach for solvent removal is based on the use of hygroscopic solutions, with common representatives being ethanol or polyethylene glycol. Hygroscopic solutions are able to attract water

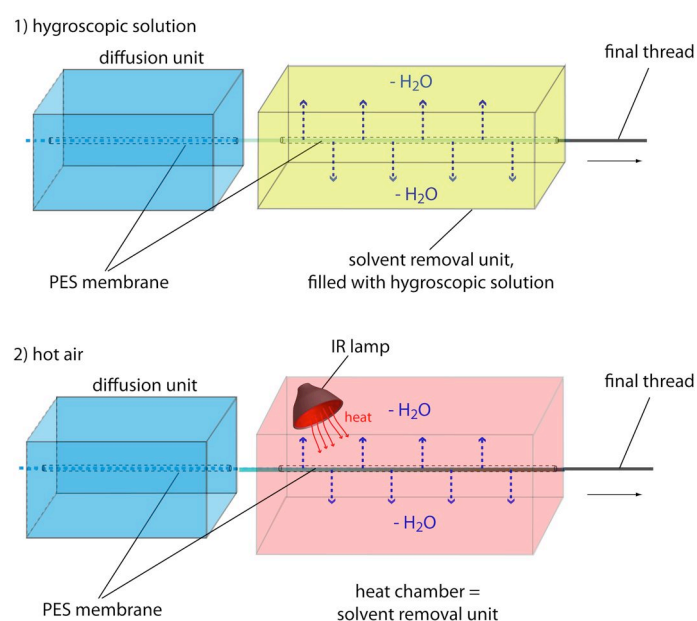


Figure 2.12 – Schematic overview of solvent removal procedures tested in this study: 1) using a unit filled with hygroscopic media, e.g. PEG or ethanol and 2) using an infrared lamp.

molecules from the surrounding environment through absorption or adsorption.

Solvent removal tests were conducted using PES membranes (MWCO = 10 kDa and 30 kDa) of 15 cm in length. Mounting those uncut membranes into the fourth generation diffusion unit (l = 10 cm) yielded a ~5 cm long membrane segment that overlapped the exit of the diffusion unit. This segment was then either placed in a small custom-built box filled with hygroscopic solutions or placed in a custom-built heat chamber, where an infrared lamp was applied to accelerate evaporation of water.

2.9.5 Mechanical characterization of natural and artificial silk fibers

2.9.5.1 Fiber preparation for tensile testing

Since the measurement of individual fibers yielded better data compared to bundles of fibers and furthermore the use of adjacent fibers resulted in reduced variability [25], a procedure to prepare individual fibers for tensile testing needed to be established. The collection of fibers on a frame that is mounted into a tensile testing apparatus has proven to be the most convenient and least manipulative method of preparing tensile test samples [278]. In literature, mostly paperboard or cardboard were used as frame material, especially with tests performed under dry conditions [25,

33, 34, 70, 195, 232, 238, 241, 246, 268, 279]. Frames were designed to define a certain gauge length by using a rectangular frame with either a circular hole [70, 268], or a rectangular hole in its center [195, 238, 241, 279] or by using a c-shaped form [232, 239, 240]. Fibers were then glued onto the frames using superglue [33, 232, 234, 239], all-purpose glue [70] or double-sided adhesive tape [238] with respect to a straight alignment. Proper specimen alignment is essential for high quality data, as misalignment between sample axis and loading direction may result in unwanted bending moment, giving rise to premature sample failure [278].

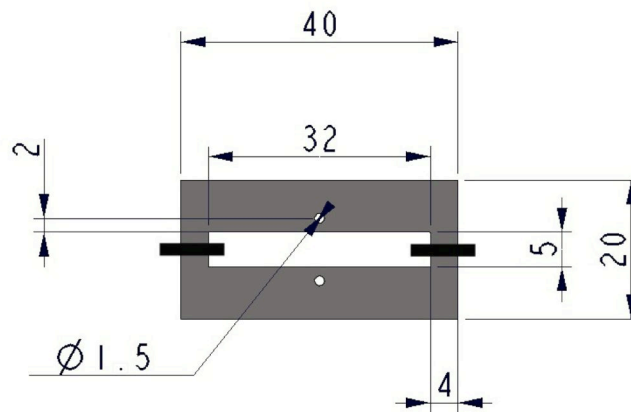


Figure 2.13 – Design of initial sample holder (shaded in grey for better illustration; numbers indicate dimensions given in mm).

Based on these descriptions, initial rectangular sample holders were manually prepared from a thick drawing paper using scissors or blades. The design of the sample holder followed the standard norm DIN 50125, describing the geometry of tensile testing samples for different materials. DIN 50125 defines the optimum ratio between sample length and diameter for a tensile testing specimen to be within the range of 5:1 to 10:1. For samples with very thin diameters, e.g. in the micron range such as natural spider silk fibers, this ratio is almost impossible to accomplish in practice. Consequently, sample holders were designed to define a gauge length of 5 mm (see Figure 2.13). For fixation of fibers, nail polish was used initially and the glue was applied to the edges of the hole to ensure that fiber length matches the defined gauge length. Proper fixation was monitored with a Zeiss 475002 stereo microscope, an easy method for fixation and alignment verification applied in other studies as well [280]. Fibers were measured within one day after collection and sample preparation to allow proper hardening of adhesive and to avoid any aging influences that were described by other groups [66, 255]. Prior to tensile testing, the sample holder mounted between the grips was cut along the black lines (see Figure 2.13), leaving the fiber as the only connection between movable and fixed body of the instrument. Therefore, any load measured

during tensile testing was a result of the fiber's resistance to deformation.

2.9.5.2 Installation and establishment of a tensile testing setup

For the mechanical characterization of natural and synthetic silk fibers as well as other artificial silk morphologies, amongst others a high precision tensile testing equipment compromising the control of environmental conditions needed to be installed at the chair. The evaluation of different tensile testing devices considered for installation at the chair is summarized in Table 7.1. A major drawback of using commercial tensile testing system for mechanical characterization is the lack of data accuracy, as these systems were typically designed to measure conventional samples, whose size and load-bearing capacity are at least an order of magnitude larger than that of silk fibers. Furthermore, it should be considered that the accuracy of load cells typically depends on the measurement regime it is assigned for, with the most accurate load cells (load resolution of 0.1 mN) are normally being assigned for the low Newton regime [278]. Due to the high elasticity of silk fibers compared to synthetic fibers, resulting in reasonable displacements during measurements, common commercial displacement actuators can be used. The BOSE Electroforce[®] 3220 system appeared to be a promising setup as it yielded, in contrast to the other devices, satisfactory load-displacement curves during initial testing. While most commercial tensile testing systems are based on servo-hydraulic or electro-mechanical motors, the BOSE Electroforce[®] is provided with a linear moving-magnet motor. This linear actuator is believed to offer several advantages compared to traditional setups, enabling the coverage of a broad test range of forces (nN to kN) and displacement (nm up to 25 mm) without loss of precision or efficiency [281]. Furthermore, this system also offered the potential to test a variety of other morphologies, such as films and non-woven, produced at the chair. The measurement accuracy for the BOSE Electroforce[®] 3220 was initially calibrated to $\pm 0.5\%$ of the measurement range prior to shipping, matching the precision requirements for this work.

Mechanical properties of natural silk fibers depend on environmental conditions, and in particular on humidity [66, 68, 242, 282]. As a consequence, a setup to control the humidity conditions during tensile testing was established. A specific saline bath chamber allowing temperature control in aqueous environments was purchased from Bose Electroforce[®] Inc. and successfully applied. A box with similar dimensions was custom-built using Macrolon[®] and used for humidity controlled experiments. The box was equipped with a removable front and top cover enabling easier access for sample mounting. To control humidity conditions inside this box, a microcontroller and sensor, a humidifier and a dehumidifier were purchased (Electro-Tech Systems, Inc.) and humidity could successfully be controlled between 0 % to 100 % relative humidity with an accuracy of 2 %

at room temperature (product information obtained from www.electrotechsystems.com).

2.9.5.3 Tensile testing

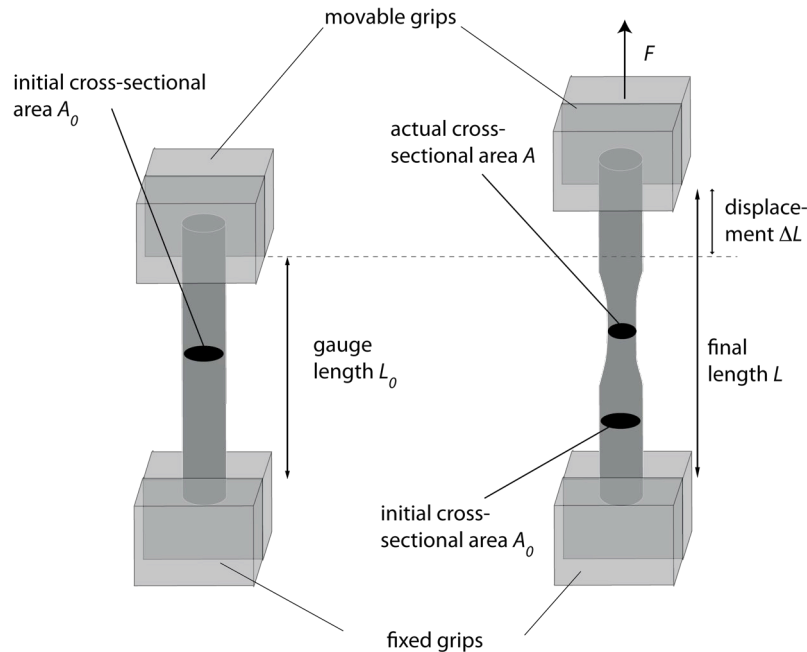


Figure 2.14 – Illustration of a tensile test procedure.

In a tensile test, the specimen is fixed between two grips of which one is movable while the other one is fixed (see Figure 2.14). The movable grip is displaced continually in axial direction of the specimen at defined rates away from the fixed grip resulting in a force acting on the specimen. A software records the signals obtained from the displacement transducer and the load cell.

Tensile tests were carried out using a BOSE Electroforce[®] 3220 instrument, equipped with a 250 gf (= 2.2 N) submersible load cell and custom-built flat grips. Initial tests with natural spider silk fibers revealed strong noise effects in the load displacement curves related to vibrations caused e.g. by the motor. For these influences, a noise reduction filter included in the WinTest[®] software was applied at 50 Hz and successfully improved the data. Consequently, the 50 Hz filter was applied in all future tensile testing measurements. Measurements were performed at a linear pulling rate of 0.05 mm s^{-1} at 30 % and 70 % relative humidity or in the presence of water.

Relative humidity was controlled in a custom-built chamber using a setup consisting of a Micro-controller and sensor unit, an ultrasonic humidifier and a dry gas dehumidification system. All samples were incubated for one hour to adopt to humidity conditions before each measurement, a

time frame supposedly sufficient enough for stabilization and adaptation of silk fibers to environmental conditions, since it was observed that water absorption takes place within a few seconds [76]. Measurements in the presence of water were performed in a commercial saline bath with samples being incubated for five minutes before testing, thus circumventing supercontraction effects during the measurement. Furthermore, the water bath was filled to a level so that the upper grip fixture did not have to pass through the water-air interface circumventing the build-up of surface tension forces much greater than the tensile forces to be measured [190].

Mechanical data were collected with WinTest[®] 4.1 and plotted as true stress - true strain curves using Origin 8.1G. True stress values were calculated instead of engineering stress values, since these values display more realistically the stress experienced by highly extensible fibers, such as spider silk (see Section 1.3.2.1). For data analysis, only fibers that showed the characteristic double breakage due to their bave structure were taken into account [283]. A determination of Young's modulus throughout this work was not pursued, since the elastic region was not reproducible for silk fibers in the low strain regime. Artificial fibers were plotted applying a polynomial fit of an order determined by best fit analysis (i.e. which polynomial fit achieved max R^2) using Origin 8.1G.

During tensile testing two sources for measurement errors were observed and are shown by exemplary stress-strain curves in figure Figure 2.15.

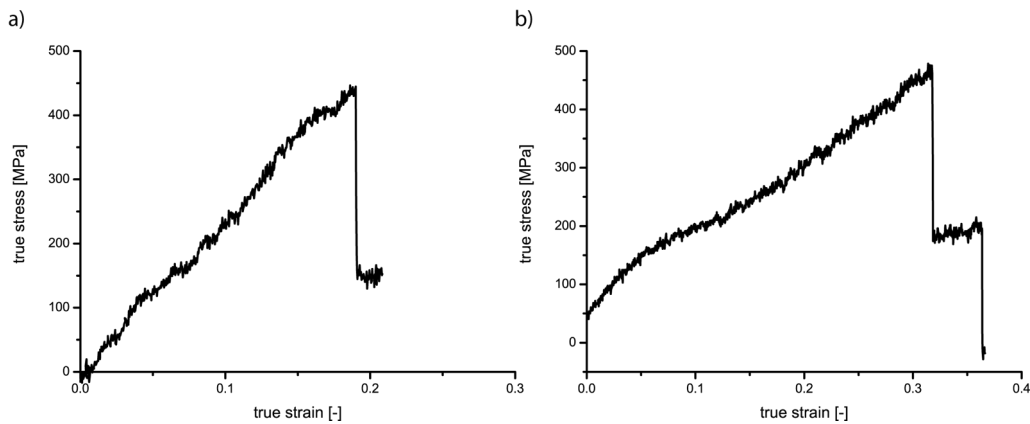


Figure 2.15 – Exemplary error sources during tensile testing: a) loose attachment of fiber and b) pre-loaded fiber

One potential source for measurement errors proved to be fibers that were loosely attached, i.e. fibers had a higher gauge length than the defined 2 mm. Upon application of load, response load did not increase although the fiber was elongated. However, this error could easily be corrected by adding the displacement measured before stress started to increase to the initial gauge length,

thus obtaining a new "corrected" gauge length. The other potential error source is caused by fibers that were fixed straight and under small tension. As a result, stress-strain curves of these specimen displayed a pre-stress behavior, indicated by stress values above zero at zero strain, and often also shown by stress values fallen below zero after breaking. Since the first error could easily be circumvented by correcting the gauge length, fibers in this study were mounted loose for tensile testing.

3 Results

3.1 Preparation and characterization of a concentrated aqueous silk spinning dope

3.1.1 Preparation of a concentrated solution from regenerated silk fibroin

RSF prepared according to the procedure described in Section 2.4.1 typically yielded aqueous solutions with concentrations between 1.2 % (w/v) and 3 % (w/v). Thereby, nearly 60 % of the initial bulk material was lost due the removal of insoluble impurities and low-molecular non-proteinaceous components. Moreover, ~ 20 % of raw silk were lost during the degumming and washing procedure as observed earlier [263].

The resulting concentrations between 1.2 % (w/v) and 3 % (w/v) are well below the range of 10 % (w/v) to 30 % (w/v) required for successful spinning. Yan and coworkers for instance have shown that concentrations between 13 % (w/v) and 19 % (w/v) were best suited for successful wet-spinning from RSF solutions [213]. As a consequence, two approaches to increase the concentration of the RSF solution were considered: 1) increasing the initial amount of raw silk or 2) increasing the concentration by applying suitable techniques. Due to the limited maximum solubility of silk fibers (~ 15 % (w/v) [263]) in $\text{CaCl}_2\text{--EtOH--H}_2\text{O}$, the first approach was discarded and the study was focused on the investigation of suitable concentration techniques. Table 3.1 summarizes the most commonly used techniques for preparation of concentrated protein or polymer solutions and the corresponding procedures tested in this work. Ultrafiltration is a prominent technique to concentrate polymer solutions but has been rather rarely used for shear sensitive silk solutions [204] due to the application of centrifugal forces or high pressure. Consequently, careful sample handling and processing conditions are inevitable to avoid premature aggregation when using this technique. Reverse dialysis is the most common concentration technique applied to silk solutions, enabling the achievement of high concentrations due to the application of low osmotic stresses [37, 176]. Other rarely applied methods to concentrate protein solutions (up to 20 % (w/v)) involve air-flow induced convection [45, 217] or the use of a chemical water absorbent agent.

Figure 3.1 shows that the simplest concentration technique involving commercially available ul-

3.1 Preparation and characterization of a concentrated aqueous silk spinning dope

Table 3.1 – Overview on common concentration techniques applied in literature and the corresponding procedure investigated in this work.

general technique	procedure
ultrafiltration [204, 284]	centrifugation with Vivaspin® 20 (MWCO 10 kDa)
solvent removal using a hygroscopic medium [176, 178, 213]	dialysis against 20 % (w/v) PEG (20 kDa)
solvent removal using dry air	evaporation, using dry air stream
solvent removal using a drying agent	Spectra/Gel® absorbent

trafiltration devices (e.g. Vivaspin® 20 centrifugal tubes) appears to be the most efficient one, reaching the desired concentration range within a couple of hours (at 4000 x g) [285]. Reverse dialysis processes using hygroscopic PEG solutions yielded fibroin concentrations between 10 % (w/v) and 30 % (w/v) within 10 hours (at room temperature) [176] or three days (at 5 °C) [178, 213]. These results indicate that reverse dialysis is a function of temperature as well as PEG concentration, so that both parameters had to be taken into account for this study. In order to reduce premature fibril formation of fibroin, the temperature for the reverse dialysis was selected to be 5 °C. To compensate for the lower temperature, PEG (20 kDa) concentration was raised to 20 % (w/v). In good agreement with earlier studies [178, 213], reverse dialysis required on average more than 20 hours to reach the desired concentration range [285]. Air-flow induced convective solvent removal and the Spectra/Gel® absorbent (data not shown) on the other hand appeared to be not useful to concentrate silk solutions for two reasons: a) both procedures provided significant challenges during sample handling and processing; and b) both procedures revealed a characteristic, extended lag phase (~20 h) without any increase in concentration, which ultimately led to a very long time until the desired concentration range was reached [285]. Moreover, once the lag phase was surpassed, the concentration increased very rapidly, usually resulting in the formation of aggregates.

3.1.2 Preparation of a concentrated spinning dope from recombinant (AQ)₂₄NR3

Table 3.2 – Summary of conditions tested for preparation of aqueous (AQ)₂₄NR3 solutions.

denaturant	dialysis conditions
8 M urea	10 mM Tris/HCl, pH8
6 M GdmSCN	10 mM Tris/HCl, pH8
	10 mM Tris/HCl, pH8, 100 mM NaCl
	10 mM Tris/HCl, pH8, 100 mM NaCl & 10 mM sodium cholate

Aqueous solutions of (AQ)₂₄NR3 were prepared as described in Section 2.4.2. Table 3.2 sum-

3.1 Preparation and characterization of a concentrated aqueous silk spinning dope

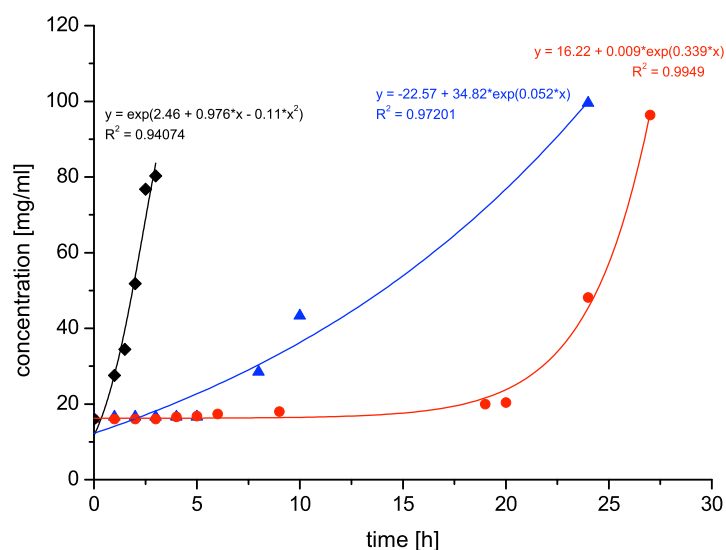


Figure 3.1 – Concentrating aqueous fibroin solutions by ultrafiltration at 4000 x g (black diamonds), PEG (20 % (w/v), 5 °C) dialysis (blue triangles) and solvent removal by air-flow induced convection (red circles).

marizes the dissolving and dialysis conditions tested in this study. (AQ)₂₄NR3 was shown to be intrinsically soluble in aqueous solutions at concentrations below 5 % (w/v) [160] due to its more hydrophilic repetitive sequence [185]. However, during preparation, significant amounts of (AQ)₂₄NR3 were lost due to aggregation throughout the dialysis step. Moreover, earlier studies showed that (AQ)₂₄NR3 solutions experience liquid-liquid phase separation into a protein-poor and a protein-rich phase within one day, if solution concentration is above 4 % (w/v) and the temperature is below 10 °C [161]. This characteristic feature imposes a great challenge to the technical spinning process, by requiring an additional step for the separation of the protein-rich from the protein-poor phase. During initial tests regarding the dialysis conditions for preparation of (AQ)₂₄NR3 solutions (Table 3.2), it was observed that the addition of 10 mM sodium cholate (a mild ionic detergent) to the dialysis buffer reduced the probability of phase separation and significantly enhanced (AQ)₂₄NR3 stability in aqueous solutions. Aqueous solutions of (AQ)₂₄NR3 could be stored for up to two weeks at 4 °C without visible aggregation or phase separation. As a consequence, throughout this work, aqueous (AQ)₂₄NR3 solutions with high concentrations, e.g. for spinning or rheology studies, were prepared using dialysis buffer C (see Section 2.1.2).

Similar to RSF solutions, the successful spinning of fibers from aqueous (AQ)₂₄NR3 solutions required concentrations in the range of 10 % (w/v) to 20 % (w/v).

3.1 Preparation and characterization of a concentrated aqueous silk spinning dope

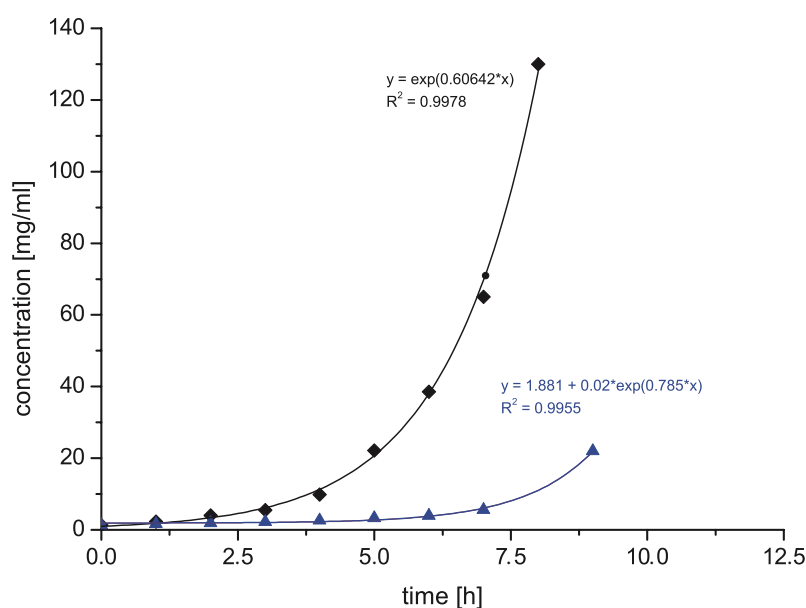


Figure 3.2 – Concentrating aqueous (AQ)₂₄NR3 solutions by ultrafiltration at 4000 x g (black diamonds) or PEG (20 % (w/v), 5 °C) dialysis (blue triangles) [285] (Permission for reprint granted by Green Materials, ICE Publishing).

As Figure 3.2 indicates, concentrating an aqueous (AQ)₂₄NR3 solution showed similar behavior in comparison to a RSF solution (see Section 3.1.1). Once again, reverse dialysis against a 20 % (w/v) PEG (20 kDa) solution required significantly long enough time to achieve the desired level of protein concentration [285]. In order to avoid aggregation as observed for RSF solutions, PEG dialysis experiments were usually stopped after 10 hours. Based upon the results obtained with RSF solutions (see Section 3.1.1) solvent removal by air-flow induced convection and via application of a water absorbent were not considered for (AQ)₂₄NR3 solutions. On the other hand, the application of Vivaspin[®] 20 ultrafiltration centrifugal tubes again proved to be the most efficient method [285]. Centrifugation for 6 hours resulted in concentrations in the range of 10 % (w/v) to 15 % (w/v). However, the concentration process was still hampered by a relatively low reproducibility. The factor by which the concentration of an aqueous (AQ)₂₄NR3 solution ($c_0 = 1.4$ % (w/v)) increased after 6 hours was determined to be 2.72 ± 0.85 , with the deviation corresponding to a variability of ~ 30 %.

It should be pointed out that centrifugation at temperatures below 10 °C frequently resulted in liquid-liquid phase separation, while at centrifugation above 17 °C no liquid-liquid phase separation was observed. Moreover, even after performing the concentrating procedures above 17 °C, (AQ)₂₄NR3 solutions in dialysis buffer C maintained their stability against aggregation and phase separation upon storage at 4 °C. The procedure for preparation of a concentrated aqueous

3.1 Preparation and characterization of a concentrated aqueous silk spinning dope

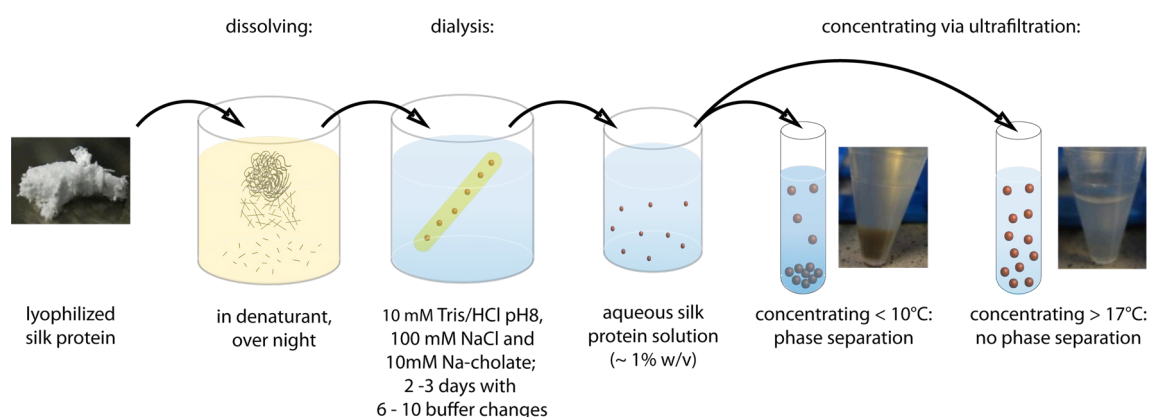


Figure 3.3 – Procedure for preparation of a concentrated aqueous (AQ)₂₄NR3 solution.

(AQ)₂₄NR3 solution is summarized in Figure 3.3.

3.1.3 Analysis of the effects of stabilizing agents on the stability of (AQ)₂₄NR3 solutions

As shown in the previous section, the preparation of concentrated spinning dopes from (AQ)₂₄NR3 was hampered by solution stability. To improve solution stability, stabilizing agents were added and their effects were investigated at room temperature (see Table 2.5).

The addition of sorbitol as shown in Figure 3.4a) did not significantly affect the stability of (AQ)₂₄NR3 at sorbitol concentrations of 10 % (w/v) and 20 % (w/v). However, (AQ)₂₄NR3 stability was reduced by nearly 30 % if more than 30 % (w/v) sorbitol were added. These results are in good agreement with other studies on the effects of sorbitol on protein stability [286] (and references therein). The addition of PEG at concentrations above 2 % (w/v) significantly reduced stability of (AQ)₂₄NR3 by more than 75 %, while at PEG concentrations below 2 % (w/v), reduction was only 20 % (Figure 3.4b). This finding is in good agreement with studies on interactions between PEG and protein [287] (and references therein). The addition of an equimolar arginine and glutamic acid solution had only little effect on the stability of (AQ)₂₄NR3 (Figure 3.4c). The addition of TMAO also reduced protein stability with increasing additive concentration (Figure 3.4d). Strikingly, the stability of (AQ)₂₄NR3 was observed to increase between day 1 and day 14 for 1 M TMAO, probably caused by a delayed solution equilibrium between (AQ)₂₄NR3 and TMAO. The addition of urea revealed a very slight reduction in (AQ)₂₄NR3 stability, usually below 10 % (Figure 3.4e). This result is in good agreement with earlier observations and confirms the assumption that urea at lower concentrations stabilizes a protein [287, 288]. A mixed solution containing 0.2 M TMAO and 0.4 M urea showed a behavior similar to that of its individual components, although it

3.1 Preparation and characterization of a concentrated aqueous silk spinning dope

appears that urea was the dominating additive in this mixture.

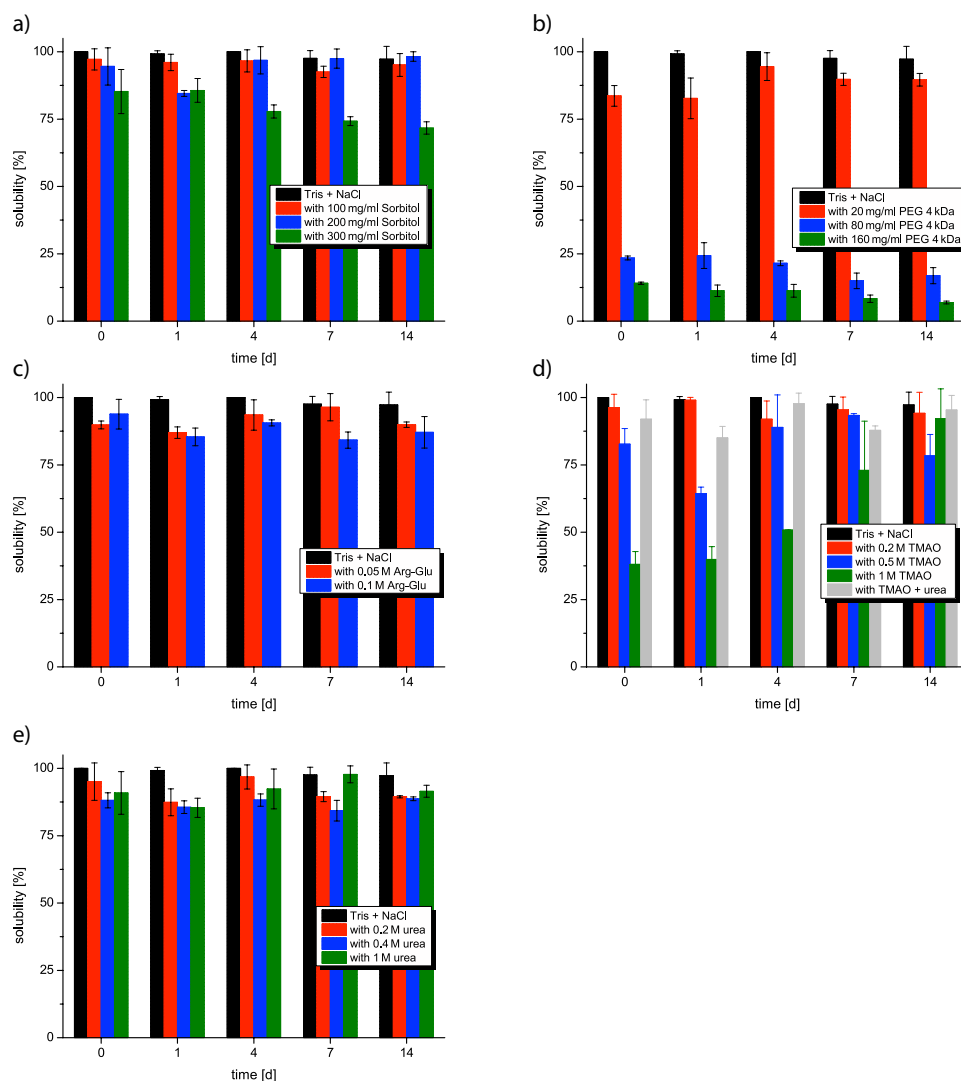


Figure 3.4 – Influence of stabilizing agents on the solution stability of aqueous (AQ)₂₄NR3 as determined by UV spectroscopy: a) Sorbitol, b) PEG, c) Arg-Glu, d) TMAO and e) urea.

In general, Figure 3.4 reveals, that the addition of stabilizing agents reduced (AQ)₂₄NR3 solution stability over time, with a positive correlation with additive concentration. These data are confirmed by the SEM images of some films cast from solutions containing exemplary additives (Figure 7.1), indicating that the presence of both (AQ)₂₄NR3 and solubility additive in a binary solution significantly affected their individual solution stability in water.

3.1 Preparation and characterization of a concentrated aqueous silk spinning dope

3.1.4 Rheological characterization of flow behavior of aqueous (AQ)₂₄NR3 and RSF solutions

A highly concentrated silk solution is one prerequisite for successful fiber spinning, but an additional attribute for qualitative silk "spinnability" and fiber production is the flow behavior of the silk solution, usually assessed by rheometry [211], and displayed in form of a viscosity against shear rate curve. In the following, the flow behavior of RSF and (AQ)₂₄NR3 solutions with different concentrations is analyzed in detail.

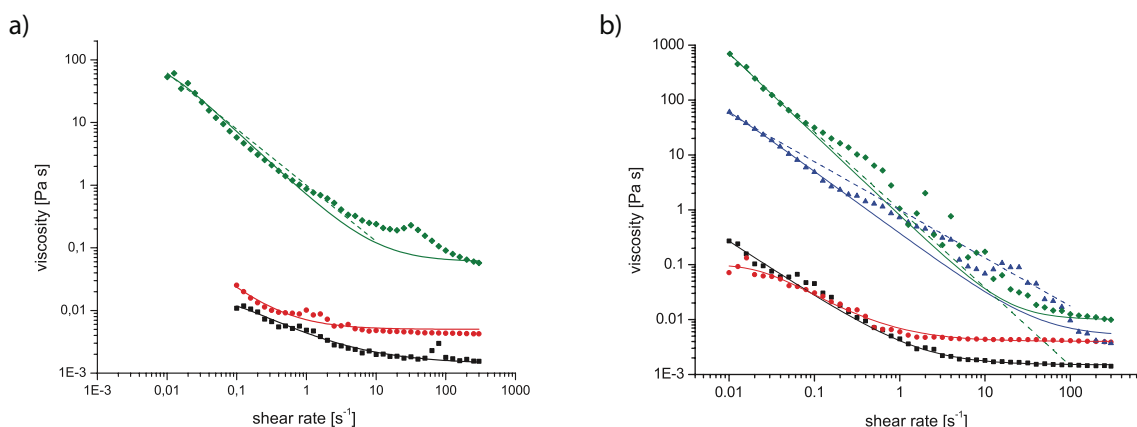


Figure 3.5 – Rheological behavior of a) (AQ)₂₄NR3 solutions of different concentrations (black squares = 1.5 % (w/v), red circles = 3 % (w/v) and green diamonds = 13 % (w/v)) and b) RSF solutions of different concentrations (black squares = 1.5 % (w/v), red circles = 6 % (w/v), blue triangles = 15 % (w/v) and green diamonds = 22 % (w/v)); the straight line illustrates a Carreau-Yasuda fit, the dotted line a Power Law fit [285] (Permission for reprint granted by Green Materials, ICE Publishing).

Figure 3.5 displays a strong concentration dependence of flow behavior for aqueous (AQ)₂₄NR3 and RSF solutions, which is in good agreement with studies on polymer solutions and earlier measurements of RSF solutions [14, 30, 211] and natural silk dope [211]. It should be noted that the rheological curves measured in this study showed considerable variability between the samples as observed in earlier studies, assumed to be caused by shear history effects induced upon sample loading [133].

Apart from their concentration dependence, the flow curves of the silk solutions also displayed one of the most common rheological features of complex (non-Newtonian) fluids: shear thinning behavior as shown by a nonlinear relationship between shear stress σ and shear rate $\dot{\gamma}$. Most polymeric systems typically display a decrease in steady shear viscosity $\eta_{\dot{\gamma}}$ (i.e. the ratio of the measured shear stress to the imposed shear rate at steady state) with increasing deformation rate due to increasing flow-alignment of the underlying microstructure [188]. Aqueous (AQ)₂₄NR3

3.1 Preparation and characterization of a concentrated aqueous silk spinning dope

solutions of 1.5 % (w/v) and 3 % (w/v), as well as aqueous RSF solutions of 1.5 % (w/v) and 6 % (w/v) displayed shear thinning behavior in the low shear rate region ($<1 \text{ s}^{-1}$) [285]. This result is in agreement with data obtained for diluted *Nephila* silk dope solutions with concentrations below 1 % (w/v) [121], but is in contrast to earlier studies on reconstituted silk solutions exhibiting Newtonian-like flow behavior [172, 211]. Interestingly, with increasing shear rates, the shear thinning became less pronounced and shifted towards a shear rate independent, so-called Newtonian behavior at shear rates above 10 s^{-1} [285]. The flow characteristics of shear thinning followed by a transition to Newtonian behavior with increasing shear rates can be best described by the Carreau-Yasuda equation [226, 289]. The Carreau-Yasuda model considers the rate of creation and destruction of molecular entanglements in concentrated polymer solutions or melts:

$$\eta(\dot{\gamma}) = \eta_{\infty} + (\eta_0 - \eta_{\infty}) \cdot [1 + (\dot{\gamma} \cdot \lambda)^a]^n \quad (3.1)$$

with η_{∞} being the viscosity at infinitively high shear rate [Pas], η_0 being the zero shear viscosity, $\dot{\gamma}$ being the shear rate, λ being the relaxation time of the viscoelastic fluid (its inverse is the critical shear rate marking the onset of shear thinning) [s], n being the power-law exponent characterizing the shear thinning regime observed at high shear rates, and a describing the rate of transition between the zero shear-rate region and the power-law region.

In contrast, concentrated aqueous silk solutions ($>10 \text{ % (w/v)}$) displayed a strong power-law shear thinning behavior between shear rates of 0.01 s^{-1} and 10 s^{-1} characteristic for natural silk dopes and molten polymers [133, 211, 285]:

$$\eta = K \cdot (\dot{\gamma})^b \quad (3.2)$$

with η being the viscosity, $\dot{\gamma}$ being the shear rate and K and b being fitting parameters [225].

In earlier studies on native silk dopes, a simple linear relationship between stress and rate (i.e. the fluid approaches the limit of a simple Newtonian fluid) at low shear rates was detected, and the steady shear viscosity approached a constant value defined as the zero-shear rate viscosity η_0 [44, 133, 188, 211, 227]. However, in this work, this behavior could not be assessed due to technical limitations of the setup in the very low shear regime and thus was estimated via non-linear regressions.

Non-linear regression of Carreau - Yasuda parameters for (AQ)₂₄NR3 and RSF solutions yielded values characteristic for a shear thinning fluid [289]. Table 3.3 reveals that the rate of shear thin-

3.1 Preparation and characterization of a concentrated aqueous silk spinning dope

Table 3.3 – Fitting parameters of silk solutions obtained in this work compared with parameters of natural silk solutions described in literature.

Sample	Carreau - Yasuda model		Power - Law model	
	zero-shear viscosity [Pa s]	n	a	b
1.5 % (w/v) (AQ) ₂₄ NR3	0.016	- 0.30	2.0	
3 % (w/v) (AQ) ₂₄ NR3	1.4	- 0.05	17.8	
13 % (w/v) (AQ) ₂₄ NR3	92.1	- 0.52	2.0	-0.89
1.5 % (w/v) fibroin	172.3	- 0.50	2.0	
6 % (w/v) fibroin	0.1	- 0.54	2.0	
15 % (w/v) fibroin	443	- 0.95	1.2	-0.88
22 % (w/v) fibroin		- 0.74	2.0	-1.42
<i>N. clavipes</i> gland extract [188]	3500	0.18	0.7	
<i>N. clavipes</i> native dope [133]				-0.61
<i>B. mori</i> native dope [133]				-0.78

ning for the 13 % (w/v) (AQ)₂₄NR3 solution following the power-law trend with $b = -0.895$ and for the 15 % (w/v) RSF solution with $b = -0.88$ [285] corresponds well with data obtained for native silk dopes from spiders ($b = -0.61$) and from silkworms ($b = -0.78$) [133]. However, the zero-shear viscosity estimated via non-linear regression of a 13 % (w/v) (AQ)₂₄NR3 solution (<100 Pa s) and a 15 % (w/v) RSF solution (450 Pa s) [285] is orders of magnitude lower than that determined for natural silk dopes in earlier studies (2000 Pa s to 5000 Pa s) [44, 188]. This can be explained by the fact that η_0 increases almost exponentially with increasing protein concentration [30, 36]. The deviating parameter values for 3 % (w/v) (AQ)₂₄NR3 and 1.5 % (w/v), and in particular the low η_0 measured for 6 % (w/v) RSF as well as the extremely high η_0 measured for 22 % (w/v) RSF are likely caused by fitting inaccuracies due to data scattering in the low shear regime. The critical shear rate for the onset of shear thinning observed in recent studies on natural silk dopes was typically in the range of 0.5 s^{-1} to 4 s^{-1} [44, 133, 188, 227]. Measurements in this work revealed shear thinning right from the beginning, with critical shear rates starting at $\sim 0.01 \text{ s}^{-1}$ [285].

3.1 Preparation and characterization of a concentrated aqueous silk spinning dope

3.1.5 Analysis of the effects of polymeric additives on the viscosity of (AQ)₂₄NR3 solutions

The viscosities of the engineered dopes obtained within the range of feasible protein concentrations were below those measured for natural silk dopes. This will likely result in mechanical properties of spun fibers being inferior than natural fibers, since higher viscosity induces a higher degree of molecular chain orientation which yields higher mechanical strength of the fiber [26]. Since polymer solution viscosity positively correlates with the molecular weight of the polymer, viscosity can be increased by using higher molecular weight polymer additives [37, 175, 290, 291]. Thus it was tested whether polymer additives support the preparation of concentrated silk dopes for fiber spinning. In recent attempts, aqueous silk solutions were successfully blended with high molecular weight polymers, e.g. PEG, improving spinnability of regenerated silk solutions, in particular for electrospinning [37, 175, 290, 291]. In general, spinnability of a solution can be improved by increasing the extensional viscosity of the fluid and by preventing the capillary break-up of fluid jets [188].

Preliminary tests revealed that the addition of polymers which require strongly acidic conditions for their solubilization, such as poly acrylonitrile (PAN), chitosan and viscose [292, 293], was detrimental as their addition lowered the pH value of the (AQ)₂₄NR3 solution leading to protein aggregation [63, 160]. Therefore, only polymers were used that could be readily dissolved in water (see Table 3.4).

Fibers were successfully wet-spun from blends of *B. mori* fibroin and PVA, a cheap, water-soluble, non-toxic, biocompatible and degradable polymer. Blending an aqueous silk solution with up to 50 % (w/v) of PVA was shown to increase the tenacity and elongation at break of the fibers (at the expense of the breaking strength) [216].

Upon blending polymeric additives with (AQ)₂₄NR3 solutions, two observations were made: 1) the total sample volume was lower than expected from the theoretical addition of both initial volumes; and 2) with the exception of alginate, PAA (5 MDa) and glycerol, all blend solutions showed significant co-aggregation of polymer and protein. The first observation can be explained by the thermodynamic properties of real mixtures, in which an excess molar volume effect leads to a volume reduction [294]. As a consequence, the final silk and polymer concentrations are higher than their initial concentrations, as determined for (AQ)₂₄NR3 concentrations in blends with alginate, PAA (5 MDa) and glycerol (using UV spectroscopy, see Table 3.4). Strikingly, the increase in concentration is equal for all three blends, giving rise to the assumption that the thermodynamic effects in those mixtures were similar. The second observation, co-aggregation, is confirmed by the significant decrease of (AQ)₂₄NR3 concentrations shown in Table 3.4. Polymer

3.1 Preparation and characterization of a concentrated aqueous silk spinning dope

Table 3.4 – Overview of blends prepared from aqueous 3% (w/v) (AQ)₂₄NR3 solutions and polymeric additives.

polymer	polymer/ (AQ)₂₄NR3 [% (v/v) /% (v/v)]	(AQ)₂₄NR3 [% (w/v)]	blend density ρ [g cm⁻³]
25 % (w/v) PEG (35 kDa) ($\rho = 1.2 \text{ g cm}^{-3}$)	20/80	0.6	1.179
	50/50	0.6	1.195
	80/20	0.5	1.199
2.5 % (w/v) PEG (600 kDa) ($\rho = 1.21 \text{ g cm}^{-3}$)	20/80	1.4	1.057
	50/50	1.2	1.133
	80/20	1.1	1.187
100 % (w/v) Glycerol ($\rho = 1.261 \text{ g cm}^{-3}$)	20/80	4.1	1.216
	50/50	n.a.	1.248
	80/20	n.a.	1.258
50 % (w/v) PAA (10 kDa) ($\rho = 1.189 \text{ g cm}^{-3}$)	20/80	1.1	1.171
	50/50	2.6	1.178
	80/20	0.6	1.188
2.5 % (w/v) PAA (5 MDa) ($\rho = 0.75 \text{ g cm}^{-3}$)	20/80	4.2	0.958
	50/50	n.a.	0.888
	80/20	n.a.	0.809
15 % (w/v) PVA ($\rho = 1.25 \text{ g cm}^{-3}$)	20/80	1.1	1.183
	50/50	0.8	1.235
	80/20	0.6	1.247
2 % (w/v) alginate ($\rho = 0.56 \text{ g cm}^{-3}$)	20/80	4.0	0.921
	50/50	n.a.	0.795
	80/20	n.a.	0.658

concentrations after mixing, however, could not be assessed in this study, but based on the findings above, the same assumptions for polymer concentration might be appropriate. The observation of co-aggregation is in good agreement with other studies on silk-polymer blends, in which macroscopic phase separation in presence of PAA [295] or pronounced gelation in presence of PEG [175, 290] were observed. The formation of specific intermolecular interactions between silk and added polymer e.g. via hydrogen bonds accounted for the observed mixing behavior and resulting blend properties [295] (and references therein). The strong propensity of lower molecular weight PEG to interact with (AQ)₂₄NR3, as indicated by the strongest reduction of (AQ)₂₄NR3 concentration (Table 3.4), had also been observed for mixtures of PEG and silk fibroin. Upon addition of PEG (3.4 kDa) a macroscopic phase separation occurred, while upon addition of PEG (900 kDa), no such macroscopic phase separation was observed [296]. The strong decrease in (AQ)₂₄NR3 concentration upon addition of PVA (Table 3.4), could be related to a potential water immiscibility of silk and PVA, already observed for fibroin and PVA blends by Lee and coworkers [216]. In contrast to earlier studies, the addition of alginate did not result in aggregation due to intermolecular hydrogen bonds, since the alginate concentration used in this study was significantly lower (2 % (w/v) compared to nearly 30 % (w/v)) [262].

3.1 Preparation and characterization of a concentrated aqueous silk spinning dope

Table 3.4 also summarizes the densities of (AQ)₂₄NR3 and polymer blends required for rheological measurements, calculated using the following relationship for ideal binary mixtures

$$\rho = \frac{c}{V} = \frac{c_1 + c_2}{V_1 + V_2} = \frac{c_1 + c_2}{\frac{c_1}{\rho_1} + \frac{c_2}{\rho_2}} \quad (3.3)$$

with c being the mass concentration [% (w/v)] and V the solution volume [m³] and ρ being the density [g cm⁻³]; indices 1 and 2 symbolize the individual solutions.

Figure 3.6 reveals that water-soluble polymers increased the viscosity of the initial (AQ)₂₄NR3 solution significantly (up to three orders of magnitude) [285]. In general, it was expected that the increase in viscosity of the blends was more pronounced with increasing polymer content as shown for silk-PEG blends (Figure 3.6a and b)). However, numerous deviations of this behavior (Figure 3.6c-g)) were observed in this study, most noticeably for mixtures of PVA and (AQ)₂₄NR3. The deviations are likely a result of phase separation or aggregation described above.

3.1.6 Rheological characterization of the viscoelastic behavior of aqueous (AQ)₂₄NR3 and regenerated fibroin solutions

Oscillating the dope samples over a range of frequencies at a small strain amplitude (0.001) allows the analysis of dope structure and behavior, as well as a material's response to energy input over different periods of time and environmental conditions [211, 225]. The relationship between applied stress and resulting strain can be used to calculate elastic G' (storage) and viscous G'' (loss) moduli [133].

Figure 3.7 describes the angular frequency (ω) dependence of G' and G'' for aqueous solutions of (AQ)₂₄NR3 and RSF. At low concentrations (below 5 % (w/v)) a gel-like behavior was detected for (AQ)₂₄NR3, as shown by frequency independence of storage modulus (indicated by a plateau between angular frequencies 2 rad s⁻¹ and 10 rad s⁻¹) and $G' > G''$ [285]. This data is in good agreement with RSF solutions of ~1.4 % (w/v) [297], diluted samples of native silkworm dope (~4.5 % (w/v)) [36, 211] and cross-linked hydrogels produced from 2 % (w/v) solutions of eADF4(C16) [298]. In contrast to previous studies of RSF [297] or native silk dope [36, 211], the dilute solutions in this study did not display a crossover point.

At concentrations above 5 % (w/v), the aqueous silk solutions showed frequency dependence, including a crossover point at an angular frequency of 15 rad s⁻¹ to 30 rad s⁻¹ [285]. This data is in good agreement with data on native spider silk dopes ($c = 18.6$ % (w/v)) [211] and silkworm

3.1 Preparation and characterization of a concentrated aqueous silk spinning dope

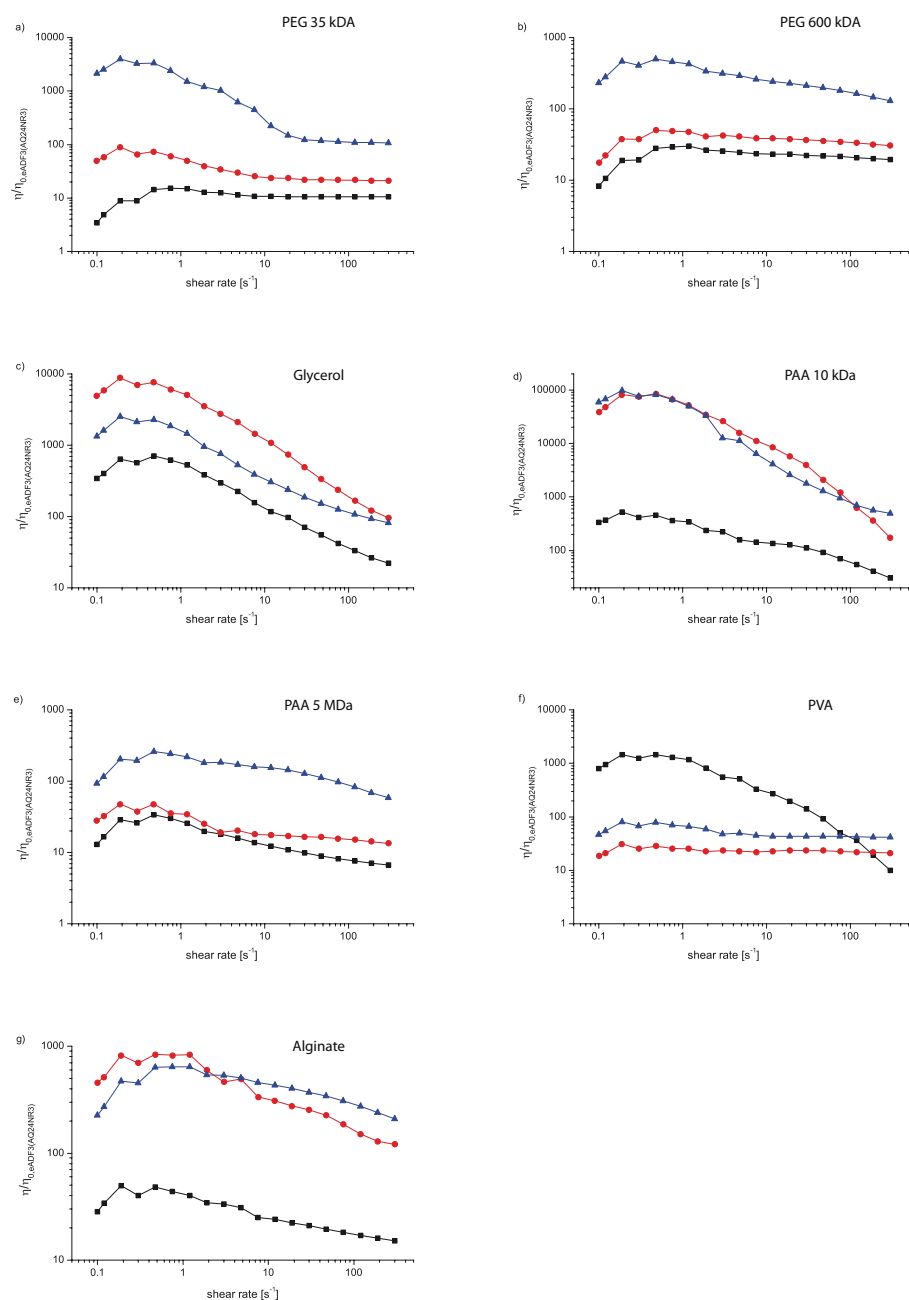


Figure 3.6 – Influence of polymeric additives on the rheological behavior of the 3 % (w/v) (AQ)₂₄NR3 solutions. A) PEG 35 kDa, b) PEG 600 kDa, c) Glycerol, d) PAA 10 kDa, e) PAA 5 MDa, f) PVA and g) Alginate (curves display rheological behavior of blends from 3 % (w/v) (AQ)₂₄NR3 and polymer stock solution with different volume ratios: black squares = ratio of silk and polymer of 80/20; red circles = 50/50 and blue triangles = 20/80) [285] (Permission for reprint granted by Green Materials, ICE Publishing).

3.1 Preparation and characterization of a concentrated aqueous silk spinning dope

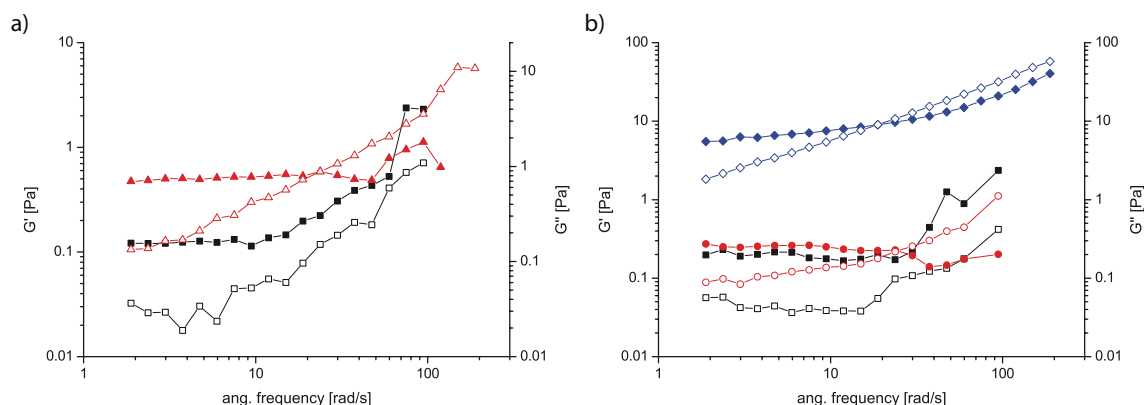


Figure 3.7 – Viscoelastic behavior as determined by oscillatory frequency sweeps performed at 1 Hz of a) engineered (AQ)₂₄NR3 solutions of different concentrations (black squares = 2 % (w/v), red triangles = 15 % (w/v)) and b) regenerated fibroin solutions of different concentrations (black square = 2 % (w/v), red circle = 5 % (w/v) and blue diamond = 15 % (w/v)); filled symbols symbolize storage modulus G' and open symbols symbolize loss modulus G'' [285] (Permission for reprint granted by Green Materials, ICE Publishing).

native dopes ($c = 25$ % (w/v)) [44]. Concentrated (AQ)₂₄NR3 and RSF solutions displayed a solid-like response over long timescales (low ω) with $G' > G''$ and G' independent of frequency. At the crossover point, a liquid-like response could be detected at shorter timescales (high ω) with $G' < G''$ and frequency-dependent G' . These observations are in contrast to concentrated native silk dopes which responded like a liquid at long timescales and displayed frequency-dependent moduli below the crossover point. Above the crossover point the moduli were relatively independent of frequency and the dopes responded more like a solid [44, 133, 211, 227]. Concentrated RSF were also observed to reveal $G'' > G'$, however these solutions typically lacked the crossover point [211, 297].

3.1.7 Analysis of the effects of salt on the rheological behavior of (AQ)₂₄NR3 and RSF solutions

During the natural spinning process, the silk dope undergoes a conformational transformation (microscopic) that results in a liquid-solid transition (macroscopic) upon exposure to acidification, ion exchange and a combination of shear and extensional flow. In the following section, the effects of salt in combination with shear flow on the silk spinning dope are investigated by rheology.

The addition of kosmotropic salts affected the rheological behavior and viscosity of (AQ)₂₄NR3 solutions, while upon addition of chaotropic chloride ions the rheological flow behavior remained unaffected apart from the decrease in viscosity due to diluting effects Figure 3.8 [285]. The addi-

3.1 Preparation and characterization of a concentrated aqueous silk spinning dope

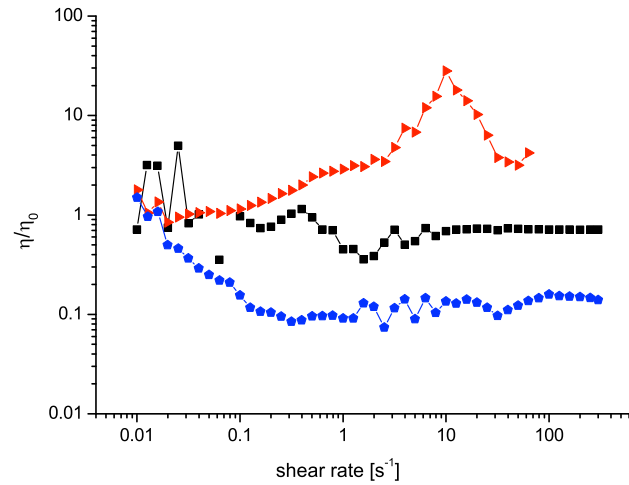


Figure 3.8 – Influence of salt addition on rheological behavior of recombinant (AQ)₂₄NR3 solutions. For better illustration, data is presented as a ratio of (AQ)₂₄NR3 with salt and initial (AQ)₂₄NR3 solution without salt $\frac{\eta}{\eta_0(AQ_{24NR3})}$, with η_0 (AQ₂₄NR3) being the viscosity of the initial (AQ)₂₄NR3 solution without salt added. (black squares: 2.2 % (w/v) (AQ)₂₄NR3 and 0.2 M PO₄[−]; red triangles: 15 % (w/v) (AQ)₂₄NR3 and 0.5 M PO₄[−] and blue pentagons: 15 % (w/v) (AQ)₂₄NR3 and 0.2 M NaCl) [285] (Permission for reprint granted by Green Materials, ICE Publishing).

tion of 0.5 M PO₄[−] to a 15 % (w/v) (AQ)₂₄NR3 solution induced pronounced shear thickening and increased viscosity confirming earlier studies [121, 180]. Upon addition of 0.2 M PO₄[−] to a 2.2 % (w/v) (AQ)₂₄NR3 solution, viscosity was only slightly affected shown by similar η and η_0 values over the whole shear rate regime although diluting effects had to be accounted. However, the shear thickening displayed upon addition of 0.5 M PO₄[−] was not observed in this case. This result confirms earlier findings that a minimum PO₄[−] concentration of 0.3 M is necessary to induce the formation of higher order protein structures that are a prerequisite for successful fiber formation [180].

3.1.8 Analysis of the effects of temperature on the rheological behavior of (AQ)₂₄NR3 and RSF solutions

The influence of temperature on natural silk spinning and the resulting silk material has been investigated in several studies, with observations often being related to the effects of temperature on the silk spinning dope [133, 191].

Figure 3.9a) reveals the influence of temperature on the rheological behavior of concentrated

3.1 Preparation and characterization of a concentrated aqueous silk spinning dope

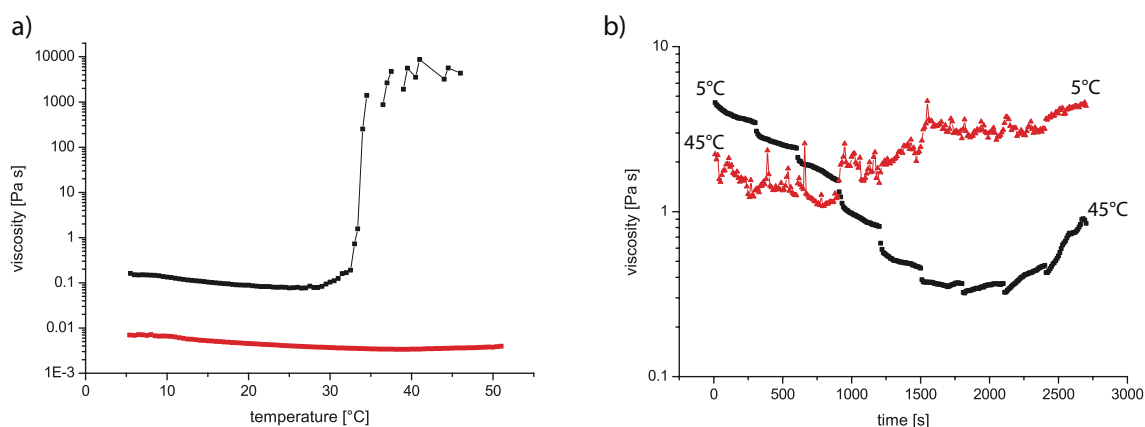


Figure 3.9 – Temperature-dependent rheological behavior of recombinant (AQ)₂₄NR3 and RSF solutions. a) influence of temperature on 15 % (w/v) (AQ)₂₄NR3 (black) and 20 % (w/v) RSF solution (red) b) temperature sweep of a 3 % (w/v) (AQ)₂₄NR3 solution (black: temperature was increased from 5 °C to 45 °C in steps of 5 °C every 5 minutes, red: temperature was decreased from 45 °C to 5 °C in steps of 5 °C every 5 minutes) [285] (Permission for reprint granted by Green Materials, ICE Publishing).

(AQ)₂₄NR3 and RSF solutions [285]. Interestingly, RSF solutions did not appear to be affected by temperature up to 50 °C, while the 15 % (w/v) (AQ)₂₄NR3 solution displayed a sudden increase in viscosity at a temperature of ~ 35 °C. The latter observation is in good agreement with results on the lower critical solution temperature (LCST) behavior for (AQ)₂₄NR3 [161]. The LCST is the critical temperature below which a polymer mixture is completely miscible; at temperatures above the LCST, aggregation has been observed. The formation of such aggregates likely leads to the sudden increase in viscosity. Furthermore, the sigmoidal shape and the critical transition temperature (T_m) observed for concentrated (AQ)₂₄NR3 had also been observed for native silkworm dope [133, 227].

Figure 3.9b) shows that the typical Arrhenius temperature dependence of viscosity [299] shifted towards a viscosity increase around ~ 2000 s, which corresponds to the aforementioned critical transition temperature range [285]. However, the temperature sweep curve also revealed that the shift towards increase in viscosity at the transition temperature is weaker for dilute (AQ)₂₄NR3 solutions. These differences correlate with the observation that MA silk at low concentration was predominantly random coil with a high T_m , while at high concentration the silk dope was dominated by helical structures with a low T_m [132]. Furthermore, the temperature effects are less pronounced upon cool down (red curve) as indicated by a weaker slope compared to the heat-up (black) curve.

3.1 Preparation and characterization of a concentrated aqueous silk spinning dope

3.1.9 Analysis of the effects of time on the rheological behavior of (AQ)₂₄NR3 and RSF solutions

Finally, the time-dependent behavior of silk solutions was investigated using a CSR loop test in order to give a relative measure of extent and speed of recovery of silk's internal structure during and after shear.

Dilute silk solutions displayed the characteristic time-independent behavior for Newtonian fluids (Figure 3.10a and b), corresponding well with their Newtonian flow behavior in that shear rate and shear stress regime (see Figure 3.5) [285]. Such time-independent behavior is also characterized by a high propensity for elastic recovery indicated by the very low difference between the first and the fifth loop (which is about 100 m to 120 minutes). Moreover, it appears that dilute solutions, in particular RSF, display a thixotropic behavior as shown by shear stress values within the recovery curve being lower than the initial values in the structure breakdown curve. This indicates that in order to initiate a structure breakdown, energy is consumed. The data scattering observed for dilute RSF in the fifth loop is likely caused by some sample evaporation during the test.

With increasing silk concentration a time-dependent behavior could be detected (Figure 3.10c and d) [285], as shown by increasing stress over time. Furthermore, the recovery curves now displayed moderately higher shear stress values than the initial structure breakdown curves, indicating an apparent rheopectic behavior. Rheopectic behavior typically describes a "thickening" of the solution with increasing time while constantly sheared, favoring the liquid-solid transition in the fiber formation process. In this case, the rheopectic behavior is not a true but only an apparent behavior, as the hysteresis of recovery and breakdown curve is not reversible but instead shows strong scattering. Moreover, the observation of visible gel-like aggregates indicates that gelling was the reason for the rheopectic-like behavior of our concentrated solutions. Interestingly, eADF3(AQ₂₄NR3) showed a stronger rheopectic-like behavior than RSF. The 7.4 % (w/v) (AQ)₂₄NR3 solution apparently assembled after the third loop (i.e. 60 m to 75 minutes), while the 9.9 % (w/v) RSF solution showed a regular hysteresis until the fifth loop (i.e. 100 m to 120 minutes) [285]. This observation was even more pronounced at higher concentrated eADF3(AQ₂₄NR3) solutions which immediately failed to recover their original state due to the formation of aggregates (see Figure 3.10e).

3.1 Preparation and characterization of a concentrated aqueous silk spinning dope

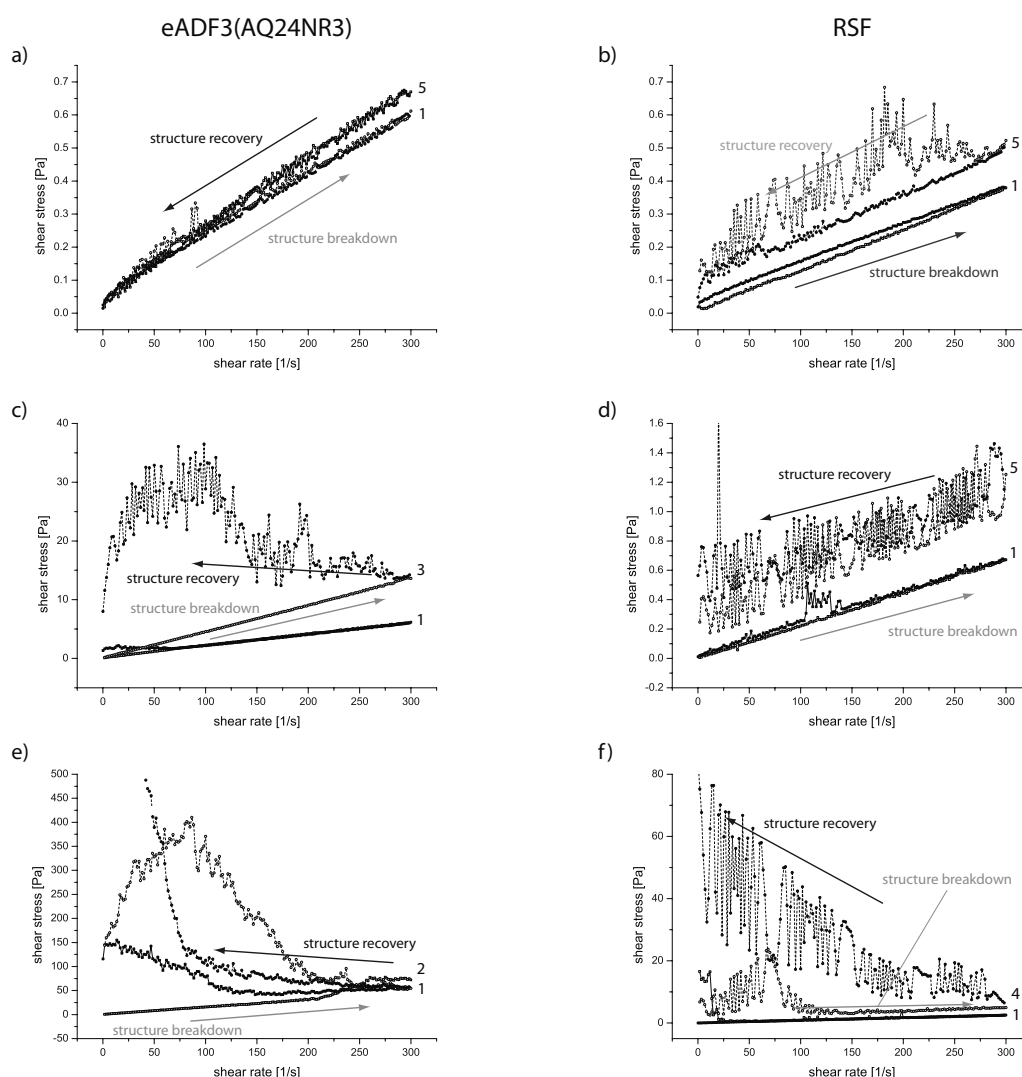


Figure 3.10 – Time-dependent (rheopectic) rheological behavior of recombinant (AQ)₂₄NR3 and RSF solutions. a) 2.1 % (w/v) (AQ)₂₄NR3, b) 1.6 % (w/v) RSF, c) 7.4 % (w/v) (AQ)₂₄NR3, d) 9.9 % (w/v) RSF, e) 16.3 % (w/v)(AQ)₂₄NR3 and f) 22.2 % (w/v) RSF. (For better illustration, only the first and the last measurable loops are shown with numbers indicating the loop count; arrows indicate structure breakdown (= shear rate increase) and structure recovery (= shear rate decrease) curve) [285] (Permission for reprint granted by Green Materials, ICE Publishing).

3.2 Process development for biomimetic spinning

3.2.1 Conception and design for a biomimetic adaption of the natural spinning duct

Initial tests using the basic setup for biomimetic spinning (as described in Section 2.5.2) revealed several drawbacks. The phosphate-PAA gel dried within a few hours, inhibiting any further ion exchange. Moreover, gel shrinking accompanied gel drying and in consequence affected the imperviousness of the initial flow channel. This problem could only be circumvented by keeping the gel wet during the process, e.g. by covering its surface with an aqueous phosphate buffer solution. Another drawback for controlled processing was hardware related: both the syringe pump and the rotating mandrel were powered by simple step-motors that could not be accurately controlled and consequently did not enable the regulation and monitoring of flow rate and reeling speed, respectively.

Based upon these observations, a second generation diffusion unit was designed and constructed (Figure 3.11). This device and all further generations described in this section were kindly provided by Tobias Martin and colleagues (Lindauer Dornier GmbH (Lindau, Germany)).

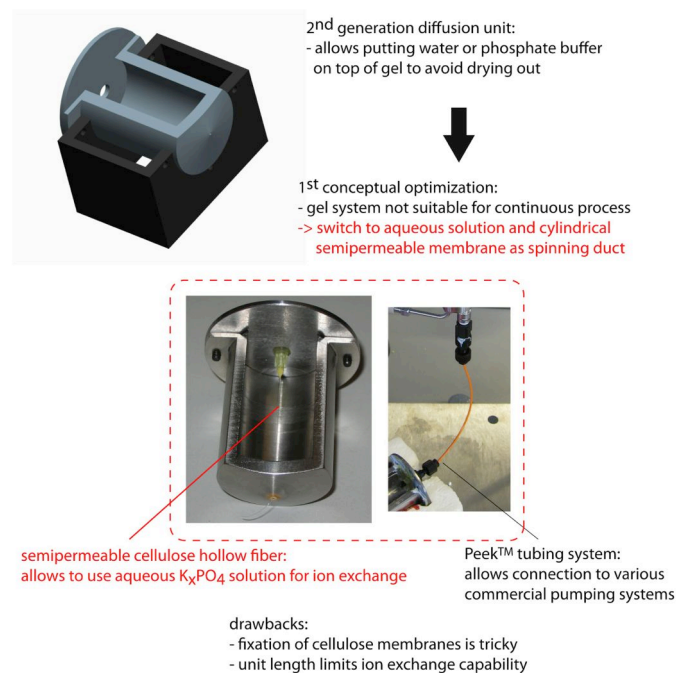


Figure 3.11 – Overview on second generation diffusion unit.

The second generation diffusion unit was constructed from a stainless steel cylinder being only

two-thirds closed and thus fully accessible from the top. This feature allowed placement of water or phosphate buffer solution on top of the phosphate-PAA gel in order to avoid gel drying. However, considerations regarding the conception of a continuous spinning device led to the conclusion that the use of a phosphate-PAA gel imposed too many limitations. The expected reduction of phosphate concentration in the gel during the ion exchange process and the challenge of avoiding gel drying being the most crucial. As a consequence, buffer solutions enabling better control of phosphate concentration and/or pH gradient within the diffusion unit were selected for future applications. In order to enable ion exchange via diffusion from a buffer into a spinning solution, a semipermeable cylindrical "spinning duct" had to be inserted into the diffusion unit. For this purpose, Thomapor[®] Biospectra semipermeable hollow fibers made from regenerated cellulose, commonly used in bundles for mass transport e.g. in dialysis processes, were purchased from Reichelt Chemietechnik. Furthermore, the implementation of a commercially available PEEK[™] tube (typically found in chromatographic applications) adapter into the unit enabled the use of commercial pumping systems for fluid transport between pump and diffusion unit. Commercial pumps significantly improved the current process by enabling accurate settings of flow rate and thus control of flow conditions during the spinning process, a significant improvement to the custom-built syringe pump used so far. Syringe pumps are the most prominent representatives of commercial pumping systems for batch systems, in particular those involving small sample amounts and low flow rates. A setup consisting of a Harvard 33 syringe pump in combination with a 1 ml syringe was used in this study for most of the spinning experiments, enabling the use of limited amounts of (AQ)₂₄NR3 solution (min. 0.1 ml) in combination with very low flow rates (min. 10 $\mu\text{l min}^{-1}$). However, for a continuous process, a syringe pump system is not suited and micro annular gear pumps that are characterized by pulsation-free running while covering a broad range of viscosities (up to 50 Pa s) appeared to be a more promising system. Therefore, micro annular gear pumps mzs-2905 and mzs-4605, both high-precision instruments enabling very low flow rates ($\sim 0.012 \text{ ml min}^{-1}$) and small volumes ($\sim 2 \mu\text{l}$) were purchased from HNP Mikrosysteme GmbH. For easier sample feeding in continuous processes, both pumps were equipped with a 30 ml reservoir that could be refilled easily during the process. Additionally, the basic custom-built rotating mandrel was replaced by the custom-built rotating mandrel constructed for forced silking (see Section 2.6.4).

Upon using the second generation diffusion unit, it became apparent that fixation and handling of the Thomapor[®] membranes was difficult. In particular the fixation, typically achieved by applying an all-purpose glue, had to be conducted with extreme care in order to avoid membrane blocking or cracking. Another drawback was delayed diffusion of phosphate ions into the membrane, since larger retention times were necessary to improve phosphate uptake (as described in detail in Section 3.2.2). The control of retention time could only be achieved either by controlling the flow rate

3.2 Process development for biomimetic spinning

or by modifying the channel length. Considering that the flow rate can only be controlled within the limitations of the pumping system which was already at the lower limits, channel length needed to be modified. Based on these results, it is expected that a retention time >11 s, corresponding to a channel length >10 cm, would provide enough time to allow the minimum phosphate concentration (~ 0.3 M) required for successful spinning of fibers from (AQ)₂₄NR3 spinning dopes [180].

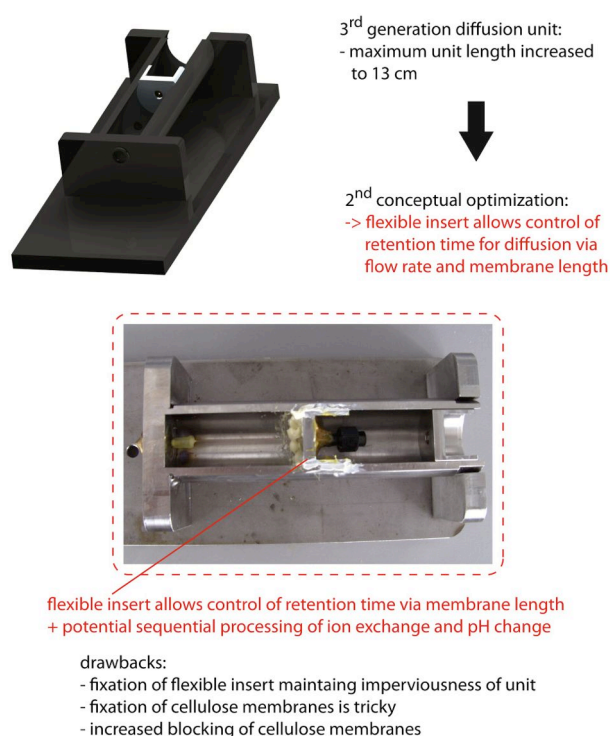


Figure 3.12 – Third generation diffusion unit.

To this purpose, a third generation diffusion unit with a length of 13 cm was constructed (see Figure 3.12). This diffusion unit was also equipped with a movable insert to vary the length of the diffusion unit, thus enabling the control of the protein solution's retention time within the diffusion unit via membrane length and flow rate. Additionally, the insert also gave rise to a potential compartmentation of the diffusion unit. This feature would enable the sequential control of individual steps of the spinning process, such as phosphate addition, acidification or water removal inside one diffusion unit. However, the extension of the diffusion unit caused process failures due to a higher propensity for blocking and cracking of increased Thomapor[®] membrane lengths.

Thus, new semipermeable materials with the following specifications were sought: MWCO be-

3.2 Process development for biomimetic spinning

tween 5 kDa to 30 kDa, allowing ion exchange while retaining the larger silk proteins (molecular weight: ~ 106 kDa); temperature resistance between 5 °C to 70 °C; pH resistance between 3 and 9 and a small inner diameter between 0.5 mm and 1 mm in order to create elongational flow forces. Besides these specifications, the mounting into the diffusion unit and a potential exchange during the process without a long process interruption were other important aspects in membrane selection. Two materials used in separation technology involving mass transport processes were selected for further consideration: ceramic and PES membranes. Ceramic membranes are mainly used due to their longevity (they can be easily purged) and higher temperature resistance [300]. However, their high investment costs as well as their brittleness, requiring extremely careful mounting (sometimes supported by special constructions) and handling, are major drawbacks. PES membranes offer small pore size distributions which gives rise to improved control of mass transfer processes. Furthermore, they are easier to handle, in particular during mounting, and are available at lower costs; although their longevity is inferior to that of ceramic membranes [300].





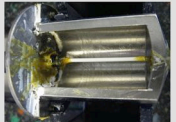

membrane:			
material:	cellulose	ceramics	polyether sulfone (PES)
pore size:	13 kDa	10 kDa	10 kDa
inner diameter:	0.2 mm	0.8 mm	0.8 mm
observations:	<ul style="list-style-type: none"> - difficult mounting - leakage - blocking - fibers rupture easily 	<ul style="list-style-type: none"> - difficult mounting - leakage - cracking upon transverse loading ° blocking (removable) 	<ul style="list-style-type: none"> + easiest mounting & handling ° reduced leakage ° blocking (removable)
in use:			

Figure 3.13 – Membrane materials tested in this study (SEM image of the cross-section of Kerafol ceramic was kindly provided by Tobias Martin (Lindauer Dornier)).

Figure 3.13 provides an overview on membrane materials tested in this study and reveals the difficulties observed during testing. In particular, accessibility and fixation of membranes during mounting were critical aspects. It should be noted that gluing appeared to be the only appropriate fixation method due to the thinness of the membranes, and in order to maintain imperviousness of the diffusion units. Based upon the observations regarding mounting and handling characteris-

3.2 Process development for biomimetic spinning

tics, PES fibers appeared to be the most promising membranes and thus were selected for future applications.

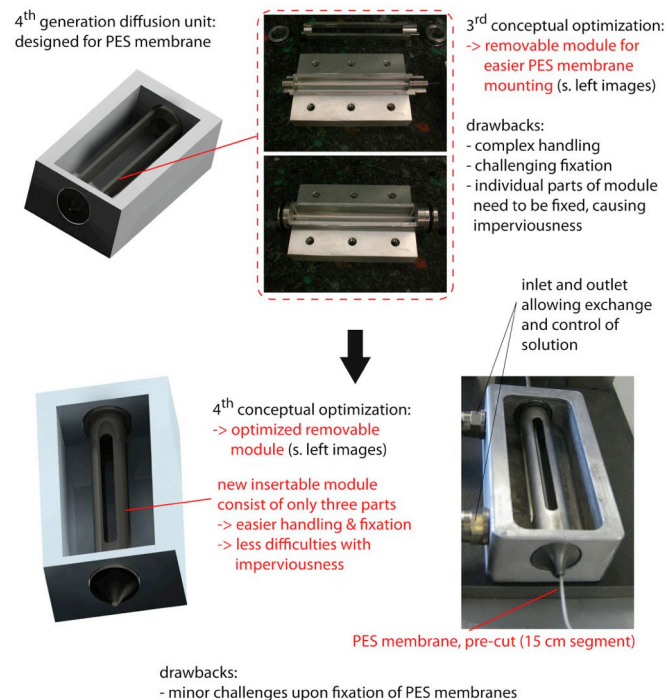


Figure 3.14 – Fourth generation diffusion units (Both photos of initial insertable module assembly were kindly provided by Tobias Martin (Lindauer Dornier).

For easier mounting of PES membranes, a fourth generation unit (see Figure 3.14) equipped with a newly designed insertable module was constructed. The module provided significantly improved handling by enabling the mounting of the membrane through a part-by-part assembly outside of the diffusion unit (see Figure 3.14 upper part). Furthermore, the module allows membrane replacement in case of problems during the spinning process, while the process itself is only interrupted for a short interval (i.e. process downtimes can be reduced drastically). However, the complex assembly and fixation of numerous small parts gave rise to new problems regarding the unit's imperviousness. As a consequence, the insert module was redesigned into a three part module in which individual parts could be assembled by screwing rather than glueing, reducing the assembly's propensity for leaking and easing mounting of PES membranes significantly. Consequently, this diffusion unit became the setup in which most ion exchange and spinning experiments were conducted (see following sections). Additionally, the fourth generation unit was equipped with an inlet and outlet enabling constant exchange of buffer solution in the unit. Thereby, the membrane module was constantly bathed by the buffer solution which is supposed to enhance mass transfer

due to higher concentration gradients [300].

All units shared their horizontal orientation, allowing accessibility from the top, which proved to be helpful during experiments. However, a typical technical setup for wet- and electrospinning is based on a vertical alignment [45, 175, 208, 210, 280]. The vertical arrangement of the spinning setup is assumed to aid fiber drawing from a viscous solution and fiber pick-up by involving gravitational forces, although the effects on thin fibers are small [301, 302]. Therefore, the fifth generation of the diffusion unit (Figure 3.15) was redesigned for a vertical orientation including a twin compartment setup. Moreover, this unit was constructed from a transparent plastic which would allow complete visual control during the spinning process. The insert module was now constructed as a single module, easing mounting, fixation, and additionally reducing difficulties with imperviousness. Since this setup was finished at the very end of this work, its practical applicability could not be tested.



Figure 3.15 – Fifth generation diffusion unit, representing the state of the art at the end of this study.

3.2.2 Analysis of the effects of semipermeable membrane material, flow rate and temperature on mass transfer of phosphate ions

The mass transfer of phosphate ions via diffusion through semipermeable membranes (Figure 3.13) was investigated as described in Section 2.9.2.

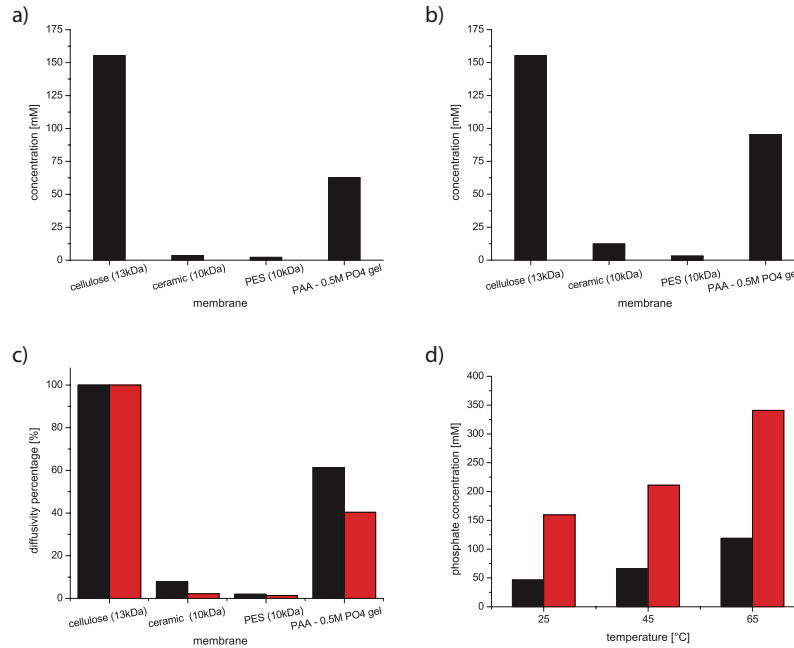


Figure 3.16 – Diffusivity studies on different membranes applied in a technical diffusion unit: a) comparison of phosphate diffusion at a constant retention time of 4.5 s; b) comparison of phosphate diffusion at a normalized diffusivity; c) percentage of phosphate diffusivity, with cellulose membrane set as 100 % benchmark (black: normalized diffusivity and red: constant retention time of 4.5 s) and d) effect of temperature on phosphate diffusivity through cellulose membrane (black: 5 mlh⁻¹ and red: 1 mlh⁻¹ volume rate).

Studies using the Thomapor[®] membrane showed that mass transfer is a function of Tris/HCl solution flow rate (Figure 3.16d), with increased phosphate transfer observed at decreased flow rates (i.e. increasing retention time). A flow rate of 1 mlh⁻¹ showed promising results by yielding a phosphate concentration of ~ 0.16 M inside the Thomapor[®] membrane. Based upon Equation 2.12 the applied flow rate of 1 mlh⁻¹ through the membrane with l being 5 cm, and inner diameter being 0.2 mm corresponds to a retention time of 4.5 s. This retention time was set for all membranes (with membrane dimensions shown in Table 3.5) by calculating the flow rate according to Equation 2.12 as follows

$$\dot{V} = \frac{r^2 \cdot \pi \cdot l}{\tau} \quad (3.4)$$

3.2 Process development for biomimetic spinning

The flow rates obtained were 16 ml h^{-1} for the ceramic membrane, 12 ml h^{-1} for the PAA-phosphate gel and 36 ml h^{-1} for PES. The resulting mass transfer is shown in Figure 3.16a) and displays significant differences in phosphate concentration between the four membranes. A phosphate concentration of $\sim 0.16 \text{ M}$ was achieved using the Thomapor[®], and only the PAA-phosphate gel reached comparable phosphate concentrations of $\sim 0.06 \text{ M}$. In contrast, the ceramic and PES membranes only achieved a $\sim 3 \text{ mM}$ phosphate concentration within the membranes. A potential explanation might be given by the different layer thicknesses and therefore "resistances" of membranes against mass transfer.

Table 3.5 – Overview on membrane dimensions and the related calculated diffusivity factor

membrane	layer thickness [μm]	length [cm]	lateral area [cm^2]	diffusivity factor [-]
Thomapor [®]	16	4	0.27	0.169
ceramic	60	4	1.76	0.029
PES	50	9	3.68	0.074
PAA-phosphate gel	10	4	1.01	0.101

For better comparison, mass transfer was now evaluated as a function of layer thickness, using diffusivity instead of retention time. The calculation of diffusivity is defined by a modified version of Fick's first law for mass transfer through a semipermeable membrane as

$$D_i = D \cdot A \cdot \frac{(c_2 - c_1)}{b} \quad (3.5)$$

with D_i = diffusivity, D = diffusion coefficient [cm^2/s], A = lateral area of the membrane, c_2 = concentration in the surrounding fluid, c_1 = concentration within the membrane and b = layer thickness [m].

The lateral area A for a cylindrical geometry is defined as $A = 2 \cdot \pi \cdot r \cdot l$, with r = radius of cylinder and l = length of cylinder.

By assuming a constant diffusion coefficient D for potassium phosphate (with $D_{\text{KH}_2\text{PO}_4} = 1.27 \times 10^{-5} \text{ cm}^2 \text{ s}^{-1}$) [303], Equation 3.5 can be used to calculate the diffusivity factor for each membrane, with the results shown in Table 3.5.

Based on the promising results obtained with Thomapor[®] membrane (see above), the diffusivity factors of the other membranes were set in relation, resulting in the following diffusivity factors: $D_{\text{cellulose}} = D_{\text{PAA-phosphate gel}} \cdot 1.67 = D_{\text{PES}} \cdot 2.3 = D_{\text{ceramic}} \cdot 5.8$. These factors were used to recalculate the retention time by multiplying the 4.5 s with the according factor in order to theoretically

account for the different diffusivities. The recalculated retention times were 26 s for the ceramic, 10 s for PES and 7.5 s for the PAA-phosphate gel. Based on these results, the flow rates were readjusted with Equation 3.4 using the membrane lengths given in Table 3.5. The new flow rates obtained were 3 ml h^{-1} for the ceramic, 7 ml h^{-1} for the PAA-phosphate gel and 16 ml h^{-1} for PES. The phosphate concentrations achieved via adjusted diffusion is displayed in Figure 3.16b), with the Thomapor[®] membrane still setting the benchmark with a phosphate concentration of $\sim 0.16 \text{ M}$. These results indicated a significant improvement in phosphate mass transfer concerning the PAA-phosphate gel and the ceramic membrane. The PAA-phosphate gel now yielded a reasonable phosphate concentration of $\sim 0.1 \text{ M}$, which is an improvement by $\sim 67 \%$. The improvement of mass transfer into the ceramic membrane was $\sim 400 \%$, now yielding a phosphate concentration of $\sim 12 \text{ mM}$. Nonetheless, the total amount of phosphate transferred through the ceramic membrane is still far below the amount required for salting out the silk proteins. Strikingly, the PES membrane did not show any considerable improvement, still displaying a meager phosphate transfer of $\sim 3 \text{ mM}$. In general, performing the phosphate transfer based on normalized diffusivity followed the same trend as that based on retention time, although more or less improvement was observed for each membrane, as shown in Figure 3.16c). Tests using PES membranes with increased retention time (60 s, i.e. a flow rate of 3 ml h^{-1}) (data not shown), showed no improvement in mass transfer. During spinning of (AQ)₂₄NR3, increased solution turbidity at the exit of the membrane was observed, being a good indicator for conformational changes towards a higher β -sheet content. These findings are however, contrary to the mass transfer studies. To investigate if shear and elongational forces during flow accounted for the induction of this conformational transition, the phosphate buffer in the diffusion unit was replaced by a Tris/HCl buffer. Indeed, no turbidity of (AQ)₂₄NR3 solution at the exit of the membrane was observed.

Studies on the effect of temperature on phosphate mass transfer revealed a strong temperature dependence (see Figure 3.16d), as expected from the temperature dependence of the diffusion coefficient described by the Stokes-Einstein relation:

$$D = \frac{R \cdot T}{6 \cdot \pi \cdot r \cdot \eta \cdot N_A} \quad (3.6)$$

Phosphate concentrations within the Thomapor[®] membrane were increased by $\sim 50 \%$ at 45°C and $\sim 100 \%$ at 65°C for both flow rates. However, these results have to be treated with care, as evaporation during the measurement likely affected the actual phosphate concentration measured. Evaporation at elevated temperature excluded further experiments with the first four generations of the diffusion unit at elevated temperatures. The fifth generation unit with its online control of buffer conditions and temperature, however, might be a promising setup for more detailed studies

on temperature effects.

3.2.3 Characterization of solvent removal during liquid-solid transition in the spinning process

Solvent removal plays a critical role in the final stage of fiber spinning. In nature, water removal is accomplished by resorption through cells along the wall of the spinning duct and evaporation in air [32, 53, 168].

In this study, two solvent removal procedures involving either hygroscopic solutions or heat-induced evaporation (see Section 2.9.4) were compared. Tests with aqueous ethanol mixtures indicated that ethanol diffusing into the membrane induced conformational transition of (AQ)₂₄NR3, as shown by increased solution turbidity and formation of viscous aggregates at the end of the membrane. However, comparable to findings on eADF4(C16) [180, 184], these prematurely formed gel-like aggregates could not be elongated into fibers. Alternatively, highly concentrated PEG solutions provide a prominent tool for solvent removal due to their induction of osmotic stresses via dialysis [37, 176]. Studies using a 20 % (w/v) PEG (20 kDa) revealed similar results as with ethanol. Choosing a molecular weight of PEG above the MWCO of the PES membrane limited PEG transfer into the protein solution. However, the slow osmotic process kinetics for PEG (compare to concentration studies in Section 3.1.1) were insufficient to achieve reasonable solvent removal within the retention times (i.e. flow rates) tested.

By comparison, experiments using an infrared lamp to generate heat in the vicinity of the membrane showed more promising results. Putting the overlapping membrane segment within an enclosed heat chamber allowed generation of temperatures of $\sim 40^{\circ}\text{C}$ to 60°C near the membrane, inducing evaporation of water within the imposed retention times as shown by the formation of small water droplets at the outside of the PES membrane (see Figure 3.17). The resulting viscous (AQ)₂₄NR3 drop at the membrane exit could then be elongated (thereby removing more water) after some additional drying time into a fiber (as will be described in more detail in Section 3.2.4).

In order to gain more insight into solvent removal induced by the heat-induced evaporation approach, so-called pan-weighing experiments were performed as described in Section 2.9.3.

The mass loss over time curves obtained by pan-weighing experiments for (AQ)₂₄NR3 and RSF solutions are shown in Figure 3.18. The internal water diffusion coefficient D_{ss} could be determined from the results of the pan-weighing experiments using Equation 2.15 and Equation 2.16. Table 3.6 summarizes the data with ρ_T being 1 g l^{-1} and x being calculated to 1.04 mm based on

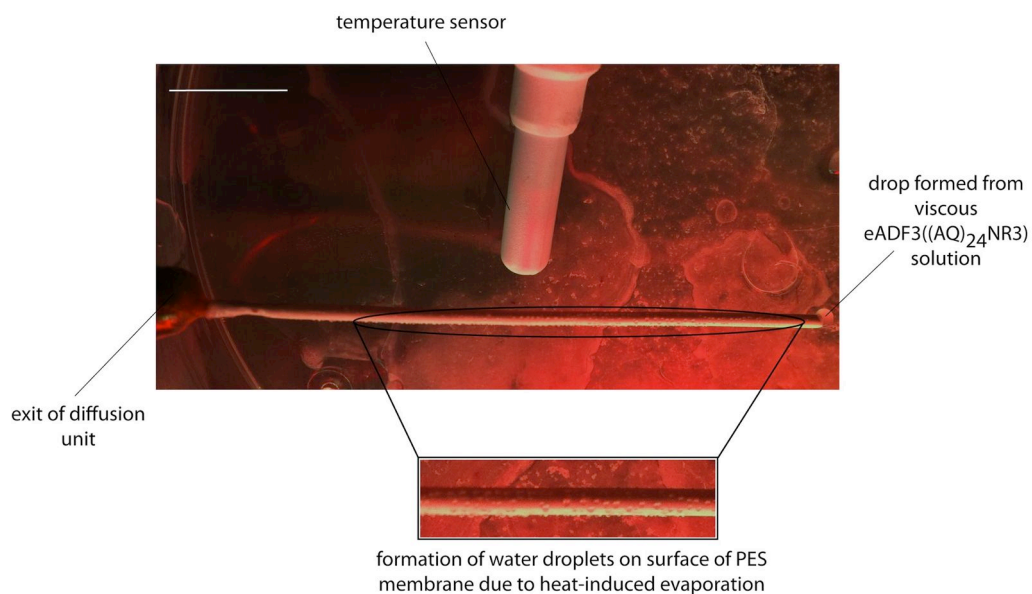


Figure 3.17 – Photograph of water droplet formation on the surface of PES membrane induced by heat generated by an infrared lamp (white scale bar = 1 cm).

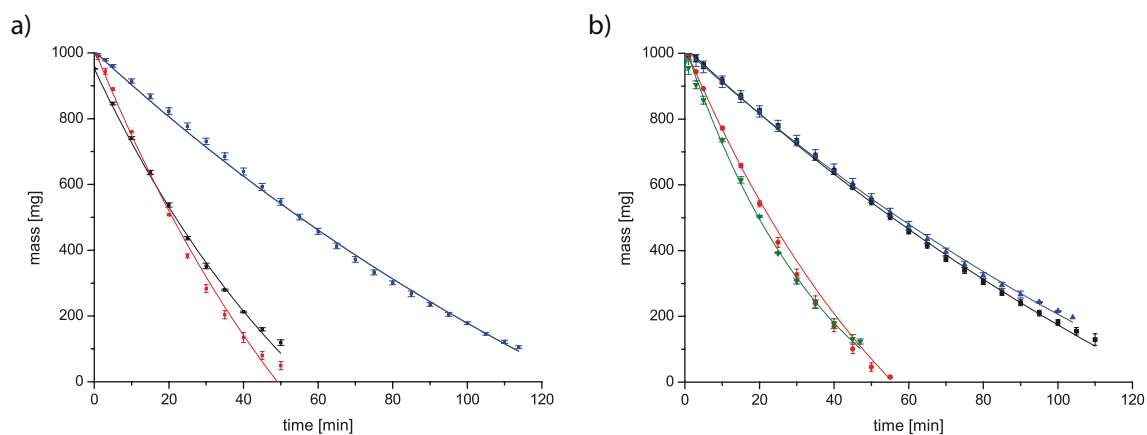


Figure 3.18 – Mass loss over time for a) (AQ)₂₄NR₃ solutions with 2 % (w/v) at 45 °C (blue), 70 °C (red) and 8 % (w/v) at 70 °C (black); and b) RSF solutions with 2 % (w/v) at 45 °C (black), 70 °C (red) and with 8 % (w/v) at 45 °C (blue), 70 °C (green).

3.2 Process development for biomimetic spinning

Table 3.6 – Determination of D_{ss} for (AQ)₂₄NR3 and RSF solutions at 45 °C and 70 °C.

sample	T [°C]	t [s]	$\rho_{w, \text{theoret.}}$ [mg/ml]	$\rho_{w, \text{exp.}}$ [mg/ml]	D_{ss} [mm ² s ⁻¹]
2% (w/v) (AQ) ₂₄ NR3	45	6600	980	895	1.50×10^{-4}
2% (w/v) (AQ) ₂₄ NR3	70	3300	980	943	3.15×10^{-4}
8% (w/v) (AQ) ₂₄ NR3	70	3300	920	875	3.12×10^{-4}
2% (w/v) RSF	45	6600	980	872	1.46×10^{-4}
2% (w/v) RSF	70	3300	980	985	3.29×10^{-4}
8% (w/v) RSF	45	6600	920	804	1.43×10^{-4}
8% (w/v) RSF	70	3300	920	873	3.11×10^{-4}

petri dish dimensions and sample volume. The data revealed that the water diffusion coefficient of (AQ)₂₄NR3 and RSF solution is a function of temperature. D_{ss} at 70 °C was typically twice as high as D_{ss} at 45 °C. Interestingly, there was almost no difference between (AQ)₂₄NR3 and RSF solutions and further, D_{ss} did not display any concentration dependence. Although the general observation correlates well with findings made by Kojic et al. on *N. clavipes* dope [168], the slopes of the mass loss curves obtained in this work were much steeper hinting towards a higher internal water diffusion. The data presented in Table 3.6 confirms these assumptions, showing that D_{ss} in this study ($\sim 3.15 \times 10^{-4} \text{ mm}^2 \text{ s}^{-1}$) was higher than the diffusion coefficient ($D_{\text{water-dope}} \sim 2.15 \times 10^{-5} \text{ mm}^2 \text{ s}^{-1}$) determined for *N. clavipes* dope [167, 168]. This is very likely a consequence of the higher temperatures applied in these pan-weighing experiments compared to their studies, which were performed at 25 °C while constantly blowing air at 150 ml min^{-1} [167, 168]. It should be noted that the experiments conducted at 45 °C apparently did not completely remove water ($\rho_{w, \text{exp}}$ values varied considerably from $\rho_{w, \text{theoret.}}$ values calculated using Equation 2.16) due to the limitations (max. running time and balance accuracy) of the instrument.

3.2.4 Production of artificial (AQ)₂₄NR3 fibers

Pulling fibers from a viscous solution, also referred to as "hand-drawing", is a simple but effective method to produce artificial fibers with decent properties from a small amount of silk protein solution [161, 215]. Rather than simply pulling fibers manually with fine tweezers from a viscous drop, the procedure in this study was refined by instantaneously transferring the fiber to a rotating mandrel (see Figure 2.2) and collecting fibers at a constant and controlled reeling speed (see Figure 3.19) [304]. This method enabled the production of fibers up to 1 m in length at reeling speeds below 20 mm s^{-1} , which corresponds well with a take-up speed of fibers used in a capillary dry spinning process (30 mm s^{-1}) [45].

Hand drawing experiments revealed that at concentrations below 4.5 % (w/v) fibers could not be

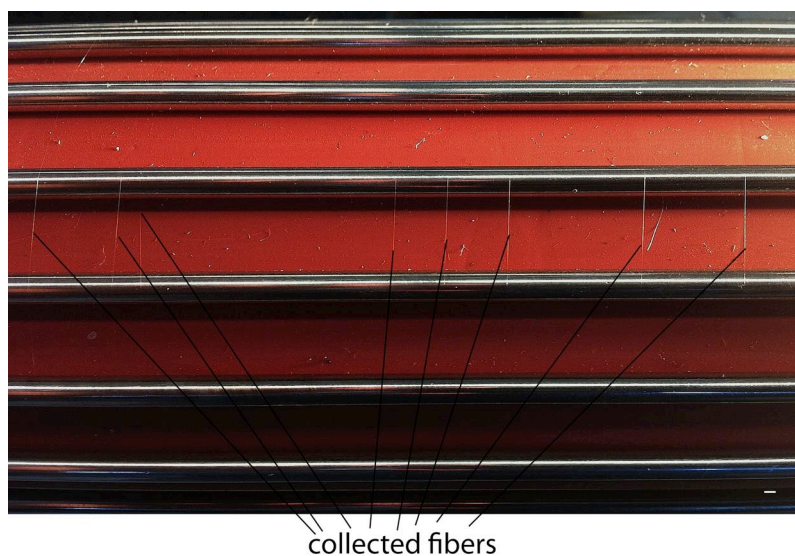


Figure 3.19 – Photograph of hand drawn fibers collected on the rotating mandrel (white scale bar = 1 mm).

produced at any spinning condition. In contrast, (AQ)₂₄NR3 solutions above 4.5 % (w/v) that appeared to be "oily" yielded the best spinnability and could be drawn into fibers upon addition of potassium phosphate (pH 8). It was also observed that a minimum concentration of 300 mM potassium phosphate (pH 8) was necessary for successful fiber formation (Table 3.7), confirming previous findings [180].

Table 3.7 – Influence of potassium phosphate (pH 8) concentration on time required for hand drawing fibers from aqueous 5 % (w/v) (AQ)₂₄NR3 solutions (concentrations are final concentrations after mixing).

C_{buffer} [mM]	lag time [s]	fiber length [cm]	comment
50	-	-	no fibers formed
100	-	-	no fibers formed
150	-	-	no fibers formed
200	-	-	no fibers formed
250	> 120	< 5	fibers only occasionally formed
300	> 30	20 - 100	
350	> 20	20 - 100	
400	10 - 20	20 - 100	
450	10	20 - 100	
500	< 10	20 - 100	

Moreover, the time required until fibers could be drawn from the solution correlated with phosphate concentration, as increasing phosphate concentration reduced lag time before fiber drawing (see Figure 3.20). Further investigations revealed that spinning from aqueous (AQ)₂₄NR3 solu-

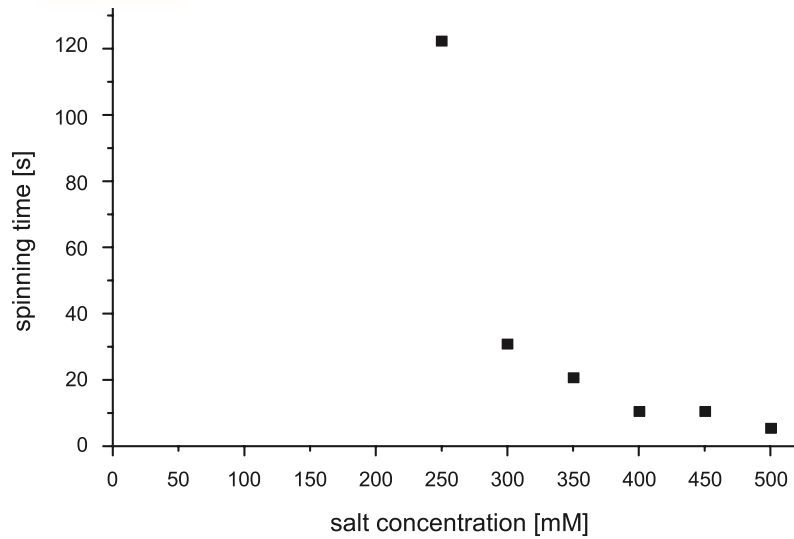


Figure 3.20 – Time required for spinning as a function of potassium phosphate buffer concentration.

tions depends predominantly on the salt applied rather than the pH conditions [304].

Table 3.8 – Influence of salt on hand drawing from aqueous (AQ)₂₄NR3 solutions (concentrations are final concentrations after mixing).

$c_{(AQ)_{24}NR3}$ [% (w/v)]	salt	c_{buffer} [M]	lag time [s]	fiber length [cm]
5 - 10	potassium phosphate (pH 8)	0.5	5 - 30	10 - 100
> 7	(NH ₄) ₂ HPO ₄ (pH 7.9)	0.5	>20	< 30
5 - 7	(NH ₄) ₂ SO ₄ (pH 5)	0.5	>20	20 - 50
5 - 7	NaH ₂ PO ₄ (pH 4)	0.5	>20	< 30

Table 3.8 reveals that in the presence of potassium phosphate (pH 8) fibers up to 1 m in length could be produced, displaying a smooth and homogeneous morphology, as shown by SEM images (see Figure 3.21b). In contrast, the addition of (NH₄)₂HPO₄ (pH 7.9), (NH₄)₂SO₄ (pH 5) and NaH₂PO₄ (pH 4) required a longer incubation phase before fibers could be drawn. The resulting fibers, in particular those prepared from (NH₄)₂SO₄, were shorter and in some cases were still covered with salt crystals (see Figure 3.21c and d). It should be noted that fibers could be drawn less frequently upon addition of salt solutions other than potassium phosphate. Nonetheless, all fibers revealed a relatively smooth surface morphology and slight variation in fiber diameter as a consequence of controlled reeling speed. This is in contrast to most wet-spun fibers that typically show a sponge-like appearance [207] or a high variability in diameter despite their smooth morphology [206].

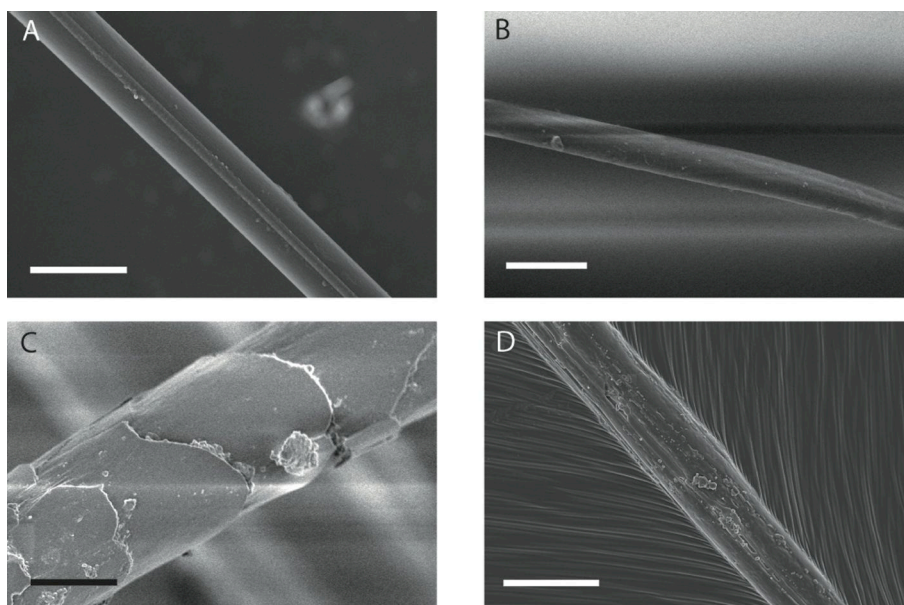


Figure 3.21 – SEM images of natural *A. diadematus* silk fiber (A) and fibers drawn from aqueous (AQ)₂₄NR3 solution in the presence of different salts (B - D): B) in presence of potassium phosphate; C) NaH₂PO₄ and D) (NH₄)₂SO₄ (scale bars represent 5 μ m for A and 10 μ m for B - D) [304] (Permission for reprint granted by Bioinspired, Biomimetic and Nanobiomaterials, ICE Publishing).

The simplicity of hand drawing fibers from concentrated silk solutions made it a useful tool in order to verify the spinnability of the silk solution. Thus, it was generally applied prior to biomimetic spinning experiments and only solutions that could successfully be hand drawn into fibers were used for biomimetic spinning. Figure 3.22 shows CAD images of both biomimetic spinning setups applied in this work: a) the setup using the Harvard 33 syringe pump for small volumes of (AQ)₂₄NR3 and b) the setup using the mzs-4605 pump for larger volumes. Furthermore, this figure shows a photo of an exemplary spinning setup, consisting of the mzs-4605 pump, the custom-built diffusion unit and the rotating mandrel device.

Figure 3.23 provides an exemplary photograph of a successful biomimetic spinning process, with the close-up showing a fiber elongated from a viscous droplet formed at the end of the diffusion unit. However, it should be noted that this fiber only formed after suspending the process to further dry the droplet. Under continuous processing conditions, fibers could not be pulled directly from the viscous droplet, although the spinnability of the (AQ)₂₄NR3 solution was approved by hand drawing (see Table 3.9). The flow rates applied in these experiments were typically in the range of 15 μ l min⁻¹ to 30 μ l min⁻¹, which is an order higher than the flow rates used in capillary dry spinning (1 μ l min⁻¹) [45] and wet-spinning (2 μ l min⁻¹ to 10 μ l min⁻¹) [204]. These observations led to the conclusion that apparently there was still too much residual water left in the spinning

Table 3.9 – Summary of biomimetic spinning experiments from aqueous (AQ)₂₄NR3 solutions (for a complete list of spinning experiments please refer to Figure 7.5).

membrane	length [cm]	c _{(AQ)₂₄NR3} [% (w/v)]	salt	c _{salt, tank} [mM]	retention time [s]	fiber formation	ext. drying time [s]
Thomapor [®]	5	< 9	K _x H _{3-x} PO ₄ buffer pH 8	0.5	n.a.	no	
Thomapor [®]	5	> 9	K _x H _{3-x} PO ₄ buffer pH 8	0.5	n.a.	yes	> 10
phosphate-PAA gel	5	6	K _x H _{3-x} PO ₄ buffer pH 8	0.5	< 770	no	
phosphate-PAA gel	5	6	K _x H _{3-x} PO ₄ buffer pH 8	0.5	> 770	yes	> 60
ceramic	4	15	K _x H _{3-x} PO ₄ buffer pH 8	1	< 60	no	
ceramic	4	15	K _x H _{3-x} PO ₄ buffer pH 8	1	> 60	no	> 60 s
ceramic	9	15	K _x H _{3-x} PO ₄ buffer pH 8	1	< 60	no	
ceramic	4	15	K _x H _{3-x} PO ₄ buffer pH 8 & 4% PEG (20 kDa)	1	> 40	no	
PES	9 (tank) + 6 (air)	< 10	K _x H _{3-x} PO ₄ buffer pH 8	1	> 90	no	
PES	9 (tank) + 6 (air)	< 13	K _x H _{3-x} PO ₄ buffer pH 8	1	< 90	no	
PES	9 (tank) + 6 (air)	< 13	K _x H _{3-x} PO ₄ buffer pH 8	1	> 90	yes	> 2
PES	9 (tank) + 6 (air)	> 13	K _x H _{3-x} PO ₄ buffer pH 8	1	< 60	no	
PES	9 (tank) + 6 (air)	> 13	K _x H _{3-x} PO ₄ buffer pH 8	1	> 90	yes	> 2
PES	9 (tank) + 6 (air)	> 13	K _x H _{3-x} PO ₄ buffer pH 8	1	> 90	yes	> 2
PES	9 (tank) + 6 (EtOH)						
PES	9 (tank) + 6 (20% PEG)	> 13	K _x H _{3-x} PO ₄ buffer pH 8	1	> 90	yes	> 2
PES	10 (tank) + 5 (IR heat box)	< 7	K _x H _{3-x} PO ₄ buffer pH 8	1	> 300	no	

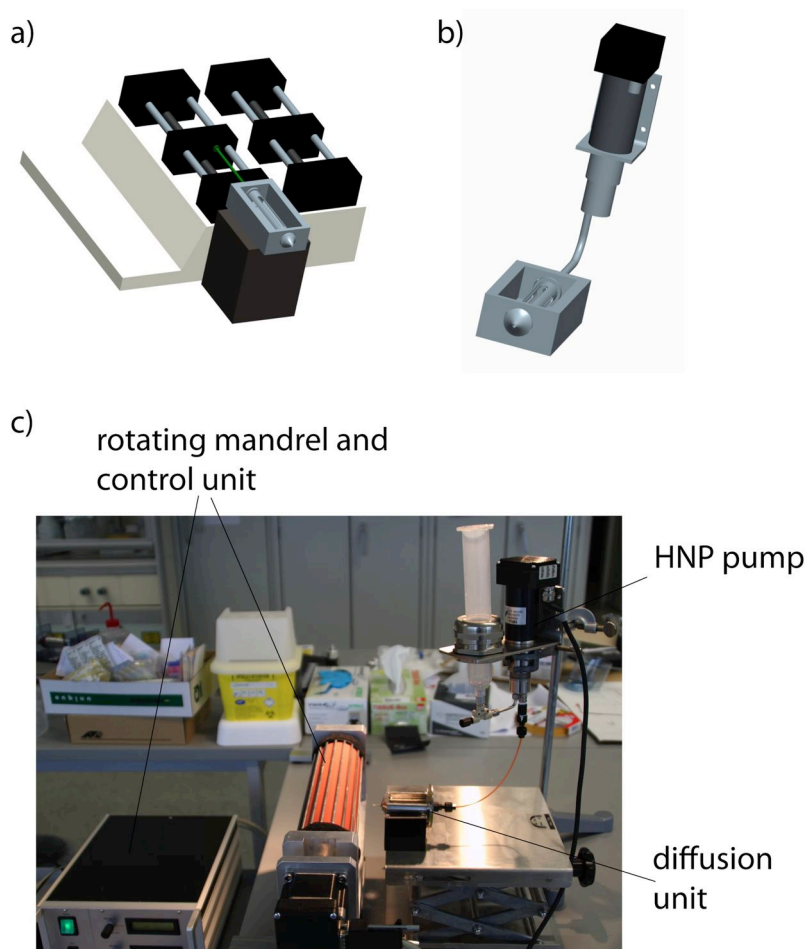


Figure 3.22 – CAD Images of biomimetic spinning setups used in this study, using a) Harvard 33 Syringe pump for small (AQ)₂₄NR3 volumina and b) HNP pump for (AQ)₂₄NR3 volumina; c) Overview of complete biomimetic spinning device, including HNP mzt-4605 pump, rotating mandrel and its control unit.

solution at the exit of the setup. However, the equipment used did not allow to reduce flow rates below the tested range.

As mentioned, drawing fibers was possible after a short period of drying of the droplet. A 7 % (w/v) (AQ)₂₄NR3 solution in combination with the phosphate-PAA gel (cast into the second generation diffusion unit) at a retention time of 77 s allowed drawing of fibers after an extended period (> 60 s) of drying. Similar observations were made using the Thomapor[®] membrane with a retention time of 6.3 s and a ceramic membrane (installed in the fourth generation unit) with a retention time of 60 s. In both cases, membranes were surrounded by a 1 M potassium phosphate (pH 8) solution. In contrast, PES membranes surrounded by a 1 M potassium phosphate (pH 8) solution with

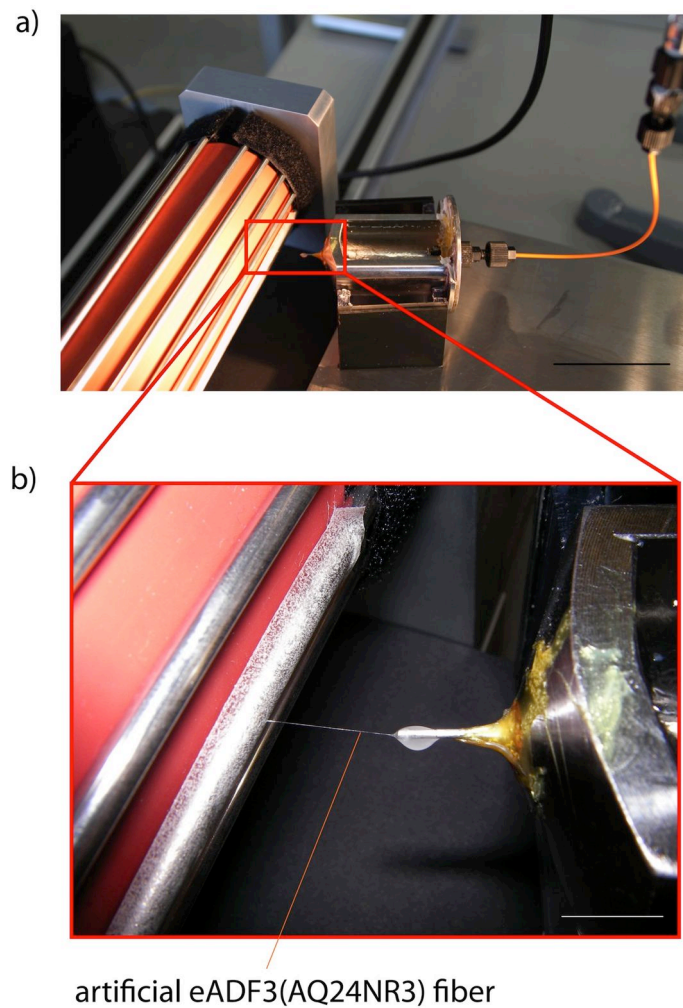


Figure 3.23 – a) Photograph of biomimetic spinning experiment, with fiber formation being highlighted in b) (scale bars represent 5 cm for a) and 5 mm for b).

a retention time of 100 s to 200 s allowed drawing of fibers within 2 s to 5 s after drop pick-up. In contrast to the other spinning experiments, the PES membrane spinning experiments included the application of solvent removal by heat-induced evaporation (see Section 3.2.3), which in particular is assumed to account for the reduced drying period following fiber pick-up.

3.3 Mechanical characterization of natural and artificial spider silk fibers

Silk fibers require proper specimen gripping, in particular to prevent slipping during testing [278]. Since suitable grips were not commercially available, grips for sample mounting were custom built

3.3 Mechanical characterization of natural and artificial spider silk fibers

(see Figure 3.24) from aluminum to save weight. The design of the grips was adopted to match perfectly with the custom-made sample holders (see Section 2.9.5.1).

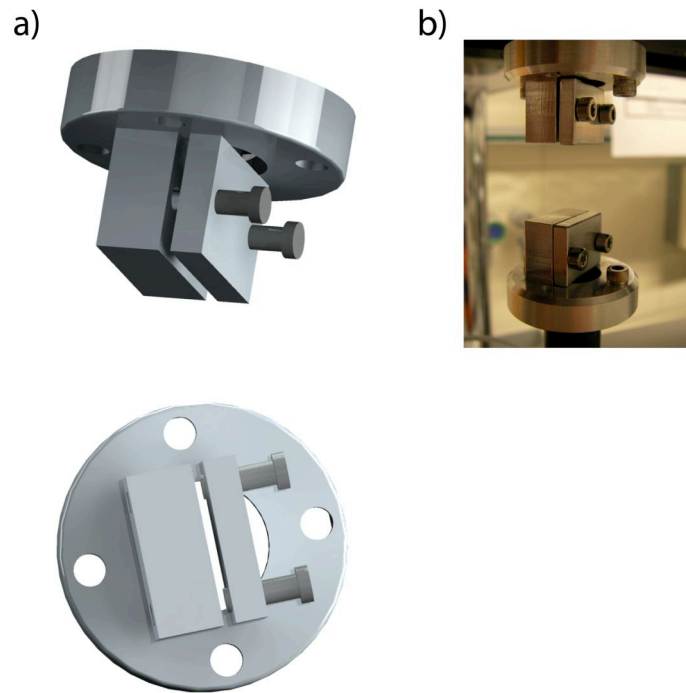


Figure 3.24 – a) CAD images of the custom-made grips for tensile testing of fibers, non-wovens and films; b) Photograph of the custom-built grips.

Those sample holders were modified in the course of this work. First, in order to improve the ratio of length to diameter, the rectangular hole width was reduced to 2 mm and further set as the new gauge length of the fibers. Secondly, considering that tensile testing should also be carried out in humid conditions and even in the presence of water, the initial sample holders prepared from drawing paper were replaced using transparency sheets made from cellulose acetate. The application of a laser cutting device allowed a high number of sample holders to be produced in a short period of time (~ 100 sample holders within a few minutes) with extremely high precision and reproducibility. The sample holders (see Figure 3.25) were designed using CorelDRAW[®] X4, and laser cutting was performed at the Handwerkskammer Oberfranken (in Bayreuth) using an Epilog Mini 24 (EpilogLaser, Golden, CO, USA).

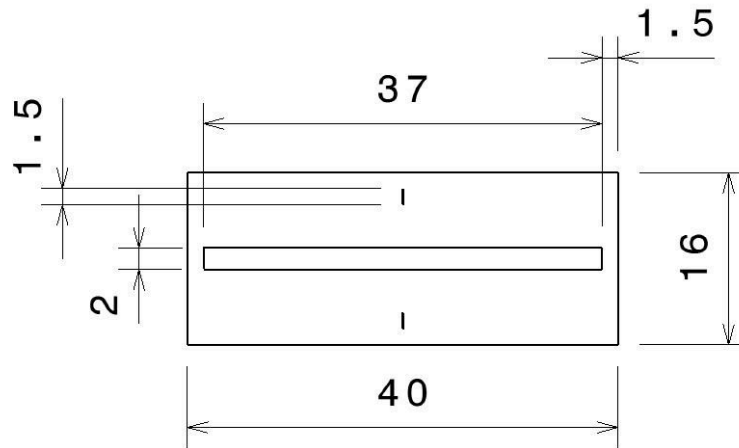


Figure 3.25 – Design of the new sample holder including dimensions (given in mm).

3.3.1 Establishing a fiber sample preparation procedure

In order to guarantee that the displacement of the load cell is only caused by fiber elongation it is essential to ensure proper fixation of the fiber sample [70]. Due to the high sensitivity and thinness of the silk fibers, several adhesives were first tested with natural silk fibers from *A. diadematus* and *B. mori* silkworm silk with regard to a firm and water resistant fixation, and a rapid hardening process that still enables minor corrections after sample immobilization. Most importantly, the fixation should neither show creeping behavior during tensile testing nor influence the fiber properties, e.g. by turning an elastic fiber brittle. Adhesives commonly found in literature for fiber fixation included superglue [33, 232, 234, 239], all-purpose glue [70] or double-sided adhesive tape [238]. Furthermore, nail polish and UV adhesive were also tested. The observations made with all glues tested in this work are summarized in Table 7.2. Nail polish, that was initially used for fiber fixation at the beginning of this work due to its easy handling and rapid hardening properties, proved to be useless for tests in an aqueous environment due to softening and loosening of sample fixation. Except for the model making glue, all other glues showed detrimental handling properties.

During preparation and testing of artificial silk fibers, the model making glue revealed a major drawback of liquid adhesives: the artificial fibers appeared to be covered and soaked with the glues as shown in Figure 3.26. As a consequence, the artificial fibers turned extremely brittle and tensile testing experiments could not be conducted. Therefore, double-sided adhesive tape was selected as the alternative for fixation of artificial silk fiber. Placing a small cover onto the adhesive tape made the fixation sufficiently firm for tensile testing experiments in this work.

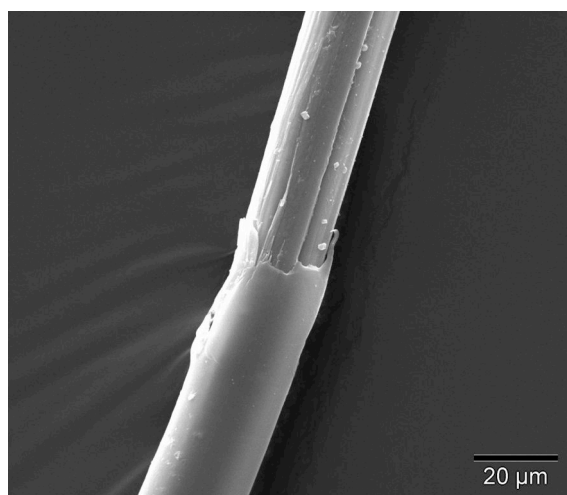


Figure 3.26 – SEM image showing the influence of a liquid adhesive on the morphology of an (AQ)₂₄NR3 fiber, with the lower part of the fiber being covered by adhesive while the upper part is not.

3.3.2 Fiber diameter determination using LM or SEM

As mentioned, mechanical properties of fibers are usually characterized based on their tensile strength characteristics [48]. With stress in this case being defined as the force applied on a fiber's cross-sectional area (Equation 1.4), it is essential to determine the diameters of fine silk threads accurately [277] (as highlighted in Figure 3.27).

Even small deviations in fiber diameter can result in significant errors concerning the calculation of tensile strength. The thinness of these fibers (μm range) requires the application of high resolution imaging techniques. As of today, two different imaging techniques have been typically employed to determine the diameter of silk fibers: PLM [70, 277] or SEM [67, 191, 246]. It should be noted that the determination of spider silk fiber diameters using these top-view techniques is enabled due to assumption of a circular fiber cross-section [26, 31, 67, 246]. For SEM imaging, samples are usually fixed on specific specimen stubs and sputter coated in a vacuum environment. Consequently, these fibers can not be further used and have to be analyzed after tensile testing [67, 246]. In contrast, fibers analyzed by PLM or LMBF do not require modification or pretreatment but could be imaged readily, enabling fiber diameter determination prior to or after tensile testing, rendering it the only method accounting for the variability in silk fiber diameters [277].

Based upon results by Blackledge and coworkers, showing that PLM is equal with SEM concerning fiber diameter determination [277], our fibers were investigated using SEM and light microscopy. However, the light microscopy images in this study were obtained in Bright Field mode

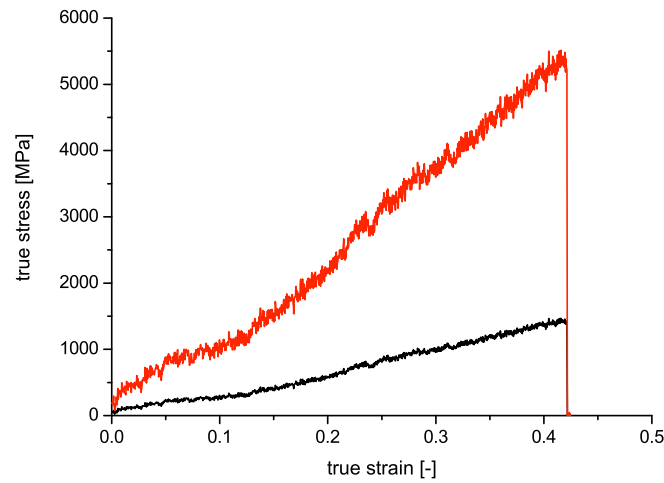


Figure 3.27 – Comparison of stress-strain curves calculated based on fiber diameter determined by LMBF (black) or by SEM (red)

instead of polarized mode, as this mode yielded sharper images easing diameter determination (see Figure 7.2). Moreover, the birefringence of fibers in polarized mode is supposed to result in diameter overestimation and increased variability [277].

Figure 3.28 shows that almost all diameters of forcibly silked *A. diadematus* fibers obtained from LMBF images were significantly higher than those obtained from SEM images (as indicated by all data points in Figure 3.28 c) being above the straight line). This is in agreement with an earlier study comparing PLM with SEM measurements [277]. These results can be related to the sample preparation procedure for SEM, which involves sputter coating and measurement in a vacuum environment. Vacuum is known to generate dehydration, which ultimately results in shrinkage of fibers [277] as most silks readily absorb water and are partially hydrated in native state [20, 21].

Fibers silked at a reeling speed of 60 mm s^{-1} (FS60) had an average diameter of $8.98 \pm 1.61 \mu\text{m}$ determined by LMBF and $5.26 \pm 3.18 \mu\text{m}$ determined by SEM. This corresponds to a variation for LMBF diameters of 17.9 % and for SEM diameters of 60.5 %. Fibers silked at a reeling speed of 200 mm s^{-1} (FS200) had an average diameter of $5.01 \pm 0.62 \mu\text{m}$ determined by LMBF and $2.86 \pm 0.78 \mu\text{m}$ determined by SEM. The variation for LMBF diameters was determined to be 12.4 % and for SEM diameters of 27.3 %. The differences between the different microscopic techniques were significant in this study, with a difference of $3.87 \pm 1.72 \mu\text{m}$ and $2.15 \pm 0.16 \mu\text{m}$ for FS60 and FS200 fibers, respectively. Blackledge and coworkers, by comparison consistently

3.3 Mechanical characterization of natural and artificial spider silk fibers

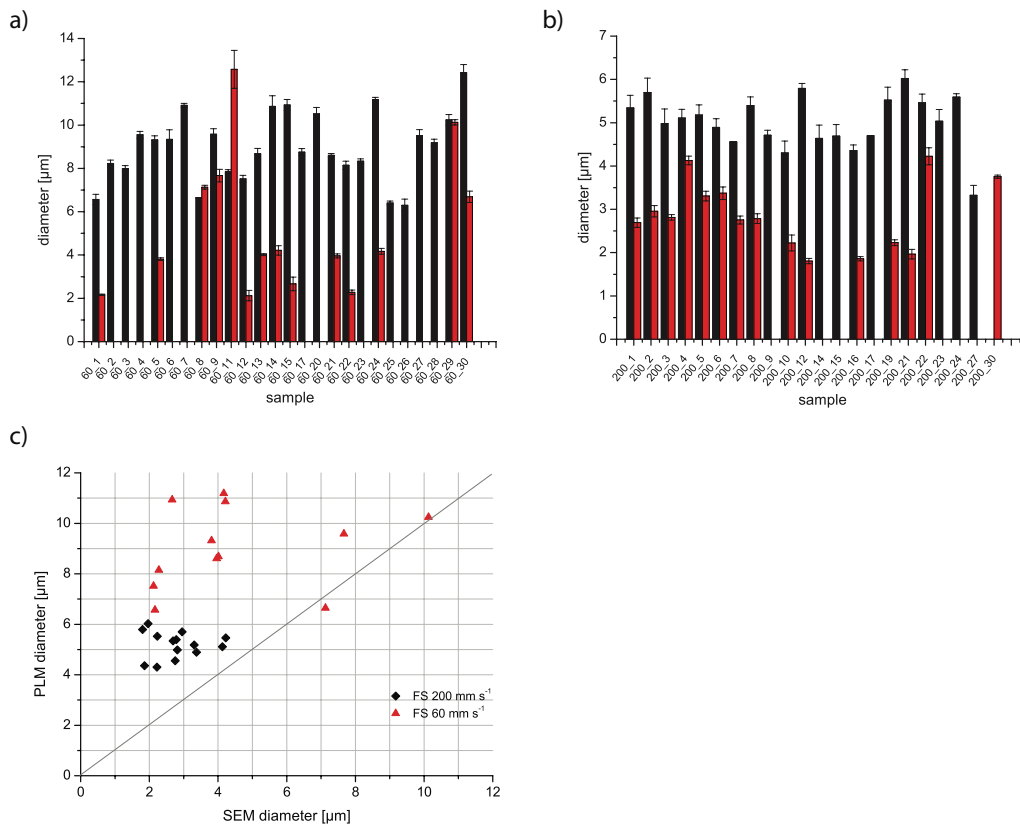


Figure 3.28 – Comparison of fiber diameter determined by LMBF (black) and SEM (red) for forcibly silked fibers: a) at 60 mm s^{-1} and b) 200 mm s^{-1} ; c) relates diameter determined by LMBF or by SEM.

measured larger diameters for PLM by only $0.16 \pm 0.13 \mu\text{m}$ [277]. That group determined diameter variations in PLM of $8.6 \pm 1.4 \%$ and in SEM of $7.7 \pm 1.1 \%$ [277], which is well below the variations obtained here. Interestingly, the variability in fiber diameter decreased significantly for FS200 compared to FS60 fibers, which is in good agreement with data on decreasing silk diameter increasing spinning speed observed for *B. mori* silk [279]. Furthermore, the data presented for forcibly silked fibers reveals that fiber diameter is a function of reeling speed, with diameters decreasing from $\sim 8 \mu\text{m}$ to less than $6 \mu\text{m}$ with increasing reeling speeds [304]. This result is in good agreement with earlier studies on spider silk [191] and *B. mori* silk [279]. Remarkably, variability in fiber diameter also decreased with increasing reeling speed, as was shown by Khan et al. [279]. These findings confirm the consideration that the control of fiber diameter is an important tool used by the spider to manage and alter the physical performance of its dragline silk fibers [60, 277].

3.3.3 Mechanical characterization of *A. diadematus* dragline silk fibers

Spider silk reveals extraordinary mechanical properties, in particular, its unique combination of high tensile strength and elasticity, distinguishing it from most other natural or synthetic fibers [47, 48, 51–55]. The following section will provide a comprehensive set of data for silk and other typical fibers, such as aramid (Kevlar[®]), cotton and *B. mori* silk fibers. Furthermore, *A. diadematus* dragline silk fibers collected directly from orb-webs or by forced silking are characterized. Only one study dealt with such a comparison on silk from *A. diadematus*, however, the results did not provide clear evidence for any dependence [64]. Dragline silk from *A. diadematus* has a brin structure [283], i.e. the parallel alignment of two filaments also observed in *B. mori* [29] and Argiope spiders [66]. These two filaments were observed to break sequentially and not simultaneously. Although the silk fibers were carefully collected and prepared, it remained challenging to obtain the individual double bave filaments. Instead, collected fibers often appeared as twisted multiples of bave filaments as shown by multiple breaking during tensile testing (see Figure 3.30). For mechanical analysis, the first and final circumference of forcibly silked fibers collected around the mandrel was usually discarded, since Guinea and coworkers showed that these fiber segments behaved differently [268].

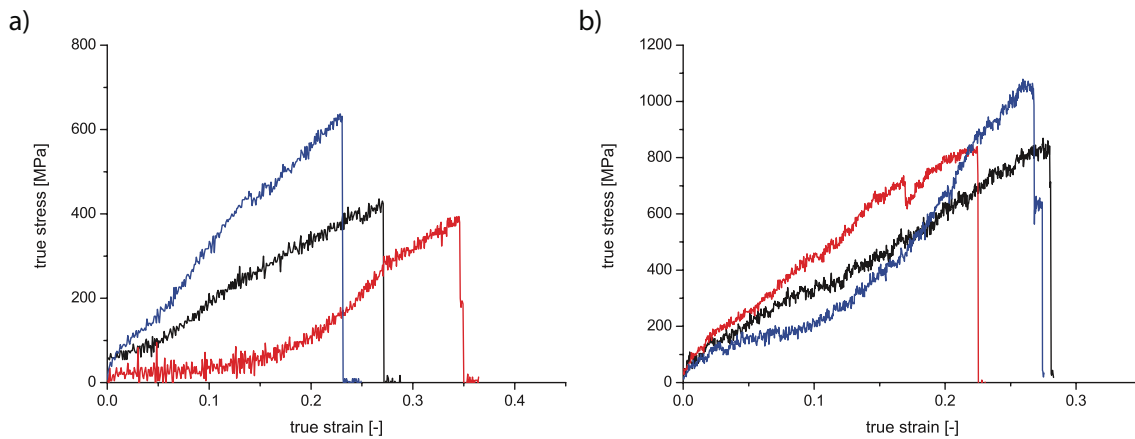


Figure 3.29 – Comparison of silk fibers from *A. diadematus* collected a) from web and b) by forced silking (different colors symbolize different samples).

The stress-strain curves of silk fibers from *A. diadematus* spiders revealed a dependence on the collection method, as shown in Figure 3.29 and Table 7.3. To highlight the extraordinary mechanical properties of spider silk, other well-known fibers, such as Kevlar[®] 49, cotton and *B. mori* silk were tensile tested and results corresponded well with data from literature (see Table 7.3).

Fibers collected directly from the orb-web and then tested at an extension rate of 0.1 mm s^{-1} displayed an average tensile strength of $581 \pm 267 \text{ MPa}$ and an average elongation to break of 29.7

3.3 Mechanical characterization of natural and artificial spider silk fibers

$\pm 10\%$. This result is significantly different to data obtained for *A. diadematus* silk collected from web and tested at an extension rate of 0.6 mm s^{-1} [230], displaying an average tensile strength of $1154 \pm 140 \text{ MPa}$ and an average elongation to break of $39.4 \pm 3.3\%$. The difference is too significant to simply relate it to the higher extension rate applied in the latter study. Moreover, fibers forcibly silked at a speed of 60 mm s^{-1} (FS60) revealed a higher average tensile strength of $770 \pm 181 \text{ MPa}$, with elongation to break at $28.7 \pm 5.4\%$ [304] compared to our orb-web data, but displayed significantly lower values than the orb-web data presented in the Kohler study [230]. The forcibly silked fibers tested in this work showed the increased tensile strength accompanied by decreased elongation at break, as observed in earlier studies on *Argiope trifasciata* [66] or *B. mori* silk [27]. The discrepancy to the Kohler study might be caused by several factors, such as false diameter assumption or different spider condition (body weight).

Figure 3.29 displays the intraspecific variability in mechanical properties among naturally spun fibers although collected from a single web, confirming observations in earlier studies [48, 64]. This large variability of properties was interpreted as a contribution to the survival ability of the spider [64, 234].

3.3.4 Influence of spinning speed on mechanical properties of *A. diadematus* dragline silk

Earlier studies have revealed that spinning speeds have an impact on resilience, strain at breaking, breaking energy, initial Young's modulus, yield point and ductility (most likely related to the variation in diameter of a single fiber) [64, 68, 78, 137, 191, 193, 234]. The silk of *A. diadematus* appears to be more sensitive to reeling speeds than that of other species [234]. The following section describes the influence of spinning speed on the mechanical properties of dragline silk from *A. diadematus*.

Table 3.10 – Overview of collected data of *A. diadematus* fibers reeled at different speeds and under different environmental conditions (n = number of samples, rH = relative humidity) [304].

sample	n	rH	elongation to break	tensile strength	toughness	diameter
		[%]	[%]	[MPa]	[MJ m ⁻³]	[μm]
FS200	6	30	26.7 ± 3.9	1256 ± 317	164.4 ± 59.9	6.3 ± 1.4
FS200	7	70	30.8 ± 3.8	1148 ± 187	151.3 ± 26.6	5.3 ± 0.6
FS200	7	in water	26.7 ± 5.1	833 ± 142	98.3 ± 34.5	5.5 ± 0.4
FS60	7	30	28.7 ± 5.4	770 ± 181	113.9 ± 20.9	8.2 ± 1.2
FS60	7	70	33.5 ± 7.4	574 ± 131	92.1 ± 31.9	8.5 ± 0.8
FS60	7	in water	26.7 ± 4.3	352 ± 73	43.6 ± 11.5	9.6 ± 1.5

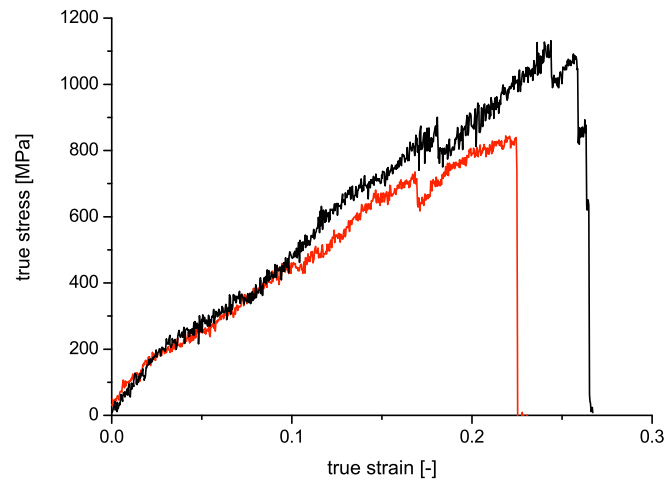


Figure 3.30 – Influence of reeling speed on mechanical properties of *A. diadematus* silk fibers (black = FS200, red = FS60) [304] (Permission for reprint granted by Bioinspired, Biomimetic and Nanobiomaterials, ICE Publishing).

The stress-strain curves of forcibly silked fibers from *A. diadematus* spiders show a strict dependence on spinning speeds with a positive correlation as revealed in Table 3.10 and Figure 3.30. FS200 fibers display an average tensile strength of 1256 ± 317 MPa. In comparison, FS60 samples revealed a significantly lower average tensile strength of 770 ± 181 MPa. Interestingly, FS200 showed a similar average of elongation to break with 26.7 ± 3.9 % compared to FS60 fibers with 28.7 ± 5.4 % [304]. These results are in good agreement with published data of forcibly silked fibers from *A. diadematus* [64, 234], fibers from other spider species [78, 191, 193] and *B. mori* silkworm silk [27]. The toughness of FS200 fibers at 164.4 ± 59.9 MJ m⁻³ correlated well with the data published in literature [52]. However, the toughness of FS60 fibers was significantly lower at 113.9 ± 20.9 MJ m⁻³, explained by the significantly reduced tensile strength. At reeling speeds above 266 mms⁻¹, however, fibers started to show inferior strength, reduced by nearly 30 % to ~ 800 MPa (data not shown) compared to FS200, also observed in an earlier study and related to the effects of very high spinning speeds on silk composition [191]. These results confirm other studies that showed that fibers collected above a critical reeling speed started to become brittle and displayed less mechanical stability [27, 191]. This observation was related to a higher probability for defects within the molecular structure at higher silking speeds due to reduced time for proper orientation [191, 268]. The standard deviation for tensile strength and elongation to break typically ranged from 10 % to 25 % of the mean values [304], constituting valid data given the aforementioned variability of natural spider silk fibers [234, 239, 246]. At higher reeling speeds,

a larger strain hardening regime in the stress-strain curve was observed (Figure 3.30). This can be related to an increased content of intramolecular β -sheets present in the fiber, knowingly affected by the reeling speeds of silk fibers [235].

Occasionally, the stress-strain curves of forcibly silked fibers showed sudden slight drops in stress, in particular, close to the point of failure (Figure 3.30) [304]. However, the stress-strain curves quickly recovered to their previous stiffness. SEM images revealed that these drops only occurred when multi-stranded fibers, i.e. smaller submicron filaments were twisted around the fiber, collected at higher reeling speed were tested. Therefore, the fibers were likely snapping around one another, suddenly loosening and then regaining stress. This observation had previously been published by Blackledge and coworkers [232].

3.3.5 Influence of humidity on mechanical properties of *A. diadematus* dragline silk

Earlier studies on other spider species have revealed that mechanical properties of dragline silk are greatly influenced upon contact with water or a relative humidity greater than 60 %, turning dragline silk into a rubber-like material [51, 52, 66, 68, 242, 282].

Therefore, the influence of humidity on the mechanical properties of dragline silk from *A. diadematus*, that is supposed to be more prone to humidity influences than other silk based on the higher proline content and the related larger amorphous network [78, 305, 306], was investigated. The mechanical properties are summarized in Table 3.10 [304]. FS60 fibers displayed on average a higher tensile strength of 770 ± 181 MPa at 30 % rH compared to 574 ± 131 MPa at 70 % rH and 352 ± 73 MPa in water. In contrast, the average elongation to break was 28.7 ± 5.4 % at 30 % rH compared to 33.5 ± 7.4 % at 70 % rH and 26.7 ± 4.3 % in water. The toughness followed the trend observed for tensile strength, decreasing with increasing humidity: 113.9 ± 20.9 MJ m⁻³ at 30 % rH, 92.1 ± 31.9 MJ m⁻³ at 70 % rH and 43.6 ± 11.5 MJ m⁻³ in water. FS200 fibers showed an average tensile strength of 1256 ± 317 MPa at 30 % rH compared to 1148 ± 187 MPa at 70 % rH and 833 ± 142 MPa in water. The average elongation to break was 26.7 ± 3.9 % at 30 % rH, 30.8 ± 3.8 % at 70 % rH and 26.7 ± 5.1 % in water. The toughness decreased with increasing humidity, with 164.4 ± 59.9 MJ m⁻³ at 30 % rH, 151.3 ± 26.6 MJ m⁻³ at 70 % rH and 98.3 ± 34.5 MJ m⁻³ in water. These results are in agreement with previous studies on the influence of humidity on mechanical properties of silk from other spider species [66, 68, 242, 282].

Figure 3.31 displays the dependence of *A. diadematus* dragline silk's mechanical properties on humidity [304]. Strikingly, the dependence is more pronounced for FS60 fibers than for FS200 fibers.

3.3 Mechanical characterization of natural and artificial spider silk fibers

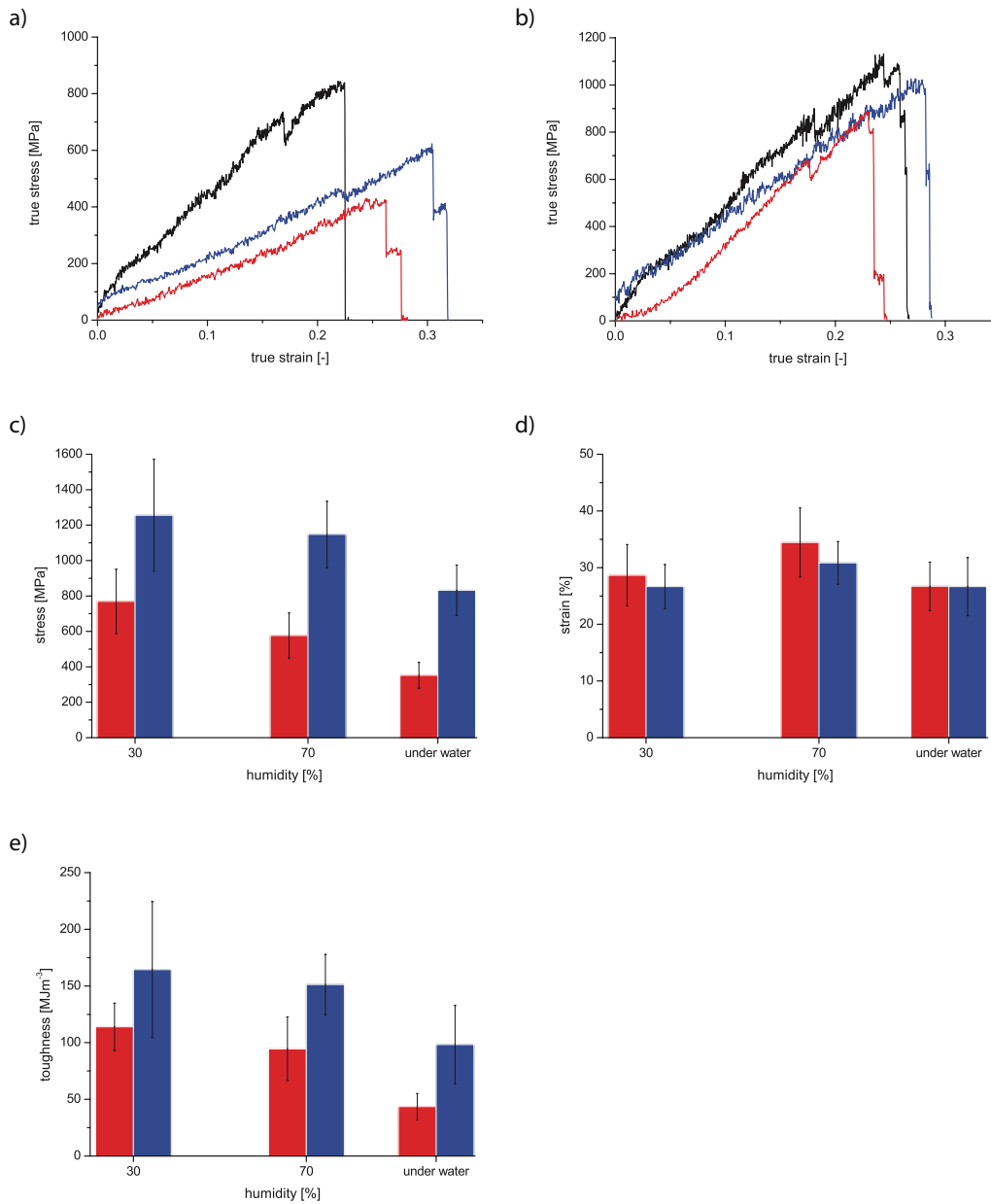


Figure 3.31 – Influence of humidity on *A. diadematus* silk fibers, forcibly silked at a) 60 mm s⁻¹ and b) 200 mm s⁻¹ (black: 30 % rH; blue: 70 % rH and red: in water) [304] (Permission for reprint granted by Bioinspired, Biomimetic and Nanobiomaterials, ICE Publishing). Diagrams c-e) reveal the degradation of mechanical properties with increasing water content (red: FS60 and blue: FS200).

3.3 Mechanical characterization of natural and artificial spider silk fibers

3.3.6 Mechanical characterization of (AQ)₂₄NR3 silk fibers

Previously described fibers produced from recombinant silk proteins by wet-spinning, revealed mechanical properties inferior to those of native silks [154, 157, 195, 196, 204, 215]. In the following section, mechanical data of fibers hand drawn from concentrated (AQ)₂₄NR3 solutions are presented.

Table 3.11 – Overview of collected data for fibers made of recombinant proteins.

sample	solvent	molecular weight [kDa]	elongation to break [%]	tensile strength [MPa]	toughness [MJ m ⁻³]	diameter [μm]
avg. (AQ) ₂₄ NR3	aq. buffer	106.3	10.8 ± 3.1	64.6 ± 26.0	3.0 ± 0.2	11.7 ± 4.2
best (AQ) ₂₄ NR3	aq. buffer	106.3	32.3	143.4	24.6	10
avg. (AQ) ₂₄ NR3 post-treated	aq. buffer + EtOH vapor	106.3	7.4	72.11	2.3	11.7 ± 4.2
best (AQ) ₂₄ NR3 post-treated	aq. buffer + EtOH vapor	106.3	29.9	152.3	23.6	10

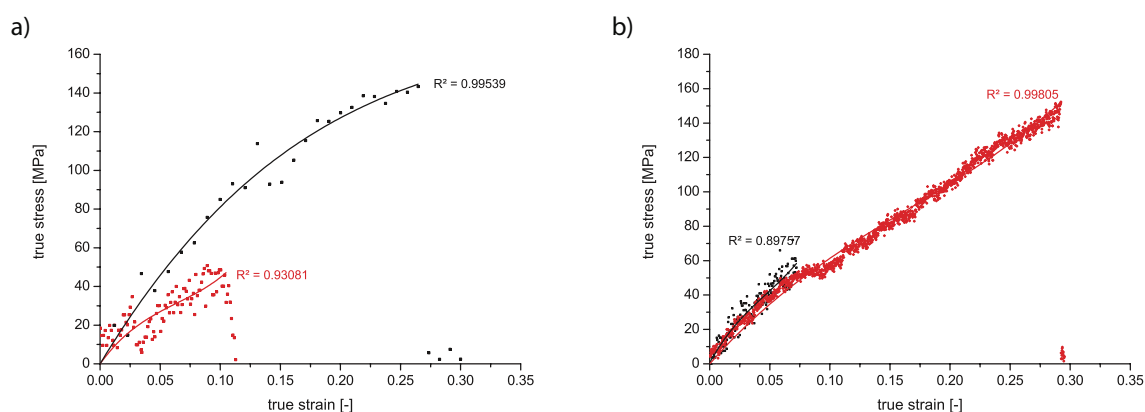


Figure 3.32 – Stress-strain curves of fibers drawn from aqueous (AQ)₂₄NR3 solutions fitted with a polynomial regression fit of third order: a) as-hand drawn (black: best curve; red: average curves) [304] (Permission for reprint granted by Bioinspired, Biomimetic and Nanobiomaterials, ICE Publishing) and b) post-treated using ethanol vapor (black: average curves; red: best curve).

The mechanical properties of silk fibers drawn from solutions of (AQ)₂₄NR3 are in the range of that of other fibers produced from recombinant silk proteins with comparable molecular weights (see Table 1.1) [304]. The tensile strength of (AQ)₂₄NR3 fibers was on average 64.6 ± 26.0 MPa and elongation to break was 10.8 ± 3.1 % (mean ± S.D., n = 6), but reached 143.3 MPa and 32.3 % in the best case. The (AQ)₂₄NR3 fibers revealed diameters between 7 μm to 16 μm without post-spin drawing, matching that of natural and hand-drawn artificial fibers, such as fibers

3.3 Mechanical characterization of natural and artificial spider silk fibers

successfully produced by hand-drawing at reasonable speeds (0.5 cm min^{-1} to 1 cm min^{-1} from an aqueous solution (0.08% (w/v)) prepared from regenerated *N. edulis* silk fibers [198]. These fibers showed a tensile strength on average of $125 \pm 15 \text{ MPa}$ and elongation to break of $18.5 \pm 8.5 \%$, with fibers having a diameter of $\sim 9 \mu\text{m}$ and an apparently rough surface morphology [198]. Wet-spun fibers, in contrast were usually between $40 \mu\text{m}$ to $75 \mu\text{m}$ in diameter before being post-stretched [195–197, 304]. Artificial fibers originally showing mechanical properties inferior to those obtained from aqueous (AQ)₂₄NR3 solutions were shown to be improved upon application of post-spinning procedures such as immersion and post-spin stretching in alcohol-water mixtures [195, 196]. As a consequence, the production of artificial silk fibers relies on post-stretching procedures to improve mechanical properties of the fibers by improving molecular alignment and increasing crystallinity [178, 195, 196, 207, 213, 216, 217]. Figure 3.32b) shows preliminary results of post-treatment tests. Strikingly, the mechanical properties of the best curves did not reveal significant changes, although on average, the post-treated curves appeared to display higher tensile strength but less extensibility.

3.3.7 Structural characterization of biotech and natural silk fibers using FT-IR and polarized FT-IR

In order to clarify the large discrepancies between mechanical properties of biotech and natural silk fibers, structural characterization of these fibers using FT-IR and polarized FT-IR were performed. It is well established that the mechanical properties of silks are related to their structural design and orientation of stiff crystalline segments embedded in an amorphous matrix [52, 101, 212, 247].

FT-IR spectra of forcibly silked fibers and fibers drawn from engineered (AQ)₂₄NR3 solutions (using potassium phosphate) shown in Figure 3.34 are similar, although the spectra of (AQ)₂₄NR3 fibers also showed a significant absorption band at 1080 cm^{-1} (phosphate) [304].

Table 3.12 – Structural data obtained by FSD-analysis for natural and biomimetic fibers [304]

sample	β -sheet [%]	α -helical [%]	random coil [%]	β -turns [%]
FS60	34.3 ± 5.3	6.3 ± 0.7	23.8 ± 1.5	23.7 ± 4.3
FS200	34.5 ± 4.6	5.5 ± 0.7	23.2 ± 1.9	21.0 ± 3.5
avg. (AQ) ₂₄ NR3	18.0 ± 2.4	13.9 ± 2.2	26.2 ± 1.6	33.7 ± 5.5
best (AQ) ₂₄ NR3	30.1 ± 0.3	7.5 ± 0.3	27.1 ± 1.3	25.5 ± 0.3

FSD-analysis data of the amide I band (1705 cm^{-1} to 1590 cm^{-1} , Figure 2.8 using the amide I assignments according to Hu et al. [173] is summarized in Table 3.12. The data reveals that the

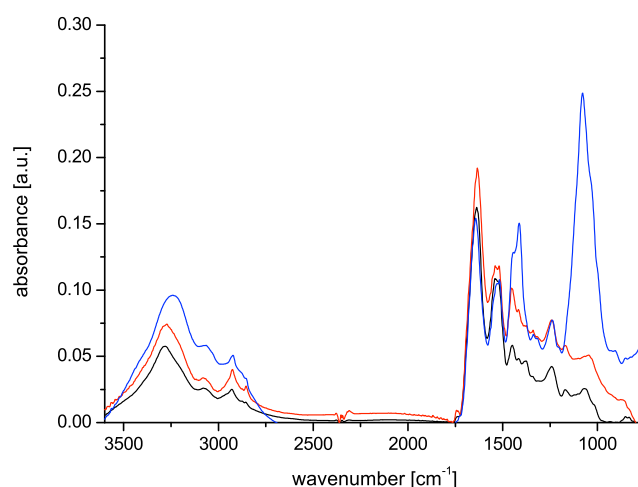


Figure 3.33 – FT-IR spectra of spider silk fibers from *A. diadematus* and (AQ)₂₄NR3 fibers (black: FS60 fibers; red: FS200 fibers and blue: (AQ)₂₄NR3 fiber) [304] (Permission for reprint granted by Bioinspired, Biomimetic and Nanobiomaterials, ICE Publishing).

forcibly silked fibers from *A. diadematus* displayed a β -sheet content of 34.3 ± 5.3 % (FS60) and 34.5 ± 4.6 % (FS200), respectively [304]. This corresponds well with results obtained by Raman spectroscopy studies on dragline silks from *A. diadematus* [73] and *Nephila* spiders [22, 307, 308], as well as X-ray scattering [99, 309, 310] and NMR studies [100, 101] on dragline silk from *N. clavipes*. In contrast, the fibers pulled from (AQ)₂₄NR3 showed on average a significantly lower β -sheet content with 18.0 ± 2.4 % [304]. Only individual fibers showed secondary structures similar to those of natural fibers with a β -sheet content of 30.1 ± 0.3 % [304]. This observation is assumed to be a consequence of an incomplete conformational transition of the recombinant proteins during fiber drawing. A study on films cast from (AQ)₂₄NR3 solutions revealed that post treatment using potassium phosphate or methanol increased the β -sheet content of these as-cast films significantly from 28 % to around 40 % [258].

Polarized FT-IR spectroscopy was used to analyze the mean orientation and molecular order parameter of fibers [273]. S^{mol} values of 0 and 1 correspond to isotropic and perfectly aligned transition moments and are typically calculated at wavenumber 966 cm^{-1} which corresponds to the vibrations of poly-alanine β -sheet crystals. S^{mol} calculations in this study yielded equivalent values of 1.0 ± 0.06 for measurements parallel to the fiber axis (0°) and 1.0 ± 0.01 for measurements perpendicular to the fiber axis (90°) [304]. In contrast, a study by Papadopoulos and coworkers on dragline silk fibers from *Nuctenea sclopetaria* obtained S^{mol} above 0.9 for measurements at 0° and

significantly lower values for measurements at 90° [273]. While polarized FT-IR measurements displayed dichroism indicative of strong parallel axial alignment of alanine-rich β -sheet crystals in native silk fibers [273, 311], regenerated or artificial silk fiber lacked the dichroism indicating that alanine-rich β -sheet crystals are distributed randomly in the fiber [198].

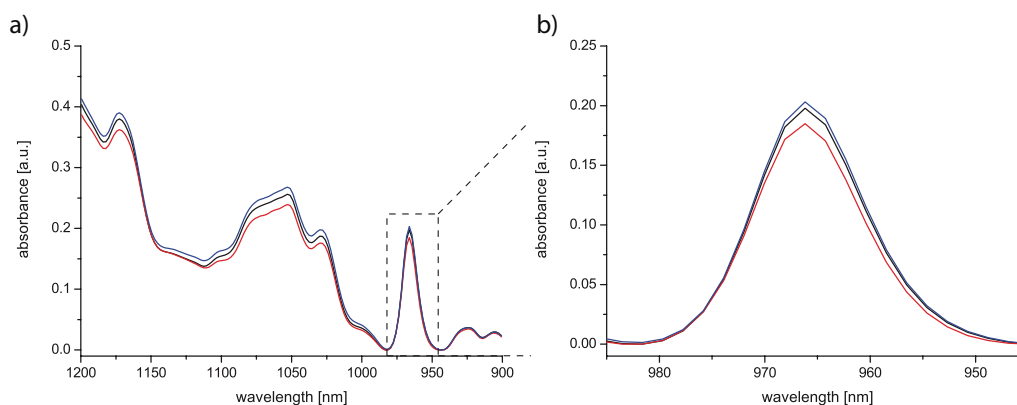


Figure 3.34 – Polarized FT-IR spectra of spider silk fibers from (AQ)₂₄NR3 fibers (black: without polarizer, blue: polarizer at 90° and red: polarizer at 0°).

It should be noted that the FT-IR measurements to obtain quantitative information about the conformation and orientation in native and artificial silk fibers provided a challenging task due to the fiber's thinness. This problem was already observed earlier by a group who related these difficulties to the size of the fibers, being below the diffraction limit of most infrared microscopes [276].

4 Discussion

4.1 Analysis of an aqueous (AQ)₂₄NR3 silk spinning dope

4.1.1 Influence of stabilizing agents on (AQ)₂₄NR3 solution stability

The preparation of aqueous (AQ)₂₄NR3 solutions from purified proteins using dialysis was typically limited to concentrations well below the range required for spinning, confirming observations in earlier studies with (AQ)₂₄NR3 and other recombinant proteins due to their tendency to self-assemble into microfibrils upon small energy inputs [9, 23]. Although the deviation in solution stability between native and recombinant proteins is not yet well understood, it is assumed that the NRN-domain [144] (and references therein), the presence of metallic ions [36] and other spidroins [185] play an important role in contributing to the stability of the native spinning dope.

The addition of stabilizing agents known to mediate interactions between proteins in aqueous solutions is well established for globular proteins, however, in this work their effects on silk proteins were investigated for the first time. A previously described screening method [288, 312] involving various buffer conditions and potential solubility enhancing additives (see Section 3.1.3) was applied and revealed that some additives improved the stability of (AQ)₂₄NR3 solutions while others reduced the solution stability. This observation can be explained by distinguishing solubility enhancing additives with respect to their chemical properties and their respective mode of action into 1) cosolvents that either destabilize protein-protein interactions to prevent aggregation and 2) cosolvents that enhance native protein stability (Table 4.1) [265, 287, 288, 312, 313].

Table 4.1 – List of cosolvents that may promote protein solubility and their mode of action.

	additive	mode of action
detergents	sodium cholate	destabilization of protein-protein interactions
chaotropes	urea	destabilization of protein-protein interactions
osmolytes	L-arginine (Arg) & L-glutamic acid (Glu)	destabilization of protein-protein interactions
	sorbitol	stabilization through preferential hydration
	PEG (4 kDa)	stabilization through preferential hydration
	TMAO	stabilization through preferential hydration

The stability of (AQ)₂₄NR3 was found to be governed by its amphiphilic pattern [160, 161, 218, 314], its low hydrophobicity [140, 152, 315], the α -helical structure of its NRC-domain [160, 257] and the protein's net charge [185, 316]. At low concentrations, (AQ)₂₄NR3 favorably interacts with the aqueous solvent by adopting a thermodynamically favored (reduction of free energy) conformation, e.g. micelles, which excludes the hydrophobic residues from water, while hydrophilic or polar groups remain in contact with water and thus avoid premature aggregation [37, 160, 218, 257, 314, 317]. That observation is similar to globular proteins which are soluble in aqueous solutions by adopting a compact spheroidal conformation in their native state. Recently, a group observed that silk proteins in solution (both *in vivo* and *in vitro*) are composed of two diffusing populations: a high proportion of "native" solubilized proteins and a small amount of high molecular weight oligomers [318]. However, with increasing concentration, the propensity of amphiphilic recombinant fibrous proteins shifts towards the spontaneous organization into ordered structures, a process known as self-assembly [6, 7, 37, 94, 114, 158]. For regenerated or recombinant silk solutions concentrated with techniques applying osmotically driven water loss, it was observed that even at higher concentrations, proteins still adopted micellar structures [30, 37]. Thus, the self-assembly process driven by preferential interactions between hydrophobic residues of the protein molecules, which require less energy than trying to minimize the exposure of these hydrophobic residues to water [189], results in coalescence of those micelles into larger globules (see Figure 4.1) [37].

Therefore, destabilizing additives that weaken hydrophobic intermolecular interactions between proteins have an effect on both, globular and in particular on the aggregation-prone fibrous proteins. (AQ)₂₄NR3 solutions showed an improved solution stability upon addition of cosolvents that destabilize protein-protein interactions such as detergents, chaotropic and charged cosolvents. These additives form preferential interactions (hydrophobic with the peptide group or electrostatic with charged residues, respectively), weakening intermolecular interactions e.g. between hydrophobic groups of (AQ)₂₄NR3 [287, 288, 312, 319]. Upon addition of sodium cholate (anionic detergent) and urea at concentrations below 1 M, a reduced phase separation/aggregation and improved solution stability of (AQ)₂₄NR3 was observed. The addition of an equimolar mixture of charged amino acids Arg and Glu apparently revealed a similar effect on (AQ)₂₄NR3 solution stability as urea or sodium cholate. Due to the negligible number of charged residues in (AQ)₂₄NR3 [160], this observation must also be linked to the formation of preferential hydrophobic interactions between Arg/Glu and (AQ)₂₄NR3 rather than electrostatic effects [313].

In contrast to destabilizing cosolvents, sorbitol, PEG and TMAO enhance the stability of the native protein. Since the native conformation of (AQ)₂₄NR3 is intrinsically unfolded while globular proteins are typically present in a folded conformation, the effects upon addition of stabilizing agents

are unclear. For globular proteins, sorbitol below a critical concentration (below 40 % (w/v)) was found to stabilize the protein's native conformation by stabilizing its surrounding water structure which led to preferential hydration of the protein [286, 288, 312]. However, the addition of sorbitol (below 30 % (w/v)) to an (AQ)₂₄NR3 solution led to a decreasing stability. This effect was more pronounced with increasing sorbitol concentration and is likely caused by increasing protein-sorbitol interactions [286, 288]. The addition of a PEG (4 kDa) solution showed a similar correlation between PEG concentration and (AQ)₂₄NR3 solution stability as sorbitol, and might be related to a high propensity of PEG and (AQ)₂₄NR3 to form hydrophobic interactions [287]. Furthermore, a two-phase system was observed for these solutions due to an excluded volume effect, resulting in increased local protein concentration and, thus, aggregation [265]. The addition of TMAO also reduced (AQ)₂₄NR3 solution stability with increasing TMAO concentration due to a solvophobic effect exerted on the peptide backbone that disfavors interactions between (AQ)₂₄NR3 and water [287, 312]. The assumption that the addition of destabilizing cosolvents results affects the stability of (AQ)₂₄NR3 solutions more is confirmed upon addition of a mixture of stabilizing TMAO and destabilizing urea, revealing a domination of stabilizing effects by urea.

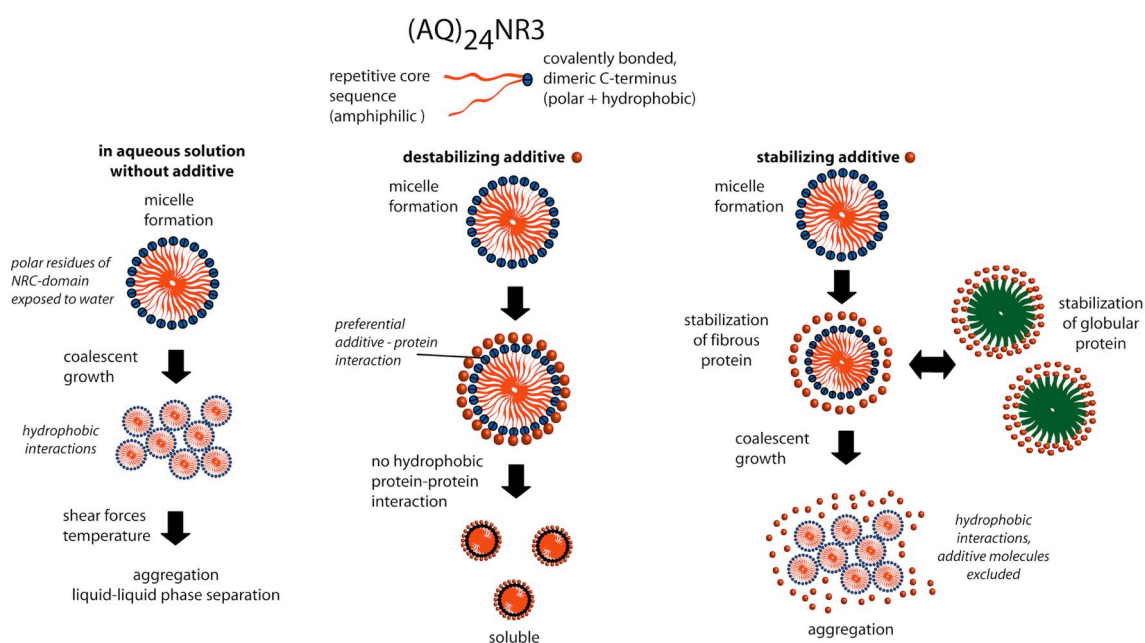


Figure 4.1 – Model for stabilization of concentrated solutions from (AQ)₂₄NR3

Based on these results, a model for stabilization of concentrated solutions from (AQ)₂₄NR3 is proposed and displayed in Figure 4.1. As a consequence, the stability of (AQ)₂₄NR3 solutions

was ensured by adding sodium cholate, as the preparation of the Arg-Glu and urea buffers was considered to be economically inefficient and their application was not further pursued in this work. Following addition of sodium cholate, the shear sensitive (AQ)₂₄NR3 could be concentrated by ultrafiltration up to 20 % (w/v) and stored for 14 days.

4.1.2 Rheological characterization of aqueous (AQ)₂₄NR3 and RSF solutions

Rheological flow characteristics of dilute (AQ)₂₄NR3 and RSF solutions revealed the characteristic shear thinning in the low shear rate regime and a transition into Newtonian behavior with increasing shear rates confirming observations for dilute native and regenerated silk solutions [30, 36, 133, 172, 297]. The shear thinning behavior likely results from an unstable balance between shear forces (trying to uncoil molecules) and solvent effects (trying to return them into compact coiled conformations) [172], while the Newtonian behavior is believed to be caused by the extension of silk chains, which gives rise to an increased number of intermolecular interactions. The resulting compact coiled structures were found to remain stable even under high shearing conditions due to strong interactions with solvent molecules [30, 172], thereby forming an extended gel network (typical for random coil conformations) already observed in dilute native and regenerated silk solutions [36, 133, 297].

Higher concentrated (AQ)₂₄NR3 and RSF solutions showed a different behavior compared to concentrated native silk solutions, although the characteristic power-law shear thinning of natural silk dopes [133] and molten polymers with increasing shear rates was detected, however less pronounced. Furthermore, the critical shear rate for onset of their shear thinning was found to be well in the regime of estimated shear rates (at the walls) within the distal part of spinning duct [44]. Concentrated native silk solutions are typically characterized by a zero-shear viscosity and shear thickening behavior in the low shear rate regime. Shear thickening, commonly reported for associating polymer systems, is believed to arise from the intermolecular interactions between hydrophobic dangling ends [121, 180, 189], with an increasing collision probability in the presence of an imposed deformation [177, 189], and ultimately resulting in orientation and elongation of polymers [36] (and references therein). The concentrated (AQ)₂₄NR3 and RSF solutions, however, did not display this shear thickening behavior in the low shear regime, likely caused by the lower molecular weight of the (AQ)₂₄NR3 and the lower solution concentrations of (AQ)₂₄NR3 and RSF compared to the native silk dope [36, 44, 121]. To increase silk solution viscosity, high molecular weight polymers were added to the (AQ)₂₄NR3 solutions and increased the viscosity by five orders of magnitude (see Section 3.1.5). However, the blending of aqueous polymeric additive solutions with (AQ)₂₄NR3 solutions was hampered by phase separation and aggregation upon

mixing. Thus, the addition of high molecular weight polymers to aqueous silk solutions did not improve the spinnability of engineered silk solutions and was not further pursued.

Although concentrated (AQ)₂₄NR3 and RSF solutions revealed a crossover point (i.e. the inverse of the relaxation time), indicating a transformation within the spinning dope found to be critical for successful silk spinning [45], both solutions behaved contrary to native silk dopes below and above the crossover point, displaying solid-like viscoelastic behavior over long time scales (low shear regime) and liquid-like behavior over short time scales (high shear regime). These observations were related to structural and conformational differences between native and artificial proteins [297]. At low shear rates, (AQ)₂₄NR3 and RSF solutions showed similar behavior as dilute solutions, displaying micellar structures typical for recombinant or regenerated silk solutions arranged in an extended gel network. The liquid-like behavior of native silk dope in the low shear regime is related to the lack of flexibility of the molecules within a concentrated environment, and corresponds well with the entangled polymer network model developed to describe storage conditions of concentrated silk solutions in the glands [36, 40, 133, 260, 297]. Polymer rheology thus suggested that concentrated native silk dopes behaved like undiluted polymers of high molecular weight acting as liquids or very weak gels [133, 225, 320]. It is suggested that the elasticity of native silk solutions arises from structures formed through ionic bonding between fibroin molecules and divalent metallic ions which are not present in regenerated solutions [36]. Regenerated silk proteins were observed to show a higher propensity to form intramolecular interactions at higher concentrations [297]. Thus, concentrated (AQ)₂₄NR3 and RSF solutions, tended to form intramolecular and intermolecular interactions enhanced by shearing, which forced the molecules into contact. As a consequence, the proteins lost their flexibility (compare entangled polymer network model) and the solutions displayed the liquid-like behavior with higher shear rates.

Strikingly, upon addition of at least 0.5 M phosphate (AQ)₂₄NR3 and RSF solutions displayed strong shear thickening behavior with increasing shear rates (see Section 3.1.7). In contrast, the addition of chloride (which is present in the lumen during silk protein storage) did not reveal such a behavior. These results confirmed earlier studies that indicated that upon addition of sodium chloride no protein aggregation was observed [117], while the addition of a critical phosphate concentration (approx. 0.5 M) induced formation of highly hydrophobic β -sheet structures [117, 121, 125, 165, 180, 257], due to increase of surface tension of water and promotion of hydrophobic interactions between proteins [63]. A similar effect was observed while increasing the temperature of the concentrated (AQ)₂₄NR3 solution, although not for the concentrated RSF solution (see Section 3.1.8). These results confirm that high temperatures favor hydrophobic interactions and thus the formation of β -sheet structures [124, 129]. The sharp increase of viscosity at a critical

4.1 Analysis of an aqueous (AQ)₂₄NR3 silk spinning dope

transition temperature can be related to the high kinetic process phase transition from random coil to β -sheet rich and is illustrated by the transformation of dope from opaque to white solid [133, 227]. Time effects on (AQ)₂₄NR3 and RSF solutions were analyzed (see Section 3.1.9) and a time-dependent behavior of (AQ)₂₄NR3 and RSF solutions as a function of concentration was determined. The effects were more pronounced for (AQ)₂₄NR3, which displays a strong sensitivity against shearing as revealed by irreversibly deformed internal structures. RSF solutions, in contrast, show a great extent and speed of recovery of initial structure. The results of (AQ)₂₄NR3 solution can be interpreted by increases in molecular bonding, with shear probably orienting molecules within a timescale allowing formation of stable structures transforming from gel to solid [133]. The effects of pH on silk fiber assembly, e.g. through controlled dimerization of the amino-terminal domain of spider silk proteins, have been demonstrated recently [112, 114]. However, due to lack of time, the influence of pH on rheological properties of silk solutions could not be investigated in this work.

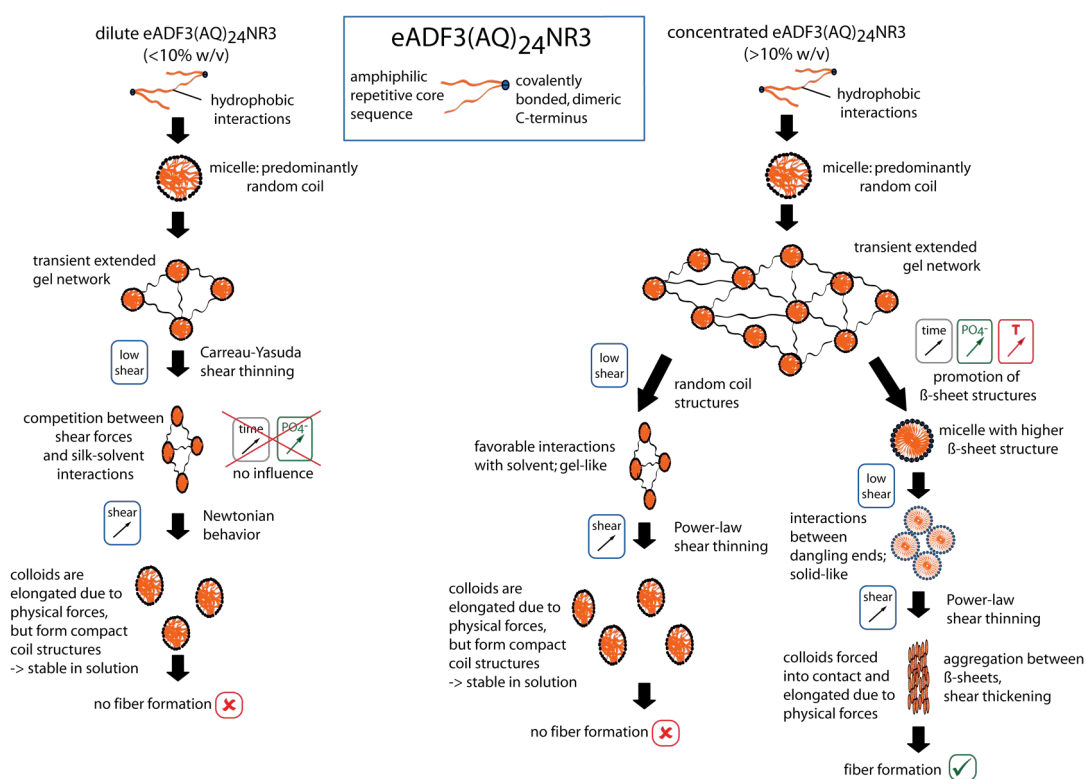


Figure 4.2 – Model for (AQ)₂₄NR3 assembly in solution based on rheological studies [285] (Permission for reprint granted by Green Materials, ICE Publishing).

Based on the findings a model for the assembly mechanism of (AQ)₂₄NR3 in solution into a spinning dope as a function of (AQ)₂₄NR3 concentration, shear forces and solution environment (ionic

strength and temperature) was proposed (see Figure 4.2). Conclusively, the rheological data highlights the importance of concentrated solution and distinct solution conditions such as presence of phosphate and shear as a prerequisite for successful fiber formation. Furthermore, these results approve the observation that the NR3 domain of (AQ)₂₄NR3 acts as a trigger for controlled assembly and stabilization upon addition of salting-out ions and salting-in ions, respectively [107, 117]. Nonetheless, the data presented also reveal that there is a difference between engineered silk solutions and native silk dopes, which will impact fiber processing and mechanical properties of the fibers.

4.2 Biomimetic adaptation of the natural spinning process

In order to enable the relevant mass transfer processes for silk spinning, a concept of an existing diffusion unit was redesigned for a continuous biomimetic spinning process and refined within the course of this work (Figure 4.3). The precise flow control of small amounts of (AQ)₂₄NR3 solutions at very low rates could be achieved using a syringe pump system (Harvard 33) with a 1 ml syringe. For future application in a continuous spinning process, a high precision micro annular gear pump (mzr-4605) equipped with a refillable sample reservoir for continuous processing was also tested and successfully installed.

A major redesign step towards a continuous spinning process involved the switch from a phosphate-PAA gel to a phosphate buffer solution due to persistent gel-drying upon extended utilization periods. For the successful generation of mass transfer processes using the buffer solution, different types of membranes, such as a Thomapor[®] Biospectra cellulose membrane, a ceramic membrane and a PES membrane were selected, tested and evaluated with respect to their mass transfer properties (see Section 3.2.2) and their handling (in particular fixation) properties. As a consequence of the frequent handling difficulties due to imperviousness and fixation issues for the very thin Thomapor[®] Biospectra cellulose and ceramic membrane, the PES membrane appeared to be the most suitable. Mass transfer experiments revealed that mass transfer is a function of retention time as well as temperature. A retention time of 4.5 s was detected to yield phosphate concentrations (approx. 0.16 M) close to that required for spinning inside the cellulose membrane. However, the phosphate mass transfer into the other membranes was significantly lower due to thicker membrane layers. Therefore, the diffusivity obtained via Fick's first law (see Equation 3.5) was now used as the parameter for flow rate and mass transfer control. This led to improved phosphate mass transfer for the PAA-phosphate gel (by nearly two thirds) and the ceramic membrane (by four times), however, the mass transfer measured for the PES membrane remained at a very low level, even at higher retention times. Mass transfer

4.2 Biomimetic adaptation of the natural spinning process

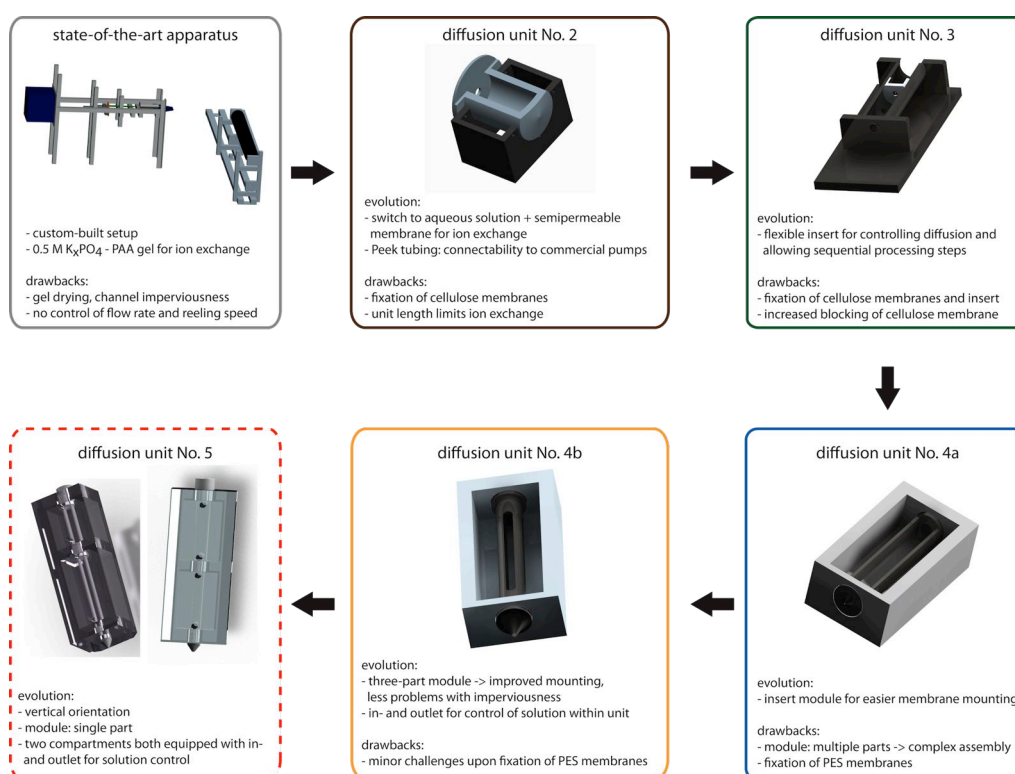


Figure 4.3 – Summary on evolution of diffusion unit.

at elevated temperatures revealed an improvement with increasing temperatures, however, the results of these studies could not be used to draw any conclusions due to issues with evaporation. In contrast to these mass transfer results, only in presence of potassium phosphate an increased $(AQ)_{24}NR3$ solution turbidity at the exit of the diffusion unit was observed during spinning tests using that PES membrane. The observed turbidity is a good indicator for conformational changes from random coil to β -sheet structures initiated by phosphate transferred into the membrane. The negligible number of charged residues in $(AQ)_{24}NR3$ leads to the conclusion that electrostatic interactions between $(AQ)_{24}NR3$ and phosphate can be excluded as an explanation for the increased mass transfer during spinning tests. Thus, the mass transfer results did not reflect the actual transfer of phosphate into the PES (or other) membranes and the data should therefore be treated carefully.

Water resorption within the spinning duct and evaporation in air, accounting for the liquid-solid phase transition that results in fiber formation [32, 53, 168], were technically mimicked by using hygroscopic solutions or by heat-induced evaporation (see Section 3.2.3). The application of hygroscopic solutions did not yield a sufficient solvent removal to enable fiber formation within given retention times. Moreover, it was observed that ethanol diffused into the membrane (instead

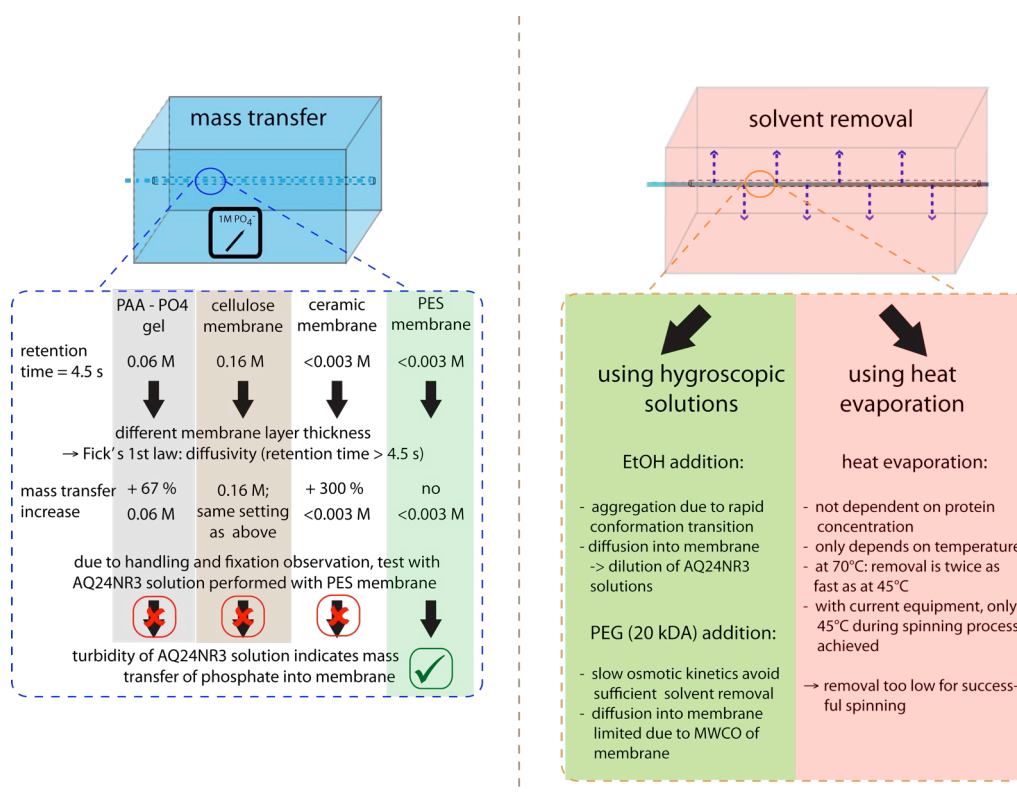


Figure 4.4 – Summary of mass transfer and solvent removal results

of removing water), which turned (AQ)₂₄NR3 solutions turbid although the viscosity was not increased. Furthermore, diffusion of ethanol into the membrane led to premature formation of gel-like (AQ)₂₄NR3 aggregates that could not be elongated into fibers. This is likely a consequence of the more pronounced and rapid conformational transition into β -sheet structures induced by ethanol [217, 222]. Upon addition of a 20 % (w/v) PEG (20 kDa) solution, solvent removal behaved similar. This result was in contrast to an earlier study, in which the addition of PEO likely accelerated the assembly of RSF into a silk I structure as well as defined the final morphology of the fibers [37]. The difference is likely related to the application of indirect (via mass transfer) instead of direct addition of PEG, suggesting that the osmotic process kinetics of PEG are too slow to initiate assembly within the given time frame in this work. A setup to investigate heat-induced using an infrared lamp was established and enabled the generation of temperatures between 40 °C to 50 °C in the vicinity of the membrane. Thereby, water was removed from the (AQ)₂₄NR3 solution as shown by significant droplet formation along the outside edges of the PES membrane. Remarkably, after inducing water evaporation by heat, fibers could be drawn from the viscous droplets at the exit of the membrane bearing another short period of drying, e.g. between tweezer-

ers. Pan-weighing experiments revealed that the water diffusion coefficients of (AQ)₂₄NR3 and RSF solutions are a function of temperature, being almost twice as high at 70 °C than at 45 °C, but independent of concentration and silk solution applied (see Section 3.2.3). These findings confirm that the diffusion coefficient can be regarded as a constant at a defined temperature, which is beneficial concerning the resistance to internal water diffusion and distinguishes silk solutions from most synthetic polymer solutions [168]. D_{ss} values determined were higher than those of native *N. clavipes* spinning dope [167, 168]. This finding reflects the aforementioned temperature dependence, as Kojic et al. induced evaporation at 25 °C while constantly blowing air at 150 ml min⁻¹. Conclusively, the results indicate that higher temperatures in the vicinity of the PES membrane result in increased water removal and thus shorten the time until fibers can be drawn. For successful spinning, temperatures near the PES membrane likely need to be increased to ~70 °C or even higher. However, this was not feasible with the setup applied in this work and requires a use of more advanced techniques to induce heat evaporation.

4.3 Processing of silk fibers from (AQ)₂₄NR3 solutions

Although biomimetic spinning experiments were conducted at flow rate settings (15 µl min⁻¹ to 30 µl min⁻¹) in the regime of other technical spinning procedures [45, 204], and with (AQ)₂₄NR3 solutions whose spinnability was approved by a simple hand-drawing technique [161, 215], fibers could not be drawn directly from the spinning apparatus. Instead, fibers could only be drawn from the viscous droplets formed at the exit of the membrane after an additional period of drying e.g. in-between tweezers. This observation was independent of membrane applied, although the time required for the additional drying step varied, and correlated with the aforementioned observations concerning water removal and ion exchange. This can be explained as during the natural spinning process, when a *Nephila* spider draws out a thread at a typical speed of 20 mm s⁻¹, flow rates were found to be an order of magnitude lower (around 0.25 nl s⁻¹) [27, 32]. Consequently, the time allowed for mass transfer and solvent removal processes is significantly higher in nature than in the technical setup. This finding is confirmed when the retention time for mass transfer was extended to 100 s to 200 s and additional heat-induced evaporation was applied. The resulting fibers could then be drawn within 2 s to 5 s from the viscous drop formed at the exit of the spinning apparatus (PES membrane surrounded by a 1 M potassium phosphate (pH 8) solution). Furthermore, in the natural process, solvent removal occurs already within the final part of the spinning duct and only the remaining water is squeezed out after the spigot to lock molecules into their final orientation [169, 187]. This is in contrast to the pure external solidification draw down as found in industrial spinning processes. Moreover, it was observed that for polymers or spider silk, the process of

orientation requires time as quick solidification proved to be disadvantageous for the orientation due to the immobility of molecular chains. It was assumed that a cross-section of the spinning dope spends around 20 s in the spinning duct [168].

Due to the inability to spin fibers directly from the biomimetic apparatus, artificial silk fibers were typically produced by a modified hand-drawing procedure. The technique of hand-drawing fibers from a viscous solution has allowed the investigation of spinning parameters using a small amount of silk protein solution and further enabled the production of artificial fibers with decent properties for mechanical characterization [161, 215]. This method was refined in this work by using a rotating mandrel to collect fibers up to 1 m in length at maximum reeling speeds of 20 mm s^{-1} [304]. This collection speed is well in the range of take-up speeds used in other fiber spinning studies (10 mm s^{-1} to 30 mm s^{-1}) [45, 168], but at the lower limit of spinning speeds observed in the natural process (15 mm s^{-1} to 120 mm s^{-1}) [47, 80]. The rotating mandrel enabled the production of smooth fibers with reduced diameter variations, while wet-spun fibers typically display a spongy-like appearance [206, 207]. This appearance is caused by the coagulating solvent entrapped inside the fiber, which evaporates upon drying and leaves behind numerous pores, requiring post-spin applications to improve fiber morphologies [207].

Hand-drawing experiments revealed, that a concentration of 4.5 % (w/v) and distinct solution characteristics ("oily-like") were necessary to successfully produce fibers. The "oily-like" appearance reflects the formation of (AQ)₂₄NR3 dimers or oligomeric micellar-like coagulates as determined by dynamic light scattering [161]. The successful production of fibers from the N-terminal region depleted (AQ)₂₄NR3 protein is in good agreement with observations by Rising and coworkers. Their results indicated that the repetitive regions mediate intermolecular interactions and the C-terminal domain governs spidroin polymerization into ordered fibrous structures, while the N-terminal domain is not essential for *in vitro* fiber formation [144]. It was further observed, that fibers were only produced upon addition of chaotropic salts, such as phosphate or sulfate, at concentrations above 0.5 M and that fiber production properties did depend on the salt added. Remarkably, the addition of potassium phosphate (pH 8) allowed the quasi-instantaneous production of 1 m long fibers with a smooth and homogeneous morphology. In contrast, the addition of (NH₄)₂HPO₄, (NH₄)₂SO₄ or NaH₂PO₄ resulted in less frequent in fiber formation. If fibers were successfully formed, the time required before fibers could be drawn was significantly higher than for potassium phosphate. Furthermore, the resulting fibers, in particular those prepared from (NH₄)₂SO₄, were shorter and revealed a more inhomogeneous surface. (NH₄)₂HPO₄ and NaH₂PO₄ presumably hampered fiber production due to their slower salting-out effects, while the stronger kosmotropic salt (NH₄)₂SO₄ resulted in inferior fiber formation and morphology due to pronounced conformation transition kinetics, as had also been observed by an earlier study,

wet-spinning RSF into different $(\text{NH}_4)_2\text{SO}_4$ coagulation bath compositions [213]. These results confirmed earlier observations that silk fiber assembly depended on a distinct interaction between the salting-out ions and the silk proteins [107, 180, 182, 184].

Based on the results in this work, a potential route for successful fiber formation is illustrated and summarized in Figure 4.5. Conclusively, a potential route for successful fiber production could be shown, however, processing speeds need to be reduced to enhance mass transfer and solvent removal as well as to improve orientation of silk molecules.

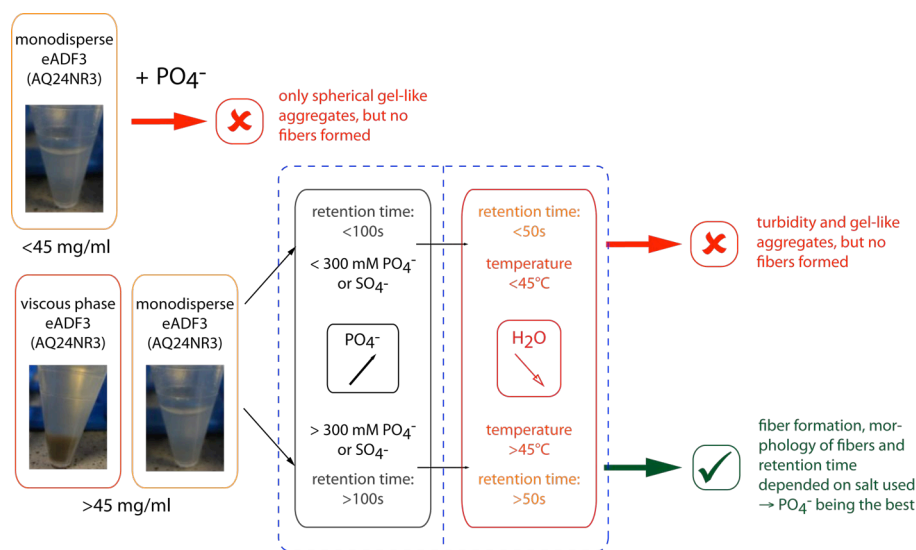


Figure 4.5 – Schematic display of route to successful production of fibers from a concentrated $(\text{AQ})_{24}\text{NR3}$ solution

4.4 Mechanical characterization of silk fibers

Dragline silk fibers of *A. diadematus* spiders revealed a strong dependance on spinning speed and humidity [304], confirming published data of forcibly silked *A. diadematus* fibers [64, 234] as well as observations that dragline silk from *A. diadematus* is more prone to humidity influences than any other silk [59, 78, 79, 91, 96, 97, 101, 105, 132, 305, 306, 321]. These observations can be related to the structure of *A. diadematus* MA silk, containing a low volume fraction of very small crystals separated by rather long amorphous chains and a high proline content.

The classic model for dragline silks assumes that β -sheet nanocrystallites are linked via amorphous chains or hydrogen bonds to form an entangled network [21, 51, 247, 322]. Actually, two types of β -sheet structures have been identified in silks: 1) intramolecular β -sheets (non-

crystalline β -sheets) [101] and 2) intermolecular β -sheet crystallites that crosslink individual silk protein molecules and form the molecular network [51, 101, 273, 323]. The intermolecular β -sheet crystallites were found to consist of highly oriented and poorly oriented crystallites, with the latter ones being important in effectively coupling the highly oriented crystalline domains and the amorphous regions [101]. Under stretching, the intramolecular β -sheets within the amorphous regions unfold to release the length of protein chains, while the β -crystallites remain unaffected. This gives rise to a high extension of draglines up to the yield point without breaking the intermolecular linkages. Stretching beyond the yield point results in breakage of weak intramolecular hydrogen bonds and the randomly arranged chains extend and slide past each other, resulting in plastic deformation [101, 105, 247, 323]. As more chains are extended, the load will begin to be taken up by the crystalline regions until load cannot be accommodated anymore and the interchain hydrogen bonds are finally broken [22]. The stiffness of the intermolecular nanocrystals is thus highly essential for specific deformation mechanisms displayed by silk and crucial for its mechanical properties [323]. Thus, the molecular network will be stretched to support the load resulting in stiffer filaments, a process referred to as "strain-hardening" [314]. These observations are displayed in the stress-strain curves of silk, revealing an initial stiff, elastic region which is followed by a yield region (indicated by a decrease in the slope of the stress-strain curve due to major structural transitions in the fiber) and further stiffening until failure [21, 32, 55, 199, 230, 235, 239, 245, 246, 306, 324].

With increasing reeling speeds, stiffness and tensile strength increased while extensibility was reduced as a consequence of improved molecular orientation within the fiber [47, 64, 68, 78, 191, 193, 234, 307, 325–327], and reduced size of β -sheet nanocrystals [247, 328, 329]. The improved orientation (i.e. enhanced formation of β -sheet crystalline regions) has been observed to be a consequence of the spider's ability to actively manipulate the tensile behavior of its fibers by using a friction brake mechanism to control the tension applied to its silks upon drawing [60, 192, 232] or by actively controlling the protein flow through the spinning apparatus, thereby varying fiber diameter and microstructure [32, 66] without resorting to a change in polymer composition, spinning rate or processing temperature [60]. It was observed that the forces exerted by their friction brake differ up to 20-fold between the different spinning behaviors, such as web building or forced silking, and enables the spider to react to a broad range of conditions [64, 192, 193, 234], but also resulting in a large variability of stress strain curves. The mechanical data of orb-web collected silk revealed a significantly higher variance than that of forcibly silked fibers, which can be explained by the irregular speed pattern during web building and regular web refurbishments [60, 67]. The latter observation is characteristic for *A. diadematus* spiders which reconstructed and rebuilt their web on a daily basis in this study, while *Nephila* spiders, in contrast, were found to repair damaged sections [135, 191]. Forcibly silked fibers on the other hand had shown acceptable

reproducibility if tested under defined conditions and without spider's anesthetization [64, 68, 268, 269]. It should be noted, that variability allows production of material either matching environmental (interspecific) or individual requirements (intraspecific and intraindividual) and thus can also become a user-controlled aspect of artificial spinning if properly characterized and exploited [234, 239, 246].

Silks revealed characteristics of a rubber-like material with increasing humidities, displaying decreased tensile strength and toughness (lowest in presence of water), while the elongation to break increased simultaneously [304], confirming earlier findings that the shape of the stress-strain curves varies significantly upon changing the humidity [51, 52, 66, 68, 80, 82, 242, 282]. Stress-strain curves measured at a relative humidity of 30 % revealed two linear regimes which is consistent with data obtained for *Nephila* spiders [242] and characteristic for rigid, polymeric solids and further can be related to the limited mobility of their amino acid chains [305]. AFM indentation tests revealed that with respect to silk's core-shell structure a purely elastic behavior was typically observed in the outer core under these conditions, while a plastic effect was detected in the inner core, producing a highly resilient material [330]. The presence of microfibrils in the thread's core (oriented parallel to the fiber axis [33]) and being pulled out during fracture, similar to failure of man-made fiber-reinforced composites [29], is believed to contribute to the silk fiber's toughness [22]. Measurements at 70 % rH, in contrast, displayed a transition from stiff (glassy) to compliant (rubbery) in the stress-strain curve, with an extremely low value of elastic modulus at small deformations and a significant increase of stiffness at large deformations [51, 68, 77, 80, 82, 186, 242, 248, 249, 282, 331]. Fibers tested in the presence of water revealed the rubber-like behavior (elastomeric tensile characteristic with very low initial elastic modulus and large (above 50 %) elongation to break) as had been observed for wet *A. diadematus* fibers [74, 190] or *A. trifasciata* fibers [66]. The elastic regimes at low deformations are significant compared to the characteristic elastomeric behavior observed above 75 % rH in most other studies. This can be explained as fibers in this work were kept wet throughout testing, to avoid supercontraction effects that result in the shape of stress-strain curves appearing more like those of semi-crystalline polymers, since wetted and then re-dried silk shrank (if unrestrained) or the forces were generated within (if restrained) [51, 68, 72, 76, 190, 205, 332]. Upon increasing humidity or immersion in water, the outer core shifts towards a plastic behavior and weakens the fiber as a whole [330], since water molecules infiltrate the disordered amorphous domains by disrupting some of the hydrogen bonds initially present in the dry state, thereby reducing molecular orientation and turning the wet fibers more compliant [51, 52, 66, 68, 73, 74, 77–80, 82, 186, 223, 242, 247–249, 330, 332, 333]. Remarkably, the effects of humidity were more significant for fibers spun at lower speeds (FS60), confirming earlier observations [81]. The results indicate that FS60 fibers can be considered to be in a late stage of the transition regime, while FS200 fibers are more likely in an early stage.

The (AQ)₂₄NR3 biotech fibers, the first artificial fibers produced by an all-aqueous process, displayed mechanical properties well below their natural counterparts, but comparable to fibers produced from other recombinant silk analogs with similar molecular weights [195, 196, 198, 304]. However, its mechanical properties were also inferior to those of artificial fibers spun from higher molecular weight silk analogs, such as a native-sized recombinant protein that was wet-spun and displayed the highest tensile strength (508 ± 108 MPa) so far for artificial fibers and a reasonable elongation to break (15 ± 5 %) [157]. These results confirm the assumption that molecular weight plays a significant role in order to achieve mechanical properties of native counterparts as larger protein molecules give rise to more intermolecular interactions [195]. Moreover, the characteristics of the stress-strain curve of artificial fibers (in particular "hand-drawn") in all studies differed from that of native fibers, displaying the typical behavior of "cold-drawing" (lacking the yield point) observed for polymer materials [197, 198, 304]. The inferior stress-strain behavior can be related to the application of a rather simple self-assembling process during hand-drawing compared to the complex liquid crystal spinning process in natural spinning [32, 198]. Earlier studies on reconstituted silk showed that those silk fibers had lost all the key features of silk including the mechanical properties, albeit having the correct amino acid composition and sequence [26, 211, 214]. These observations were confirmed by FT-IR data revealing that forcibly silked fibers from *A. diadematus* displayed a β -sheet content of nearly 35 %, correlating well with other studies [22, 73, 99–101, 304, 307–310], while the data obtained for biotech fibers pulled from (AQ)₂₄NR3 by comparison typically showed a significantly lower β -sheet content (18 %) [304]. RSF fibers and *B. mori* silk fibers exhibited the same tendencies in this work as well as in earlier studies [206]. This led to the conclusion that forcing a higher percentage of the alanines to crystallize in the β -sheet conformation is a prerequisite for successful spinning of artificial fibers and for improving the mechanical properties [206].

Polarized FT-IR results indicated that biotech fibers also lacked orientation of their alanine-rich β -sheet crystals, as shown by similar values of S^{mol} at different angles to fiber axis. In contrast, earlier studies on dragline silk fibers revealed a strong parallel axial alignment of alanine-rich β -sheet crystals as indicated by NMR and x-ray scattering data [123, 186] as well as significantly differing S^{mol} values in polarized FT-IR [273, 311]. These results confirm earlier findings that pointed out the necessity of a post-stretching procedure for artificial silk fibers, e.g. in alcohol or water, to improve the mechanical properties (up to 10 fold), by improving molecular alignment and increasing crystallinity [45, 104, 136, 154, 178, 195, 196, 198, 206, 207, 212, 213, 216, 217, 219–221]. However, fibers produced from (AQ)₂₄NR3 appeared to be soluble in any sort of solvent and therefore post-stretching in water or any other solvent could not be performed. As a consequence, these fibers were post-treated by using an alternative steam annealing procedure (see Section 2.5.3). Strikingly, stress-strain behavior of post-treated fibers appeared to be much more

alike that of native silk, due to improved fiber morphology and increased crystallinity attributed to improved and more uniform molecular chain alignment as a result of promoted substitution of protein-protein hydrogen bonds by water-protein hydrogen bonds (plasticization by water and steam) [139, 154, 207, 213]. Post-stretched fibers were now no longer soluble in water because the tightly packed hydrophobic β -sheet regions remained immobile in the presence of water [104, 195]. However, the mechanical properties such as tensile strength of the best post-treated curves tested so far did reveal only a weak improvement of around 10 %.

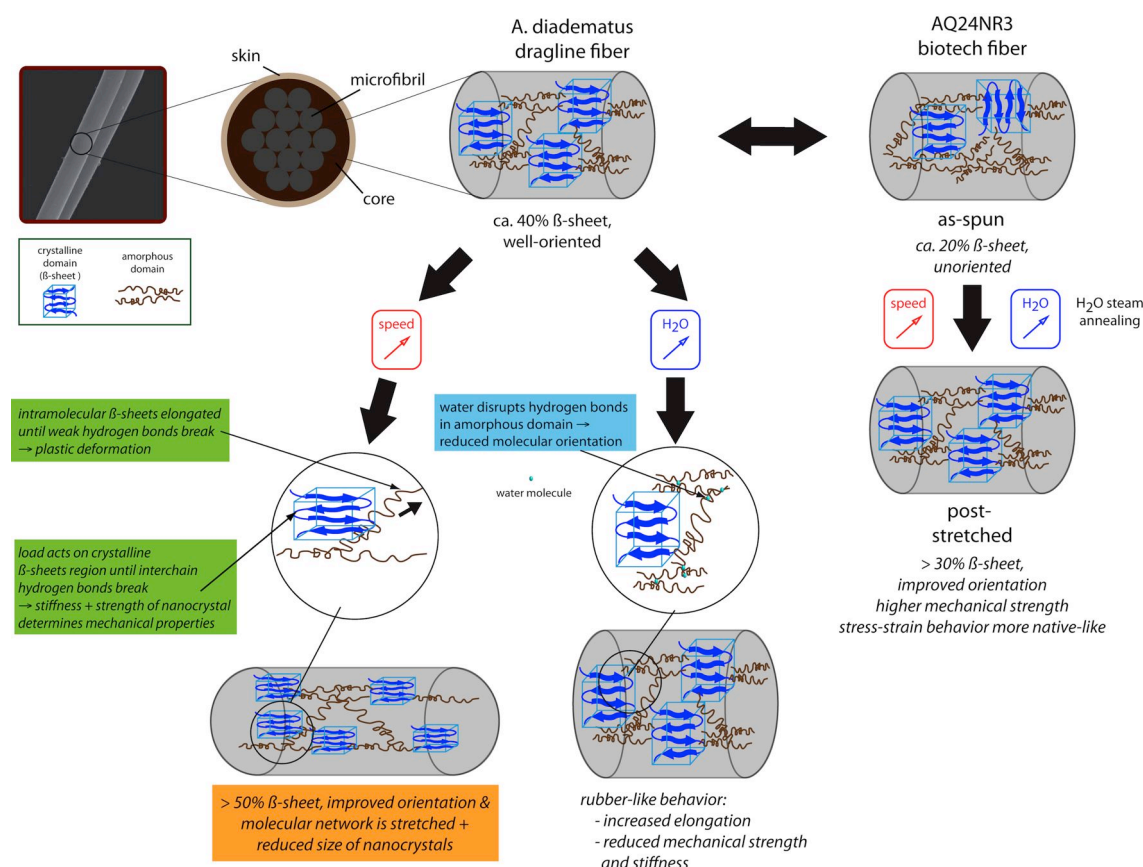


Figure 4.6 – Schematic illustration of the mechanical model proposed for native and artificial spider dragline silk.

5 Summary

Spider silk produced by orb-weaving spiders offers a large variety of technical applications due to its combination of mechanical strength and extensibility. However the utilization of spider silk in technical applications has so far been hampered by its limited availability, a consequence of spider's cannibalistic behavior. Furthermore, the artificial production of fibers as of today did not yield fibers with comparable mechanical properties due to differences in molecular structure, molecular weight, protein concentration and most importantly in the spinning process.

In this work, artificial fibers - for the first time produced in an all-aqueous biomimetic process - from the recombinant spider silk protein (AQ)₂₄NR3, which is based on the sequence (except the NRN-domain) of the dragline silk protein eADF3 of the European garden spider *A. diadematus*, are characterized. The influence of silk spinning dope properties (silk concentration, viscosity and solution stability), processing parameters (ion exchange and water removal) and spinning conditions (silk spinning speed and humidity) on fiber production and properties are systematically studied.

The addition of destabilizing cosolvents (sodium cholate and urea amongst others) improved the solution stability of (AQ)₂₄NR3, as determined by UV/Vis spectroscopy and SEM analysis, by weakening intermolecular protein interactions. In contrast, the addition of stabilizing agents (such as sorbitol or PEG) led to pronounced aggregation and precipitation of (AQ)₂₄NR3. Upon application of an ultrafiltration technique, (AQ)₂₄NR3 solutions (stabilized by sodium chlorate) could be prepared with concentrations up to 20 % (w/v) (i.e. close to the native range).

Rheological characterization of dilute (AQ)₂₄NR3 and RSF solutions revealed the characteristic flow behavior of shear thinning and transition into Newtonian behavior as observed in dilute native silk solutions. In contrast, the rheological behavior of concentrated (AQ)₂₄NR3 and RSF solutions distinguished in kind from that of native silk solutions, related to lower concentration, molecular weight and thus viscosity as well as structural and conformational differences. With (AQ)₂₄NR3 being the largest recombinant silk molecule available in this work, and the preparation of highly concentrated solutions hampered by aforementioned stability issues, viscosity of the solution was increased by adding water-soluble high molecular weight polymers such as PEG or PAA. Although viscosity of the silk solutions was significantly increased, blending of polymer

and (AQ)₂₄NR3 was limited in this work due to pronounced co-aggregation. However, this feature could provide a promising alternative for the preparation of highly viscous and aqueous silk spinning dopes in future works. During natural spinning and in *in vitro* studies of silk assembly, the addition of phosphate was observed to trigger the formation of β -sheet structure and further to account for the strength of the final fiber. Therefore, the addition of phosphate to (AQ)₂₄NR3 solutions and its effect on the rheological behavior was analyzed and revealed that the presence of phosphate and shear is essential for successful fiber formation. Moreover, temperature and time as additional parameters that can be influenced during technical spinning and their effects on silk solutions were also characterized and indicated strong dependence in particular for concentrated solutions. Thereby, exposure to increased temperatures revealed a similar behavior as addition of phosphate.

For successful biomimetic adaptation of the natural spinning process, a so-called diffusion unit enabling the important processes within the spinning process, such as ion exchange and water removal, was modified and optimized for application in a continuous spinning process. Therefore, a precise pumping system was installed and different membrane types (cellulose, ceramic and PES) were evaluated with respect to installation as well as mass transfer properties. Thorough testing revealed that the PES membrane appeared to guarantee longest running times in a technical process due to very limited operational failures compared to the other two types. Mass transfer studies to investigate the ion exchange were performed using conductivity which limited the measurement to mass transfer from phosphate buffer into Tris/HCl buffer. As expected, the studies revealed that mass transfer of phosphate is a function of flow rate. However, the mass transfer into the PES membrane appeared to be lower than that into the cellulose or ceramic membrane. This was in contrast to initial spinning tests with (AQ)₂₄NR3 solutions which indicated a phosphate transfer into the membrane as (AQ)₂₄NR3 solutions due to observed silk solution turbidity at the end of the diffusion unit.

Water removal was approached by two different methods: removal using hygroscopic solutions such as PEG and EtOH or heat evaporation. The first approach did not reveal any positive effects on water removal due to diffusion effects or processing kinetics. The effects of heat evaporation were analyzed using a so-called pan-weighing procedure and revealed strong temperature dependence of the diffusion coefficient, while no dependence on the silk protein concentrations was observed. Pan-weighing studies showed that with temperatures around 70 °C water could be completely removed in the pan-weighing experiments. However, with the current biomimetic spinning setup, heat evaporation yielded only temperatures of around 45 °C. For future works, installing a heat generation setup that will achieve temperatures around 70 °C will be an important factor for successful production of fibers. As a consequence of insufficient heat evaporation, fibers could not

be directly produced using the biomimetic spinning setup.

Therefore, artificial fibers with up to 1 m length were produced by a modified hand-drawing procedure. The hand-drawing studies revealed a minimum concentration (4.5 % (w/v)) and "oily-like" solution behavior as prerequisites for successful fiber formation as well as a dependence of fiber formation from the type of salt added. Fibers with high homogeneity and smoothness could be easily produced upon addition of potassium phosphate while upon addition of ammonium sulphate or other kosmotropic salts, fiber production was less frequent, required more time and the resulting fibers appeared brittle and less smooth.

For a better understanding of underlying differences between natural and biotech silk fibers, a mechanical and structural characterization of these fibers was performed. Tensile testing of natural *A. diadematus* fibers revealed a strong dependence on silking speed and humidity as observed for other natural spider silk fibers. Fibers spun (or forcibly silked) at higher speeds showed higher stiffness, strength but less extensibility while fibers spun at higher humidity displayed a rubber-like behavior, characterized by higher extensibility and lower strength and stiffness. Artificially produced fibers displayed mechanical properties inferior to their native counterparts and artificial fibers produced from high molecular weight silk analogs, but comparable to fibers produced from silk analogs with similar molecular weight. Moreover the stress-strain characteristics of artificial fibers were different to those of native silk, displaying the typical cold-drawing behavior observed for many polymers. From earlier studies, it is well known that post-treatment improved the mechanical properties of artificial fibers therefore a few initial tests were conducted at the end of the work and reveal the promising potential of post-spin steam annealing in order to improve mechanical strength. Apparently, the stress-strain characteristics of post-treated fibers now displayed the typical behavior of native silk fiber. To investigate the origin of the differences between mechanical properties, FT-IR and polarized FT-IR measurements were conducted. The results indicate that artificial fibers displayed less β -sheet content than native fibers and that β -sheet crystals in artificial fibers showed significantly less orientation.

Overall, this work provides information about the preparation of concentrated recombinant spider silk solutions and how the production of fibers from these solutions may be affected and controlled by varying processing parameters. The results reveal insights into the differences between artificial and native silk solutions and fiber, providing essential knowledge for future approaches to produce fibers from an all aqueous solution with mechanical properties comparable to native silk fibers.

6 Zusammenfassung

Spinnenseide produziert von Radnetzspinnen bietet durch seine Kombination aus mechanischer Stärke und Dehnbarkeit eine Vielzahl an Möglichkeiten für den Einsatz in technischen Anwendungen. Allerdings ist die Verwendung von Spinnenseide durch die limitierte Verfügbarkeit, eine Konsequenz des kannibalistischen Verhaltens von Spinnen, eingeschränkt. Darüber hinaus wiesen künstliche Spinnenseidenfasern bisher deutlich schlechtere mechanische Eigenschaften auf im Vergleich zur natürlichen Spinnenseide. Die Gründe hierin werden in Unterschieden in der Molekülstruktur, dem Molekulargewicht, der Proteinkonzentration und vor allem im Spinnprozess vermutet.

In dieser Arbeit wurden künstliche Fasern zum allerersten Mal in einem rein wässrigen biomimetischen Prozess aus dem rekombinanten Spinnenseidenprotein (AQ)₂₄NR3 hergestellt und charakterisiert. Das rekombinante Protein leitet sich von der Sequenz (mit Ausnahme der nicht-repetitiven aminoterminalen Domäne) des eADF3-Proteins, ein Hauptbestandteil des Abseilfaden der europäischen Gartenkreuzspinne *A. diadematus* ab. Der Einfluss von Lösungseigenschaften (Konzentration, Viskosität und Stabilität), Prozessparameter (Ionenaustausch und Wasserentfernung) und Spinnbedingungen (Spinngeschwindigkeit und Feuchte) auf Faserherstellung und -eigenschaften wurden systematisch untersucht.

Durch Zugabe von destabilisierenden Reagenzien (z.B. Natriumcholat oder Harnstoff) konnte die Stabilität der (AQ)₂₄NR3 Lösungen durch Schwächung der intermolekularen Proteinwechselwirkungen verbessert werden wie UV/Vis-Spektroskopie und REM Analysen zeigten. Im Gegensatz hierzu resultierte die Zugabe von stabilisierenden Reagenzien (z.B. Sorbitol oder PEG) in verstärkter Aggregation von (AQ)₂₄NR3. Mittels Ultrafiltration konnten - durch Natriumcholat stabilisierte - (AQ)₂₄NR3 Lösungen mit Konzentrationen bis zu 20 % (w/v) (nahe am natürlichen Bereich) hergestellt werden.

Rheologische Untersuchungen verdünnter (AQ)₂₄NR3 und RSF Lösungen zeigte die charakteristischen scherverdünnenden Fließeigenschaften und den Übergang in Newton'sches Verhalten wie er auch in verdünnten nativen Seidenlösungen beobachtet wurde. Im Gegensatz dazu unterschied sich das rheologische Verhalten konzentrierter (AQ)₂₄NR3 und RSF Lösungen, bedingt durch niedrigere Konzentrationen, niedrigeres Molekulargewicht und daher niedrigeren Viskositäten

sowie durch strukturelle und konformative Unterschiede deutlich von dem natürlicher Seidenlösungen. Da (AQ)₂₄NR3 das größte am Lehrstuhl verfügbare Protein darstellt und die Herstellung hochkonzentrierter Lösungen wie oben beschrieben durch Stabilitätsprobleme eingeschränkt war, wurde versucht durch Zugabe von wasserlöslichen Polymeren mit hohem Molekulargewicht (z.B. PEG oder PAA) die Viskosität der Spinnlösung zu verbessern. Obwohl die Viskosität dadurch deutlich erhöht werden konnte stellte das Herstellen der Polymer- und der (AQ)₂₄NR3 Mischung durch verstärkte Co-Aggregation noch ein deutliches Hindernis in dieser Arbeit dar. Nichtsdestotrotz könnte dieser Ansatz in Zukunft eine vielversprechende Alternative zur Herstellung hoch viskoser wässriger Spinnlösungen darstellen. Im Rahmen des natürlichen Spinnprozesses und *in vitro* Studien zur Seidenassemblierung zeigte sich, dass die Zugabe von Phosphat die Bildung von β -Faltblattstrukturen auslöst und sich damit für die mechanischen Eigenschaften der Faser verantwortlich ist. Daher wurde die Zugabe von Phosphat zu (AQ)₂₄NR3 Lösungen und der Einfluss auf die rheologischen Eigenschaften analysiert und zeigte, dass die Gegenwart von Phosphat und Scherkräften ein entscheidender Bestandteil für ein erfolgreiches Verspinnen darstellt. Des Weiteren wurden mit Temperatur- und Zeiteinflüssen weitere mögliche Parameter die im Spinnprozess eingestellt werden können und deren Auswirkungen auf die Spinnlösung untersucht. Dabei zeigte sich eine starke Abhängigkeit insbesondere der konzentrierten Seidenlösungen von beiden Parametern. Unter Temperatureinfluss zeigten die Seidenlösungen dabei ein ähnliches Verhalten wie unter Zugabe von Phosphat.

Für eine erfolgreiche biomimetische Adaption des natürlichen Spinnprozesses wurde eine sogenannte Diffusionseinheit die die wichtigsten Prozesse innerhalb des Spinnprozesses, Ionenaustausch und Wasserentzug ermöglicht, modifiziert und hinsichtlich einer Anwendung in einem kontinuierlichen Spinnprozess optimiert. Dafür wurden ein präzises Pumpsystem installiert und verschiedene Membrantypen - Zellulosehohlfaser, Keramik und PES - vor allem hinsichtlich Einbau und Stofftransporteigenschaften evaluiert. Ausführliche Tests zeigten das die PES Membran die längste ausfallfreie Laufzeit im technischen Prozess im Vergleich zu den anderen Membrantypen garantieren kann. Untersuchungen zum Ionenaustausch wurden mit Leitfähigkeitsmessungen durchgeführt, allerdings messtechnisch bedingt nur für den Austausch zwischen Phosphatpuffer und Tris/HCl-Puffer. Wie erwartet zeigten die Ergebnisse eine Abhängigkeit der Stofftransports von der Verweilzeit, die durch die Durchflussrate kontrolliert wird. Interessanterweise zeigten die Stofftransportmessungen mit der PES Membran niedrigeren Ionenaustausch als mit den anderen Membranen. Bei ersten Spinnversuchen in der Apparatur mit (AQ)₂₄NR3 Lösungen zeigte sich allerdings ein offensichtlicher Phosphataustausch, dargestellt durch eine Trübung der (AQ)₂₄NR3 Lösung am Ausgang der Diffusionseinheit.

Wasserentfernung wurde in dieser Arbeit durch zwei verschiedene Ansätze verfolgt: zum Einen

durch hygroskopische Lösungen wie PEG oder Ethanol und zum Anderen durch Verdampfung mittels Hitze. Mittels hygroskopischer Lösungen konnte dabei kein Erfolg erzielt werden, da die kinetischen Prozesse entweder zu langsam (PEG) oder zu schnell (Ethanol) stattfinden oder die Lösung durch Diffusion von Ethanol in die Membran verdünnt und beeinflusst wurde. Der Einfluss der Temperatur auf die Verdampfungskinetiken wurde mittels sogenannter *pan-weighing* Experimente ermittelt und zeigte eine starke Abhängigkeit des Diffusionskoeffizienten von Wasser von der Temperatur ab. Interessanterweise zeigte sich allerdings keine Abhängigkeit von der Proteinkonzentration (bzw. zu entfernenden Wassermenge). Die Ergebnisse dieser Studie zeigten ferner das mit Temperaturen um 70 °C das Wasser komplett aus den Seidenlösungen entfernt werden konnte. Jedoch konnten mit dem gegenwärtigen Spinnapparat nur Temperaturen im Bereich von 45 °C generiert werden. Damit war der Wasserentzug für ein erfolgreiches Verspinnen der Lösung zu gering. Für zukünftige Arbeit zeigen diese Erkenntnisse aber auch, dass der Einsatz einer Verdampfungseinheit, die Temperaturen um die 70 °C ermöglicht, ein wichtiger Bestandteil für die Etablierung eines erfolgreichen Spinnprozesses darstellt.

Durch die unzureichende Verdampfung konnten keine Fasern direkt aus dem biomimetischen Spinnapparat gesponnen werden. Daher wurden künstliche Fasern mit bis zu 1 m Länge durch ein modifiziertes *hand-drawing* Verfahren hergestellt. Dabei zeigte sich dass für ein erfolgreiches *hand-drawing* eine minimale Spinnlösungskonzentration von 4.5 % (w/v) und einem "ölgigen" Erscheinungsbild bedeutende Voraussetzungen für eine erfolgreiche Faserherstellung sind. Des Weiteren wurde eine Abhängigkeit der Faserherstellung vom zugesetzten Salz gezeigt. Fasern mit hoher Homogenität und Glattheit konnten relativ einfach nach Zugabe von Phosphat gezogen werden, während nach Zugabe von Ammoniumsulfat oder anderen kosmotropischen Salzen Fasern deutlich seltener bzw. erst nach längerer Zeit gezogen werden konnten. Darüber hinaus waren diese Fasern sehr spröde sowie weniger homogen und deutlich rauher.

Für ein besseres Verständnis der Unterschiede zwischen natürlichen und künstlichen Seidenfasern wurden mechanische und strukturelle Untersuchungen an diesen Fasern durchgeführt. Zugprüfungen an natürlichen *A. diadematus* Fasern zeigten eine starke Abhängigkeit von Spinnengeschwindigkeit und Luftfeuchtigkeit, die auch für Fasern von anderen Spinnen gefunden wurde. Fasern die bei höheren Geschwindigkeiten produziert wurden, z.B. durch *forced silking* zeigten eine höhere Steifigkeit und mechanische Stärke aber weniger Dehnbarkeit. Dahingegen zeigten Fasern bei höherer Luftfeuchtigkeit ein gummiartiges Verhalten, charakterisiert durch höhere Dehnbarkeit während Steifigkeit und mechanische Stärke deutlich schwächer waren. Künstliche Fasern hingegen wiesen deutlich schwächere mechanische Eigenschaften auf als natürliche Fasern und künstliche Fasern die aus Proteinen mit höherem Molekulargewicht hergestellt wurden. Im Vergleich zu künstlichen Fasern, die aus Proteinen mit ähnlichem Molekulargewicht

unter Nutzung organischer Lösungsmittel gesponnen wurden, zeigten die Fasern in dieser Arbeit vergleichbare Eigenschaften. Die Spannungs-Dehnungs-Kurven künstlicher Fasern zeigten das typische Verhalten kaltgezogener Polymere auf und unterschieden sich damit deutlich von der Charakteristik natürlicher Spinnenseide, Frühere Studien haben gezeigt dass durch Nachbehandlung (z.B. Nachziehen) der Fasern deren mechanische Eigenschaften verbessert werden konnten. Hier wurden gegen Ende der Arbeit daher ein paar Versuche durchgeführt und Ergebnisse nach Dampfnachbehandlung (ohne Zug) zeigten, dass diese Methode ein vielversprechendes Potenzial für künftige Arbeiten darstellen kann um die Eigenschaften der künstlichen Fasern zu verbessern. Interessanterweise zeigten nachbehandelte Fasern nun das typische Spannungs-Dehnungs-Kurven Verhalten der natürlichen Seidenfasern. Um die Unterschiede der mechanischen Eigenschaften zwischen natürlichen und künstlichen Fasern zu untersuchen wurden FT-IR und polarisiertes FT-IR Messungen durchgeführt. Die Ergebnisse dieser Untersuchungen zeigten dabei das der β -Faltblattanteil in den künstlichen Fasern deutlich geringer ausfällt, und darüber hinaus dass die Orientierung dieser β -Faltblatt Kristalle deutlich weniger ausgeprägt war wie in natürlicher Seide.

Zusammengefasst liefert diese Arbeit wichtige Erkenntnisse zur Herstellung konzentrierter rekombinanter Spinnenseidenlösungen und wie die Herstellung von Fasern aus diesen Lösungen durch die Prozessparameter beeinflusst und kontrolliert werden kann. Die Ergebnisse dieser Arbeit geben auch einen Einblick in die Unterschiede zwischen künstlicher und natürlicher Spinnenseidenlösung und -fasern, und liefern somit wichtige Erkenntnisse für zukünftige Ansätze zur Herstellung von Fasern aus wässrigen Lösungen mit mechanischen Eigenschaften vergleichbar zur natürlichen Seide.

7 Appendix

Table 7.1 – Overview on tensile testing instrument evaluation for installation at the chair of biomaterials, UBT.

	INSTRON 5564-69	DIASTRON LEX810	BOSE Electroforce® 3220
instrument type	vertical table-top	vertical or horizontal table-top	vertical or horizontal table-top
force resolution	n.a.	0.05 - 0.5 mN	mN
applications	biomaterials	micro fibers, hair	biomaterials, soft tissue, films
advantages	easy-to-use	smooth curves	variety of applications, low noise
disadvantages	strong noise effects, sensitive to environmental influences	reduced noise (software plots moving average value), complex sample handling procedure	sensitive to environmental influences, short displacement

Table 7.2 – Overview on adhesives tested

adhesive	dosing	hardening	water resistance	connectivity with overhead transparency	creeping	effect on artificial fiber properties
superglue	+	++	o	++	++	-
model making glue	++ (mini canula)	+	+	++	+	-
all-purpose glue	o	-	-	+	-	-
nail polish	o (brush)	+	+	+	+	-
UV adhesive	++	- (only with UV light)	o	+	+	n.a.
double-sided adhesive tape	++	+	n.a.	+	o	++

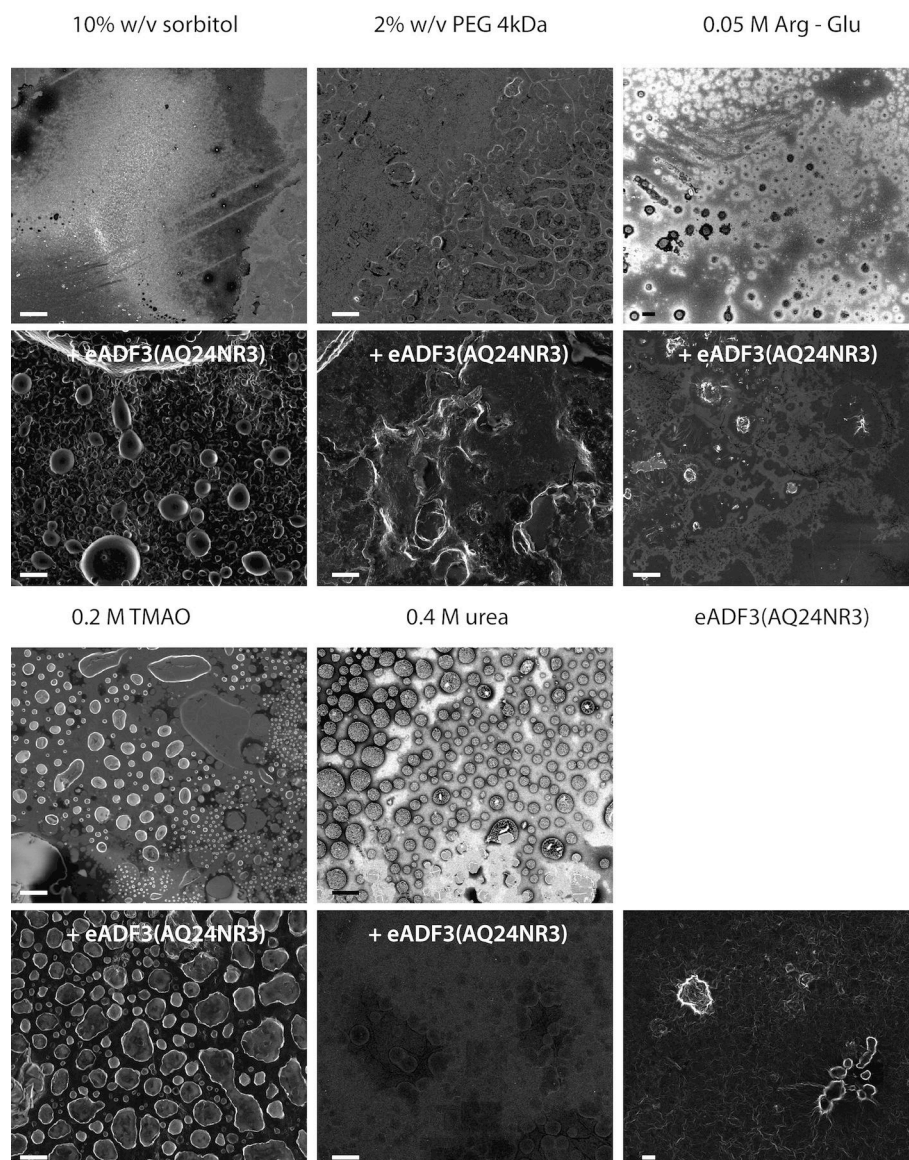


Figure 7.1 – SEM images comparing films cast from (AQ)₂₄NR3 solutions containing solubility additives after 14 days (scale bars correspond to 10 μ m).

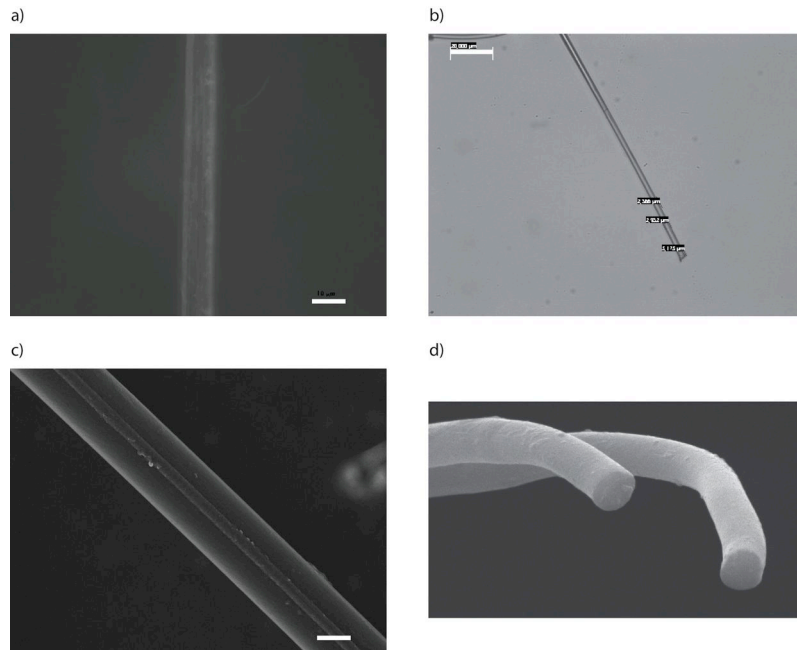


Figure 7.2 – Comparison of different imaging techniques for fiber diameter characterization: a) PLM, b) LMBF and c) SEM. Image d) reveals the circular cross-section of natural silk fibers (white scale bars: a) and c) correspond to 10 μm ; b) 20 μm).

Table 7.3 – Overview of data for *A. diadematus* silk, *B. mori* silk, cotton and Kevlar[®] fibers from literature or tested in this work (n = number of samples, rH = relative humidity).

sample	n	rH [%]	elongation to break [%]	tensile strength [MPa]	diameter [μm]
<i>A. diadematus</i> orb web	8	35 - 45	30 ± 10	581 ± 267	5
<i>A. diadematus</i> FS60	7	30	29 ± 5	770 ± 181	8.2 ± 1.2
<i>A. diadematus</i> orb web [230]	6	45	39 ± 3	1154 ± 140	n.a.
<i>B. mori</i> silk	5	30	19 ± 4	613 ± 59	11.7
<i>B. mori</i> silk [22]	10	50 ± 5	22 ± 4	400 ± 100	50 ± 7
<i>B. mori</i> silk [29]	10	60	15 ± 2	650 ± 40	n.a.
<i>B. mori</i> silk [334]	6	60	22 ± 2	530	n.a.
cotton	5	30	10 ± 4	310 ± 173	12.5
cotton	5	70	14 ± 2	457 ± 140	12.5
wool [52]	n.a.	100	50	200	n.a.
Kevlar [®] 49	5	30	13 ± 1	2995 ± 182	13.7
Kevlar [®] 29 [55]	n.a.	n.a.	4	2800	n.a.
FS20 [234]	30	50	28 ± 4	1080 ± 160	n.a.

membrane	ID	pore size [nm]	length [mm]	salt solution	C _{sp} [mg/ml]	protein	C _{protein} [mg/ml]	pump [type]	rate [mg/min]	problems during process	fiber formation (at the membrane exit) (after acid drying, ground)	add-on water removal	observations
Thomapor	0.2	50	50	KPO4 - buffer pH8	500	AQ24, no ps	520	custom	na	blockage	✗	0	only turbidity
	0.2	50	50	KPO4 - buffer pH8	500	AQ12, no ps	850	custom	na	blockage	✗	10	
	0.2	35	35	KPO4 - buffer pH8	1000	Fibroin		mzr-4605	0.083	blockage	✗		
	0.2	30	30	KPO4 - buffer pH8	1000	Fibroin	65	mzr-4605	0.166	blockage	✗		
	0.9	50	50	20% acrylamide (200μl APS + 100μl TEMED) + PO4	500	Fibroin	65	mzr-4605	0.083	blockage	✗		visible aggregation
Gel	0.9	50	50	20% acrylamide (200μl APS + 100μl TEMED) + PO4	500	Fibroin	115	mzr-4605	0.02 - 0.083	none	✗		visible aggregation, close to fiber formation
	1.1	50	50	20% acrylamide (200μl APS + 100μl TEMED) + PO4	500	Fibroin	65	mzr-4605	0.02 - 0.166	slight blockage	✗		visible aggregation
Gel	0.7	50	50	20% acrylamide (200μl APS + 100μl TEMED) + PO4	500	Fibroin	115	mzr-4605	0.083	slight blockage	✗		visible aggregation
	0.9	50	50	20% acrylamide (200μl APS + 100μl TEMED) + SO4	500	Fibroin	65	mzr-4605	0.02 - 0.083	part. blockage, gel was brittle	✗		visible aggregation, close to fiber formation
Gel	0.9	50	50	20% acrylamide (200μl APS + 100μl TEMED) + SO4	500	Fibroin	115	mzr-4605	0.02 - 0.083	brittle gel	✗		visible aggregation, close to fiber formation
	0.5	50	50	20% acrylamide (200μl APS + 100μl TEMED) + PO4	500	no ps	600	mzr-4605	0.0015	blockage	✗	-	
Gel	0.7	50	50	20% acrylamide (200μl APS + 100μl TEMED) + PO4	500	no ps, oily	600	mzr-4605	0.0015	none	✗	60 - 120	
	1	50	50	20% acrylamide (200μl APS + 100μl TEMED) + PO4	500	no ps	600	mzr-4605	0.0015	none	✗	-	
ceramic	0.8	10	36	KPO4 - buffer pH8	1000	Fibroin	65	mzr-4605	0.083	blockage after 5min	✗		visible aggregation
	0.8	10	86	KPO4 - buffer pH8	1000	no ps	1500	mzr-4605	0.2	none	✗	-	
	0.8	10	86	KPO4 - buffer pH8	1000	no ps	1500	mzr-4605	0.05	none	✗	-	
	0.8	10	86	KPO4 - buffer pH8	1000	no ps	1500	mzr-4605	0.02	blockage	✗	-	
	0.8	10	36	KPO4 - buffer pH8	1000	no ps	1500	mzr-4605	0.02	blockage	✗	-	
	0.8	10	36	KPO4 - buffer pH8	1000	no ps	1500	mzr-4605	0.03	blockage	✗	-	
	0.8	10	36	KPO4 - buffer pH8	1000	no ps	1500	mzr-4605	0.05	blockage	✗	-	
	0.8	10	36	KPO4 - buffer pH8	1000	no ps	1500	mzr-4605	0.05	blockage	✗	60	
	0.8	10	36	4% PEG (200000 g/mol) + KPO4 - buffer pH8	1000	no ps	1500	mzr-4605	0.05	none	✗	-	
	0.8	10	36	4% PEG (200000 g/mol) + KPO4 - buffer pH8	1000	no ps	1500	mzr-4605	0.03	blockage	✗	-	
Microdyn PES	0.8	10	36	KPO4 - buffer pH8	1000	no ps	1500	Harvard 33	0.05	(V too low)	✗	-	too much water
	0.8	10	36	KPO4 - buffer pH8	1000	no ps	360	Harvard 33	0.05	none	✗	-	too much water
	0.8	10	36	KPO4 - buffer pH8	1000	no ps	360	Harvard 33	0.01	none	✗	-	dryer
	0.8	160 (Tank: 90; Lair: 60)	160	KPO4 - buffer pH8	1000	PS	1200	Harvard 33	0.03	none	✗	-	turbid, but no fiber
	0.8	160 (Tank: 90; Lair: 60)	160	KPO4 - buffer pH8	1000	PS	1200	Harvard 33	0.015	(p to low)	✗	-	
Microdyn PES	0.8	10	160 (Tank: 90; Lair: 60)	KPO4 - buffer pH8	1000	PS, oily	1200	Harvard 33	0.03	none	✗	2-5	membrane (drop extremely viscous, small water)

Figure 7.3 – Full list of biomimetic spinning experiments - page 1

Microdyn PES	0.8	10	160 (Tank: 90; Lair: 60)	KPO4 - buffer pH8	1000	PS, oily	1200	Harvard 33	0.03	none	✗	✓	2-5	in air	droplets outside of membrane)
Microdyn PES	0.8	10	160 (Tank: 90; Lair: 60)	KPO4 - buffer pH8	1000	PS, oily	1300	Harvard 33	0.03	none	✗	✓	2-5	membrane in air	(drop extremely viscous, tears after short elongation, small water droplets outside of membrane)
Microdyn PES	0.8	10	160 (Tank: 90; Lair: 60)	KPO4 - buffer pH8	1000	PS, oily	1300	Harvard 33	0.025	none	✗	✓	2-5	membrane in air	(drop extremely viscous, tears after short elongation, small water droplets outside of membrane)
Microdyn PES	0.8	10	160 (Tank: 90; Lair: 60)	KPO4 - buffer pH8	1000	PS, oily	1300	Harvard 33	0.02	none	✗	✓	2-5	membrane in air	(drop extremely viscous, tears after short elongation, small water droplets outside of membrane)
Microdyn PES	0.8	10	160 (Tank: 90; Lair: 60)	KPO4 - buffer pH8	1000	PS, oily	1300	Harvard 33	0.015	none	✗	✓	2-5	membrane in air	(drop extremely viscous, tears after short elongation, small water droplets outside of membrane)
Microdyn PES	0.8	10	160 (Tank: 90; Lair: 60)	KPO4 - buffer pH8	1000	PS, oily	1300	Harvard 33	0.02	none	✗	✓	2-5	membrane in air	(drop extremely viscous, tears after short elongation, small water droplets outside of membrane)
Microdyn PES	0.8	10	160 (Tank: 90; Lair: 60)	KPO4 - buffer pH8	1000	PS, oily	1300	Harvard 33	0.015	none	✗	✓	2-5	membrane in air	(drop extremely viscous, tears after short elongation, small water droplets outside of membrane)
Microdyn PES	0.8	10	160 (Tank: 90; Lair: 60)	KPO4 - buffer pH8	1000	PS, oily	1400	Harvard 33	0.03	none	✗	✗	-	membrane in air	water, gel-like aggregates instead of fiber
Microdyn PES	0.8	10	160 (Tank: 90; Lair: 60)	KPO4 - buffer pH8	1000	dialyzed against 10 mM Tris (pH8); PS	1400	Harvard 33	0.02	none	✗	✓	30-45	dryer	water, gel-like aggregates instead of fiber
Microdyn PES	0.8	10	160 (Tank: 90; Lair: 60)	KPO4 - buffer pH8	1000	PS	1400	Harvard 33	0.01	(V too low)	✗	✗	-	membrane in air	no transport
Microdyn PES	0.8	10	160 (Tank: 90; Lair: 60)	KPO4 - buffer pH8	1000	PS	1500	Harvard 33	0.03	none	✗	✗	-	membrane in air	water, gel-like aggregates instead of fiber
Microdyn PES	0.8	10	160 (Tank: 90; Lair: 60)	KPO4 - buffer pH8	1000	dialyzed against 10 mM NaCO (pH10.4); PS	1500	Harvard 33	0.02	none	✗	✓	30-45	dryer	water, gel-like aggregates instead of fiber
Microdyn PES	0.8	10	160 (Tank: 90; Lair: 60)	KPO4 - buffer pH8	1000	PS	1500	Harvard 33	0.01	(V too low)	✗	✗	-	membrane in air	no transport
Microdyn PES	0.8	10	160 (Tank: 90; Lair: 60)	KPO4 - buffer pH8	1000	PS	1300	Harvard 33	0.03	none	✗	✓	20-30	membrane in air	(drop extremely viscous, tears after short elongation, small water droplets outside of membrane but less than above due to higher lab humidity)
Microdyn PES	0.8	10	160 (Tank: 90; Lair: 60)	KPO4 - buffer pH8	1000	PS	1300	Harvard 33	0.015	none	✗	✓	20-30	membrane in air	(drop extremely viscous, tears after short elongation, small water droplets outside of membrane but less than above due to higher lab humidity)
Microdyn PES	0.8	10	160 (Tank: 90; Lair: 60)	KPO4 - buffer pH8	1000	dialyzed against 10 mM NaCO (pH10.4); PS	1500	Harvard 33	0.03	none	✗	✓	30	membrane in air	too much water
Microdyn PES	0.8	10	160 (Tank: 90; Lair: 60)	KPO4 - buffer pH8	1000	PS	1500	Harvard 33	0.02	none	✗	✓	30-45	membrane in air	too much water
Microdyn PES	0.8	10	160 (Tank: 90; Lair: 60)	KPO4 - buffer pH8	1000	PS	1500	Harvard 33	0.03	none	✗	✗	-	membrane in air	20% EtOH, EtOH diffuses into membrane
Microdyn PES	0.8	10	160 (Tank: 90; Lair: 60)	KPO4 - buffer pH8	1000	PS	1500	Harvard 33	0.03	none	✗	✓	45-60	membrane in air	80% EtOH, EtOH diffuses into membrane
Microdyn PES	0.8	10	160 (Tank: 90; Lair: 60)	KPO4 - buffer pH8	1000	PS	1500	Harvard 33	0.03	none	✗	✓	45-60	membrane in air	too much water
Microdyn PES	0.8	10	100 (Tank: 90; Lair: 10)	KPO4 - buffer pH8	1000	oil	750	Harvard 33	0.03	none	✗	✓	3-5	membrane in air	not enough phosphate? - droplets outside of membrane // adding PO4 to viscous drop enabled fiber formation
Microdyn PES	0.8	10	100 (Tank: 90; Lair: 10)	KPO4 - buffer pH8	1000	oil	750	Harvard 33	0.003	none	✗	✓	3-5	membrane in air	not enough phosphate? - droplets outside of membrane // adding PO4 to viscous drop enabled fiber formation

Figure 7.4 – Full list of biomimetic spinning experiments - page 2

Microdyn PES	0.8	10	160 (Tank: 90; Lair: 60)	KPO4 - buffer pH8	1000	olly	750	Harvard 33	0.03	none	✗	✓	3 - 5	membrane in air	
Microdyn PES	0.8	10	150 (Tank: 100; Lair: 50)	KPO4 - buffer pH8	1000	olly	867	Harvard 33	0.03	none	✗	✗	-	membrane in air	too much water
Microdyn PES	0.8	10	150 (Tank: 100; Lair: 50)	KPO4 - buffer pH8	1000	olly	867	Harvard 33	0.01	none	✗	✗	-	membrane in air	too much water
Microdyn PES	0.8	10	150 (Tank: 100; Lair: 50)	KPO4 - buffer pH8	1000	olly	867	Harvard 33	0.01	none	✗	✗	-	membrane (L = 5 cm) in 5% PEG 100KDa;	too much water
Microdyn PES	0.8	10	100	KPO4 - buffer pH8	1000	Fibroin (oly) + 300 mM PO4	102.145046	Harvard 33	0.2	none	✗	✗	-		too much water
Microdyn PES	0.8	10	100	KPO4 - buffer pH8	1000	Fibroin (oly) + 300 mM PO4	102.145046	Harvard 33	0.05	none	✗	✗	-		too much water
Microdyn PES	0.8	10	100	KPO4 - buffer pH8	1000	Fibroin (oly) + 300 mM PO4	102.145046	Harvard 33	0.01	none	✗	✗	-		too much water
Microdyn PES	0.8	10	100	KPO4 - buffer pH8	1000	Fibroin (oly) + 300 mM PO4	102.145046	Harvard 33	0.005	none	✗	✗	-		too much water
Microdyn PES	0.8	10	150 (Tank: 100; Lair: 50)	KPO4 - buffer pH8	1000	Fibroin (oly) + 300 mM PO4	102.145046	Harvard 33	0.015	none	✓	✓	>10	membrane in air	(drop extremely viscous, small water droplets outside of membrane)
Microdyn PES	0.8	10	150 (Tank: 100; Lair: 50)	KPO4 - buffer pH8	1000	Fibroin (oly) + 300 mM PO4	102.145046	Harvard 33	0.015	none	✗	✗	-	membrane in IR box	T= 36-45°C; no fiber formation
Microdyn PES	0.8	10	150 (Tank: 100; Lair: 50)	KPO4 - buffer pH8	1000	Fibroin (oly) + 300 mM PO4	102.145046	Harvard 33	0.02	none	✗	✗	-	membrane in IR box	T= 36-45°C; no fiber formation
Microdyn PES	0.8	10	150 (Tank: 100; Lair: 50)	KPO4 - buffer pH8	1000	Fibroin (oly) + 300 mM PO4	102.145046	Harvard 33	0.01	none	✗	✓	>60	membrane in IR box	T = 45°C; fiber formation only enabled using separated viscous droplet (~15cm)
Microdyn PES	0.8	10	150 (Tank: 100; Lair: 50)	KPO4 - buffer pH8	1000	Fibroin (oly) + 400 mM PO4	102.145046	Harvard 33	0.01	none	✓	✓	>10	membrane in IR box	T = 49°C; close to fiber drawing from droplet at membrane exit @ v=0.02; interrupting process enabled fiber drawing from membrane exit after extend. Period of drying
Microdyn PES	0.8	10	150 (Tank: 100; Lair: 50)	KPO4 - buffer pH8	1000	Fibroin (oly) + 300 mM PO4	102.145046	Harvard 33	0.01	none	✓	✓	>120	membrane in IR box	T = 43 - 48°C; close to fiber drawing from droplet at membrane exit @ v=0.02; interrupting process enabled fiber drawing from membrane exit after extended period of drying
Microdyn PES	0.8	10	150 (Tank: 100; Lair: 50)	KPO4 - buffer pH8	1000	AQ24NR3 (oly) + 300 mM PO4	564.4402634	Harvard 33	0.02	none	✗	✗	-	membrane in IR box	T = 48 - 52°C; RH = 45%; no viscous droplet
Microdyn PES	0.8	10	150 (Tank: 100; Lair: 50)	KPO4 - buffer pH8	1000	AQ24NR3 (oly) + 300 mM PO4	564.4402634	Harvard 33	0.015	none	✗	✗	-	membrane in IR box	T = 48 - 52°C; RH = 45%; no viscous droplet
Microdyn PES	0.8	10	150 (Tank: 100; Lair: 50)	KPO4 - buffer pH8	1000	AQ24NR3 (oly) + 300 mM PO4	564.4402634	Harvard 33	0.01	none	✗	✗	-	membrane in IR box	T = 48 - 52°C; RH = 45%; no viscous droplet
Microdyn PES	0.8	10	150 (Tank: 100; Lair: 50)	10mM Tris/HCl - buffer pH8 + 100mM NaCl + 10mM Na-Cholat					0.015	none	✗	✗	-	membrane in IR box	solution clear as in front of tank => PO4 required for spinning
Microdyn PES	0.8	10	150 (Tank: 100; Lair: 50)	KPO4 - buffer pH6	1000	AQ24NR3 (oly)	564.4402634	Harvard 33	0.015	none	✗	✗	-	membrane in IR box	too watery for spinning

Figure 7.5 – Full list of biomimetic spinning experiments - page 3

3µl each of protein + salt mixed using tweezers; after a few second fibers were drawn and transferred to rotating mandrel (rot. speed =16,7 mm/s)

protein	C _{protein} [mmol]	salt	C _{salt} [mmol]	lag time prior to spinning [s]	fiber length [cm]	polymer	C _{polymer} [mmol]	Comments
AQ24NR3 (25806)	629.59	KPO4 - buffer pH8	500	>20	2 - 3			
AQ24NR3 (25806)	314.79	KPO4 - buffer pH8	500	10	2	C32NR4	22.41	fiber broke immediately after drawing
AQ24 (101106)	811.55	KPO4 - buffer pH8	500	10	2			
AQ24NR3 (101106)	605.36	KPO4 - buffer pH8	500	10	2			
AQ24NR3 (050507)	705.55	KPO4 - buffer pH8	500	10	2			
AQ24NR3 (201109)	705.55	KPO4 - buffer pH8	500	>20	2 - 5			
AQ24NR3 (201109)	705.55	NH4SO4	1000	>20	2 - 5			
AQ24NR3 (190210)	752.59	KPO4 - buffer pH8	1000	30	5 - 10			
AQ24NR3 (020310)	752.59	KPO4 - buffer pH8	1000	>20	10			
AQ24NR3 (120310)	752.59	KPO4 - buffer pH8	500	5 - 10	2 - 10			
AQ24NR3 (270410)	585.51	KPO4 - buffer pH8	500	>50	2 - 5			from viscous phase of phase separated sol. extremely difficult
AQ24NR3 (140410) - 14d	690.73	KPO4 - buffer pH8	500	2 - 5	5 - 10			
AQ24NR3 (120310) - 30d	752.59	KPO4 - buffer pH8	500	30	15			from viscous phase of phase separated sol.
AQ24NR3 (270111)	517.40	KPO4 - buffer pH8	500	>10	10			
AQ24NR3 (080211)	838.66	KPO4 - buffer pH8	500	5 - 10	30 - 50			
AQ24NR3 (080211) - 7d	838.66	KPO4 - buffer pH8	500	>20	10 - 20			
AQ24NR3 (150211)	918.16	KPO4 - buffer pH8	500	5 - 10	5 - 30			
AQ24NR3 (150211) - 8d	918.16	KPO4 - buffer pH8	500	5 - 10	30 - 100			
AQ24NR3 (150211) - 14d	459.08	KPO4 - buffer pH8	500	5 - 10	5 - 10	PEG 100KDa		125 only short fiber, but thicker?
AQ24NR3 (150211) - 14d	459.08	KPO4 - buffer pH8	500	5 - 10	5 - 10	PEG 35KDa		1785.71 influence on turbidity, also on fiber?
AQ24NR3 (150211) - 14d	459.08	KPO4 - buffer pH8	500	5 - 10	5 - 10	PAA 10KDa		12500 only AQ fiber, no mixture?
AQ24NR3 (150211) - 14d	459.08	KPO4 - buffer pH8	500	5 - 10	5 - 10	glycerol		2714.74 no fibers, solution shows weak turbidity and decrease viscosity
AQ24NR3 (150211) - 14d	459.08	KPO4 - buffer pH8	500	-	-	alginate	50	
AQ24NR3 (150211) - 14d	459.08	KPO4 - buffer pH8	500	5 - 10	20 - 80	PVA		851.31 only short fiber, but thicker?
AQ24NR3 (170311) - 7d	705.55	NH4HP04	500	>20	10 - 30			
AQ24NR3 (170311) - 7d	705.55	NH4SO4	500	>20	10 - 30			
AQ24NR3 (170311) - 14d	705.55	KPO4 - buffer pH8	500	>30	10 - 60			
AQ24NR3 (170311) - 14d	705.55	NH4HP04	500	>20	10 - 30			
AQ24NR3 (170311) - 14d	705.55	NH4SO4	500	>20	20 - 100			
AQ24NR3 (170311) - 14d	705.55	NH4HP04	500	>20	10 - 30			
AQ24NR3 (140411) - 6d	498.59	KPO4 - buffer pH8	50	-	-			
AQ24NR3 (140411) - 6d	498.59	KPO4 - buffer pH8	100	-	-			
AQ24NR3 (140411) - 6d	498.59	KPO4 - buffer pH8	150	-	-			
AQ24NR3 (140411) - 6d	498.59	KPO4 - buffer pH8	200	-	-			
AQ24NR3 (140411) - 6d	498.59	KPO4 - buffer pH8	250	> 120	< 5			time required before fiber can be drawn
AQ24NR3 (140411) - 6d	498.59	KPO4 - buffer pH8	300	>30	20 - 100			decreases with increasing phosphate conc.
AQ24NR3 (140411) - 6d	498.59	KPO4 - buffer pH8	350	>20	20 - 100			post-treated with ethanol
AQ24NR3 (140411) - 6d	498.59	KPO4 - buffer pH8	400	10 - 20	20 - 100			
AQ24NR3 (140411) - 6d	498.59	KPO4 - buffer pH8	450	10 - 20	20 - 100			
AQ24NR3 (140411) - 6d	498.59	KPO4 - buffer pH8	500	5 - 10	20 - 100			
AQ24NR3 (140411) - 6d	498.59	KPO4 - buffer pH8	500	5 - 10	20 - 100			
AQ24NR3 (140411) - 14d	564.44	KPO4 - buffer pH8	500	10 - 20	80			
AQ24NR3 (310511)	564.44	KPO4 - buffer pH8	500	5 - 10	20 - 100			post-treated with isopropanol vapor, or immersed in isopropanol (fiber breaks, no post-stretching due to thickness possible)
AQ24NR3 (300911)	564.44	KSO4	500	-	-			
AQ24NR3 (300911)	564.44	NH4HP04	500	-	-			
AQ24NR3 (300911)	564.44	NH4SO4	500	>20	10 - 50			difficult to draw
AQ24NR3 (300911)	564.44	NH4HP04	500	>20	5 - 10			good spinability, but dries faster / post-treated using isopropanol vapor
AQ24NR3 (121011)	658.51	Cl6 (Martha)	1677.15	5 - 10	10 - 80			

Figure 7.6 – Full list of hand-drawing experiments

Bibliography

- [1] C. Sanchez, H. Arribart, and M. M. Giraud Guille. "Biomimetism and bioinspiration as tools for the design of innovative materials and systems". In: *Nature Materials* 4 (2005), pp. 277–288.
- [2] N. Huebsch and D. J. Mooney. "Inspiration and application in the evolution of biomaterials". In: *Nature* 462 (2009), pp. 426–32.
- [3] I. Grunwald, K. Rischka, S. M. Kast, T. Scheibel, and H. Bargel. "Mimicking biopolymers on a molecular scale: nano(bio)technology based on engineered proteins". In: *Philosophical Transactions of the Royal Society A: Mathematical, Physical and Engineering Sciences* 367 (2009), pp. 1727–1747.
- [4] W. Nachtigall. *Bionik: Grundlagen und Beispiele für Ingenieure und Naturwissenschaftler*. 2nd. Springer Berlin / Heidelberg, 2002.
- [5] A. M. Kushner and Z. Guan. "Modular Design in Natural and Biomimetic Soft Materials". In: *Angewandte Chemie International Edition* 50 (2011), pp. 9026–9057.
- [6] J. F. V. Vincent. "Making biological materials". In: *Journal of Bionic Engineering* 2 (2006), pp. 209–237.
- [7] T. Scheibel. "Protein fibers as performance proteins: new technologies and applications". In: *Current Opinion in Biotechnology* 16 (2005), pp. 427–433.
- [8] A. Lammel, D. Keerl, L. Roemer, and T. Scheibel. "Proteins: Polymers of natural origin". In: *Recent Advances in Biomaterials Research*. Ed. by J. Hu. Kerala, India: Transworld Research Network, 2008, pp. 1–22.
- [9] F. G. Omenetto and D. L. Kaplan. "New Opportunities for an Ancient Material". In: *Science* 329 (2010), pp. 528–531.
- [10] J. Vincent. *Structural Biomaterials*. Princeton University Press, 1990.
- [11] T. Scheibel and L. Serpell. "Physical Methods for Studies of Fiber Formation and Structure". In: ed. by J. Buchner and T. Kiefhaber. Vol. 3. Protein Folding Handbook. Wiley-VCH Verlag GmbH, 2005, pp. 197–253.
- [12] B. Alberts. *Molecular Biology of the Cell: Reference Edition*. Molecular Biology of the Cell: Reference Edition Band 1. Garland Publishing Inc., 2008.
- [13] M. J. Buehler, S. Keten, and T. Ackbarow. "Theoretical and computational hierarchical nanomechanics of protein materials: Deformation and fracture". In: *Progress in Materials Science* 53 (2008), pp. 1101–1241.
- [14] E. Iizuka. "The physico-chemical properties of silk fibers and the fiber spinning process". In: *Cellular and Molecular Life Sciences* 39 (1983), pp. 449–454.
- [15] T. E. Creighton. *Proteins: Structures and Molecular Properties*. W. H. Freeman & Co, 1993.
- [16] C. Brandén and J. Tooze. *Introduction to Protein Structure*. Garland Publishing, Incorporated, 1999.
- [17] J. G. Hardy, L. M. Romer, and T. R. Scheibel. "Polymeric materials based on silk proteins". In: *Polymer* 49 (2008), pp. 4309–4327.
- [18] W. Bergmann. "Werkstofftechnik". In: *Werkstofftechnik 1*. Carl Hanser Verlag GmbH & Co. KG, 2008.
- [19] S. SenGupta and T. Scheibel. "Folding, self-assembly and conformational switches of proteins". In: *Protein Folding-Misfolding: Some Current Concepts of Protein Chemistry*. Ed. by J. P. Zbilut and T. Scheibel. Nova Science Publishers Inc., 2007.
- [20] F. Vollrath. "Biology of spider silk". In: *International Journal of Biological Macromolecules* 24 (1999), pp. 81–88.

-
- [21] J. M. Gosline, M. E. Demont, and M. W. Denny. "The Structure and Properties of Spider Silk". In: *Endeavour* 10 (1986), pp. 37–43.
- [22] J. Sirichaisit, V. L. Brookes, R. J. Young, and F. Vollrath. "Analysis of structure-property relationships in silkworm (*Bombyx mori*) and spider dragline (*Nephila edulis*) silks using Raman Spectroscopy". In: *Biomacromolecules* 4 (2003), pp. 387–394.
- [23] G. H. Altman, F. Diaz, C. Jakuba, T. Calabro, R. L. Horan, J. Chen, H. Lu, J. Richmond, and D. L. Kaplan. "Silk-based biomaterials". In: *Biomaterials* 24 (2003), pp. 401–416.
- [24] T. Asakura, K. Umemura, Y. Nakazawa, H. Hirose, J. Higham, and D. Knight. "Some observations on the structure and function of the spinning apparatus in the silkworm *Bombyx mori*". In: *Biomacromolecules* 8 (2007), pp. 175–181.
- [25] J. Pérez-Rigueiro, C. Viney, J. Llorca, and M. Elices. "Silkworm silk as an engineering material". In: *Journal of Applied Polymer Science* 70 (1998), pp. 2439–2447.
- [26] F. Vollrath and D. Porter. "Silks as ancient models for modern polymers". In: *Polymer* 50 (2009), pp. 5623–5632.
- [27] Z. Shao and F. Vollrath. "Surprising strength of silkworm silk". In: *Nature* 418 (2002), p. 741.
- [28] P. Jiang, H. Liu, C. Wang, L. Wu, J. Huang, and C. Guo. "Tensile behavior and morphology of differently degummed silkworm (*Bombyx mori*) cocoon silk fibres". In: *Materials Letters* 60 (2006), pp. 919–925.
- [29] P. Poza, J. Perez-Rigueiro, M. Elices, and J. Llorca. "Fractographic analysis of silkworm and spider silk". In: *Engineering Fracture Mechanics* 69 (2002), pp. 1035–1048.
- [30] A. Matsumoto, A. Lindsay, B. Abedian, and D. L. Kaplan. "Silk fibroin solution properties related to assembly and structure". In: *Macromolecular Bioscience* 8 (2008), pp. 1006–1018.
- [31] D. L. Dunaway, B. L. Thiel, S. G. Srinivasan, and C. Viney. "Characterizing the Cross-Sectional Geometry of Thin, Noncylindrical, Twisted Fibers (Spider Silk)". In: *Journal of Materials Science* 30 (1995), pp. 4161–4170.
- [32] F. Vollrath and D. P. Knight. "Liquid crystalline spinning of spider silk". In: *Nature* 410 (2001), pp. 541–548.
- [33] O. Hakimi, D. P. Knight, M. M. Knight, M. F. Grahn, and P. Vadgama. "Ultrastructure of insect and spider cocoon silks". In: *Biomacromolecules* 7 (2006), pp. 2901–2908.
- [34] H.-P. Zhao, X.-Q. Feng, and H.-J. Shi. "Variability in mechanical properties of *Bombyx mori* silk". In: *Materials Science and Engineering: C* 27 (2007), pp. 675–683.
- [35] J. G. Hardy and T. R. Scheibel. "Composite materials based on silk proteins". In: *Progress in Polymer Science* 35 (2010), pp. 1093–1115.
- [36] A. Ochi, K. S. Hossain, J. Magoshi, and N. Nemoto. "Rheology and Dynamic Light Scattering of Silk Fibroin Solution Extracted from the Middle Division of *Bombyx mori* Silkworm". In: *Biomacromolecules* 3 (2002), pp. 1187–1196.
- [37] H. J. Jin and D. L. Kaplan. "Mechanism of silk processing in insects and spiders". In: *Nature* 424 (2003), pp. 1057–1061.
- [38] P. J. Willcox, S. P. Gido, W. Muller, and D. L. Kaplan. "Evidence of a cholesteric liquid crystalline phase in natural silk spinning processes". In: *Macromolecules* 29 (1996), pp. 5106–5110.
- [39] S. I. Inoue, J. Magoshi, T. Tanaka, Y. Magoshi, and M. Becker. "Atomic force microscopy: *Bombyx mori* silk fibroin molecules and their higher order structure". In: *Journal of Polymer Science Part B - Polymer Physics* 38 (2000), pp. 1436–1439.
- [40] C. Dicko, J. M. Kenney, and F. Vollrath. "beta-silks: Enhancing and controlling aggregation". In: *Advances in Protein Chemistry* 73 (2006), pp. 17–53.
- [41] Y. Cao and B. Wang. "Biodegradation of silk biomaterials". In: *International Journal of Molecular Sciences* 10 (2009), pp. 1514–1524.
-

-
- [42] J. D. Bunning and J. E. Lydon. "The cellular optical texture of the lyotropic nematic phase of the caesium pentadecafluoro-octanoate (CsPFO) water system in cylindrical tubes". In: *Liquid Crystals* 20 (1996), pp. 381–385.
- [43] C. Dicko, F. Vollrath, and J. M. Kenney. "Spider silk protein refolding is controlled by changing pH". In: *Biomacromolecules* 5 (2004), pp. 704–710.
- [44] A. E. Terry, D. P. Knight, D. Porter, and F. Vollrath. "pH induced changes in the rheology of silk fibroin solution from the middle division of *Bombyx mori* silkworm". In: *Biomacromolecules* 5 (2004), pp. 768–772.
- [45] W. Wei, Y. Zhang, Y. Zhao, J. Luo, H. Shao, and X. Hu. "Bio-inspired capillary dry spinning of regenerated silk fibroin aqueous solution". In: *Materials Science and Engineering C* 31 (2011), pp. 1602–1608.
- [46] F. Lucas. "Spiders and their silks". In: *Discovery* 25 (1964), pp. 20–26.
- [47] P. M. Cunniff, S. A. Fossey, M. A. Auerbach, and J. W. Song. "Mechanical Properties of major ampullate gland silk fibers extracted from *Nephila clavipes* spiders". In: *Silk Polymers. Materials Science and Biotechnology*. Ed. by D. L. Kaplan, W. Adams, B. Farmer, and C. Viney. Washington D.C.: American Chemical Society, 1994, pp. 234–251.
- [48] M. Denny. "Physical properties of spiders silk and their role in design of orb-webs". In: *Journal of Experimental Biology* 65 (1976), pp. 483–506.
- [49] O. Emile, A. L. Floch, and F. Vollrath. "Time-Resolved Torsional Relaxation of Spider Draglines by an Optical Technique". In: *Physical Review Letters* 98 (2007), pp. 167402/1–167402/4.
- [50] L. Eisoldt, A. Smith, and T. Scheibel. "Decoding the secrets of spider silk". In: *Materials Today* 14 (2011), pp. 80–86.
- [51] J. M. Gosline, M. W. Denny, and M. E. Demont. "Spider Silk as Rubber". In: *Nature* 309 (1984), pp. 551–552.
- [52] J. M. Gosline, P. A. Guerette, C. S. Ortlepp, and K. N. Savage. "The mechanical design of spider silks: From fibroin sequence to mechanical function". In: *Journal of Experimental Biology* 202 (1999), pp. 3295–3303.
- [53] M. Heim, D. Keerl, and T. Scheibel. "Spider Silk: From Soluble Protein to Extraordinary Fiber". In: *Angewandte Chemie-International Edition* 48 (2009), pp. 3584–3596.
- [54] D. L. Kaplan, S. J. Lombardi, W. S. Muller, and S. A. Fossey. "Silks: chemistry, properties and genetics". In: *Biomaterials: novel materials from biological sources*. Ed. by D. Byrom. New York: Stockton Press, 1991, pp. 1–53.
- [55] F. K. Ko and J. Jovicic. "Modeling of mechanical properties and structural design of spider web". In: *Biomacromolecules* 5 (2004), pp. 780–785.
- [56] V. Gerritsen. "The tiptoe of an airbus". In: *Protein Spotlight* 24 (2002), pp. 1–2.
- [57] F. Vollrath. "Strength and structure of spiders' silks". In: *Reviews in Molecular Biotechnology* 74 (2000), pp. 67–83.
- [58] L. Romer and T. Scheibel. "The Elaborate Structure of Spider Silk: Structure and Function of a Natural High Performance Fiber". In: *Prion* 2 (2008). Ed. by T. Scheibel, pp. 154–161.
- [59] A. E. Brooks, H. B. Steinkraus, S. R. Nelson, and R. V. Lewis. "An Investigation of the Divergence of Major Ampullate Silk Fibers from *Nephila clavipes* and *Argiope aurantia*". In: *Biomacromolecules* 6 (2005), pp. 3095–3099.
- [60] M. A. Garrido, M. Elices, C. Viney, and J. Perez-Rigueiro. "Active control of spider silk strength: comparison of drag line spun on vertical and horizontal surfaces". In: *Polymer* 43 (2002), pp. 1537–1540.
- [61] C. Dicko, D. Porter, J. Bond, J. M. Kenney, and F. Vollrath. "Structural disorder in silk proteins reveals the emergence of elastomericty". In: *Biomacromolecules* 9 (2008), pp. 216–221.
- [62] F. Vollrath and E. K. Tillinghast. "Glycoprotein Glue beneath a Spider Webs Aqueous Coat". In: *Naturwissenschaften* 78 (1991), pp. 557–559.
-

-
- [63] T. Scheibel. "Spider silks: recombinant synthesis, assembly, spinning, and engineering of synthetic proteins". In: *Microbial Cell Factories* 3 (2004), p. 14.
- [64] R. W. Work. "Force-Elongation Behavior of Web Fibers and Silks Forcibly Obtained from Orb-Web-Spinning Spiders". In: *Textile Research Journal* 46 (1976), pp. 485–492.
- [65] O. Emile, A. Le Floch, and F. Vollrath. "Biopolymers: shape memory in spider draglines". In: *Nature* 440 (2006), p. 621.
- [66] M. Elices, J. Perez-Rigueiro, G. R. Plaza, and G. V. Guinea. "Finding inspiration in Argiope trifasciata spider silk fibers". In: *JOM* 57 (2005), pp. 60–66.
- [67] J. Pérez-Rigueiro, M. Elices, J. Llorca, and C. Viney. "Tensile properties of Argiope trifasciata drag line silk obtained from the spider's web". In: *Journal of Applied Polymer Science* 82 (2001), pp. 2245–2251.
- [68] M. Elices, G. R. Plaza, J. Pérez-Rigueiro, and G. V. Guinea. "The hidden link between supercontraction and mechanical behavior of spider silks". In: *Journal of the Mechanical Behavior of Biomedical Materials* 4 (2011), pp. 658–669.
- [69] C. Boutry and T. A. Blackledge. "The Common House Spider Alters the Material and Mechanical Properties of Cobweb Silk in Response to Different Prey". In: *Journal of Experimental Zoology Part a-Ecological Genetics and Physiology* 309A (2008), pp. 542–552.
- [70] D. B. Zax, D. E. Armanios, S. Horak, C. Malowniak, and Z. T. Yang. "Variation of mechanical properties with amino acid content in the silk of Nephila clavipes". In: *Biomacromolecules* 5 (2004), pp. 732–738.
- [71] K. H. Guehrs, B. Schlott, F. Grosse, and K. Weisshart. "Environmental conditions impinge on dragline silk protein composition". In: *Insect Molecular Biology* 17 (2008), pp. 553–564.
- [72] J. Perez-Rigueiro, M. Elices, and G. V. Guinea. "Controlled supercontraction tailors the tensile behaviour of spider silk". In: *Polymer* 44 (2003), pp. 3733–3736.
- [73] Z. Shao, F. Vollrath, J. Sirichaisit, and R. J. Young. "Analysis of spider silk in native and supercontracted states using Raman spectroscopy". In: *Polymer* 40 (1999), pp. 2493–2500.
- [74] Z. Z. Shao and F. Vollrath. "The effect of solvents on the contraction and mechanical properties of spider silk". In: *Polymer* 40 (1999), pp. 1799–1806.
- [75] I. Agnarsson, C. Boutry, S.-C. Wong, A. Baji, A. Dhinojwala, A. T. Sensenig, and T. A. Blackledge. "Supercontraction forces in spider dragline silk depend on hydration rate". In: *Zoology* 112 (2009), pp. 325–31.
- [76] G. V. Guinea, M. Elices, J. Perez-Rigueiro, and G. Plaza. "Self-tightening of spider silk fibers induced by moisture". In: *Polymer* 44 (2003), pp. 5785–5788.
- [77] F. I. Bell, I. J. McEwen, and C. Viney. "Fibre science: supercontraction stress in wet spider dragline". In: *Nature* 416 (2002), p. 37.
- [78] Y. Liu, Z. Z. Shao, and F. Vollrath. "Relationships between supercontraction and mechanical properties of spider silk". In: *Nature Materials* 4 (2005), pp. 901–905.
- [79] L. W. Jelinski, A. Blye, O. Liivak, C. Michal, G. LaVerde, A. Seidel, N. Shah, and Z. T. Yang. "Orientation, structure, wet-spinning, and molecular basis for supercontraction of spider dragline silk". In: *International Journal of Biological Macromolecules* 24 (1999), pp. 197–201.
- [80] A. Schafer, T. Vehoff, A. Glisovic, and T. Salditt. "Spider silk softening by water uptake: an AFM study". In: *European Biophysics Journal with Biophysics Letters* 37 (2008), pp. 197–204.
- [81] K. N. Savage, P. A. Guerette, and J. M. Gosline. "Supercontraction Stress in Spider Webs". In: *Biomacromolecules* 5 (2004), pp. 675–679.
- [82] G. V. Guinea, M. Elices, J. Perez-Rigueiro, and G. R. Plaza. "Stretching of supercontracted fibers: a link between spinning and the variability of spider silk". In: *Journal of Experimental Biology* 208 (2005), pp. 25–30.
-

-
- [83] T. Scheibel and D. Hummerich. *Method and Device for Producing a Thread from Silk Proteins*. WO2007/031301A2. 2007.
- [84] D. Vollrath F. Knight. *Apparatus and Method for selective assembly of protein*. WO2005/017237A2. 2005.
- [85] F. Vollrath and D. P. Knight. *Apparatus and Method for Forming Materials*. WO01/38614 A1. 1999.
- [86] D. P. Knight and F. Vollrath. "Liquid crystals and flow elongation in a spider's silk production line". In: *Proceedings of the Royal Society of London Series B-Biological Sciences* 266 (1999), pp. 519–523.
- [87] F. Vollrath and D. P. Knight. "Structure and function of the silk production pathway in the Spider *nephila edulis*". In: *International Journal of Biological Macromolecules* 24 (1999), pp. 243–249.
- [88] A. Spohner, E. Unger, F. Grosse, and W. Klaus. "Differential polymerization of the two main protein components of dragline silk during fibre spinning". In: *Nature Materials* 4 (2005), pp. 772–775.
- [89] A. Spohner, W. Vater, S. Monajembashi, E. Unger, F. Grosse, and K. Weisshart. "Composition and Hierarchical Organisation of a Spider Silk". In: *Plos One* 2 (2007), e998.
- [90] C. Viney, A. E. Huber, D. L. Dunaway, K. Kerkam, and S. T. Case. "Optical Characterization of Silk Secretions and Fibers". In: *Silk Polymers. Materials Science and Biotechnology*. Ed. by D. L. Kaplan, W. Adams, B. Farmer, and C. Viney. Washington D.C.: American Chemical Society, 1994, pp. 120–136.
- [91] W. A. Gaines and W. R. Marcotte Jr. "Identification and characterization of multiple Spidroin 1 genes encoding major ampullate silk proteins in *Nephila clavipes*". In: *Insect Molecular Biology* 17 (2008), pp. 465–474.
- [92] G. C. Candelas and J. Cintron. "A Spider Fibroin and Its Synthesis". In: *Journal of Experimental Zoology* 216 (1981), pp. 1–6.
- [93] A. Spohner, E. Unger, F. Grosse, and K. Weisshart. "Conserved C-termini of Spidroins are secreted by the major ampullate glands and retained in the silk thread". In: *Biomacromolecules* 5 (2004), pp. 840–845.
- [94] A. Spohner, W. Vater, W. Rommerskirch, F. Vollrath, E. Unger, F. Grosse, and K. Weisshart. "The conserved C-termini contribute to the properties of spider silk fibroins". In: *Biochemical and Biophysical Research Communications* 338 (2005), pp. 897–902.
- [95] E. Bini, D. P. Knight, and D. L. Kaplan. "Mapping domain structures in silks from insects and spiders related to protein assembly". In: *Journal of Molecular Biology* 335 (2004), pp. 27–40.
- [96] S. O. Andersen. "Amino Acid Composition of Spider Silks". In: *Comparative Biochemistry and Physiology* 35 (1970), pp. 705–711.
- [97] M. S. Creager, J. E. Jenkins, L. A. Thagard-Yeaman, A. E. Brooks, J. A. Jones, R. V. Lewis, G. P. Holland, and J. L. Yarger. "Solid-State NMR Comparison of Various Spiders' Dragline Silk Fiber". In: *Biomacromolecules* 11 (2010), pp. 2039–2043.
- [98] L. Eisoldt, C. Thamm, and T. Scheibel. "Review the role of terminal domains during storage and assembly of spider silk proteins". In: *Biopolymers* 97 (2012), pp. 355–361.
- [99] A. D. Parkhe, S. K. Seeley, K. Gardner, L. Thompson, and R. V. Lewis. "Structural studies of spider silk proteins in the fiber". In: *Journal of Molecular Recognition* 10 (1997), pp. 1–6.
- [100] J. Kummerlen, J. D. van Beek, F. Vollrath, and B. H. Meier. "Local structure in spider dragline silk investigated by two-dimensional spin-diffusion nuclear magnetic resonance". In: *Macromolecules* 29 (1996), pp. 2920–2928.
- [101] A. H. Simmons, C. A. Michal, and L. W. Jelinski. "Molecular orientation and two-component nature of the crystalline fraction of spider dragline silk". In: *Science* 271 (1996), pp. 84–87.
- [102] D. H. Hijirida, K. G. Do, C. Michal, S. Wong, D. Zax, and L. W. Jelinski. "¹³C NMR of *Nephila clavipes* major ampullate silk gland". In: *Biophysical Journal* 71 (1996), pp. 3442–3447.
- [103] J. D. van Beek, S. Hess, F. Vollrath, and B. H. Meier. "The molecular structure of spider dragline silk: Folding and orientation of the protein backbone". In: *Proceedings of the National Academy of Sciences of the United States of America* 99 (2002), pp. 10266–10271.
-

-
- [104] G. P. Holland, M. S. Creager, J. E. Jenkins, R. V. Lewis, and J. L. Yarger. "Determining Secondary Structure in Spider Dragline Silk by CarbonCarbon Correlation Solid-State NMR Spectroscopy". In: *Journal of the American Chemical Society* 130 (2008), pp. 9871–9877.
- [105] S. Keten and M. J. Buehler. "Nanostructure and molecular mechanics of spider dragline silk protein assemblies". In: *Journal of the Royal Society Interface* 7 (2010), pp. 1709–1721.
- [106] R. V. Lewis, M. Hinman, S. Kothakota, and M. J. Fournier. "Expression and purification of a spider silk protein: A new strategy for producing repetitive proteins". In: *Protein Expression and Purification* 7 (1996), pp. 400–406.
- [107] F. Hagn, L. Eisoldt, J. G. Hardy, C. Vendrely, M. Coles, T. Scheibel, and H. Kessler. "A conserved spider silk domain acts as a molecular switch that controls fibre assembly". In: *Nature* 465 (2010), pp. 239–244.
- [108] R. Beckwitt and S. Arcidiacono. "Sequence conservation in the C-terminal region of spider silk proteins (Spidroin) from *Nephila clavipes* (Tetragnathidae) and *Araneus bicentenarius* (Araneidae)". In: *Journal of Biological Chemistry* 269 (1994), pp. 6661–6663.
- [109] A. Rising, G. Hjälm, W. Engström, and J. Johansson. "N-Terminal Nonrepetitive Domain Common to Dragline, Flagelliform, and Cylindric Spider Silk Proteins". In: *Biomacromolecules* 7 (2006), pp. 3120–3124.
- [110] J. E. Garb, N. A. Ayoub, and C. Y. Hayashi. "Untangling spider silk evolution with spidroin terminal domains". In: *BMC Evolutionary Biology* 10 (2010), p. 243.
- [111] W. A. Gaines, M. G. Sehorn, and W. R. Marcotte. "Spidroin N-terminal Domain Promotes a pH-dependent Association of Silk Proteins during Self-assembly". In: *Journal of Biological Chemistry* 285 (2010), pp. 40745–40753.
- [112] G. Askarieh, M. Hedhammar, K. Nordling, A. Saenz, C. Casals, A. Rising, J. Johansson, and S. D. Knight. "Self-assembly of spider silk proteins is controlled by a pH-sensitive relay". In: *Nature* 465 (2010), pp. 236–238.
- [113] D. Motriuk-Smith, A. Smith, C. Y. Hayashi, and R. V. Lewis. "Analysis of the conserved N-terminal domains in major ampullate spider silk proteins". In: *Biomacromolecules* 6 (2005), pp. 3152–3159.
- [114] F. Hagn, C. Thamm, T. Scheibel, and H. Kessler. "pH-Dependent Dimerization and Salt-Dependent Stabilization of the N-terminal Domain of Spider Dragline Silk—Implications for Fiber Formation". In: *Angewandte Chemie International Edition* 50 (2010), pp. 310–313.
- [115] M. Landreh, G. Askarieh, K. Nordling, M. Hedhammar, A. Rising, C. Casals, J. Astorga-Wells, G. Alvelius, S. D. Knight, J. Johansson, H. Jörnvall, and T. Bergman. "A pH-Dependent Dimer Lock in Spider Silk Protein". In: *Journal of Molecular Biology* 404 (2010), pp. 328–336.
- [116] F. Vollrath, D. P. Knight, and X. W. Hu. "Silk production in a spider involves acid bath treatment". In: *Proceedings of the Royal Society of London Series B-Biological Sciences* 265 (1998), pp. 817–820.
- [117] L. Eisoldt, J. G. Hardy, M. Heim, and T. R. Scheibel. "The role of salt and shear on the storage and assembly of spider silk proteins". In: *Journal of Structural Biology* 170 (2010), pp. 413–419.
- [118] J. A. Wallace and J. K. Shen. "Unraveling a Trap-and-Trigger Mechanism in the pH-Sensitive Self-Assembly of Spider Silk Proteins". In: *The Journal of Physical Chemistry Letters* 3 (2012), pp. 658–662.
- [119] T. Lefèvre, S. Boudreault, C. Cloutier, and M. Pézolet. "Conformational and Orientational Transformation of Silk Proteins in the Major Ampullate Gland of *Nephila clavipes* Spiders". In: *Biomacromolecules* 9 (2008), pp. 2399–2407.
- [120] A. Plazaola and G. C. Candelas. "Stimulation of fibroin synthesis elicits ultrastructural modifications in spider silk secretory cells". In: *Tissue Cell* 23 (1991), pp. 277–284.
- [121] X. Chen, D. P. Knight, and F. Vollrath. "Rheological characterization of *Nephila* spidroin solution". In: *Biomacromolecules* 3 (2002), pp. 644–648.
-

-
- [122] T. Lefevre, J. Leclerc, J. F. Rioux-Dube, T. Buffeteau, M. C. Paquin, M. E. Rousseau, I. Cloutier, M. Auger, S. M. Gagne, S. Boudreault, C. Cloutier, and M. Pezolet. "Conformation of spider silk proteins in situ in the intact major ampullate gland and in solution". In: *Biomacromolecules* 8 (2007), pp. 2342–2344.
- [123] M. Hronska, J. D. van Beek, P. T. F. Williamson, F. Vollrath, and B. H. Meier. "NMR characterization of native liquid spider dragline silk from *Nephila edulis*". In: *Biomacromolecules* 5 (2004), pp. 834–839.
- [124] J. M. Kenney, D. Knight, M. J. Wise, and F. Vollrath. "Amyloidogenic nature of spider silk". In: *European Journal of Biochemistry* 269 (2002), pp. 4159–4163.
- [125] D. P. Knight and F. Vollrath. "Changes in element composition along the spinning duct in a *Nephila* spider". In: *Naturwissenschaften* 88 (2001), pp. 179–182.
- [126] G. De Luca and A. D. Rey. "Dynamic interactions between nematic point defects in the spinning extrusion duct of spiders". In: *Journal of Chemical Physics* 124 (2006), p. 144904.
- [127] A. D. Rey. "Liquid crystal models of biological materials and processes". In: *Soft Matter* 6 (15 2010), pp. 3402–3429.
- [128] D. Knight and F. Vollrath. "Hexagonal columnar liquid crystal in the cells secreting spider silk". In: *Tissue & Cell* 31 (1999), pp. 617–620.
- [129] C. Dicko, D. Knight, J. M. Kenney, and F. Vollrath. "Structural conformation of spidroin in solution: a synchrotron radiation circular dichroism study". In: *Biomacromolecules* 5 (2004), pp. 758–767.
- [130] C. W. P. Foo, E. Bini, J. Hensman, D. P. Knight, R. V. Lewis, and D. L. Kaplan. "Role of pH and charge on silk protein assembly in insects and spiders". In: *Applied Physics a-Materials Science & Processing* 82 (2006), pp. 223–233.
- [131] T. Lefèvre, S. Boudreault, C. Cloutier, and M. Pézolet. "Diversity of Molecular Transformations Involved in the Formation of Spider Silks". In: *Journal of Molecular Biology* 405 (2011), pp. 238–253.
- [132] C. Dicko, D. Knight, J. M. Kenney, and F. Vollrath. "Secondary structures and conformational changes in flagelliform, cylindrical, major, and minor ampullate silk proteins. Temperature and concentration effects". In: *Biomacromolecules* 5 (2004), pp. 2105–2115.
- [133] C. Holland, A. E. Terry, D. Porter, and F. Vollrath. "Comparing the rheology of native spider and silkworm spinning dope". In: *Nature Materials* 5 (2006), pp. 870–874.
- [134] L. R. Fox. "Cannibalism in Natural-Populations". In: *Annual Review of Ecology and Systematics* 6 (1975), pp. 87–106.
- [135] S. Zschokke and M. E. Herberstein. "Laboratory methods for maintaining and studying web-building spiders". In: *Journal of Arachnology* 33 (2005), pp. 205–213.
- [136] J. P. O'Brien, S. R. Fahnestock, Y. Termonia, and K. C. H. Gardner. "Nylons from nature: Synthetic analogs to spider silk". In: *Advanced Materials* 10 (1998), pp. 1185–1195.
- [137] X. Chen, Z. Z. Shao, and F. Vollrath. "The spinning processes for spider silk". In: *Soft Matter* 2 (2006), pp. 448–451.
- [138] C. Vendrely and T. Scheibel. "Biotechnological production of spider-silk proteins enables new applications". In: *Macromolecular Bioscience* 7 (2007), pp. 401–9.
- [139] M. Yang, J. Kawamura, Z. Zhu, K. Yamauchi, and T. Asakura. "Development of silk-like materials based on *Bombyx mori* and *Nephila clavipes* dragline silk fibroins". In: *Polymer* 50 (2009), pp. 117–124.
- [140] J. G. Hardy and T. R. Scheibel. "Silk-inspired polymers and proteins". In: *Biochemical Society Transactions* 37 (2009), pp. 677–681.
- [141] S. R. Fahnestock and S. L. Irwin. "Synthetic spider dragline silk proteins and their production in *Escherichia coli*". In: *Applied Microbiology and Biotechnology* 47 (1997), pp. 23–32.
- [142] J. T. Prince, K. P. Mcgrath, C. M. Digirolamo, and D. L. Kaplan. "Construction, Cloning, and Expression of Synthetic Genes Encoding Spider Dragline Silk". In: *Biochemistry* 34 (1995), pp. 10879–10885.
-

-
- [143] J. A. Kluge, U. Rabotyagova, G. G. Leisk, and D. L. Kaplan. "Spider silks and their applications". In: *Trends in Biotechnology* 26 (2008), pp. 244–251.
- [144] A. Rising, M. Widhe, J. Johansson, and M. Hedhammar. "Spider silk proteins: recent advances in recombinant production, structure–function relationships and biomedical applications". In: *Cellular and Molecular Life Sciences* 68 (2011), pp. 169–184.
- [145] Y. Fukushima. "Genetically engineered syntheses of tandem repetitive polypeptides consisting of glycine-rich sequence of spider dragline silk". In: *Biopolymers* 45 (1998), pp. 269–279.
- [146] Y. T. Zhou, S. X. Wu, and V. P. Conticello. "Genetically directed synthesis and spectroscopic analysis of a protein polymer derived from a flagelliform silk sequence". In: *Biomacromolecules* 2 (2001), pp. 111–125.
- [147] F. Teule, A. R. Cooper, W. A. Furin, D. Bittencourt, E. L. Rech, A. Brooks, and R. V. Lewis. "A protocol for the production of recombinant spider silk-like proteins for artificial fiber spinning". In: *Nature Protocols* 4 (2009), pp. 341–355.
- [148] S. R. Fahnestock and L. A. Bedzyk. "Production of synthetic spider dragline silk protein in *Pichia pastoris*". In: *Applied Microbiology and Biotechnology* 47 (1997), pp. 33–39.
- [149] F. Teule, C. Aube, M. Ellison, and A. Abbott. "Biomimetic manufacturing of customised novel fibre proteins for specialised applications". In: *AUTEX Research Journal* 3 (2003), pp. 160–165.
- [150] L. A. Barr, S. R. Fahnestock, and J. J. Yang. "Production and purification of recombinant DP1B silk-like protein in plants". In: *Molecular Breeding* 13 (2004), pp. 345–356.
- [151] J. Scheller, K. H. Guhrs, F. Grosse, and U. Conrad. "Production of spider silk proteins in tobacco and potato." eng. In: *Nature Biotechnology* 19 (2001), pp. 573–577.
- [152] D. Huemmerich, T. Scheibel, F. Vollrath, S. Cohen, U. Gat, and S. Ittah. "Novel assembly properties of recombinant spider dragline silk proteins". In: *Current Biology* 14 (2004), pp. 2070–2074.
- [153] Y. Miao, Y. Zhang, K. Nakagaki, T. Zhao, A. Zhao, Y. Meng, M. Nakagaki, E. Y. Park, and K. Maenaka. "Expression of spider flagelliform silk protein in *Bombyx mori* cell line by a novel Bac-to-Bac/BmNPV baculovirus expression system". In: *Applied Microbiology and Biotechnology* 71 (2006), pp. 192–199.
- [154] A. Lazaris, S. Arcidiacono, Y. Huang, J. F. Zhou, F. Duguay, N. Chretien, E. A. Welsh, J. W. Soares, and C. N. Karatzas. "Spider silk fibers spun from soluble recombinant silk produced in mammalian cells". In: *Science* 295 (2002), pp. 472–476.
- [155] H. T. Xu, B. L. Fan, S. Y. Yu, Y. H. Huang, Z. H. Zhao, Z. X. Lian, Y. P. Dai, L. L. Wang, Z. L. Liu, J. Fei, and N. Li. "Construct synthetic gene encoding artificial spider dragline silk protein and its expression in milk of transgenic mice". In: *Animal Biotechnology* 18 (2007), pp. 1–12.
- [156] F. Teulé, Y.-G. Miao, B.-H. Sohn, Y.-S. Kim, J. J. Hull, M. J. Fraser, R. V. Lewis, and D. L. Jarvis. "Silkworms transformed with chimeric silkworm/spider silk genes spin composite silk fibers with improved mechanical properties". In: *Proceedings of the National Academy of Sciences* 109 (2012), pp. 923–928.
- [157] X.-X. Xia, Z.-G. Qian, C. S. Ki, Y. H. Park, D. L. Kaplan, and S. Y. Lee. "Native-sized recombinant spider silk protein produced in metabolically engineered *Escherichia coli* results in a strong fiber". In: *Proceedings of the National Academy of Sciences* 107 (2010), pp. 14059–14063.
- [158] C. W. P. Foo, E. Bini, J. Huang, S. Y. Lee, and D. L. Kaplan. "Solution behavior of synthetic silk peptides and modified recombinant silk proteins". In: *Applied Physics a-Materials Science & Processing* 82 (2006), pp. 193–203.
- [159] O. S. Rabotyagova, P. Cebe, and D. L. Kaplan. "Self-Assembly of Genetically Engineered Spider Silk Block Copolymers". In: *Biomacromolecules* 10 (2009), pp. 229–236.
- [160] D. Huemmerich, C. W. Helsen, S. Quedzuweit, J. Oschmann, R. Rudolph, and T. Scheibel. "Primary structure elements of spider dragline silks and their contribution to protein solubility". In: *Biochemistry* 43 (2004), pp. 13604–13612.
-

-
- [161] J. H. Exler, D. Hummerich, and T. Scheibel. "The amphiphilic properties of spider silks are important for spinning". In: *Angewandte Chemie International Edition* 46 (2007), pp. 3559–3562.
- [162] M. Baron. "Definitions of basic terms relating to low-molar-mass and polymer liquid crystals - (IUPAC recommendations 2001)". In: *Pure and Applied Chemistry* 73 (2001), pp. 845–895.
- [163] M. Rubinstein and R. Colby. *Polymer Physics*. Oxford University Press, 2003.
- [164] D. P. Knight and F. Vollrath. "Spinning an elastic ribbon of spider silk". In: *Philosophical Transactions of the Royal Society of London Series B-Biological Sciences* 357 (2002), pp. 219–227.
- [165] C. Dicko, J. M. Kenney, D. Knight, and F. Vollrath. "Transition to a beta-sheet-rich structure in spidroin in vitro: The effects of pH and cations". In: *Biochemistry* 43 (2004), pp. 14080–14087.
- [166] D Saravanan. "Spider Silk - Structure, Properties and Spinning". In: *Journal of Textile and Apparel, Technology and Management* 5 (2005).
- [167] N. Kojic, A. Kojic, and M. Kojic. "Numerical determination of the solvent diffusion coefficient in a concentrated polymer solution". In: *Communications in Numerical Methods in Engineering* 22 (2006), pp. 1003–1013.
- [168] N. Kojic, M. Kojic, S. Gudlavalleti, and G. McKinley. "Solvent removal during synthetic and Nephila fiber spinning". In: *Biomacromolecules* 5 (2004), pp. 1698–1707.
- [169] D. P. Knight, M. M. Knight, and F. Vollrath. "Beta transition and stress-induced phase separation in the spinning of spider dragline silk". In: *International Journal of Biological Macromolecules* 27 (2000), pp. 205–210.
- [170] F. Vollrath, D. Porter, and C. Holland. "There are many more lessons still to be learned from spider silks". In: *Soft Matter* 7 (2011), pp. 9595–9600.
- [171] T. Arai, D. L. Wilson, N. Kasai, G. Freddi, S. Hayasaka, and M. Tsukada. "Preparation of silk fibroin and polyallylamine composites". In: *Journal of Applied Polymer Science* 84 (2002), pp. 1963–1970.
- [172] X. Chen, D. P. Knight, Z. Z. Shao, and F. Vollrath. "Regenerated Bombyx silk solutions studied with rheometry and FTIR". In: *Polymer* 42 (2001), pp. 9969–9974.
- [173] X. Hu, D. Kaplan, and P. Cebe. "Determining beta-sheet crystallinity in fibrous proteins by thermal analysis and infrared-spectroscopy". In: *Macromolecules* 39 (2006), pp. 6161–6170.
- [174] T. Huang, P. Ren, and B. Huo. "Atomic force Microscopy of the topography of regenerated observations of the silk fibroin aggregations". In: *Journal of Applied Polymer Science* 106 (2007), pp. 4054–4059.
- [175] H.-J. Jin, S. V. Fridrikh, G. C. Rutledge, and D. L. Kaplan. "Electrospinning Bombyx mori Silk with Poly(ethylene oxide)". In: *Biomacromolecules* 3 (2002), pp. 1233–1239.
- [176] U. J. Kim, J. Y. Park, C. M. Li, H. J. Jin, R. Valluzzi, and D. L. Kaplan. "Structure and properties of silk hydrogels". In: *Biomacromolecules* 5 (2004), pp. 786–792.
- [177] A. Matsumoto, J. Chen, A. L. Collette, U. J. Kim, G. H. Altman, P. Cebe, and D. L. Kaplan. "Mechanisms of silk fibroin sol-gel transitions". In: *Journal of Physical Chemistry B* 110 (2006), pp. 21630–21638.
- [178] G. Q. Zhou, Z. Z. Shao, D. P. Knight, J. P. Yan, and X. Chen. "Silk fibers extruded artificially from aqueous solutions of regenerated Bombyx mori silk Fibroin are tougher than their natural counterparts". In: *Advanced Materials* 21 (2009), pp. 366–370.
- [179] M. Stark, S. Grip, A. Rising, M. Hedhammar, W. Engstrom, G. Hjalml, and J. Johansson. "Macroscopic fibers self-assembled from recombinant miniature spider silk proteins". In: *Biomacromolecules* 8 (2007), pp. 1695–1701.
- [180] S. Rammensee, U. Slotta, T. Scheibel, and A. R. Bausch. "Assembly mechanism of recombinant spider silk proteins". In: *Proceedings of the National Academy of Sciences of the United States of America* 105 (2008), pp. 6590–6595.
-

-
- [181] Q. X. Ruan, P. Zhou, B. W. Hu, and D. Ji. "An investigation into the effect of potassium ions on the folding of silk fibroin studied by generalized two-dimensional NMR-NMR correlation and Raman spectroscopy". In: *FEBS Journal* 275 (2008), pp. 219–232.
- [182] M. G. Cacace, E. M. Landau, and J. J. Ramsden. "The Hofmeister series: salt and solvent effects on interfacial phenomena". In: *Quarterly Reviews of Biophysics* 30 (1997), pp. 241–277.
- [183] Y. Zhang and P. S. Cremer. "Interactions between macromolecules and ions: the Hofmeister series". In: *Current Opinion in Chemical Biology* 10 (2006), pp. 658–663.
- [184] U. Slotta, S. Rammensee, S. Gorb, and T. Scheibel. "An Engineered Spider Silk Protein Forms Microspheres". In: *Angewandte Chemie International Edition* 47 (2008), pp. 4592–4594.
- [185] J. P. Zbilut, T. Scheibel, D. Huemmerich, C. L. Webber, M. Colafranceschi, and A. Giuliani. "Statistical approaches for investigating silk properties". In: *Applied Physics a-Materials Science & Processing* 82 (2006), pp. 243–251.
- [186] C. Riekkel and F. Vollrath. "Spider silk fibre extrusion: combined wide- and small-angle X-ray microdiffraction experiments". In: *International Journal of Biological Macromolecules* 29 (2001), pp. 203–210.
- [187] Y. Liu, Z. Z. Shao, and F. Vollrath. "Extended wet-spinning can modify spider silk properties". In: *Chemical Communications* (2005), pp. 2489–2491.
- [188] N. Kojic, J. Bico, C. Clasen, and G. H. McKinley. "Ex vivo rheology of spider silk". In: *Journal of Experimental Biology* 209 (2006), pp. 4355–4362.
- [189] A. Tripathi, K. C. Tam, and G. H. McKinley. "Rheology and dynamics of associative polymers in shear and extension: Theory and experiments". In: *Macromolecules* 39 (2006), pp. 1981–1999.
- [190] R. W. Work. "Viscoelastic Behavior and Wet Supercontraction of Major Ampullate Silk Fibers of Certain Orb-Web-Building Spiders (Araneae)". In: *Journal of Experimental Biology* 118 (1985), pp. 379–404.
- [191] F. Vollrath, B. Madsen, and Z. Z. Shao. "The effect of spinning conditions on the mechanics of a spider's dragline silk". In: *Proceedings of the Royal Society of London Series B-Biological Sciences* 268 (2001), pp. 2339–2346.
- [192] C. S. Orltapp and J. M. Gosline. "Consequences of forced silking". In: *Biomacromolecules* 5 (2004), pp. 727–731.
- [193] J. Perez-Rigueiro, M. Elices, G. Plaza, J. I. Real, and G. V. Guinea. "The effect of spinning forces on spider silk properties". In: *Journal of Experimental Biology* 208 (2005), pp. 2633–2639.
- [194] A. Ziabicki. "Effects of molecular weight on melt spinning and mechanical properties of high-performance poly(ethylene terephthalate) fibers". In: *Textile Research Journal* 66 (1996), pp. 705–712.
- [195] B. An, M. B. Hinman, G. P. Holland, J. L. Yarger, and R. V. Lewis. "Inducing -Sheets Formation in Synthetic Spider Silk Fibers by Aqueous Post-Spin Stretching". In: *Biomacromolecules* 12 (2011), pp. 2375–2381.
- [196] F. Teulé, B. Addison, A. R. Cooper, J. Ayon, R. W. Henning, C. J. Benmore, G. P. Holland, J. L. Yarger, and R. V. Lewis. "Combining flagelliform and dragline spider silk motifs to produce tunable synthetic biopolymer fibers". In: *Biopolymers* 97 (2012), pp. 418–431.
- [197] A. E. Brooks, S. M. Stricker, S. B. Joshi, T. J. Kamerzell, C. R. Middaugh, and R. V. Lewis. "Properties of synthetic spider silk fibers based on Argiope aurantia MaSp2". In: *Biomacromolecules* 9 (2008), pp. 1506–1510.
- [198] Z. Z. Shao, F. Vollrath, Y. Yang, and H. C. Thogersen. "Structure and behavior of regenerated spider silk". In: *Macromolecules* 36 (2003), pp. 1157–1161.
- [199] C. Viney. "Silk Fibers: Origins, Nature and Consequences of Structure". In: *Structural Biological Materials: Design and Structure-Property Relationships*. Ed. by M. Elices. Vol. 10. Washington D.C.: American Chemical Society, 2000, pp. 295–333.
- [200] R. Lock. *Process for making silk fibroin fibers*. US5252285. 1993.
-

-
- [201] J. O' Brien. *Polypeptide fibers and processes for making them*. WO002003060207A1. 2003.
- [202] C. Mello, S. Arcidiacono, and M. Butler. *Methods for purification and aqueous fiber spinning of spider silks and other structural proteins*. US7335739B2. 2008.
- [203] S. Islam, C. Karatzas, A. Rodenhiser, A. Alwattari, Y. Huang, and C. Turcotte. *Methods and apparatus for spinning spider silk protein*. US7057023. 2006.
- [204] S. Arcidiacono, C. M. Mello, M. Butler, E. Welsh, J. W. Soares, A. Allen, D. Ziegler, T. Laue, and S. Chase. "Aqueous processing and fiber spinning of recombinant spider silks". In: *Macromolecules* 35 (2002), pp. 1262–1266.
- [205] M. Elices, G. V. Guinea, G. R. Plaza, C. Karatzas, C. Riekel, F. Agulló-Rueda, R. Daza, and J. Pérez-Rigueiro. "Bioinspired Fibers Follow the Track of Natural Spider Silk". In: *Macromolecules* 44 (2011), pp. 1166–1176.
- [206] A. Seidel, O. Liivak, and L. W. Jelinski. "Artificial spinning of spider silk". In: *Macromolecules* 31 (1998), pp. 6733–6736.
- [207] A. Seidel, O. Liivak, S. Calve, J. Adaska, G. D. Ji, Z. T. Yang, D. Grubb, D. B. Zax, and L. W. Jelinski. "Regenerated spider silk: Processing, properties, and structure". In: *Macromolecules* 33 (2000), pp. 775–780.
- [208] S. Sohn and S. P. Gido. "Wet-Spinning of Osmotically Stressed Silk Fibroin". In: *Biomacromolecules* 10 (2009), pp. 2086–2091.
- [209] W. Qiu, W. Teng, J. Cappello, and X. Wu. "Wet-Spinning of Recombinant Silk-Elastin-Like Protein Polymer Fibers with High Tensile Strength and High Deformability". In: *Biomacromolecules* 10 (2009), pp. 602–608.
- [210] J. M. Yao, H. Masuda, C. H. Zhao, and T. Asakura. "Artificial spinning and characterization of silk fiber from Bombyx mori silk fibroin in hexafluoroacetone hydrate". In: *Macromolecules* 35 (2002), pp. 6–9.
- [211] C. Holland, A. E. Terry, D. Porter, and F. Vollrath. "Natural and unnatural silks". In: *Polymer* 48 (2007), pp. 3388–3392.
- [212] O. Liivak, A. Blye, N. Shah, and L. W. Jelinski. "A microfabricated wet-spinning apparatus to spin fibers of silk proteins. Structure-property correlations". In: *Macromolecules* 31 (1998), pp. 2947–2951.
- [213] J. Yan, G. Zhou, D. P. Knight, Z. Shao, and X. Chen. "Wet-Spinning of Regenerated Silk Fiber from Aqueous Silk Fibroin Solution: Discussion of Spinning Parameters". In: *Biomacromolecules* 11 (2009), pp. 1–5.
- [214] M. Boulet-Audet, F. Vollrath, and C. Holland. "Rheo-attenuated total reflectance infrared spectroscopy: a new tool to study biopolymers". In: *Physical Chemistry Chemical Physics* 13 (2011), pp. 3979–3984.
- [215] F. Teule, W. A. Furin, A. R. Cooper, J. R. Duncan, and R. V. Lewis. "Modifications of spider silk sequences in an attempt to control the mechanical properties of the synthetic fibers". In: *Journal of Materials Science* 42 (2007), pp. 8974–8985.
- [216] K. H. Lee, D. H. Baek, C. S. Ki, and Y. H. Park. "Preparation and characterization of wet spun silk fibroin/poly(vinyl alcohol) blend filaments". In: *International Journal of Biological Macromolecules* 41 (2007), pp. 168–172.
- [217] Y. P. Zhang, W. Wei, H. L. Shao, and X. C. Hu. "Posttreatment of the dry-spun fibers obtained from regenerated silk fibroin aqueous solution in ethanol aqueous solution". In: *Journal of Materials Research* 26 (2011), pp. 1100–1106.
- [218] V. G. Bogush, O. S. Sokolova, L. I. Davydova, D. V. Klinov, K. V. Sidoruk, N. G. Esipova, T. V. Neretina, I. A. Orchanskyi, V. Y. Makeev, V. G. Tumanyan, K. V. Shaitan, V. G. Debabov, and M. P. Kirpichnikov. "A novel model system for design of biomaterials based on recombinant analogs of spider silk proteins". In: *Journal of Neuroimmune Pharmacology* 4 (2009), pp. 17–27.
- [219] G. P. Holland, J. E. Jenkins, M. S. Creager, R. V. Lewis, and J. L. Yarger. "Solid-state NMR investigation of major and minor ampullate spider silk in the native and hydrated states". In: *Biomacromolecules* 9 (2008), pp. 651–657.
-

- [220] G. P. Holland, J. E. Jenkins, M. S. Creager, R. V. Lewis, and J. L. Yarger. "Quantifying the fraction of glycine and alanine in beta-sheet and helical conformations in spider dragline silk using solid-state NMR". In: *Chemical Communications* (2008), pp. 5568–5570.
- [221] J. E. Jenkins, M. S. Creager, R. V. Lewis, G. P. Holland, and J. L. Yarger. "Quantitative Correlation between the Protein Primary Sequences and Secondary Structures in Spider Dragline Silks". In: *Biomacromolecules* 11 (2010), pp. 192–200.
- [222] X. Chen, Z. Z. Shao, D. P. Knight, and F. Vollrath. "Conformation transition kinetics of Bombyx mori silk protein". In: *Proteins-Structure Function and Bioinformatics* 68 (2007), pp. 223–231.
- [223] J Pérez-Rigueiro, C Viney, J Llorca, and M Elices. "Mechanical properties of silkworm silk in liquid media". In: *Polymer* 41 (2000), pp. 8433–8439.
- [224] J. W. Goodwin and R. W. Hughes. *Rheology for Chemists: An Introduction*. DOI: 10.1039/9781847558046: RSC Publishing, 2008.
- [225] J. D. Ferry. *Viscoelastic properties of polymers*. 3rd. John Wiley & Sons, Inc., 1980.
- [226] R. B. Bird, R. C. Armstrong, and O. Hassager. *Fluid-Mechanics. Dynamics of Polymeric Liquids*. Vol. 1. John Wiley & Sons, Inc., 1987, p. 784.
- [227] M. Moriya, F. Roschztardt, Y. Nakahara, H. Saito, Y. Masubuchi, and T. Asakura. "Rheological Properties of Native Silk Fibroins from Domestic and Wild Silkworms, and Flow Analysis in Each Spinneret by a Finite Element Method". In: *Biomacromolecules* 10 (2009), pp. 929–935.
- [228] D. O. Olagunju. "A 1-D theory for extensional deformation of a viscoelastic filament under exponential stretching". In: *Journal of Non-Newtonian Fluid Mechanics* 87 (1999), pp. 27–46.
- [229] G. H. McKinley and A. Tripathi. "How to extract the Newtonian viscosity from capillary breakup measurements in a filament rheometer". In: *Journal of Rheology* 44 (2000), pp. 653–670.
- [230] T. Kohler and F. Vollrath. "Thread Biomechanics in the 2 Orb-Weaving Spiders Araneus-Diadematus (Araneae, Araneidae) and Uloborus-Walckenaerius (Araneae, Uloboridae)". In: *Journal of Experimental Zoology* 271 (1995), pp. 1–17.
- [231] H. Bargel and G. Schulze. *Werkstoffkunde*. Springer Berlin / Heidelberg, 2005.
- [232] T. A. Blackledge, J. E. Swindeman, and C. Y. Hayashi. "Quasistatic and continuous dynamic characterization of the mechanical properties of silk from the cobweb of the black widow spider Latrodectus hesperus". In: *Journal of Experimental Biology* 208 (2005), pp. 1937–1949.
- [233] G. V. Guinea, J. Perez-Rigueiro, G. R. Plaza, and M. Elices. "Volume constancy during stretching of spider silk". In: *Biomacromolecules* 7 (2006), pp. 2173–2177.
- [234] B. Madsen, Z. Z. Shao, and F. Vollrath. "Variability in the mechanical properties of spider silks on three levels: interspecific, intraspecific and intraindividual". In: *International Journal of Biological Macromolecules* 24 (1999), pp. 301–306.
- [235] N. Du, Z. Yang, X. Y. Liu, Y. Li, and H. Y. Xu. "Structural Origin of the Strain-Hardening of Spider Silk". In: *Advanced Functional Materials* 21 (2011), pp. 772–778.
- [236] M. Elices, G. R. Plaza, M. A. Arnedo, J. Pérez-Rigueiro, F. G. Torres, and G. V. Guinea. "Mechanical Behavior of Silk During the Evolution of Orb-Web Spinning Spiders". In: *Biomacromolecules* 10 (2009), pp. 1904–1910.
- [237] G. V. Guinea, M. Cerdeira, G. R. Plaza, M. Elices, and J. Pérez-Rigueiro. "Recovery in Viscid Line Fibers". In: *Biomacromolecules* 11 (2010), pp. 1174–1179.
- [238] E. P. S. Tan, S. Y. Ng, and C. T. Lim. "Tensile testing of a single ultrafine polymeric fiber". In: *Biomaterials* 26 (2005), pp. 1453–1456.
- [239] B. O. Swanson, T. A. Blackledge, J. Beltran, and C. Y. Hayashi. "Variation in the material properties of spider dragline silk across species". In: *Applied Physics a-Materials Science & Processing* 82 (2006), pp. 213–218.

-
- [240] B. O. Swanson, T. A. Blackledge, and C. Y. Hayashi. "Spider capture silk: performance implications of variation in an exceptional biomaterial". In: *Journal of Experimental Zoology Part A: Ecological Genetics and Physiology* 307 (2007), pp. 654–666.
- [241] I. Agnarsson and T. A. Blackledge. "Can a spider web be too sticky? Tensile mechanics constrains the evolution of capture spiral stickiness in orb-weaving spiders". In: *Journal of Zoology* 278 (2009), pp. 134–140.
- [242] T. Vehoff, A. Glisovic, H. Schollmeyer, A. Zippelius, and T. Salditt. "Mechanical properties of spider dragline silk: Humidity, hysteresis, and relaxation". In: *Biophysical Journal* 93 (2007), pp. 4425–4432.
- [243] I. Agnarsson, M. Kuntner, and T. A. Blackledge. "Bioprospecting finds the toughest biological material: extraordinary silk from a giant riverine orb spider". In: *PLoS One* 5 (2010), e11234.
- [244] C. Baley. "Analysis of the flax fibres tensile behaviour and analysis of the tensile stiffness increase". In: *Composites Part A: Applied Science and Manufacturing* 33 (2002), pp. 939–948.
- [245] F. Vollrath and D. Porter. "Spider silk as a model biomaterial". In: *Applied Physics a-Materials Science & Processing* 82 (2006), pp. 205–212.
- [246] M. A. Garrido, M. Elices, C. Viney, and J. Perez-Rigueiro. "The variability and interdependence of spider drag line tensile properties". In: *Polymer* 43 (2002), pp. 4495–4502.
- [247] Y. Termonia. "Molecular Modeling of Spider Silk Elasticity". In: *Macromolecules* 27 (1994), pp. 7378–7381.
- [248] D. Sapède, T. Seydel, V. T. Forsyth, M. A. Koza, R. Schweins, F. Vollrath, and C. Riekell. "Nanofibrillar structure and molecular mobility in spider dragline silk". In: *Macromolecules* 38 (2005), pp. 8447–8453.
- [249] F. Vollrath and D. T. Edmonds. "Modulation of the Mechanical-Properties of Spider Silk by Coating with Water". In: *Nature* 340 (1989), pp. 305–307.
- [250] M. Widhe, J. Johansson, M. Hedhammar, and A. Rising. "Current progress and limitations of spider silk for biomedical applications". In: *Biopolymers* 97 (2012), pp. 468–478.
- [251] K. Spiess, A. Lammel, and T. Scheibel. "Recombinant spider silk proteins for applications in biomaterials". In: *Macromolecular Bioscience* 10 (2010), pp. 998–1007.
- [252] A. Leal-Egana and T. Scheibel. "Silk-based materials for biomedical applications". In: *Biotechnology and Applied Biochemistry* 55 (2010), pp. 155–167.
- [253] D. M. Kane, A. M. Joyce, G. R. Staib, and M. E. Herberstein. "Optical surface profiling of orb-web spider capture silks". In: *Bioinspiration & Biomimetics* 5 (2010), p. 036004.
- [254] D. M. Kane, N. Naidoo, and G. R. Staib. "Atomic force microscopy of orb-spider-web-silks to measure surface nanostructuring and evaluate silk fibers per strand". In: *Journal of Applied Physics* 108, 073509 (2010), p. 073509.
- [255] I. Agnarsson, C. Boutry, and T. A. Blackledge. "Spider silk aging: Initial improvement in a high performance material followed by slow degradation". In: *Journal of Experimental Zoology Part a-Ecological Genetics and Physiology* 309A (2008), pp. 494–504.
- [256] M. Humenik, A. M. Smith, and T. Scheibel. "Recombinant Spider Silks - Biopolymers with Potential for Future Applications". In: *Polymers* 3 (2011), pp. 640–661.
- [257] D. Huemmerich, U. Slotta, and T. Scheibel. "Processing and modification of films made from recombinant spider silk proteins". In: *Applied Physics a-Materials Science & Processing* 82 (2006), pp. 219–222.
- [258] U. Slotta, M. Tammer, F. Kremer, P. Koelsch, and T. Scheibel. "Structural analysis of spider silk films". In: *Supramolecular Chemistry* 18 (2006), pp. 465–471.
- [259] B. Liebmann, D. Huemmerich, T. Scheibel, and M. Fehr. "Formulation of poorly water-soluble substances using self-assembling spider silk protein". In: *Colloids and Surfaces a-Physicochemical and Engineering Aspects* 331 (2008), pp. 126–132.
- [260] K. Schacht and T. Scheibel. "Controlled Hydrogel Formation of a Recombinant Spider Silk Protein". In: *Biomacromolecules* 12 (2011), pp. 2488–2495.
-

-
- [261] C. Muller, R. Jansson, A. Elfving, G. Askarieh, R. Karlsson, M. Hamedi, A. Rising, J. Johansson, O. Inganäs, and M. Hedhammar. "Functionalisation of recombinant spider silk with conjugated polyelectrolytes". In: *Journal of Materials Chemistry* 21 (2011), pp. 2909–2915.
- [262] C. X. Liang and K. Hirabayashi. "Improvements of the physical properties of fibroin membranes with sodium alginate". In: *Journal of Applied Polymer Science* 45 (1992), pp. 1937–1943.
- [263] A. Ajisawa. "Dissolution of silk fibroin with calcium chloride - ethanol aqueous solution". In: *Journal of Sericultural Science of Japan* 67 (1998), pp. 91–94.
- [264] L. Qiang, C. B. Cao, Y. Zhang, X. L. Man, and H. S. Zhu. "The preparation of insoluble fibroin films induced by degummed fibroin or fibroin microspheres". In: *Journal of Materials Science-Materials in Medicine* 15 (2004), pp. 1193–1197.
- [265] C. H. Schein. "Solubility as a Function of Protein-Structure and Solvent Components". In: *Nature Biotechnology* 8 (1990), pp. 308–315.
- [266] S. Zschokke. "The influence of the auxiliary spiral on the capture spiral in *Araneus diadematus*". In: *Bulletin of the British Arachnological Society* 9 (1993), pp. 167–173.
- [267] R. W. Work and P. D. Emerson. "An Apparatus and Technique for the Forcible Silking of Spiders". In: *Journal of Arachnology* 10 (1982), pp. 1–10.
- [268] G. V. Guinea, M. Elices, J. I. Real, S. Gutierrez, and J. Perez-Rigueiro. "Reproducibility of the tensile properties of spider (*Argiope trifasciata*) silk obtained by forced silking". In: *Journal of Experimental Zoology Part a-Comparative Experimental Biology* 303A (2005), pp. 37–44.
- [269] B. Madsen and F. Vollrath. "Mechanics and morphology of silk drawn from anesthetized spiders". In: *Naturwissenschaften* 87 (2000), pp. 148–153.
- [270] C. Cantor and P. Schimmel. *Biophysical Chemistry: Part I: The Conformation of Biological Macromolecules*. Biophysical Chemistry. W. H. Freeman, 1980.
- [271] C. N. Pace and F. X. Schmid. "How to determine the molar absorbance coefficient of a protein." In: *Protein structure: a practical approach*. Ed. by T. E. Creighton. IRL Press at Oxford University Press, Oxford UK, 1997. Chap. 10, pp. 253–259.
- [272] S. C. Gill and P. H. von Hippel. "Calculation of protein extinction coefficients from amino acid sequence data". In: *Analytical Biochemistry* 182 (1989), pp. 319–326.
- [273] P. Papadopoulos, J. Solter, and F. Kremer. "Structure-property relationships in major ampullate spider silk as deduced from polarized FTIR spectroscopy". In: *European Physical Journal E* 24 (2007), pp. 193–199.
- [274] W. H. Moore and S. Krimm. "Vibrational analysis of peptides, polypeptides, and proteins. II. beta-Poly(L-alanine) and beta-poly(L-alanylglycine)". In: *Biopolymers* 15 (1976), pp. 2465–2483.
- [275] S. Krimm and J. Bandekar. "Vibrational spectroscopy and conformation of peptides, polypeptides, and proteins". In: *Advances in Protein Chemistry*. Ed. by C. Anfinsen, J. Edsall, and F. Richards. 38. Elsevier Science, 1986, pp. 181–364.
- [276] M. Boulet-Audet, T. Lefevre, T. Buffeteau, and M. Pezolet. "Attenuated total reflection infrared spectroscopy: An efficient technique to quantitatively determine the orientation and conformation of proteins in single silk fibers". In: *Applied Spectroscopy* 62 (2008), pp. 956–962.
- [277] T. A. Blackledge, R. A. Cardullo, and C. Y. Hayashi. "Polarized light microscopy, variability in spider silk diameters, and the mechanical characterization of spider silk". In: *Invertebrate Biology* 124 (2005), pp. 165–173.
- [278] E. P. S. Tan and C. T. Lim. "Mechanical characterization of nanofibers - A review". In: *Composites Science and Technology* 66 (2006), pp. 1102–1111.
-

- [279] M. M. R. Khan, H. Morikawa, Y. Gotoh, M. Miura, Z. Ming, Y. Sato, and M. Iwasa. "Structural characteristics and properties of Bombyx mori silk fiber obtained by different artificial forcibly silking speeds". In: *International Journal of Biological Macromolecules* 42 (2008), pp. 264–270.
- [280] S.-C. Wong, A. Baji, and S. Leng. "Effect of fiber diameter on tensile properties of electrospun polycaprolactone". In: *Polymer* 49 (2008), pp. 4713–4722.
- [281] K. Biegler and R. Carreras. "Fatigue and Fracture Testing". In: *Advanced Materials & Processes* 161 (2003), pp. 41–44.
- [282] G. R. Plaza, G. V. Guinea, J. Perez-Rigueiro, and M. Elices. "Thermo-hygro-mechanical behavior of spider dragline silk: Glassy and rubbery states". In: *Journal of Polymer Science Part B-Polymer Physics* 44 (2006), pp. 994–999.
- [283] A. Glisovic, J. Thieme, P. Guttman, and T. Salditt. "Transmission X-ray microscopy of spider dragline silk". In: *International Journal of Biological Macromolecules* 40 (2007), pp. 87–95.
- [284] R. van Reis and A. Zydney. "Membrane separations in biotechnology". In: *Current Opinion in Biotechnology* 12 (2001), pp. 208–211.
- [285] D. Keerl and T. Scheibel. "Rheological characterization of silk solutions". In: *Green Materials* ahead of print (2013), pp. 1–37.
- [286] K. Gekko and T. Morikawa. "Preferential Hydration of Bovine Serum-Albumin in Polyhydric Alcohol-Water Mixtures". In: *Journal of Biochemistry* 90 (1981), pp. 39–50.
- [287] H. Hamada, T. Arakawa, and K. Shiraki. "Effect of Additives on Protein Aggregation". In: *Current Pharmaceutical Biotechnology* 10 (2009), pp. 400–407.
- [288] S. E. Bondos and A. Bicknell. "Detection and prevention of protein aggregation before, during, and after purification". In: *Analytical Biochemistry* 316 (2003), pp. 223–231.
- [289] K. Yasuda, R. C. Armstrong, and R. E. Cohen. "Shear flow properties of concentrated solutions of linear and star branched polystyrenes". In: 20 (1981), pp. 163–178.
- [290] M. Wang, H.-J. Jin, D. L. Kaplan, and G. C. Rutledge. "Mechanical Properties of Electrospun Silk Fibers". In: *Macromolecules* 37 (2004), pp. 6856–6864.
- [291] M. Wang, J. H. Yu, D. L. Kaplan, and G. C. Rutledge. "Production of Submicron Diameter Silk Fibers under Benign Processing Conditions by Two-Fluid Electrospinning". In: *Macromolecules* 39 (2006), pp. 1102–1107.
- [292] D. M. Cates and H. J. White. "Preparation and Properties of Fibers Containing Mixed Polymers - 3. Polyacrylonitrile-Silk Fibers". In: *Journal of Polymer Science* 21 (1956), pp. 125–138.
- [293] S. Hirano, T. Nakahira, M. Zhang, M. Nakagawa, M. Yoshikawa, and T. Midorikawa. "Wet-spun blend biofibers of cellulose-silk fibroin and cellulose-chitin-silk fibroin". In: *Carbohydrate Polymers* 47 (2002), pp. 121–124.
- [294] P. W. Atkins and J. de Paula. *Atkins' Physical Chemistry*. 9th. Oxford: Oxford University Press, 2009.
- [295] G. Freddi, M. Tsukada, and S. Beretta. "Structure and physical properties of silk fibroin/polyacrylamide blend films". In: *Journal of Applied Polymer Science* 71 (1999), pp. 1563–1571.
- [296] H.-J. Jin, J. Park, R. Valluzzi, P. Cebe, and D. L. Kaplan. "Biomaterial Films of Bombyx Mori Silk Fibroin with Poly(ethylene oxide)". In: *Biomacromolecules* 5 (2004), pp. 711–717.
- [297] C. Mo, C. Holland, D. Porter, Z. Shao, and F. Vollrath. "Concentration State Dependence of the Rheological and Structural Properties of Reconstituted Silk". In: *Biomacromolecules* 10 (2009), pp. 2724–2728.
- [298] S. Rammensee, D. Huemmerich, K. D. Hermanson, T. Scheibel, and A. R. Bausch. "Rheological characterization of hydrogels formed by recombinantly produced spider silk". In: *Applied Physics a-Materials Science & Processing* 82 (2006), pp. 261–264.
- [299] L. Jarecki and A. Ziabicki. "Viscosity effects in computer modeling of fiber spinning from crystallizing polymer melts". In: *Polimery* 49 (2004), pp. 101–109.

-
- [300] T Melin and R Rautenbach. *Membranverfahren: Grundlagen der Modul- und Anlagenauslegung*. Vol. 3. Berlin Heidelberg: Springer, 2007.
- [301] A. Ziabicki. “Mechanical aspects of fibre spinning process in molten polymers”. In: *Colloid & Polymer Science* 175 (1961), pp. 14–27.
- [302] A. Ziabicki and L. Jarecki. “Structure-controlled bifurcation in mathematical modelling of fibre spinning”. In: *Archives of Mechanics* 58 (2006), pp. 459–475.
- [303] W. Haynes. *CRC Handbook of Chemistry and Physics*. Vol. 92. Taylor & Francis, 2011.
- [304] D. Keerl and T. Scheibel. “Characterization of natural and biomimetic spider silk fibers”. In: *Bioinspired, Biomimetic and Nanobiomaterials* 1.10.1680/bbn.11.00016 (2012), pp. 83–94.
- [305] K. N. Savage and J. M. Gosline. “The effect of proline on the network structure of major ampullate silks as inferred from their mechanical and optical properties”. In: *Journal of Experimental Biology* 211 (2008), pp. 1937–1947.
- [306] Y. Liu, A. Spohner, D. Porter, and F. Vollrath. “Proline and processing of spider silks”. In: *Biomacromolecules* 9 (2008), pp. 116–121.
- [307] T. Lefevre, M. E. Rousseau, and M. Pezolet. “Protein secondary structure and orientation in silk as revealed by Raman spectromicroscopy”. In: *Biophysical Journal* 92 (2007), pp. 2885–2895.
- [308] M. E. Rousseau, T. Lefevre, L. Beaulieu, T. Asakura, and M. Pezolet. “Study of protein conformation and orientation in silkworm and spider silk fibers using Raman microspectroscopy”. In: *Biomacromolecules* 5 (2004), pp. 2247–2257.
- [309] D. T. Grubb and L. W. Jelinski. “Fiber morphology of spider silk: The effects of tensile deformation”. In: *Macromolecules* 30 (1997), pp. 2860–2867.
- [310] L. D. Miller, S. Putthananat, R. K. Eby, and W. W. Adams. “Investigation of the nanofibrillar morphology in silk fibers by small angle X-ray scattering and atomic force microscopy”. In: *International Journal of Biological Macromolecules* 24 (1999), pp. 159–165.
- [311] P. Papadopoulos, J. Sölter, and F. Kremer. “Hierarchies in the structural organization of spider silk - a quantitative model”. In: *Colloid & Polymer Science* 287 (2 2009), pp. 231–236.
- [312] S. Bagby, K. I. Tong, and M. Ikura. “Optimization of protein solubility and stability for protein nuclear magnetic resonance”. In: *Nuclear Magnetic Resonance of Biological Macromolecules, Pt B* 339 (2001), pp. 20–41.
- [313] A. P. Golovanov, G. M. Hautbergue, S. A. Wilson, and L. Y. Lian. “A simple method for improving protein solubility and long-term stability”. In: *Journal of the American Chemical Society* 126 (2004), pp. 8933–8939.
- [314] E. Oroudjev, J. Soares, S. Arcidiacono, J. B. Thompson, S. A. Fossey, and H. G. Hansma. “Segmented nanofibers of spider dragline silk: Atomic force microscopy and single-molecule force spectroscopy”. In: *Proceedings of the National Academy of Sciences of the United States of America* 99 (2002), pp. 6460–6465.
- [315] S. Ittah, N. Barak, and U. Gat. “A proposed model for dragline spider silk self-assembly: insights from the effect of the repetitive domain size on fiber properties”. In: *Biopolymers* 93 (2010), pp. 458–68.
- [316] J. P. Zbilut, T. Scheibel, D. Huemmerich, C. L. Webber, M. Colafranceschi, and A. Giuliani. “Spatial stochastic resonance in protein hydrophobicity”. In: *Physics Letters A* 346 (2005), pp. 33–41.
- [317] S. Vauthey, S. Santos, H. Gong, N. Watson, and S. Zhang. “Molecular self-assembly of surfactant-like peptides to form nanotubes and nanovesicles”. In: *Proceedings of the National Academy of Sciences* 99 (2002), pp. 5355–5360.
- [318] J. Leclerc, T. Lefèvre, M. Gauthier, S. M. Gagné, and M. Auger. “Hydrodynamical properties of recombinant spider silk proteins: Effects of pH, salts and shear, and implications for the spinning process”. In: *Biopolymers* 99 (2013), pp. 582–93.
-

-
- [319] Y.-S. Kim, S. P. Cape, E. Chi, R. Raffin, P. Wilkins-Stevens, F. J. Stevens, M. C. Manning, T. W. Randolph, A. Solomon, and J. F. Carpenter. "Counteracting Effects of Renal Solutes on Amyloid Fibril Formation by Immunoglobulin Light Chains". In: *Journal of Biological Chemistry* 276 (2001), pp. 1626–1633.
- [320] C. Holland, F. Vollrath, A. J. Ryan, and O. O. Mykhaylyk. "Silk and Synthetic Polymers: Reconciling 100 Degrees of Separation". In: *Advanced Materials* 24 (2012), pp. 105–109.
- [321] D. Porter, F. Vollrath, and Z. Shao. "Predicting the mechanical properties of spider silk as a model nanostructured polymer". In: *European Physical Journal E* 16 (2005), pp. 199–206.
- [322] Y. Termonia. "Molecular Modelling of the Stress-Strain Behavior of Spider Dragline". In: *Structural Biological Materials*. Ed. by M. Elices. Pergamon Press, 2000, pp. 335–349.
- [323] A. Nova, S. Keten, N. M. Pugno, A. Redaelli, and M. J. Buehler. "Molecular and nanostructural mechanisms of deformation, strength and toughness of spider silk fibrils". In: *Nano Letters* 10 (2010), pp. 2626–2634.
- [324] A. M. T. Harmer, T. A. Blackledge, J. S. Madin, and M. E. Herberstein. "High-performance spider webs: integrating biomechanics, ecology and behaviour". In: *Journal of the Royal Society Interface* 8 (2011), pp. 457–471.
- [325] C. Riekel, B. Madsen, D. Knight, and F. Vollrath. "X-ray diffraction on spider silk during controlled extrusion under a synchrotron radiation X-ray beam". In: *Biomacromolecules* 1 (2000), pp. 622–626.
- [326] T. Lefèvre, F. Paquet-Mercier, J.-F. Rioux-Dubé, and M. Pérolet. "Review structure of silk by Raman spectroscopy: From the spinning glands to the fibers". In: *Biopolymers* 97 (2012), pp. 322–336.
- [327] S. A. C. Gould, K. T. Tran, J. C. Spagna, A. M. F. Moore, and J. B. Shulman. "Short and long range order of the morphology of silk from *Latrodectus hesperus* (Black Widow) as characterized by atomic force microscopy". In: *International Journal of Biological Macromolecules* 24 (1999), pp. 151–157.
- [328] S. Keten, Z. Xu, B. Ihle, and M. J. Buehler. "Nanoconfinement controls stiffness, strength and mechanical toughness of beta-sheet crystals in silk". In: *Nature Materials* 9 (2010), pp. 359–367.
- [329] S.-M. Lee, E. Pippel, U. Gösele, C. Dresbach, Y. Qin, C. V. Chandran, T. Bräuniger, G. Hause, and M. Knez. "Greatly increased toughness of infiltrated spider silk". In: *Science* 324 (2009), pp. 488–492.
- [330] C. P. Brown, J. MacLeod, H. Amenitsch, F. Cacho-Nerin, H. S. Gill, A. J. Price, E. Traversa, S. Licoccia, and F. Rosei. "The critical role of water in spider silk and its consequence for protein mechanics". In: *Nanoscale* 3 (9 2011), pp. 3805–3811.
- [331] J. Guan, F. Vollrath, and D. Porter. "Two Mechanisms for Supercontraction in *Nephila* Spider Dragline Silk". In: *Biomacromolecules* 12 (2011), pp. 4030–4035.
- [332] R. W. Work and N. Morosoff. "A Physicochemical Study of the Supercontraction of Spider Major Ampullate Silk Fibers". In: *Textile Research Journal* 52 (1982), pp. 349–356.
- [333] X. Li, P. T. Eles, and C. A. Michal. "Water Permeability of Spider Dragline Silk". In: *Biomacromolecules* 10 (2009), pp. 1270–1275.
- [334] J. Pérez-Rigueiro, M. Elices, J. Llorca, and C. Viney. "Effect of degumming on the tensile properties of silkworm (*Bombyx mori*) silk fiber". In: *Journal of Applied Polymer Science* 84 (2002), pp. 1431–1437.

Publikationen

Publikationen:

1. D. Keerl and T. Scheibel (2013). *Rheological characterization of silk solutions*, Green Materials (2), pp. 11-23.
2. D. Keerl and T. Scheibel (2012). *Characterization of natural and biomimetic spider silk fibers*, Bioinspired, Biomimetic and Nanobiomaterials (1), pp. 83-94.
3. Keerl, D. et al. (2009). *Spider Silk: From Soluble Protein to Extraordinary Fiber*, Angewandte Chemie-International Edition (48), pp. 3584-3596.
4. Lammel, A. et al. (2008). *Proteins: Polymers of natural origin*, in: Recent Advances in Biomaterials Research. ed.: J. Hu. Kerala, India, Transworld Research Network, pp. 1-22.

Tagungsbänder:

1. Keerl, D. et al (2009). *Biomimetic spinning of recombinant silk proteins*, MRS Proceedings, 2009, Boston, MA, USA.
2. Keerl, D. et al (2009). *Verspinnen von Proteinfasern für technische Anwendungen*, 17. Symposium Verbundwerkstoffe & Werkstoffverbunde, Bayreuth

Lebenslauf

Persönliche Daten

David Keerl
Romanstr. 8, 95444 Bayreuth
E-Mail: davidkeerl79@gmail.com
Geboren am 30.08.1979 in München
Familienstand: verheiratet
Staatsangehörigkeit: deutsch

Schulbildung

09/1986 - 07/1990 Grundschule in Neukeferloh
09/1990 - 07/1991 Ernst-Mach-Gymnasium in Haar bei München
09/1991 - 07/1994 Deutsche Schule in Toulouse, Frankreich
09/1994 - 05/1999 Gymnasium Grafing bei München (Leistungskurse Mathematik und Englisch)

Studium

10/2000 - 01/2006 Chemieingenieurwesen an der TU München (Abschluß Dipl.-Ing.)

Promotion

08/2006 - 12/2007 Promotion am Lehrstuhl Biotechnologie an der TU München
01/2008 - 11/2011 Fortsetzung der Promotion am Lehrstuhl Biomaterialien, Universität Bayreuth

Beruf

11/2012 - heute Entwicklungsingenieur bei MANN+HUMMEL Innenraumfilter GmbH,
Himmelkron

February 2014, Bayreuth